PhD Dissertation

博士論文

Measurement and numerical
modeling of pedestrian flows

（人流の計測と数値モデリング）

Feliciani Claudio

フェリシャーニ　クラウディオ

Contents

Notation

This section provides a list with the common notation used in this work. The list is not complete since some symbols are used only once and only on a special purpose (in particular for empirical expressions including experimentally obtained parameters). Although every symbol is defined within the text, this section should provide a reference in case meaning is not clear or defined only several pages earlier.

Abbreviations

AI	Artificial Intelligence
$ANOVA$	Analysis of variance
AVG	Average
BI	Bidirectional
BIB	Bidirectional Balanced
BIU	Bidirectional Unbalanced
BPM	Beats Per Minute
CA	Cellular Automata
CA	Cumulative Average
CDF	Cumulative Density Function
ESC	Escalator
EXP	Experiment/Experimental
FD	Fundamental Diagram
FF	Floor Field
FFT	Fast Fourier Transform
fps	frames per second
GPS	Global Positioning System
HD	High Density
ID	Identification (number)
IT	Information Technology
LD	Low Density
LOS	Level of Service
LWR	Lighthill-Whitham-Richards (model)

MA	Moving Average	
MAC	Media Access Control	
MC	Maximum Current	
OS	Operating System	
PDF	Probability Density Function	
ROI	Region of Interest	
ST	Stairs	
STD	Standard Deviation	
$TASEP$	Totally Asymmetric Simple Exclusion Process	
UNI	Unidirectional	
VAR	Variance	

Roman

a	Car maximum acceleration	[m·s^{-2}]
A	Anticipation floor field value	
A	Area (surface)	[m^2]
b	Car breaking deceleration	[m·s^{-2}]
d	Probabilistic density	
d	Distance	[m]
D	Dynamic floor field value	
g	Gap	[m]
h	Distance (horizontal)	[m]
i	Index for horizontal direction	
j	Index for vertical direction	
J	Probabilistic flow	
k	Floor field weight	
l	Length	[m]
m	Elements in vertical direction	
n	Elements in horizontal direction	
n	Occupancy	
N	Normalization parameter	
N	Number of elements (in general)	
p	Position	[m]
p	Probability	
q	Pedestrian flow	[(m·s)$^{-1}$]

r	Flow ratio	
r, R	Rotation	$[\text{s}^{-1}]$
R	Correlation coefficient	
s	Side length	$[\text{m}]$
S	Static floor field value	
v, V	Velocity	$[\text{m/s}]$
w, W	Width	$[\text{m}]$
W	Wall floor field value	$[\text{m}]$
X	Random number	

Subscript

A	Anticipation floor field
avg	Average
bi	Bidirectional
$cong$	Congestion
$corr$	Corridor
d	Distance
D	Dynamic floor field
E	Exchange
eff	Effective
i	Horizontal direction
$inter$	Intersection
j	Vertical direction
l, L	Left
max	Maximum
min	Minimum
mj	Major
mn	Minor
$mono$	Monodirectional
ped	Pedestrian
r, R	Right
s	Side
S	Static floor field
tot	Total

trans	Transition	
uni	Unidirectional	
w	Width	
W	Wall floor field	
wa	Waiting area	

Greek

α	Diffusion (in Floor Field model)	
α	Pedestrian inflow	$[(\text{m·s})^{-1}]$
α	TASEP inflow (boundary rate)	
β	Decay (in Floor Field model)	
β	Pedestrian outflow	$[(\text{m·s})^{-1}]$
β	TASEP outflow (boundary rate)	
ϵ	Gipps model parameter	
μ	Obstruction index	$[\text{s}^{-1}]$
μ	Update probability	
ξ	Obstacle parameter	
ρ	Pedestrian density	$[\text{m}^{-2}]$
ϕ	Intersecting angle	$[°]$
ϕ	Local order parameter	
ϕ	Occupancy parameter	
Φ	Global order parameter	
ω	Angular velocity	$[\text{rad/s}]$

Abstract

The motion of pedestrians in transportation facilities has been studied for several decades now, but there are still many phenomena which are not completely understood. In the one-dimensional case (people moving in a single line), properties similar to vehicular flow are shown and jamming transition is clearly identified using the so-called fundamental diagram when pedestrian flow reaches a platoon. Also, simple mathematical models are able to describe one-dimensional systems with sufficient accuracy. However, in the case of multidimensional motion (crosswalk, sidewalk...) it is not yet clear which approach should be taken and how to predict jamming phenomena. Several simulation models have been developed, with the Cellular Automata approach and the social force model being the most used and researched. However, ad-hoc modifications of the standard models are required to reproduce particular aspects in simulation. Nonetheless, many studies build most of their conclusions on simulated results and empirical aspects are only marginally considered in research of pedestrian dynamics.

The present research starts by trying to explain some phenomena observed in bidirectional pedestrian flow (people walking in opposite directions) and propose methods to allow a more complete analysis of this particular case. Bidirectional flow was chosen because it is a very common situation observed in many transportation facilities. Corridors, sidewalks or crosswalks are a typical example of bidirectional flows. Also, they possess some common characteristic with one-dimensional cases, thus allowing the use of some methods from the past research. However, because lateral motion is possible, bidirectional flow also shows some typical characteristic of multidimensional systems, namely the capacity to lead to spontaneous organization in the form of lanes.

At first, we studied a bidirectional stream of pedestrians moving inside a corridor of a crowded train station during peak hour. We observed that large groups of passengers passing through a studied section in the corridor produce a Gaussian flow when entering and leaving the corridor. Based on the difference in the shape of the inflow and outflow we were able to distinguish between different regimes: free flow (people moving with complete freedom), organized flow (moving in lanes) and congestion (or partial/complete deadlock).

We later used the empirical measurements to validate a simulation model which was developed to deal with high density crowd. Simulation results showed that empirical results can be reproduced with sufficient accuracy, but different model parameters had to be used for different situations. Results from the simulations also suggested that pedestrians turning their body to crawl inside the dense crowd may contribute to the dissolution of deadlocks.

To study more in detail phenomena occurring during lane formation and the reasons leading to deadlock, we designed supervised experiments with two small group of pedestrians passing through each others by walking in opposite directions. Video recordings of the experiment were obtained and pedestrians trajectories were taken by tracking par-

ticipants' head with a specialized software. Results showed that anticipation (predicting others' behavior) is only minimal and pedestrians start to interact with each others only at relatively small distance. Also, when both groups were equal in size (balanced flow) participants showed the largest lateral motion during the process of lane formation. This suggests that at high density, when motion is constrained by the crowd, lane formation is more difficult and therefore congestion should appear more easily. On the other side, the balanced case shows smoother lanes and it is therefore more efficient at low density crowds. To quantify the smoothness of bidirectional flow and measure properties of the crowd in different phases, a measure characterizing the crowd vorticity has been introduced based on principles from fluid-dynamics. By applying this measure on pedestrians' trajectories, lane formation and dissolution mechanisms could be clearly distinguished and the balanced case was confirmed being the most efficient once lanes are formed.

To validate the principle of crowd vorticity we developed a system to measure body rotation directly on the pedestrians involved in the experiment. Commercial tables equipped with high-precision inertial sensors were used and data were streamed to a PC during the experiment using a wireless network. Direct measurement of body rotation confirmed that crowd vorticity (based on the trajectories from pedestrians) allows to get intrinsic properties of the crowd without the need to actually have sensors on pedestrians. On the other side, this result also showed that the opposite approach is possible: obtain information relative to the whole crowd by sensing the motion of only few pedestrians.

To provide a theoretical explanation of the phenomena observed in bidirectional flows a simple mathematical model was developed. The corridor (or similar structures) is divided in several cells along its length and each cell is assigned with one direction (main flow or counter flow) with a determined probability. The possibility to have an open path with each cell pointing in the same direction can be computed using statistical theory. A database of pedestrians' trajectories from different researchers was created and we showed that the function obtained from the mathematical model can accurately describe the transition to congestion (from organized motion). A similar approach was also used to compute the expected number of lanes of a particular bidirectional flow configuration. The general function giving the expected number of lanes allows to describe the transition from free flow to organized lanes. We therefore demonstrated that changes (or phase transitions) in pedestrian's crowds can be described using simple theoretical models also in the case of the bidirectional flow.

The methods developed during the study of bidirectional flows were later tested in a completely bidimensional environment with people moving in different and random directions. The so-called congestion level had been used in several experiments to measure the degree of organization in pedestrian motion and set a threshold for transition to congestion. The different cases considered showed that the approach proposed here with the congestion level has similarities with the concept of the fundamental diagram but also allows to describe situations which could not be explained by using flow and density alone. Also in the multidimensional case a mathematical function was proposed to describe the changes of crowd properties in regard to variations in density. The approach presented here specifically identifies a transition point therefore allowing to test universality of different approaches in measuring pedestrian crowds.

When tested on scenarios where crowd properties change in space and time, the congestion level allowed to recognize the most congested spot for evacuations through a single door and the moment during which organized structures are formed in a circular flow experiment. In the latter case, the congestion level also possibly allowed to recognize

cognitive features as participants learned from experience during the execution of the experiments. Cognitive features were also identified as being a relevant element contributing to changes in the transition to congestion observed in bidirectional flows. Although not demonstrated, our analysis suggest that cognitive processes may be the reason leading to different forms of fundamental diagrams at very high densities.

Throughout our multidirectional experiments, the measurement of pedestrian properties based on inertial sensors has been constantly researched to increase its capabilities in estimating crowd properties. In this regard, we showed that the accelerometer contained in inertial units of commercial devices allows to get an estimation of the walking speed and, if accurately calibrated, measurement accuracy is more than satisfactory. However, application to real pedestrian crowds could be limited by the fact that calibration is not possible or rather difficult in real situations and prediction accuracy depends on individual factors such as the place where the device is stored, which cannot be know in advance. Nonetheless, our analysis suggested that if the population making use of electronic devices is large enough and creates a homogenous crowd than estimation of pedestrian properties may be sufficiently accurate.

Finally, we extended our analysis on pedestrian motion to the case where also vehicles are involved by studying an unsignalized crosswalk. In this regard, we found that a specific model has to be build based on real observations and only by including the decision making process deduced empirically accurate predictions are possible. Our model for the unsignalized crosswalk allowed to predict the waiting times found for both vehicles and pedestrians, thus allowing the assessment of the Level of Service for this traffic facility. The model was later extended by including collisions between cars and pedestrians and perform comparative statements on which policy has the biggest potential in creating a safe environment for pedestrians. While speed limitation and level of distractions had clear effects on the number of fatalities obtained in simulation, we also found that concepts such as the shared space could have the same effects without having to enforce particular measures.

Chapter 1

Introduction and fundamentals

1.1   Preface

Collective motion is a subject which has fascinated scientists for decades or even centuries. Flocking of birds is probably the most common yet fascinating among the different expressions of collective motion. When birds move in large number they follow a common path, thus creating the impression that a single compact entity (composed by hundreds or thousands of individual birds) is moving in the sky. What is particular about this type of organization is the fact that in most of the cases no-one inside the group is aware of the shape taken by the moving group and that no-one has a specific function in guiding the others. Structures like the flocking of birds described now form because the different members of the group react according to a set of rules and the interactions among them produce the so-called "emergent phenomena" relative to the group as a whole. In the specific case of birds the different rules are related with natural instincts: reduce wind resistance, protect from predators and migrate toward a common destination [1]. Overall shape of the flock change depending of environmental conditions: direction and strength of wind or position of predators, but the group is kept compact during flight.

We have started the discussion with birds because they represent probably the most common and familiar scenario (especially in areas where migrations occur), but there are many more species showing organized structures in nature. Fish schools are another very common case, but also ants and sheep show a strikingly social behavior leading to some specific group structures under particular conditions. Because of their complex social structures, humans also show collective motion when moving in group and because of their cognitive capacities relationship with the surrounding environment tends to be particularly sophisticated. In the case of humans, collective structures are not only shown while walking, but driving behavior also shows some form of autonomous synchronization when drivers move along a common route [2]. The collective phenomena originating from car traffic are more simple than the ones resulting from motion by walking, because traffic regulations contribute in reducing the degree of decision freedom and in establishing a common framework under which actions should be considered.

While the concept of "flocking" has been typically applied to phenomena observed in the animal world, it can be also used to describe sudden changes in the organization of complex structures. As a consequence, although collective phenomena described so far represented cases in which individuals concretely moved in the physical space, there are other more abstract examples of collective dynamics. For example, the movements of the stock market are also related to single actions generating from individual traders (recently

automated trading also plays an important role). Although large fluctuations are usually caused by external triggers (like economical of political changes), there are cases where it is very difficult to determine which event caused a particular loss/gain. Often this is the result of a sudden synchronization occurring within the financial system, leading to a collective action resulting in a sudden change in the stock market [3].

Finally, increasing the degree of abstraction, it is worth mentioning that collective phenomena are gaining popularity in the field of Information Technology (IT) to understand, for example, how trend emerges and how to use this knowledge for marketing purposes in the e-commerce [4, 5]. Researchers are also interested in understanding how consensus emerge among individuals and if it is a sort of synchronization within the group or a consequence of a strong leadership [6]. From this point of view, research on collective dynamics has shown having many similarities with network theory, with knowledge often shared between both field of research [7].

1.2   Pedestrian dynamics

As stated above, humans are among the several species showing collective behavior when moving in group. Research on the motion of humans has been a topic of research for several decades, but the interest has grown in the recent years. Below we will examine the reasons and the motivations which have led to a grow in popularity on the research on pedestrian traffic (and pedestrian dynamics more in general).

1.2.1   Motivation and background

The planning and design of pedestrian facilities has a very long history. When humans started to live in organized and compact cities the necessity to consider location and size of public spaces became evident. Although we can assume that in the very ancient time facilities were not specifically designed considering pedestrian behavior, this aspect rapidly started playing an important role. One of the first and most remarkable examples of buildings designed to allow a smooth flow of pedestrians is the Coliseum in the ancient Roman Empire. It had more than 60 numbered entrances along its circumference, thus allowing to quickly evacuate the more than 50'000 spectators it could accommodate. Helbing and Mukerji [8] state that the particular design of the Coliseum allowed an evacuation in just 5 minutes, a remarkable performance also compared to modern structures. Several centuries later the size of cities around the globe keeps growing and the demand for mobility is contributing to a congestion in transportation facilities. According to the "2014 World Urbanization Prospects" by the United Nations [9], globally more people live in urban areas than in rural areas. While the proportion of urban population was 30% in 1950, it is projected to reach 66% by 2050. Africa and Asia are still proportionally rural regions, but urbanization is growing faster. Urban population in Tokyo account to 38 million people, the largest mega-city in the world. When air transportation is considered, the number of passengers carried worldwide passed from slightly more than 1 billion in 1990 to almost 3.5 billion in 2015 [10]. As a consequence, airports, train stations and facilities accommodating passengers are experiencing a surge in pedestrian flow (Figure 1.1 shows an example of a crowded train station in China).

Also, the different ways of transportation allow to quickly move a large number of people from far locations and it is rather easy to see large crowds during popular events. The Olympics, religious pilgrimages or the World Fair are just some examples of events which

Figure 1.1: Example of a crowded train station in Shanghai, China.

routinely gather million of people in a limited space. Several accidents have occurred in the recent past in different countries. In Japan a firework display in 2001 resulted in the death of 11 people (with 247 injured) when spectators tried to cross a bridge connecting a train station [11]. In Germany in 2010 21 people were killed (and more than 500 injured) during an open-air music festival [8]. Probably the most deadliest accident occurred in the recent past is the stampede which generated during the 2015 annual Hajj pilgrimage in Saudi Arabia. Although the figures vary depending on the source it is believed that about (or more than) thousand people died when trying to cross an intersection [12] (exact dynamic is still under investigation). Although this kind of accidents are relatively rare, the examples provided above testify that when crowd accidents do occur the consequences can be devastating. In addition, what is also characteristic of crowd accidents, is that they may occur at events which have been held without problems for several years. One reason for this is that because those accident are quite rare, there are only very few people having experienced such emergencies and it is therefore difficult to learn from experience. Also, location and/or position of entrances/exits and security personnel change quite often at mass events and it is difficult to predict in advance which area is the most risky. It is therefore important to develop some sort of technology and quantitative measure to asses the intrinsic danger of a particular crowd and help security personnel identifying risks on a real-time basis.

Even excluding the extreme case of accident, there is the need to improve the comfort of pedestrian facilities in order to increase the quality of life in crowded cities. Obviously, building new facilities to accommodate a larger number of people is always the priority, but there are many cases in which it is not possible to add a new construction because of space limitations or logistical problems. In these cases, improving the efficiency of pedestrian facilities is the only solution and this is only possible when motion of pedestrian is sufficiently known and predictable. In addition, also in the case of new constructions it is important to have adequate norms to provide sufficient space for pedestrian flows.

Here, it is important to remember that in the case of vehicular traffic active safety (seat belt, airbag, automatic breaking...) greatly contributes in making roads safer and therefore the design of road network can mostly focus on traffic/congestion issues. However, in the case of pedestrian facilities active safety does not exist and pedestrian safety can only be guaranteed by designing facilities in which accidents are very unlikely to occur. Finally, considering aspects related to policy making, research on pedestrian motion can

help defining some norms and regulations to be used when planning new facilities or considering the improvements of existing ones. In this regard, it is relevant to consider that people designing buildings and transportation facilities are usually not familiar with details of pedestrian traffic. For this reason some simple and yet adequate norms are required to determine for example the width of a corridor, the number of escalators, the number and location of exits or the guidance to be provided inside facilities. While some norms already exist, they tend to be quite outdated and modern facilities are more often designed using computer codes simulating pedestrian motion, thus creating a gap between experts setting up and running computer simulations and decision makers having to interpret the results.

To conclude and summarize it can be said that research on pedestrian dynamics is important for the following reasons:

1. To prevent accidents such as stampede and crush.

2. To improve the comfort of pedestrian facilities.

3. To create norms and regulations to be used when planning a new construction accommodating a large crowd.

To reconnect with the introduction and considering a wider context, the research on pedestrian dynamics can help in the understanding of collective (and emergent) phenomena as a whole, since (as it was discussed before) motion of group of humans possess similarities with other events observed in nature. Besides scientific and academic interest, the knowledge gained from this more wide research on collective phenomena may find application in a variety of fields with finance, computer science and marketing being only some examples.

1.2.2   Definitions and nomenclature

Before discussing more in detail specific topics of pedestrian dynamics, it is important to introduce some fundamental principles which will be used in this manuscript. In general, there are two quantities which are typically used to quantify pedestrian crowds: density and flow [1].

Pedestrian density it is defined as the number of people in a given area and it is measured in persons per square meter (shortened in m^{-2} from here on). Usually an area larger than $1\ m^2$ is required to accurately measure density, although no unique definition is provided as for what is the minimum area required for a correct measurement (a discussion on different methods is given in [13]). In real situations the density of the crowd may change from region to region and defining an overall value may be problematic (see for example Figure 1.3(b)). For this reason, it is often convenient using the term "global density" to refer to an average value resulting from a large area and "local density" to describe more subtle changes inside the crowd.

To partially overcome the problem of local density variations, some researchers [14, 13] proposed to use the so-called Voronoi cells to estimate a "personal space" of each pedestrian and therefore allow a more precise definition of density. An example for Voronoi cells

---

[1]Velocity is also important in defining crowd and pedestrian properties, but the definition is not different from that of any other physical entity (like particle speed or so on) and a detailed discussion may not be necessary.
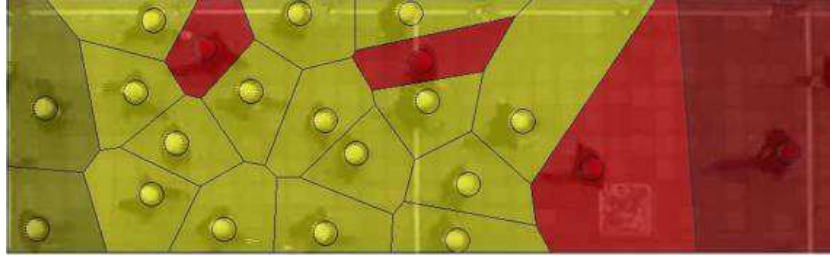
Figure 1.2: Superposition of Voronoi cells to a frame taken during an experiment with pedestrians. Colors indicate different walking directions. Note that this frame is equivalent to the situation represented in Figure 1.4.

computed from a real situation is given in Figure 1.2. It is clear that pedestrians lying in a low-density region have larger Voronoi cells compared to pedestrians in dense areas. By using Voronoi cells it is also possible to compute the density of a single individual inside the group by taking the inverse of the his/her cell's surface. Of course, using a moderate number of pedestrians to compute density is required to get a better picture, but the use of Voronoi cells allows to reduce density fluctuations due to local effects.

| (a) $\rho \approx 0.5$ m^{-2} | (b) $\rho \approx 1$ m^{-2} | (c) $\rho \approx 2$ m^{-2} | (d) $\rho \approx 4$ m^{-2} |
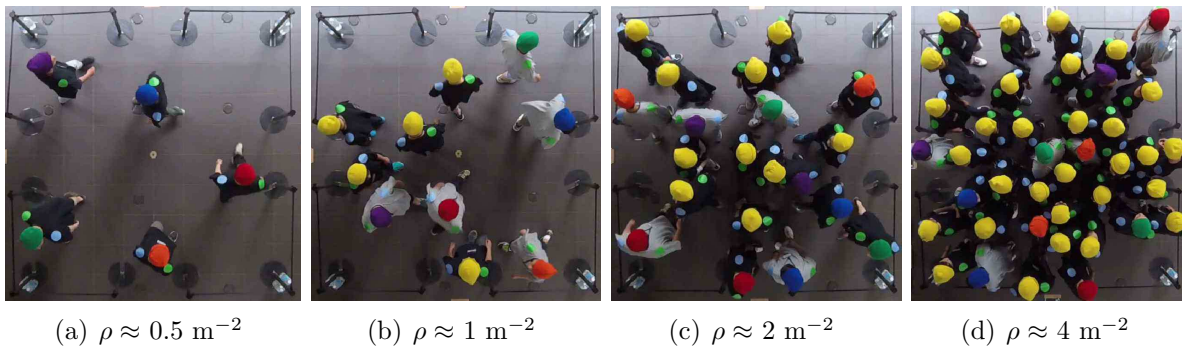
Figure 1.3: Examples of pedestrian crowds under different densities ρ. It can be also noted that in some situation the local density does not represents the global density.

To help getting a practical image on the concept of pedestrian density, Figure 1.3 provides some illustrative examples. Also, the following qualitative examples should help becoming familiar with the figures usually encountered in human crowds [2].

- $\rho \ll 0.5$ m^{-2}: complete freedom of motion, people can walk in the desired direction without having to consider other pedestrians. This condition is encountered for example in large uncongested public plazas or residential areas.

- $\rho \approx 0.5$–1 m^{-2}: freedom to select individual walking speed and direction is restricted and pedestrians need to consider others to avoid collisions. At this density emergent behavior may form, for example lanes may spontaneously form in corridors.

- $\rho \approx 1$–2 m^{-2}: walking at constant speed becomes difficult and continuous speed adjustments are required. At this density pedestrians may partially move in an intermittent way, but walking is still possible and there is no need to stop.

---

[2]There are no unique definitions for typical densities and reported figures change from author to author and in relation to several criteria. So the examples provided here are mostly based on the author's general knowledge on the subject.

- $\rho \approx 2\text{--}3 \text{ m}^{-2}$: continuously walking is very difficult and progresses are made by shuffling. Visual field is restricted and judgments are only possible based on neighboring pedestrians.

- $\rho \approx 6 \text{ m}^{-2}$: maximum density sustainable for long time. Packed trains in congested cities usually reach this value during morning rush. Although this density represents a very unconformable level it can be physically sustained for periods of several hours. However, at this density, psychological tolerance may go beyond acceptable limits if the situation does not improve on the long run. Also, shock waves are observed in the crowd if people try to move (this aspect will be considered later).

- $\rho = 8.4 \text{ m}^{-2}$: maximum density (at author's knowledge) reported for a controlled experiment under safe conditions [15]. Trained firemen walked toward a fixed wall and kept pressing on it after getting in contact with the wall. The rows of firemen were gradually increased (or added) to measure the pressure created by them on the wall. The experiment was performed under safe conditions and with trained professionals, so conditions may slightly differ from real situations.

- $\rho > 10 \text{ m}^{-2}$: almost certainly causalities will occur. This value is not uniquely defined, but analysis of video footage from stampede accidents revealed that densities higher than 10 m^{-2} were reached when people started collapsing [16]. Some authors [11] also reported densities up to 15 m^{-2} in case of accidents.

When only safety is concerned, density is without doubt the most important information on human crowds. Values above 6 m^{-2} should quickly ring an alarm necessitating a prompt and effective intervention. For densities roughly over 3 m^{-2}, motion is very limited and therefore the type of geometry (facility) considered does not play a significant role in determining comfort (while safety is relevant). Motion in walkways, corridors, intersections or crosswalks is similar under congested conditions because progresses are made by shuffling. However, at low density the type of facility considered plays an important role and density alone cannot qualitatively describe the phenomena observed.

To grasp with more accuracy crowd's condition and allow more precise statements concerning pedestrian comfort, then density alone cannot give a complete picture as it does not contain the concept of motion (density has a static definition); flow needs to be also considered. Pedestrian flow is defined as the number of people passing through a given location in a given time. It is typically measured in persons per meter width per second (old literature usually prefers minutes), shortened in $(\text{m} \cdot \text{s})^{-1}$.

Figure 1.4: Frame taken from an experiment with pedestrians walking in opposite directions. Flow can be computed at different locations like the three proposed in the figure.

For example considering the straight section of Figure 1.4, it is possible to compute the flow for each of the three points indicated (obviously any alternative location can be chosen, but the three chosen in Figure 1.4 are clearly recognizable). Considering that

pedestrians in Figure 1.4 are walking in the given direction (left to right for the yellow caps and the opposite direction for the red ones), it can be guessed that flow in location 1 and 2 will be similar and bigger than the flow in 3.

It has to be noted that flow is much more specific than density and may be representative of a particular structure. For example, for the case in Figure 1.4 the cross section of the walkway can be used to compute the flow. In the case of a four-leg intersection defining a cross section to compute flow may be more difficult and the flow in the central part can be obtained by summing up the single flows in the four legs before entering the intersection. However, for multi-directional motion, for example pedestrians wandering in large plaza, determining flow in an univocal way may become impossible. For these conditions the general definition of flow may apply. From fluid-dynamic it is known that the specific flow inside a pipe (or any structure moving fluids) can be computed from:

$$q = \rho \cdot \overline{v} \tag{1.1}$$

where ρ is the density of the fluid and $\overline{v}$ the average speed. The same definition can be used for human crowds, where ρ now stands for pedestrians' density and $\overline{v}$ for their average walking speed (this equation is sometimes also referred as the "fundamental relation" of traffic dynamics). When a scenario like the one shown in Figure 1.4 is considered, fluid-dynamic and pedestrian definitions coincide. However, pedestrian flow becomes more abstract for the example of the plaza previously discussed (like in Figure 1.3). Nonetheless, the use of the above definition allows to measure flow in any condition, thus allowing the quantitative comparison of different situations.

Finally it is important to introduce a last concept often used to quantify pedestrian streams: the capacity. The capacity of a given pedestrian facility is defined as the maximum flow which can be sustained for an indefinite time under stable conditions. Flow higher than capacity may be possible for a short time, but this will lead to congestion and ultimately to the formation of jams. The concept of capacity is related with the one of stability, whereas flows above capacity leads to unstable conditions (such as congestion). The notion of capacity is very important for the design of pedestrian facilities and it is necessary that demand never exceeds capacity except for very short time periods. Quantify these quantities is the goal of planners and represents one of the objective of pedestrian dynamics (and this study also).

As the reader may have already guessed from the short definitions provided here, defining pedestrian measures to be used in a variety of situations is not easy. In the past, several methods and standards have been established to evaluate pedestrian facilities and the next section will try presenting a brief summary of the research performed so far.

1.2.3   Empirical aspects

As we have seen, already in the ancient times city planners had to consider the behavior of people in large groups. However, the research on crowd behavior is relatively recent and the first scientific and quantitative studies were reported only during the 20th century (with few exceptions). Because of the historical events occurred during the 20th century, academics firstly started to consider sociological/anthropological aspects of human crowds. In this context, one of the most prominent works examining social and political aspects of human crowds is the book by Canetti: "Crowds and power" [17]. After witnessing the mass events occurred in the first half of the 20th century, Canetti started investigating the relationship between crowds and power and more specifically how can

the power be used to control large crowds making mass of people behaving like a single entity. In his book, Canetti provides very accurate and clear descriptions of human crowds, including the way they move, gather and disperse. Crowds are compared to elements observed in nature, like rivers, seas, fires and so on. As we will see later this river-like formulation inspired mathematical models.

Level Of Service (LOS)

Quantitative description was not among the interests of Canetti and we have to wait one decade more before the first studies considering engineering aspects of pedestrian traffic appeared around the 1970s (or late 1960s). In this regard, the work by Fruin, entitled "Pedestrian planning and design" [18], can be considered a pioneer work in the context of traffic engineering. Fruin collected results from several researchers and conducted his own research to establish some design standard to be used for pedestrian facilities. A central point in the work by Fruin is the so-called Level of Service (LOS). Depending on the type of structure considered (walkway, stair or waiting queue) different quantities are defined to set a LOS in a scale from A to F (with A being the most comfortable LOS and F an unacceptable design standard).

Table 1.1: Level of Service defined by Fruin for pedestrian flow in flat walkways [18]. Note: original values by Fruin are provided in imperial units, while values reported here were converted into metric units.

LOS	Density [m^{-2}]	Flow [(m·s)$^{-1}$]	Application example
A	<0.31	<0.38	Public wide plazas
B	0.31–0.43	0.38–0.55	Transportation facility at off-peak
C	0.43–0.72	0.55–0.82	Heavily used transportation terminal
D	0.72–1.08	0.82–1.09	Most crowded public area
E	1.08–2.15	1.09–1.37	Maximum acceptable standard
F	>2.15	>1.37	Waiting area, queuing pedestrians

The concept of LOS is still used nowadays and it has been extended to a variety of facilities also including interaction with vehicular traffic like in the case of crosswalks. The definitions for LOS are constantly updated and are contained in the "Highway capacity manual" [19], a sort of reference manual containing norms to be used by traffic planners. Some authors also tried to introduce alternative methodologies based on the same general concept [20].

In the 1970s research on pedestrian motion gained popularity and a number of studies have been published. In 1993 Weidmann summarized the research performed at that time in his work "Transportation techniques for pedestrians" [21], a book which remains a milestone in the present days. In his work, Weidmann mostly focus on pedestrian as a single entity, reporting for example how walking speed change depending on slope and climate or what is the walking speed expected for people walking uphill and downhill in stairs. Also, Weidmann provided some methodology to determine the size of pedestrian facilities, considering for example the repulsion from walls or the effect of obstacles. While the works by Fruin and Weidmann can be considered similar in several points, the biggest change is represented by a shift from grading (in Fruin) to scaling (in Weidmann). The research conducted over the years allowed to define more accurate norms thus making design of pedestrian facilities more efficient and reliable.

But the reason which made the work of Weidmann a milestone in the literature is the establishment of a universal function (or equation) for the so-called "fundamental diagram" of pedestrian traffic. Although the concept of fundamental diagram was not new (for vehicular traffic it was discovered in 1933 by Greenshields [22]), Weidmann was the first to collect multiple studies and define a universal function able to predict pedestrian speed at different conditions. Since the fundamental diagram (as the name suggest) is a central topic in traffic engineering we will devote the next part for a more detailed discussion.

Fundamental diagram

The fundamental diagram originates from vehicular traffic, but it is now a widespread concept used in different areas of traffic research. Although most of the applications are still related with vehicular traffic, there are many more systems showing similar properties to cars, with pedestrian also belonging to that group. In general, any system composed of self-propelled particles shows transitions between different states of organization and transition to a congested motion is clearly depicted in the fundamental diagram. Generally speaking, there are three types of fundamental diagrams: speed–density, flow–density and flow–speed (this one is rarely used in the case of pedestrians). The name of each refers to the properties plotted within it. We will start with the speed–density fundamental diagram, which is the one most studied in the case of pedestrians.
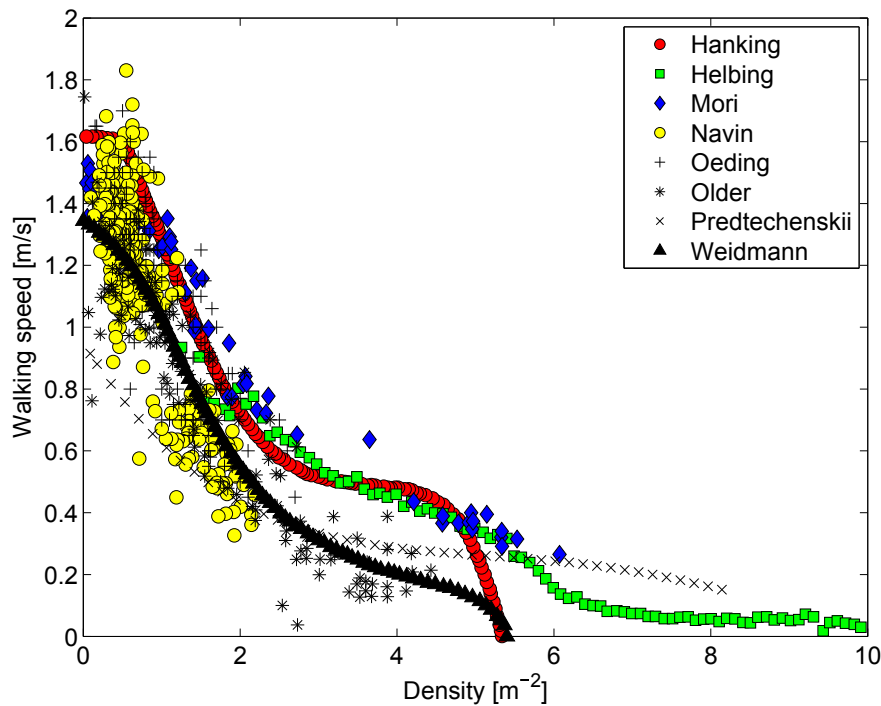
Figure 1.5: Measurement of pedestrian speed and density by several authors [23, 16, 20, 24, 25, 26, 27, 21].

Figure 1.5 shows pedestrian walking speed plotted against density for several empirical studies reported in the literature. One may notice that, although datasets differ (particularly at low densities), there is a common trend. As it can be intuitively guessed (and experience suggests), the walking speed drops when the density is increased, as motion becomes restricted. It is observed that the relationship between speed and density does not seem to be linear. Some linearity is observed for very low densities, until about 1–2

m^{-2}, but after that density increases faster for equivalent drops in velocity. Also, it is remarkable to notice that studies differ as for which density should be considered as the maximum, i.e. the moment in which velocity reaches zero and pedestrians are unable to move. Some studies set this limit at about 5.5 m^{-2}, but others observed that also at very high densities (about 10 m^{-2}) very slow motion is still observed.

Figure 1.6: Speed–density fundamental diagram from different authors [28, 29, 30, 31, 32, 21, 33].

Based on their own results several authors proposed functions to describe the speed–density relationship. Figure 1.6 shows some of the functions proposed so far with the expressions given in Table 1.2 (a complete review is given in [34]). In Figure 1.6, linear functions are given in black, while non-linear ones are plotted in blue. As we have seen from Figure 1.5, linear relationships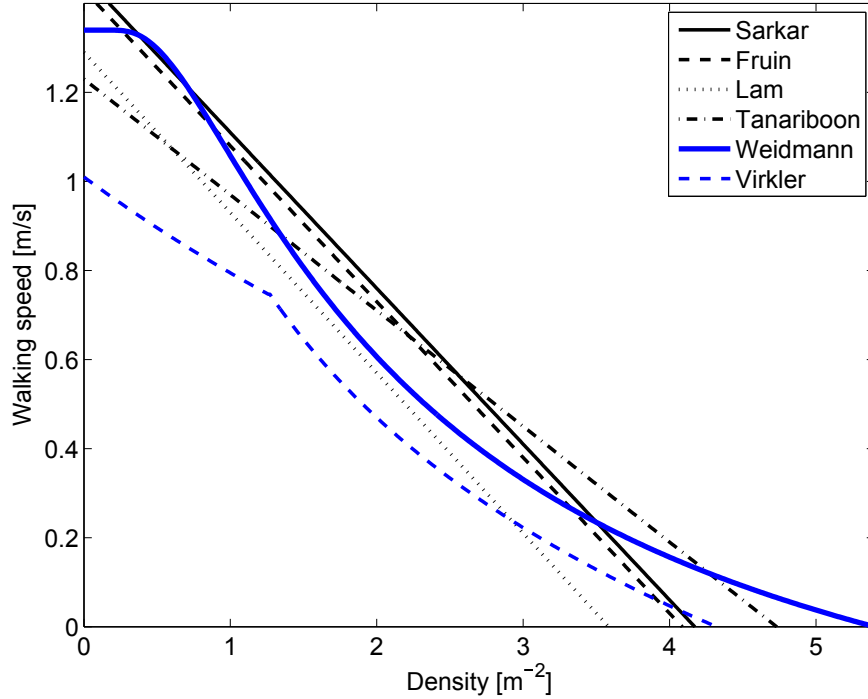 are only valid for low densities but in these conditions a linear approximation may be sufficient. Also, it should be noted that, although its name is ambiguous, the "fundamental" diagram change depending on a variety of pedestrian characteristics with age, gender, travel purpose and culture being only some of the most relevant [21, 35]. For this reason, if differentiating between different groups is the main objective, then linear relationships for low densities can be satisfactory and different functions can be defined for various types of pedestrian crowds. However, when high densities are considered, then the non-linear effects need to be accounted for. In this regard, the popularity of the function by Weidmann may be related to the fact that it is one of the first to clearly consider the non-linear effects at high densities. But still, evidence from recent research suggests that walking speed should be higher than zero also at extreme densities [16, 36, 37], thus proposing a revision of relationships to be used in the speed–density fundamental diagram.

While speed–density relation has been studied for long, the most important type of funda-

---

[3]Only first author is used for simplification.

[4]The study by Weidmann is a meta-study, i.e. he combined data from multiple sources.

Table 1.2: Speed–density relationships for the curves plotted in Figure 1.6 [28]. Density ρ is given in m^{-2}, while velocity v is in m/s.

Author [3]	Year	Country	Speed–density function
Sarkar [30]	1997	India	$v = 1.36 - 0.35\rho$
Fruin [18]	1971	U.S.	$v = 1.43 - 0.35\rho$
Lam [31]	1995	Hong Kong	$v = 1.29 - 0.36\rho$
Tanaboriboon [32]	1986	Singapore	$v = 1.23 - 0.26\rho$
Weidmann [21]	1993	Several combined [4]	$v = 1.34 \left[1 - \exp(-1.913 \cdot (\frac{1}{\rho} - \frac{1}{5.4})) \right]$
Virkler [33]	1994	U.S.	$v = \begin{cases} 1.01 \exp(\frac{-\rho}{4.17}), & \rho < 1.27 \\ 0.61 \ln(\frac{4.32}{\rho}), & \rho > 1.27 \end{cases}$

mental diagram is probably the flow–density one, which is given for the case of Weidmann in Figure 1.7. By remembering the fundamental relationship between flow and density, we can obtain the expression for flow by multiplying the function for speed with density. As a consequence, if only speed and density are measured, both types of the fundamental diagrams can be obtained. One of the advantages of the flow–density relationship is that, as shown in Figure 1.7, the transition from free flow (or more generally uncongested flow) to congestion is clearly recognizable. By considering a scenario in which pedestrian traffic gradually increases, at first flow will grow linearly with density, according to a slope represented by the free walking speed. However, as both density and flow grow, linearity is lost and the flow reach its maximum. The maximum flow is defined as capacity, as introduced earlier. It is also convenient defining density and speed at capacity, which can be done by relating with the point where the maximum is reached. The density at which a generally free motion turns into a congested crowd is also referred as critical density.

The concept of stability is defined by using the speed at capacity. The triangular region defined by the ordinate axis and the maximum flow is defined as the stable region, while the remaining half corresponds to unstable motion. The maximum flow (capacity) represents the critical point where stable motion turns into an unstable one.
For the reasons described above the fundamental diagram has been used for decades to classify the motion of pedestrians. However, as we will see later, there are some limitations relative to its use. The biggest limitation is given by the fact that, traditionally, this formulation of the fundamental diagram holds for uni-dimensional motion, i.e. for people walking in a line. The studies considered so far mostly considered more complex scenarios, like people walking on walkways or crosswalks, which are different from uni-dimensional motion (people can move laterally), but do not deviate in a large extent. A great deal of efforts have been recently made to obtain fundamental diagrams for different geometries (see for example [39, 40, 41]) and to establish a method for creating them [42]. However, it has been also shown that while the characterization of pedestrian flow based on the fundamental diagram works for fairly organized motion (like in the case of walkways or corridors), when geometries become complex (intersections for example) the fundamental diagram completely change and defining a universal measure of capacity (or stability) is not possible when only density and flow are considered [39, 36, 43].
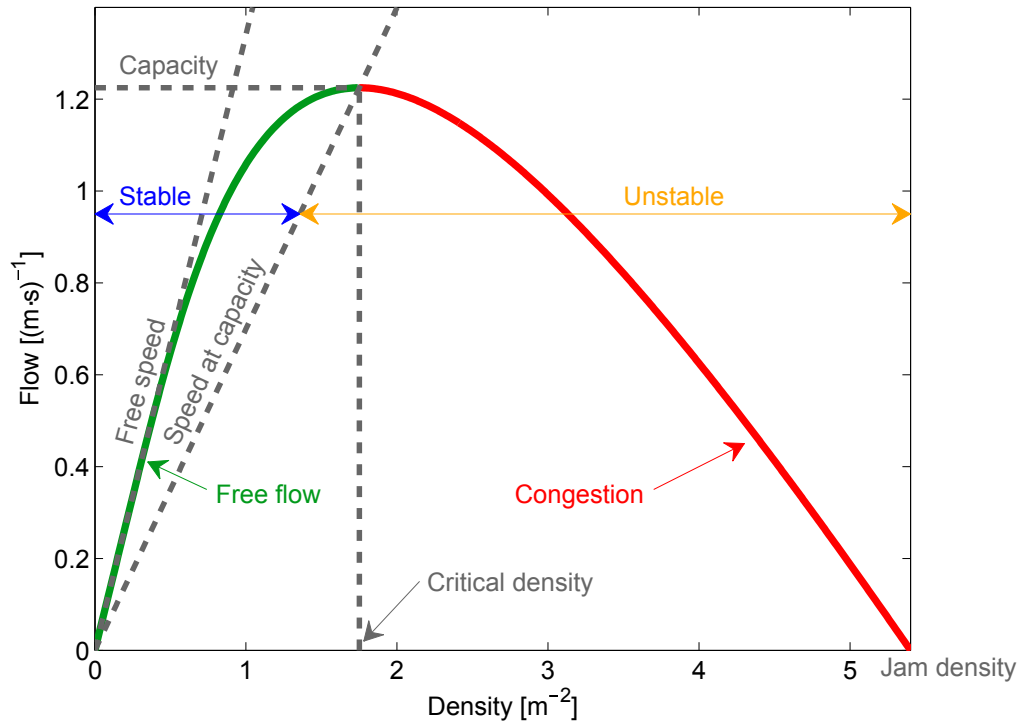
Figure 1.7: Flow–density fundamental diagram for pedestrians. The shape does not change if cars, bicycles or other similar ways of transportation are employed, although values are obviously different [28, 2, 38].

1.2.4   Theoretical aspects

Until now we have considered experimental aspects related with pedestrian dynamics. But there are some features of the fundamental diagram which can be obtained with simple mathematical models. We will consider these theoretical aspects in this section.

Cellular Automaton

The Cellular Automaton (CA) is a set of discrete models introduced by mathematicians Ulam and Von Neumann in the 1940s. Cellular Automaton has been widely studied in the 20th centuries and many famous mathematicians (like Wolfram for example) have worked on this problem. In particular, the approach used in CA is well suited for studying problems related with traffic engineering and research on pedestrians has also considered this application. In CA, the physical space is discretized using a mesh composed by cells which can take different states, such as full/empty or on/off. We will consider bidimensional representations of CA in the discussion of simulation models, since complex CA structures are usually computed using calculators since analytical solution are not possible (or very difficult).

Here we will start by considering very simple uni-dimensional cases which can be treated in an analytical way. Let's consider the CA model like the one presented in Figure 1.8. The model consists of n cells (10 in the example here), each of which can take one of the two possible states: occupied (by a single particle) or empty. In the initial configuration occupied cells will be randomly chosen in order to have a density $d = [0, 1]$ of occupied
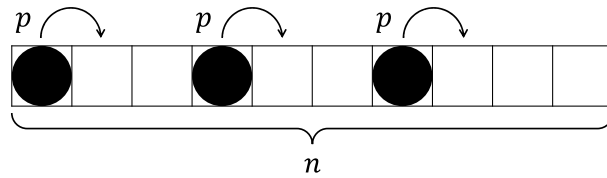
Figure 1.8: Schematic representation of a simple CA model. This specific case is also referred as Totally Asymmetric Simple Exclusion Process (TASEP). The number of cells is $n = 10$ and 3 particles are present; density is therefore $d = 0.3$.

cells [5]. As a consequence of the random attribution, same-density initial setups do not necessarily have always the same configuration.

Next, we can introduce a transportation mechanism allowing to move particles from one cell to the next one. To simplify the calculation, we assume that particles may only move in one direction (from left to right here). The possibility that one particle may (or may not) move to the neighboring cell is given by $p = [0, 1]$. At each time step all particles are updated according to the probability p. $p = 0$ represents the static case (no particle moves), while for $p = 1$ every particle will move at each step. However, there is an additional rule which needs to be introduced: only one particle is allowed for each position. This means that in some cases, some particles cannot move although they may be allowed if only probability is concerned. An example for 5 consecutive steps is given in Figure 1.9.
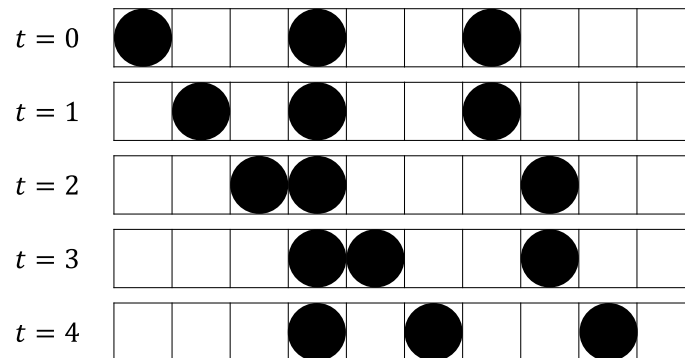
Figure 1.9: Example of successive updates for the TASEP model.

This particular type of CA model is called Totally Asymmetric Simple Exclusion Process (TASEP). The "T" in TASEP is used to indicated the fact that only one particle is allowed for each location. By changing rules it is possible to create new models and there is large literature on the subject [2]. Here we will stick to the simplest case represented by the above description. There is however one final important element which needs to be considered before examining mathematical properties of the model: the boundary conditions. Characteristics of the model change if periodic or open boundary conditions are applied and both cases need to be considered separately.

TASEP with periodic boundary conditions

The case for periodic boundary conditions is illustrated in Figure 1.10. When a particle reaches the last cell on the right-end side, it can move during the next step to the first

---

[5]In this theoretical treatment we will use d for density and J for flow, to differentiate the unit-less probabilistic quantities from ρ and q used for physical quantities.

cell on the left-end side according the same probability p. In short, the model now takes a circular form in which there is neither start nor end. Particles are placed in the beginning to reach a density of d and can then continuously move inside the system.
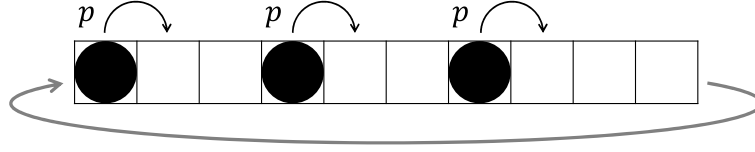
Figure 1.10: TASEP with periodic boundary conditions.

Readers may have already noticed the similarity with traffic dynamics. When particles are substituted with pedestrians, the model can be used to consider the simple case of people moving in a closed loop. What interest us is the relation between flow J and density d. Here, we need to make a further differentiation between two cases: random-sequential and parallel update of positions.

(a) Random-sequential update

(b) Parallel update
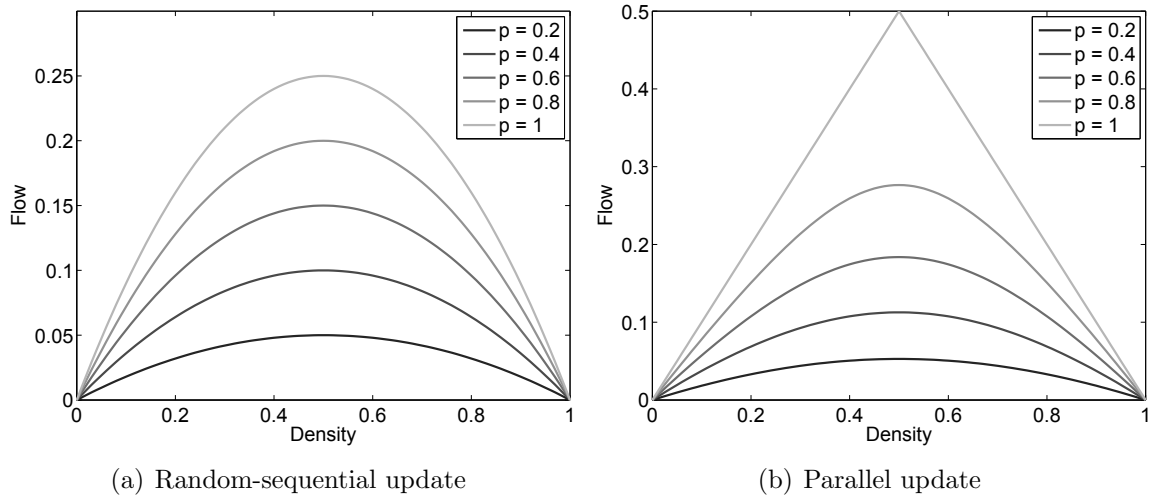
Figure 1.11: Flow–density relation for the periodic boundary TASEP model.

In random-sequential update a particle is chosen at random and its new position is computed according to the probability p. The process is repeated until all particles have been considered. During the next step the procedure will be repeated. Under this condition the order in which positions are updated will change at every step. This fact has some important consequences. If, like in the case $t = 2$ in Figure 1.9 the first particle (from left) is updated before the second one, the first one will not be able to move because the next position is occupied. However, if the update order is reversed, both are able to proceed (like in the example of Figure 1.9). In the case of parallel update all particles are updated simultaneously. At $p = 1$ the parallel update results in a shift of one position for all particles altogether.

For both update procedure variants in the periodic boundary TASEP, the functions for flow can be computed analytically. The result for the random-sequential update is:

$$J(d, p) = p \cdot d(1 - d) \tag{1.2}$$

while in the case of parallel update the exact solution is:

$$J(d, p) = \frac{1}{2} \left[1 - \sqrt{1 - 4 \cdot p \cdot d(1 - d)} \right] \tag{1.3}$$

For both cases the respective equations are plotted in Figure 1.11. The parallel update has a higher flow compared to the random-sequential update, since conflicts are resolved more efficiently. It is also relevant to notice that the shape of both curves corresponds qualitatively to the empirical fundamental diagram presented before (except the fact that empirically obtained FD shown in Figure 1.7 is asymmetric). This shows that TASEP model can be effectively used to model aspects of traffic dynamics and that a quite simple formulation already allow to depict relevant properties.

TASEP with open boundary conditions

We will now consider a different version of the TASEP model like the one shown in Figure 1.12. Open boundary conditions are now employed, which means that the last and the first cells are not connected anymore. In the case of open boundary conditions a probability α is assigned to fill the first cell and a probability β is used to move particles out of the system (in the last cell). To simplify the calculations we will now assume $p = 1$ and use only the random-sequential update.
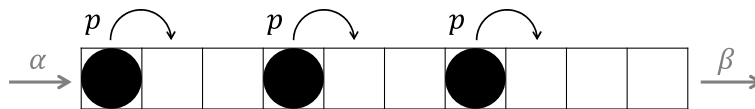
Figure 1.12: TASEP with open boundary conditions.

What it is particular in the case of open boundary conditions is the fact that flow–density relation is not anymore ubiquitous and different states (or phases) exist. It should be clear that if $\alpha > \beta$ then the system is taking particle in at a faster rate then the ones going out of from system. This quickly leads to congestion and an increase in density. This condition is therefore called high density phase (HD). On the other side, when $\beta > \alpha$, particles are taken out of the system with a rate faster then the one of insertion, thus creating a low density phase (LD). From the previous case we know that maximum flow which is sustainable within the system is $\frac{1}{4}$ for a density equal $\frac{1}{2}$. For values of $\alpha, \beta > 0.5$ the maximum flow is expected, a condition which is called maximum current (MC).
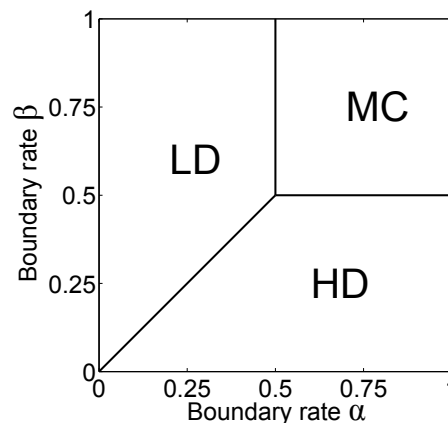
Figure 1.13: Exact phase diagram for TASEP with $p = 1$ and random-sequential update [2]. LD is low density, HD high density and MC maximum current.

The three different phases are shown in Figure 1.13 (strictly speaking sub-phases also exist within phases, but are not discussed here). For each phase it is possible to consider

flow and the density at different locations inside the model [6]. The different functions are given in Table 1.3.

Table 1.3: Flow $J(\alpha, \beta)$ and density in different position for the TASEP with $p = 1$ and random-sequential update [2]. $d_{n/2}$ refers to the density in the middle of the model, d_1 for the region close to the entrance and d_n for the one close to the exit.

Phase	Condition	$J(\alpha, \beta)$	$d_{n/2}$	d_1	d_n
Low density	$\alpha < \beta$	$\alpha(1 - \alpha)$	α	α	$\dfrac{\alpha(1 - \alpha)}{\beta}$
High density	$\beta < \alpha$	$\beta(1 - \beta)$	$1 - \beta$	$1 - \dfrac{\beta(1 - \beta)}{\alpha}$	$1 - \beta$
Maximum current	$\alpha, \beta > \dfrac{1}{2}$	$\dfrac{1}{4}$	$\dfrac{1}{2}$	$1 - \dfrac{1}{4\alpha}$	$\dfrac{1}{4\beta}$

More complex models can be created using CA and it is beyond the scope of this text to discuss their properties. It is however important to get familiar with the idea behind CA and to understand how transport phenomena can be modeled using it. Like for any phenomena considered in science, the simplest the geometry considered in reality the closer will be the result to the theoretical derivation. However, as we will see later, quite simple models may be sufficient to describe some properties found in more complex pedestrian structures, showing that the ability to describe collective phenomena may be related to the formulation of the model used, not its complexity.

Modeling by continuum equations

There is an additional approach which has been also often used to model pedestrian streams and it is the continuum approach making use of equations derived from fluid- or gas-dynamics. Although discrete probabilistic approach and continuum description are connected and it is possible to pass from one system to the other by changing the scale considered, assumptions are different. It is therefore worth considering them separately and a short description of continuum models will be provided here.
Like in the case of CA there are many possible continuous models and it is beyond the scope of this thesis to present a discussion on them (for details see [44, 45]). We will focus on the most simple model for one-dimensional dynamics, just to present the different approach compared to CA. The Lighthill-Whitham-Richards model (in short LWR model) was developed in the 1950s by the three authors [46, 47]. The central equation is the one-dimensional conservation law for traffic, given by:

$$\frac{\partial}{\partial t}\rho(x, t) + \frac{\partial}{\partial x}q(x, t) = 0 \tag{1.4}$$

where ρ is the density, t the time, x the position along the uni-dimensional axis and q is the flow [7]. As before, the flow will be dependent on density, but now q will not be

---

[6]Specific length scales are required to define beginning, middle and end of the model and a large number of cells is assumed. For details refer to [2].

[7]Now flow and density refer to physical quantities and we therefore reintroduced the original form used before (ρ for density and q for flow).

the result of our analysis, but need to be defined to solve the differential equation. It is therefore convenient to use relationships derived from empirical data and, considered the large number of functions for the fundamental diagram, it is basically a matter of choice. For simplicity we can use a linear function for the speed–density relationship, like the ones we have seen before. In general terms we can write:

$$v(x,t) = v_{free} \left(1 - \frac{\rho(x,t)}{\rho_{jam}} \right) \tag{1.5}$$

where v_{free} is the free walking velocity and ρ_{jam} is the jam density. As usual, velocity can be converted into a flow by multiplying with density. This will lead to the following equation:

$$q(x,t) = \rho(x,t) \cdot v_{free} \left(1 - \frac{\rho(x,t)}{\rho_{jam}} \right) \tag{1.6}$$

The solution for the spatiotemporal evolution of density can be obtained by putting (1.6) into (1.4) leading to the following one-dimensional partial differential equation for pedestrian motion:

$$\frac{\partial}{\partial t}\rho(x,t) + v_{free} \cdot \frac{\partial}{\partial x} \left[\rho(x,t) \left(1 - \frac{\rho(x,t)}{\rho_{jam}} \right) \right] = 0 \tag{1.7}$$

This partial differential equation can be considered as a Riemann problem for traffic flow and there are a few considerations which can be done. We can set the density at the left side as $\rho(0,x) = \rho_l$ for $x < 0$ and the one at the right side as $\rho(0,x) = \rho_r$ for $x > 0$, such that $\rho_l < \rho_r$. The characteristic speed at $t = 0$ and $x < 0$ is given by:

$$\lambda(\rho_l) = f'(\rho_l) = v_{free} \left(1 - 2\frac{\rho_l}{\rho_{jam}} \right) \tag{1.8}$$

and the characteristic speed on the opposite side is:

$$\lambda(\rho_r) = f'(\rho_r) = v_{free} \left(1 - 2\frac{\rho_r}{\rho_{jam}} \right) \tag{1.9}$$

Remembering that $\rho_l < \rho_r$, it can be observed that the characteristic velocity on the left side is higher than that on the right side and therefore characteristic curves (or straight lines) catch up. This condition produce a shock wave with speed λ, given by the Rankine-Hugoniot condition as:

$$\lambda(\rho_r - \rho_l) = f(\rho_r) - f(\rho_l) \tag{1.10}$$

This type of treatment with kinematic waves was first introduced by Lighthill and Whitham in 1955 [48]. For the shock wave problem a schematic description is also possible and is given in Figure 1.14. Both characteristic velocities meet along a common line which is defined as the propagation velocity of the shock wave.

Although more complex in nature, shock waves are indeed observed in pedestrian flows and are divided into two types: stop-state waves and go-state waves. If a single line of people walking in one direction is considered, stop-wave is observed when someone have to stop because the person in front of him/her had stopped also. Later on, that person may be able to walk again when the person in front of him/her start walking again. The situation is very common in queues observed in vehicular traffic and car drivers surely
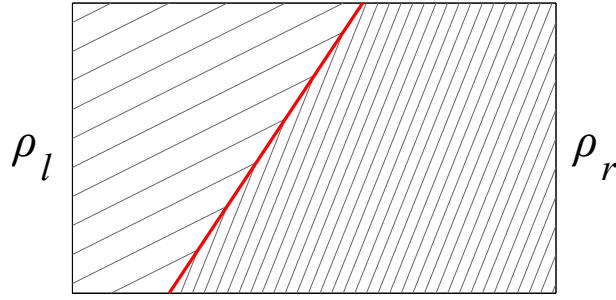
Figure 1.14: Schematic representation of a shock wave resulting from discontinuities in density.

had this type of experience. For the case of pedestrians, Zhang et al. [49] were able to measure both waves' propagation speed and observed during a mass event that stop-state waves move backward compared to the direction of motion with a speed of 0.076 m/s, while characteristic speed for go-state waves was of 0.25 m/s (also backward). On the other hand, Helbing et al. [16] were able to measure characteristic density being 6.96 and 5.62 m^{-2} for stop-state and go-state waves respectively. As one can notice, both densities correspond to a very dense crowd and it becomes therefore evident that under these conditions it may be appropriate to consider pedestrian crowds as a continuum.
Although researchers are typically divided into the ones preferring a discrete approach and the ones inclined toward the continuum one, this short discussion had the goal of showing to the reader that different approaches are possible and the choice between them is related on goals and background of a specific study.

1.2.5   Models for computer simulation

As we have seen in the previous section there are mainly two approaches to theoretically describe traffic flow and they both rely on quite complex equations which can be analytically solved only for special cases and normally only for the uni-dimensional geometry. From the 1980s the evolution of computer has allowed to solve complex differential equation in a numerical way and computer simulation has increasingly become an important part of traffic engineering and pedestrian dynamics. In this section we will describe the most common models used in the discrete and continuous approach (a complete overview and comparison of various models is given in [50, 51]). The discrete approach will be covered more in detail since a particular model will be presented later in Chapter 2.7.

Discrete models

The Cellular Automata approach presented earlier can be extended into a bidimensional grid to represent pedestrians moving in a space as it is the case in most of real situations. Here, we will focus on the Floor Field model [52] which is one of the most widely used to model pedestrians with CA. A schematic representation of a general grid used to model pedestrians in a bidimensional case is given in Figure 1.15(a).
The pedestrian under consideration is represented as in the center of the grid given in Figure 1.15(b), for which the corresponding position is i,j (see Figure 1.15(a)). Unlike the uni-dimensional case, in the bidimensional geometry there are several cells which can be considered as candidate for the following move (in the successive computational step). Here, we have to differentiate between two classes of CA models based on the type of

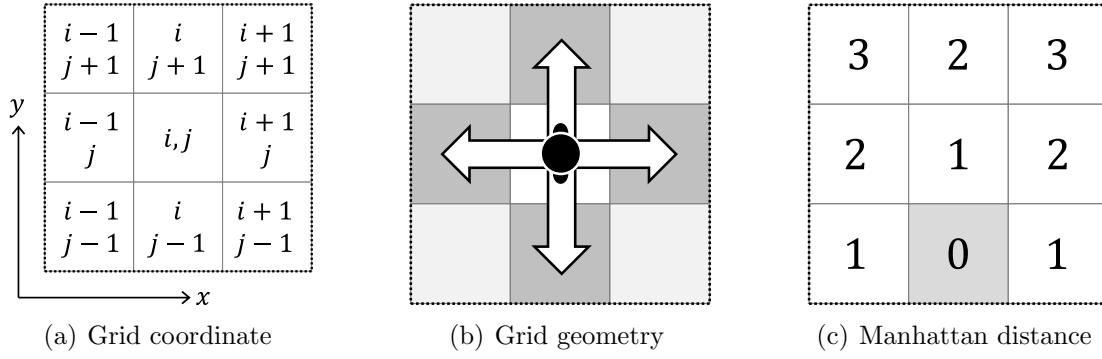| | (a) Grid coordinate | (b) Grid geometry | (c) Manhattan distance |

Figure 1.15: Geometrical configuration in the bidimensional CA model for pedestrians.

motion allowed. If Moore neighborhood is used, pedestrians are allowed to move to the next cell including the ones along the diagonal (therefore all the cells available in Figure 1.15(b) can be taken as candidate). The use of the Moore neighborhood allows a natural reproduction of pedestrian motion, but specific rules are required to consider the fact that diagonal motion is $\sqrt{2}$ times the longitudinal motion (if center to center distance is computed). To keep the discussion easier, we will focus on the Von Neumann neighborhood in which only horizontal or vertical motion is allowed (arrows in Figure 1.15(b) leading to dark cells).
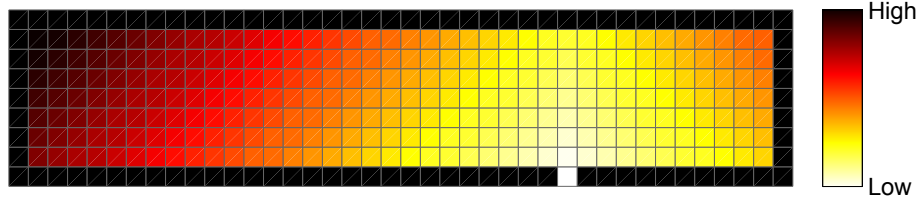
Figure 1.16: Example for a static floor field in the case of evacuation from a room. Cells having low values are assigned with light colors, cells with high values are darker. Walls are given in black.

Since the final aim is to move pedestrians toward a particular destination, it is convenient to assign different probabilities according to the direction of the destination. On this purpose the so-called static floor field is employed. The static floor field is made up by computing the Manhattan distance from the destination, which will have a value of 0. The Manhattan distance is the sum of the horizontal and vertical distance between two points inside the computational grid. In other words, it is the distance required between two points in the mesh by traveling zigzag-wise from cell to cell. A simple case is given in Figure 1.15(c) (where the destination is given in gray) and Figure 1.16 shows a larger scenario in which cells close to the exit (distance 0) are given with lighter colors compared to far cells.

By using the static floor field it is possible to compute the different transition probabilities (what we called using p in the uni-dimensional model) for the grid of Figure 1.15(a). According to the Floor Field model and assuming the considered pedestrian is in position i,j, then the transition probability to $i+1,j$ is given by:

$$p_{i+1,j} = N\xi_{i+1,j} \exp\left(-k_S S_{i+1,j}\right)\left(1 - \phi_{i+1,j}\right) \tag{1.11}$$

where N is the normalization parameter (used to scale the 4 different probabilities from 0 to 1), $\xi_{i+1,j}$ the obstacle parameter (being 0 for wall or obstacles), k_S the weight of the

static floor field, $S_{i+1,j}$ the static floor field itself and $\phi_{i+1,j}$ the settlement parameter (being 0 if a cell is taken by another pedestrian). Similarly to the example provided in (1.11) the transition probability for all neighboring cells can be computed. Note that also position i,j has its own probability and in certain cases could be the one having the highest value. In this simplest implementation of the Floor Field model it is already possible to simulate evacuation scenarios by having several people inside one common floor. Simulation will proceed by updating the position of each pedestrian either in a parallel update process or in a sequential one. If the parallel update process is chosen, it is then possible that multiple pedestrians will aim at a common cell. To overcome this problem several solutions have been proposed, but, in general, a 2-step process is used in which destinations are reserved first and pedestrian are later moved. More in detail, probabilities are computed using the above formulation and destination cell is selected based on the highest probability. Each pedestrian will therefore reserve the destination cell (with the process including all pedestrians on the floor). Finally, for the cells having multiple reservations, only one candidate is chosen with equal probability and the discarded ones are returned to their original position (this mechanism is referred as conflict resolution). When all conflicts have been resolved, pedestrians are actually moved to their destinations (although some of them may not be able to move and stay in the same position).

(a) Parallel update   (b) Sequential update
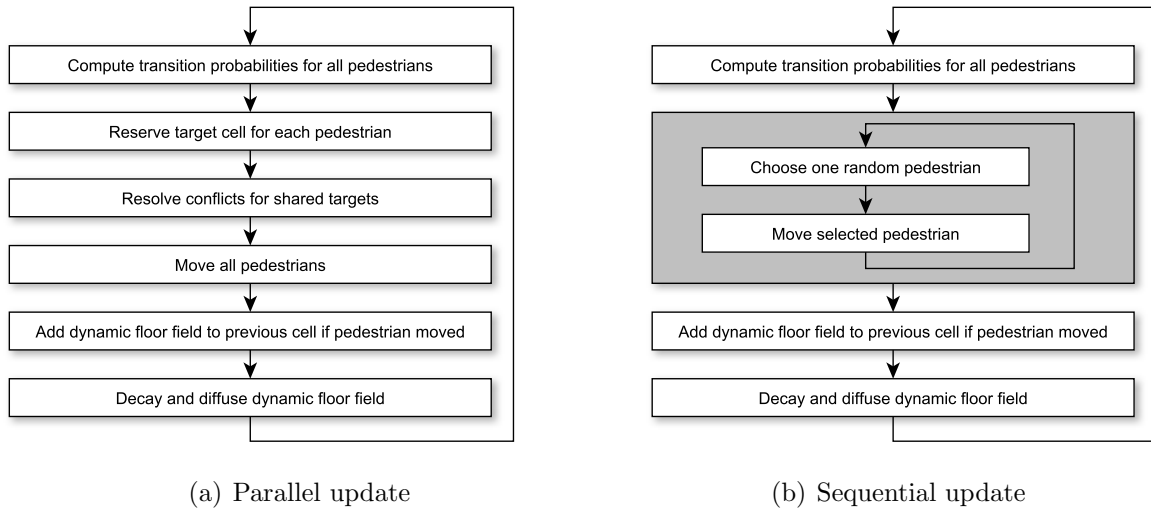
Figure 1.17: Update schemes for the CA Floor Field model using static and dynamic floor field. Differences are only related to the update of positions.

However, with the model presented until here, pedestrians do not interact with each other's and only distance from the destination is considered. This formulation may be sufficient for evacuations (like the case of Figure 1.16), but for other scenarios it may become unrealistic. In particular, it is known that pedestrians tend to follow people aiming at the same direction (destination). To reproduce this behavior a dynamic floor field is usually employed and it is spread over the surface to be simulated like in the case of the static floor field. The dynamic floor field is inspired by the motion of ants, which release a chemical substance (called pheromone) to allow other ants recognizing the path traveled. At the beginning, the dynamic floor field is 0 everywhere, but, after each time step, pedestrians increase the value of the dynamic floor field in their previous positions by one (pedestrians who did not move are excluded). A cell having accumulated high values for the dynamic floor field is a cell which has been occupied by several pedestrians

and will become attractive. However, if dynamic floor field is added at every time step, it will keep increasing and the floor will saturate. Therefore, in accordance with the process observed in ants, the dynamic floor field has the ability to diffuse to the neighbor cell (increasing by one the dynamic floor field of a neighbor cell and reducing by one the own value) or decay (simply decrease by one). Two different probabilities are assigned to the diffusion and decay process, defined respectively as α_D and β_D. At each time step diffusion and decay is computed for each cell having a dynamic floor field value larger than 0. The following behavior can finally be implemented by adding the dynamic floor field to the equation of the transition probability, leading to:

$$p_{i+1,j} = N\xi_{i+1,j} \exp\left(-k_S S_{i+1,j}\right) \exp\left(k_D D_{i+1,j}\right)\left(1 - \phi_{i+1,j}\right) \tag{1.12}$$

where $D_{i+1,j}$ is the value of the dynamic floor field at position $i+1,j$ and k_D its weighting factor. To summarize the whole process Figure 1.17 show the computational loop for the parallel and sequential update. Note that the difference is only when positions are updated.

By using only the static and dynamic floor field several phenomena observed in real crowds were reproduced in simulation. Some examples are the spontaneous lanes formation in long corridors or oscillations at bottleneck [53, 54]. One advantage of the CA approach is that new rules can be easily implemented and this has led to the creation of a variety of models over the years. In particular, on-purpose floor fields were created to reproduce specific behavior found in humans. Suma et al. [55] added an anticipation field to account for the collision avoidance in counter flow, Nishinari et al. [56] used a wall field to keep pedestrians far from walls and Henein and White [57] used a force field to assess the pressure felt by pedestrians. An additional reason for the popularity of CA models is that heterogeneity found in pedestrian crowds can be efficiently implemented by using different set of rules for different group of pedestrians. It is therefore possible to account for elderly [58] or to reproduce the behavior of social structures (groups) [59]. Also, CA model is very simple and computational requirements are modest, making it ideal for large scale simulations [60] or for real-time prediction, when short computational time is more important than accuracy [61].

Finally, it also worth mentioning that, when bi-dimensionality is accounted for, CA can be used to create more complex phase diagrams than the simple one previously considered in the analytical case. Different authors [62, 63, 64] have developed numerical models able to identify the transition between organized and congested motion (this aspect will be also discussed later in Chapter 2.3.4) and CA has allowed considering scenarios with thousands of people, very difficult to reproduce in experimental conditions.

However, the discrete nature of CA has its own limitation and, for example, accurately reproducing the Gaussian distribution for walking speed observed in reality [21, 65, 66] can become a difficult task (although some solutions were proposed [67, 68]). Also, densities considered in CA models are limited by the size of the cell used and by changing it different rules may have to be employed, limiting the flexibility in this context (although also here some solutions were proposed and are discussed later in Chapter 2.3.4 and Chapter 2.7).

Continuous models

As we have seen in the previous analytical treatment, exact solutions for continuous differential equations are obtained only for simple cases. It is however possible to discretize differential equations by employing numerical schemes and deal with complex

multi-dimensional cases. The "discretization" considered here should not be confused with the discrete approach discussed above. In CA, pedestrians can only move in the grid used for simulation; a displacement of half cell or any other non-integer quantity is not possible; space and time are both discretized. In the continuous approach, models' equations are discretized in time in order to be solved using computer, but space is continuous and pedestrians can move in any direction and at any distance from one time step to the next one.

The first continuous models were derived from fluid- or gas-dynamics equations and are based on the empirical observation that, under given conditions, people move inside the crowd in a similar fashion to particles immersed in a liquid stream or molecules inside a gas [69, 70]. To account for features typical of humans in the theoretical treatment with continuum equations, the social force model was developed [71, 72]. In its formulation, pedestrians are treated like positively charged particles which move toward a negatively charged destination (the exit in case of evacuations). Interactions between individuals are described using mathematical functions expressing the degree of repulsion (normally using exponential law expressions [73]). A consequence of this approach is that pedestrians are treated like point force field without a physical volume (or surface for bidimensional treatment). A clear advantage is that there is no limit for the density achieved since points have no surface, but this also includes unrealistic implications (infinite densities are possible). To overcome this problem, most of the social force models include special rules to account for volume exclusions of human bodies [73]. The social force model has been also able to predict several phenomena observed in reality and typically used to validate fundamental features of pedestrian models (like spontaneous lane formation or oscillations at bottleneck).

Similarly to CA models, also in the case of the social force models, several modifications have been proposed to account for more specific behaviors found in human crowds; like collision prediction [74], motion in heavily packed situations [75], memory in regard to the exit location or to simulate the crossing of streets at signalized crosswalks [76].

A clear advantage of the continuous approach (and the social force model in particular), lies in the ability to consider a continuous space thus producing smooth motion in simulation. Also, its deterministic approach allows to perform only one simulation per case, while the probabilistic nature of CA requires several simulations from which an average result is obtained. However, continuous models are computationally expensive and difficult to parallelize, requiring longer simulation time.

1.2.6   Latest trends

To conclude this introduction on methods and concepts of pedestrian dynamics, we will provide a very short discussion on the most recent trends in the research and possible future developments.

In general, industry and engineering requirements are pushing toward an increasing interest in computer simulation. With pedestrian models having reached a somehow satisfactory accuracy [77], many researchers are focusing on multi-scale approaches [78, 79]. At the moment, different approaches are required to account for the different scales observed in pedestrian motion. CA models or social force models are effective at the microscopic, individual level, but to simulate large structures problems related to route-choice or re-routing need to be considered. Different strategies are therefore used and connections are created at various levels to use results from one level as boundary conditions for the

lower level. In this scenario, connection with real data for real-time simulation is also a growing subject, in particular for industrial research [80, 61]. Computer vision has been used for many years to detect pedestrian motion, but recently alternative solutions have been proposed to overcome some technical and legal (privacy) issues related with the use of images. But we will discuss more in detail detection and measurement of pedestrian properties in Chapter 3.

Technological progresses have not only contributed in changing the way in which pedestrian motion is modeled, but also experimental aspects are starting to be analyzed with a new approach. Although still limited, virtual reality is starting to become an alternative for experiments in which people may be at risk [81, 82, 83]. Evacuations or scenarios involving decision making processes are particularly suited for this type of technique, since it is possible to partially recreate conditions which are only rarely observed in reality. In parallel, the increased possibilities offered by virtual reality and online experiments are attracting researchers from psychology, which are interested on how people make decisions relating to dangerous situations [84]. This interest in psychological aspects of crowd is contributing in making pedestrian models more heterogeneous and complex, allowing to consider each scenario according to its local and cultural particularities [85].

Empirical aspects of crowd motion are also widely investigated and, in particular, the widespread of tracking technology is making easier to obtain trajectories in controlled experiments [86, 87, 88]. A large amount of trajectory data from different sources is already openly available to researchers and more is being added every year. After many years of theories and theoretical research it is now possible to verify the different models and investigate which aspect has been correctly considered and which aspects need to be studied more deeply. On the other side, the large amount of data available is starting to interest researchers from machine learning and Artificial Intelligence (AI), who hope to use their algorithms to predict pedestrian behavior based on the analysis of past data. Although this approach has been mostly limited to vehicular traffic [89], it is predictable that pedestrian dynamics will be also subjected to similar changes.

1.3   Motivation and objectives of this study

Having given an introduction on the state-of-the-art practices in pedestrian dynamics it is now important to relate this study into the wider context of traffic engineering and understand why and how it can contribute to the understanding of pedestrian collective motion. This section will be devoted on the discussion of those aspects in detail.

This work obviously shares most fundamental motivations which have led to a shift toward quantitative research on pedestrian dynamics. Accidents prevention and increase of comfort for pedestrian facilities are definitely final objectives of pedestrian research and this study also aims at contributing in this direction. But, having discussed this broad aspect before, here we will focus on more specific and concrete objectives, while also mentioning the motivation for choosing the particular topic of "measurement" and "modeling" among the several subjects on which pedestrian traffic research focus.

As discussed above, a general trend toward computer simulation is observed in pedestrian and traffic research. However, to develop accurate simulation models it is important to understand the processes and the mechanisms which are being modeled. Traditionally, experimental science has covered this role. However, while modeling based on observations from nature is still the fundamental process driving scientific research, the large amount of data available from experiments has lead to a gradual shift from physical modeling to

algorithmic modeling. In other words, attention is increasingly put on methods ("how to reproduce") rather than phenomena ("what to model"). Although both aspects are clearly important; in the path toward knowledge, understanding what is observed should come first. For this reason, this study focused mostly on experimental aspects to provide explanations on which phenomena are observed and later also investigate how is it possible to reproduce them in computer simulation (or theoretical models more in general).

For the specific case of pedestrian dynamics, we have seen that uni-dimensional situations (a single line of people) have been studied from multiple perspectives and it is possible to predict an incoming congestion using the fundamental diagram. However, multidimensional motion is still not completely understood and while there are configurations (geometries) which can be studied using the fundamental diagram, there are also cases in which the fundamental diagram has not been effective. On the other side, pretending to understand fully multidimensional motion at this stage would be overly ambitious. For this reason, research has been particularly focused on the case of bidirectional motion, which, although being fairly simple, has many aspects which are still obscure. The bidirectional case can be considered as a bridge between the simple uni-dimensional motion and the final goal of multidimensional dynamics. With that said, as we will see by presenting this work, the results obtained from the bidirectional case later allowed us to set some new objectives on alternative methods to measure general pedestrian crowds also in complex multidimensional environments.

This aspect of "measuring" has been a guideline and a constant throughout the project. As we briefly mentioned earlier, the rarity of pedestrian accidents make it difficult to learn from experience and train people to prevent recurrence of dangerous situations. As a consequence, while understanding mechanisms and creating new knowledge on pedestrian crowds has been an important goal of this research, developing an efficient method to "measure" pedestrian crowds has been a more concrete objective. This aspect encompass a more wide objective being related on defining new standards for pedestrian safety and comfort. As we have seen, the Level of Service has been already developed, but its formulation is now outdated and a more universal approach is required. New standards are therefore required which should also take into account the technological progresses of the last decades.

Chapter 2

Bidirectional flow

2.1   Introduction

Bidirectional pedestrian flow is a common sight in urban environment. There are many examples of bidirectional flow configurations, with sidewalks, corridors, and crosswalks being the most common ones. Bidirectional flow is basically composed by two classes of pedestrians walking in different and opposite directions. From a phenomenological point of view the bidirectional case lies between the uni-dimensional and the multidimensional definition. Since the motion is usually observed in only two (opposite) directions, the degree of complexity is rather limited. However, in contrast to the simplest uni-dimensional case, in the bidirectional flow people can move laterally thus allowing the creation of "emergent phenomena" and more specifically organized lanes. In the bidirectional flow pedestrians have therefore the possibility to get organized in collective structures, although it should be said that the variety of such structures is rather limited and in fact only lanes can be distinguished as emergent phenomena.

Understanding the dynamics of bidirectional flow is therefore an important step toward defining crowd measures and models for more complex full multidimensional motion. Also, since the bidirectional flow is a very common scenario in public structures it is important to obtain reliable and accurate data which can be used to design pedestrian facilities. As we will see in the literature review, there has been a quite consistent research on the this topic, but most of the authors seemed to focus on specific aspects or to consider only the scenario on which their study was based on. In this study, we will try to consider different approaches to deal with the bidirectional case and we will also attempt to provide a more general theory which can explain most of the studies presented so far on the subject.

This chapter is organized as follows: at first definitions and nomenclature will be defined to create a basic framework to describe bidirectional streams, later an overview on the literature on the subject is provided. We will also consider several cases of bidirectional flow, starting with an empirical observation followed by different supervised experiments designed to investigate particular aspects. A statistical model able to predict transition from organized to congested motion is proposed and finally a simulation model reproducing experimental results is presented. In general, as for the introduction, we will differentiate empirical, numerical (simulation) and theoretical treatment, although we will see that it is possible to relate the three aspects.

2.2   Definitions and nomenclature

Literature is not univocal on the terms used on the bidirectional flow and it is therefore convenient to introduce at first the concepts that will be discussed in this manuscript. We tried to stick to terms generally used in the literature, but in some case we had to choose between different usages. Figure 2.1 should help understanding the notation introduced in this manuscript.

The bidirectional flow is characterized by two (monodirectional) streams moving in opposite directions. Monodirectional flow is the term we will use to describe each group of pedestrians moving in a determined direction making up the bidirectional configuration. In case the flow in one direction is bigger than the one in the opposite direction we will refer to the first one as the major flow. The smallest flow in both directions will be defined as the minor flow. When major and minor flows are equal we speak of balanced flow. In the extreme case of a non-existent minor flow, we will have a unidirectional flow (all pedestrians moving in the same direction). More in general the asymmetry of bidirectional flows can be measured using the flow ratio (sometimes called directional split) defined as:

$$r = \frac{\text{considered monodirectional flow}}{\text{minor flow} + \text{major flow}} = \frac{\text{considered monodirectional flow}}{\text{total flow}} \qquad (2.1)$$

Note that under the given definition the flow ratio r is defined in the interval $[0, 1]$. The case of balanced bidirectional flow will be equal to $\frac{1}{2} = 0.5$. When minor flow is considered (excluding the unidirectional case) the flow ratio will take values in $]0, 0.5[$ and in the case of major flow it will result in values included in $]0.5, 1[$. We will refer to counter flow as the flow in the opposite direction to the one being considered (usually we speak of counter flow referring to the the minor flow). By definition (except for the balanced case) the counter flow of a minor flow is a major flow, with the opposite case being obviously also valid. Whenever known we will use the terms minor or major to characterize a given group of pedestrians and we will use the term "monodirectional" to refer to a general case for which the specific characteristic cannot be known.
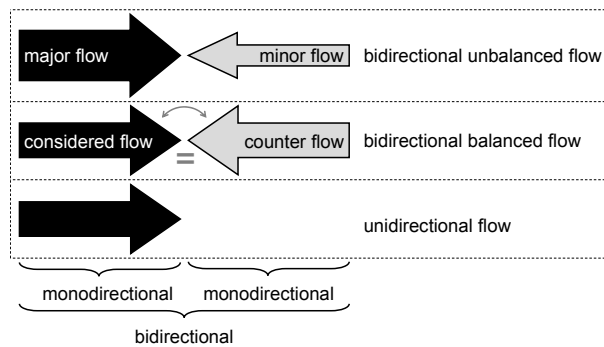
Figure 2.1: Schematic representation of bidirectional flow with definitions used in this manuscript. Note that for the balanced case both flows are equal and therefore terms are interchangeable.

At this point, it may be also necessary to add some remarks on the difference between unidirectional and uni-dimensional (or bidirectional and bidimensional). The dimensionality is a mathematical concept which is used to describe the minimum number of dimensions required to describe a phenomenon (or the number of axis from a more physical perspective). For instance, in uni-dimensional flow pedestrians move in a line (or a queue) and

overtaking or lateral motion is not allowed. In this case, only one dimension is considered and it is sufficient to describe the phenomenon. For unidirectional flow we intend a group of people walking in the same direction. This imply that someone will walk slower and someone faster than most of the group and therefore overtaking and lateral displacements may be observed. As a consequence, to describe this type of unidirectional motion bidimensional treatment is required (when people overtake or move laterally to avoid collisions). If the group is perfectly organized and everyone walk at constant and equal speed, it may be possible to simplify the description using uni-dimensional laws, but this represents an extreme case rarely observed in reality.

In general, any pedestrian crowd can be described using bidimensional laws (also stairs or vertical displacements can be considered as movements in a plane), but we will use the term multidimensional to indicate very complex scenarios like intersections with multiple legs. To summarize, the "multidimensional" term is used here to emphasize very complex structure, while "bidimensional" is used to indicate fairly simple cases which cannot however described using uni-dimensional laws.

2.3   Literature review

Bidirectional flow has been widely studied in the past and in particular a wide range of numerical models has been developed to account for collision avoidance with the counter flow. This section will provide an exhaustive summary of the most representative studies performed so far.

2.3.1   Empirical studies on the capacity of bidirectional flow

Experimental studies on bidirectional flow are the first to appear in the literature. The particular interest for this type of flow may be characterized by the fact that when standards had to be defined to uniform the width of sidewalks and crosswalks, scientific evidence became necessary. It is therefore not surprising that most of the early studies on the bidirectional flow are focused on defining the capacity and finding a function providing the relation with flow ratio.

Navin and Wheeler

The first efforts to quantify the effects of the counter flow were reported by Navin and Wheeler [24]. In their study they noted that when a small amount of pedestrians was walking in the minor flow, they occupied a proportionally larger size of the walkway compared to the major flow. As the flow became balanced (close to a flow ratio of 0.5), both groups tended to form organized lanes equally taking half of the walkway. Weidmann quantified this effect in terms of capacity reduction as illustrated in Figure 2.2(a).

Cheung

In the digital era, data acquisition became easier and Cheung was able to collect a large database of pedestrian speed and flow at different pedestrian facilities in Hong Kong [90]. The effect of counter flow was quantified in a number of situations, including stairways in both directions (up and down), escalators and different types of walkways. For the case of flat walkways, Cheung observed (similarly to Navin and Wheeler) that in the

presence of counter flow the opposing traffic contribute in reducing the capacity, but when the flow becomes balanced pedestrians in each direction share the width of the walkway equally. Cheung was able to provide an empirical function for the relation between effective capacity and flow ratio [1]:

$$q_{tot}(r) = q_{uni} \left[1 - (a_0 + a_1 r + a_2 r^2 + a_3 r^3 + +a_4 r^4 + +a_5 r^5 + a_6 r^6) \right] \qquad (2.2)$$

where q_{uni} is the unidirectional capacity (given as 1.53 (m·s)$^{-1}$) and a_i for $i = [0, 6]$ are empirically obtained parameters. It is important to remark that the function by Cheung is defined for $0 < r < 1$, which means that it is not continuous for the transition from unidirectional to bidirectional flow as shown in Figure 2.2(b) (empirical parameter are given in [90]). In the case of Cheung, the stability of balanced flow is remarkable and practically the same capacity of unidirectional flow is obtained.

Lam et al.

Some years later Lam et al. used the same approach to investigate the case of crosswalks (always in Hong Kong), creating a large database including speed and flow for two different locations (a commercial area and a shopping facility) [91]. Based on their observations they derived an empirical function for the effective flow (defined as the total flow relative to each direction), given by:

$$q_{eff}(r) = b_0 + b_1 r + b_2 r^2 + b_3 r^3 \qquad (2.3)$$

where r is the flow ratio and b_0, b_1, b_2 and b_3 are experimentally obtained parameters. To obtain the total flow (the sum of flows in both directions) the following transformation is required [2]:

$$q_{tot}(r) = r \cdot q_{eff}(r) + (1 - r) \cdot q_{eff}(1 - r) \qquad (2.4)$$
$$= c_0 + c_1 r + c_2 r^2 + c_3 r^3 + c_4 r^4 \qquad (2.5)$$

with c_0, c_1, c_2, c_3 and c_4 given by:

$$c_0 = b_0 + b_1 + b_2 + b_3 \qquad (2.6)$$
$$c_1 = -2b_1 - 3b_2 - 4b_3 \qquad (2.7)$$
$$c_2 = 2b_1 + 3b_2 + 6b_3 \qquad (2.8)$$
$$c_3 = -4b_3 \qquad (2.9)$$
$$c_4 = 2b_3 \qquad (2.10)$$

Using the empirical parameters provided by Lam et al. it is possible to plot the relation between total flow (or capacity) as shown in Figure 2.2(c). Qualitatively the result is very similar to the previous studies although the advantage gained when the flow becomes balanced is less marked.

---

[1]The function provided here is obtained by combining the relative reduction in capacity and the unidirectional capacity provided by Cheung.

[2]The interpretation of the function proposed by Lam et al. is rather controversial and there is no agreement between researchers (the author did not provide an official explanation and the presentation is rather unclear). The transformation proposed here is based on different qualitative remarks made in their work.
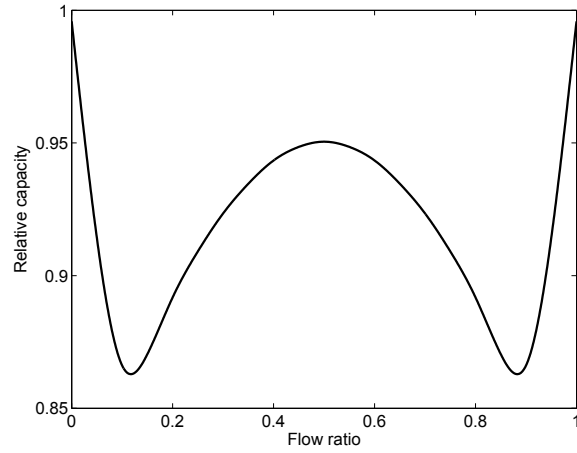
(a) Navin and Wheeler [24, 21]
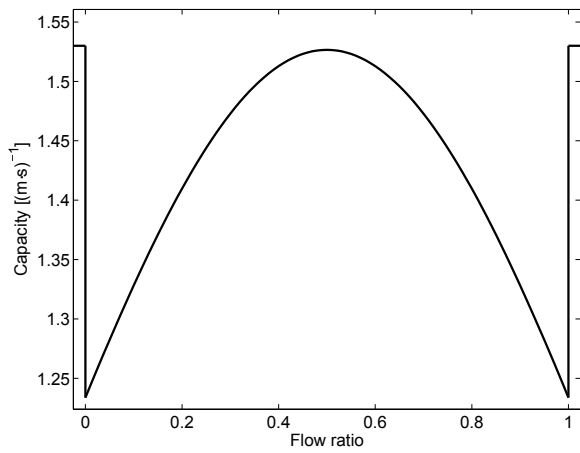
(b) Cheung [90]
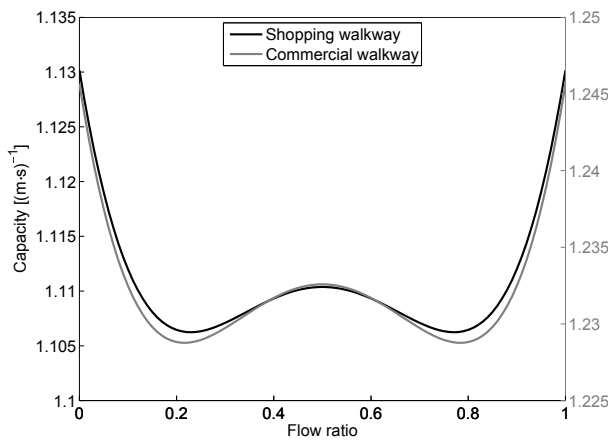
(c) Lam et al. [91]
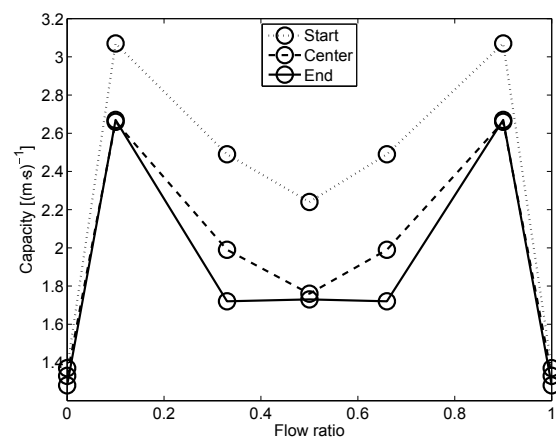
(d) Kretz et al. [92]
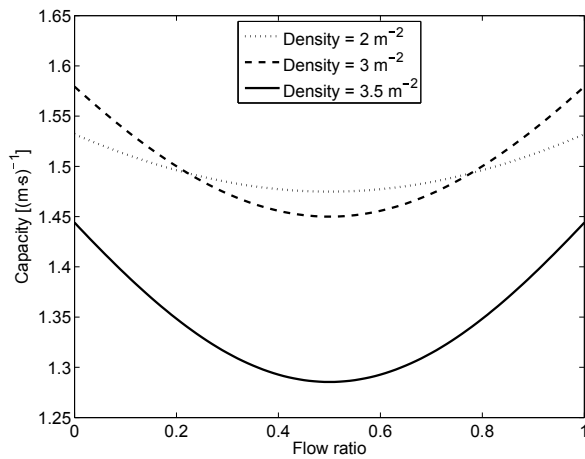
(e) Wong et al. [93]
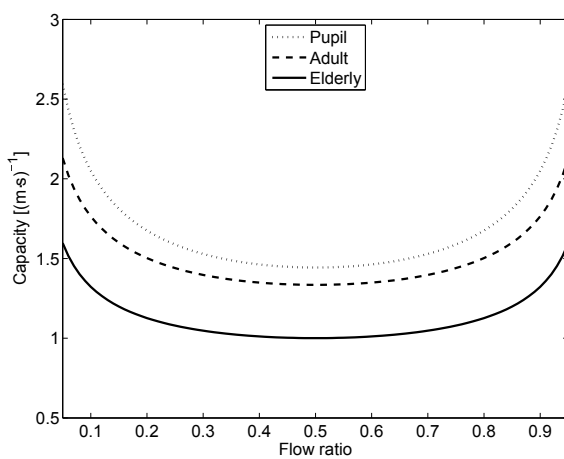
(f) Alhajyaseen and Nakamura [94]

Figure 2.2: Effect of the counter flow on capacity of bidirectional pedestrian facilities [95]. Geometries (crosswalk, sidewalk, corridor...) considered vary from author to author.

Kretz et al.

To study more in detail phenomena related with bidirectional flows, Kretz et al. performed a supervised experiment in a corridor analyzing the video recordings obtained at three positions [92]. The results of their study on counter flow effects are given in Figure 2.2(d) ("start", "center" and "end" refer to the relative position inside the corridor). In contrast to the previous researchers they found that bidirectional flow performs better than unidirectional ones in any situation. This conclusion may be partially related to the relative small group size considered (67 participants), especially when compared with the field studies presented earlier where thousands of people were observed.

Wong et al.

Wong et al. [93] have studied different configurations of cross-flows in a supervised experiment, with the bidirectional (counter) flow considered as the most extreme case of the ones studied. 90 participants were recruited for the experiment. Wong et al. developed an algorithm to extract pedestrians' position at each video frame, which allowed them to work with a large number of accurate data. The database was fitted with a function they proposed to predict pedestrian group velocity based on density ρ_{tot} and intersecting angle ϕ. With v_{free} being the free walking speed, their function is given by:

$$v_{mono}(\rho_{tot}, r, \phi) = v_{free} \exp\left[-\theta_1 \rho_{tot}^2\right] \cdot \exp\left[-\theta_2 (1 - \cos\phi)\left((1-r)\rho_{tot}\right)^2\right] \quad (2.11)$$

with θ_1 and θ_2 being experimentally determined parameters. The bidirectional counter flow case is obtained by setting $\phi = 180°$, which leads to the velocity for each monodirectional group:

$$v_{mono}(\rho_{tot}, r) = v_{free} \exp\left[-\theta_1 \rho_{tot}^2\right] \cdot \exp\left[-2 \cdot \theta_2 \left((1-r)\rho_{tot}\right)^2\right] \quad (2.12)$$

which can be promptly converted into pedestrian flow by multiplying with the corresponding density and flow ratio as follows:

$$q_{mono}(\rho_{tot}, r) = v_{mono}(\rho_{tot}, r) \cdot \rho_{tot} \cdot r \quad (2.13)$$

Finally the total flow can be computed by summing up both monodirectional components:

$$q_{tot}(\rho_{tot}, r) = q_{mono}(\rho_{tot}, r) + q_{mono}(\rho_{tot}, 1 - r) \quad (2.14)$$

Figure 2.2(e) shows the relationship of the above function for different densities by using the numerical values provided by Wong et al. ($v_{free} = 1.034$ m/s, $\theta_1 = 0.075$ m^4 and $\theta_2 = 0.019$ m^4). In the central section (around 0.5) a behavior similar to the work by Kretz et al. is observed, but the function is continuous at the transition between uni- and bidirectional flow. Also, Wong et al. predict that bidirectional flow is always performing worst than unidirectional one.

Alhajyaseen and Nakamura

Alhajyaseen and Nakamura [94] developed a drag force model based on empirical observations of signalized crosswalks. Their capacity function for the flow in one direction takes the following form:

$$q_{mono}(r) = d_0 r^{d_1} (1 - r)^{d_2} \quad (2.15)$$

where d_0, d_1 and d_2 are experimentally determined parameters. Again, we can obtain the function for the total flow by summing up both monodirectional components as follows:

$$q_{tot}(r) = q_{mono}(r) + q_{mono}(1-r) = d_0 \cdot \left[r^{d_1}(1-r)^{d_2} + (1-r)^{d_1} r^{d_2} \right] \qquad (2.16)$$

Alhajyaseen and Nakamura obtained different parameters for three age groups: pupils, adults and elderly. Their total flow for the three age groups is given in Figure 2.2(f). Their function shows similar properties with the ones previously presented: numerical values are close to the ones by Kretz et al. and function shape resembles to the one proposed by Wong et al. However, the function by Alhajyaseen and Nakamura tends to infinity for unidirectional configurations, thus not allowing a continuous transition to the bidirectional case.

Zhang et al.

Very recently Zhang et al. [96] performed a controlled experiment for the case of crosswalks. Conditions similar to reality were recreated in laboratory, with pedestrians waiting at opposite sides of a section which was later crossed by both groups simultaneously. Studied crosswalk had a length of 7.5 m and a width of 4.0 m. The number of pedestrians on both sides was changed to study flow ratio, with a maximum of 100 pedestrians in total. Similar to some previous studies, Zhang et al. concluded that capacity in one direction is given with a cubic function:

$$q_{mono}(r) = e_0 r^3 + e_1 r^2 + e_2 r \qquad (2.17)$$

where $e_0 = 8.7$ (m·s)$^{-1}$, $e_1 = -12.4$ (m·s)$^{-1}$ and $e_2 = 5.9$ (m·s)$^{-1}$ are empirical values. As usual the total capacity is obtained by summing main and counter flow, resulting in:

$$q_{tot}(r) = q_{mono}(r) + q_{mono}(1-r) = (2e_1 - 3e_0)r^2 - (2e_1 + 3e_0)r + (e_0 + e_1 + e_2) \qquad (2.18)$$

which is a simple quadratic equation. Based on their results, Zhang et al. concluded that the capacity of bidirectional flow in crosswalks is close the one for unidirectional flow in corridors. Concerning lane formation, Zhang et al. interestingly noted that it neither depends on the number of pedestrians in bidirectional flow nor on the flow ratio.

Outline

As we have seen above, different authors have provided various functions to explain the influence that counter flow has on the capacity of bidirectional flow. In addition to providing the different functions in Figure 2.2, we can compare qualitative features of each study as given in Table 2.1 and Table 2.2.

By looking at both tables and remembering the considerations performed earlier, it is possible to divide the various studies in two categories: continuous pedestrian stream (for example long time observation of walkways) and small group observations/experiments (two limited size groups of pedestrians crossing each others). In the first case a W-shape was observed in the capacity–flow ratio function, in the second one a U-shape seemed more common (with the partial exception of Kretz et al. who concluded that unidirectional flow is always less efficient). A tentative explanation for the U-shape function may be that lane formation is more difficult when there is no clear distinction between minor and major flow, thus making balanced flow less efficient compared to other bidirectional

configurations. This behavior could be particularly strong for small group of pedestrians who have only a short time to interact and determine which group should take a given portion of the corridor. However, over the long run, especially when pedestrians continue to flow at stable conditions, lanes will form separating both directions.

Table 2.1: Comparison between the different studies considered. Continuous pedestrian stream indicates a situation in which people continuously flow through the facility, while small group interaction is the case in which two groups limited in size pass each other's (as in the case of signalized crosswalks).

Author(s)	Type of study	Facility	Pedestrian stream
Navin and Wheeler	Observation	Sidewalk	Continuous
Cheung	Observation	Walkway	Continuous
Lam et al.	Observation	Crosswalk	Small groups interaction? [3]
Kretz et al.	Experiment	Corridor	Small groups interaction
Wong et a	Experiment	Corridor	Small groups interaction
Alhajyaseen and Nakamura	Observation	Crosswalk	Small groups interaction
Zhang et al.	Experiment	Crosswalk	Small groups interaction

Table 2.2: Capacity–flow ratio relationship, its shape and minimum/maximum capacity for different studies. Values given in bracket for capacity is the flow ratio at which minimum/maximum is observed; since the relation is symmetric two extrema are always found but only one is reported here for convenience.

Author(s)	Capacity function	Capacity $[(m·s)^{-1}]$	
		Maximum	Minimum
Navin and Wheeler	W-shape	1.23 (0.00)	1.05 (0.10)
Cheung	W-shape	1.53 (0.00)	1.12 (0.01)
Lam et al.	Slightly W-shape	1.25 (0.00)	1.11 (0.22)
Kretz et al.	M-shape / Center U-shaped	3.07 (0.10)	1.28 (0.00) [4]
Wong et al.	U-shape	1.62 (0.00)	1.52 (0.50)
Alhajyaseen and Nakamura	U-shape	2.62 (0.00)	1.34 (0.50)
Zhang et al.	U-shape	2.20 (0.00)	1.88 (0.50)

As several authors reported, the balanced case shows higher stability once lanes are formed, thus making it virtually no different from parallel unidirectional flows. This could be the mechanism leading to the transition into a W-shape function as reported in long time observations. This could also explain the changes observed by Kretz et al. as pedestrians moved from the "start" to the "end" position.

2.3.2   Other experimental studies

Although a consistent part of the empirical literature on bidirectional flow has been devoted in quantifying the impact of counter flow there have been other studies focusing on

---

[3]The term "crosswalk" suggests an interaction between small groups, but the image provided in [91] implies that possibly the flow was rather continuous.

[4]If bidirectional flow only is considered then minimum is found at the balanced case equal 0.5.

different aspects and will be presented here.

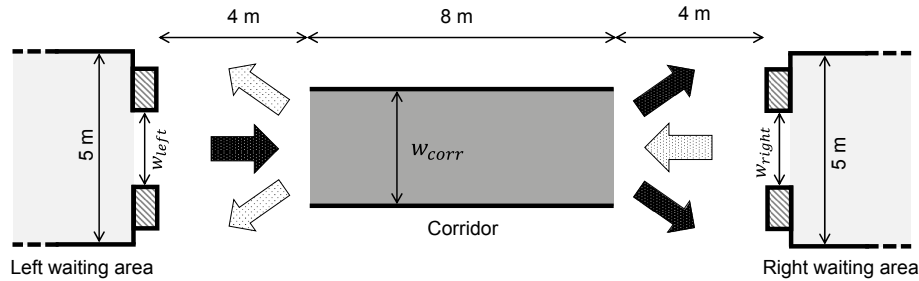**Bidirectional flow fundamental diagram**

Figure 2.3: Geometrical setup used by Zhang et al. for their experiments. Two opposite located waiting rooms are used to gather participants who walk in the central corridor. Variable sizes are given using symbols, fixed dimensions are provided with numbers. Diagram is adapted from [97].

Zhang et al. [39, 42] have performed one of the largest experimental campaign on the bidirectional flow, gathering about 350 participants and conducting experiments for a whole day. The data collected have been openly shared and consequently other researchers have also worked on their data. We will also analyze those data (as discussed in Chapter 2.5.5 and Chapter 2.6) and therefore the most important aspects of their study are summarized here.

Figure 2.3 shows the geometrical setup of their experiment. A corridor placed between two waiting rooms was created in a large exposition hall. Waiting rooms were created to gather participants before the start of each experiment. Each waiting room had a door with settable width, thus creating a bottleneck. When the starting signal was given, participants started to flow out from the respective waiting rooms, crossed the corridor and left from the opposite side (arrows in Figure 2.3 should help understanding the concept). The width of each door has been used to adjust the flow in each direction, having a control on the total flow and the flow ratio. This particular configuration allowed Zhang et al. to study different types of uni- and bidirectional flow without having to take big changes on the experimental setup.

Table 2.3: Configurations tested by Zhang et al. during their experimental campaign. Detailed figures are given in [13, 97, 98]. Codename is based on the following acronyms: UNI for unidirectional and BI for bidirectional (with BIB being bidirectional balanced and BIU bidirectional unbalanced). For balanced configurations w_{left} and w_{right} are set equal. When exit direction was freely chosen participants were allowed to leave the corridor from whichever side, under fixed destination the side was decided beforehand by organizers.

Codename	Configuration	Flow ratio	Exit	w_{corr}	w_{left}	w_{right}
UNI	Unidirectional	0.0	Free	3.00 m	3.00 m	0.80–3.00 m
BIB-free	Bidirectional	0.5	Free	3.60 m	0.50–1.60 m	
BIB-fixed	Bidirectional	0.5	Fixed	3.00 m	0.50–1.00 m	
BIB-fixed	Bidirectional	0.5	Fixed	3.60 m	0.50–2.50 m	
BIU-fixed	Bidirectional	≈0.4	Fixed	3.00 m	0.50–0.80 m	0.70–1.20 m

As shown in Table 2.3, the first configuration being studied has been the simple unidirectional case which has been created by setting the opening of the left waiting room equal to the width of the corridor. Participants simply exited the left waiting room and walked directly into the right waiting room. Different width for the door of the right waiting room were used to test different level of congestion (a bottleneck formed on the right side of the corridor). Participants were not given particular instructions on how to walk, but were simply asked to cross the corridor and enter the opposite located waiting room. By using the same principle a bidirectional flow configuration was also tested. To create a balanced flow the same door width has been chosen in both waiting rooms. To avoid having congestion formed after passing the corridor, participants were asked to leave it by exiting from one of the sides which they found more convenient (as for the arrows given in Figure 2.3) and take a long path at the external side of the respective waiting area (they did not re-enter from the "front" door as in the unidirectional case). This led to the formation of well organized lanes with pedestrians from each direction occupying the right half of the corridor (as clearly shown in Figure 2.4(a) and Figure 2.4(b)). This can be regarded as an unconscious consequence of traffic regulations (the experiment was performed in Germany which is a right driving country).

Later, different instructions were given to participants without changing the geometry employed. This time, half of the participants in each waiting room were asked to leave the corridor from the left side and the remaining half to the right side (ID numbers provided to them beforehand were used to determine exit direction on a even/odd basis). As a consequence, the flow inside the corridor became more chaotic and no preferential direction was observed. In Figure 2.4(c) and Figure 2.4(d) it is clearly observed that lanes cannot form in this configuration or are very unstable.

Finally the openings were set at different widths to create an unbalanced flow. Width of the left and right door was gradually changed by keeping a flow ratio close to ≈ 0.4 (in fact the unbalanced case tested by Zhang et al. was not much different from the balanced configuration). In the unbalanced case participants were always asked to leave the corridor from different sides as in the last configuration described. Trajectories obtained for the unbalanced configuration were similar to the one obtained in the balanced case with fixed exit directions.

Zhang et al. analyzed their experiments in terms of the fundamental diagram (see Figure 2.5). Their conclusions are that although there are differences between the uni- and bidirectional flow fundamental diagram, the different configurations of bidirectional flow are similar. This implies that by using the fundamental diagram it is possible to highlight some universal features which are common among the uni- and bidirectional motion (with the typical shape also found in theoretical representations), but on the other side it is not possible to grasp the more subtle changes observed in the different configurations of bidirectional flow.

Velocity distributions and fluctuations

Saberi et al. [99, 66] analyzed the data by Zhang et al. from a different perspective and investigated how velocity distributions changed in the various experimental configurations. At first the velocity profile along the width of the corridor is discussed. Helbing [100] theoretically predicted that for the case of pedestrian unidirectional motion (in group), velocity profile follows a hyperbolic form rather than the parabolic form observed for pipe flow in fluid dynamics. This hypothesis was later rejected by Zhang et al. [49] who analyzed data gained during a mass event in China and found that fully developed laminar

(a) BIB-free for $w_{left} = w_{right}$=0.75 m

(b) BIB-free for $w_{left} = w_{right}$=1.20 m

(c) BIB-fixed for $w_{left} = w_{right}$=0.75 m

(d) BIB-fixed for $w_{left} = w_{right}$=1.20 m
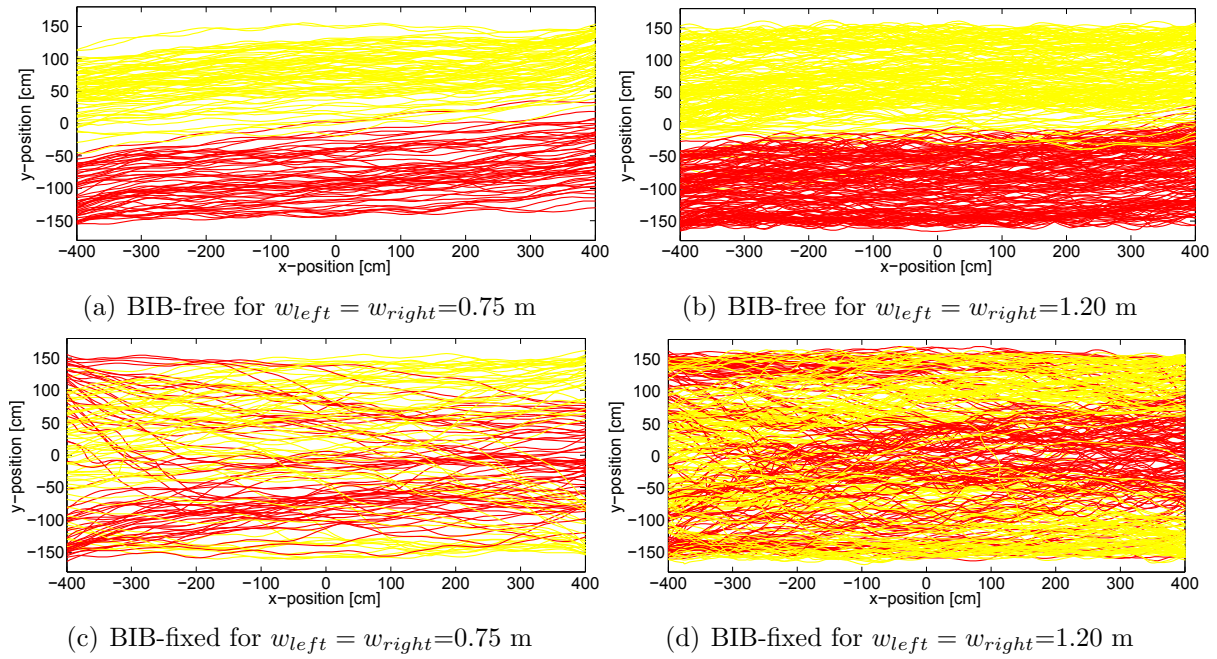
Figure 2.4: Pedestrian trajectories for the bidirectional experimental campaign by Zhang et al. (data are available in [98]). In BIB-free pedestrians are free to leave the corridor from the side they want, in BIB-fixed directions are determined. Yellow trajectories are relative to the left-to-right motion, red ones to the opposite direction. x-coordinate represent the corridor's length, while y refers to its width. Center of the corridor is set at the $0, 0$ coordinate.

(a) Uni- and bidirectional flow

(b) Different types of bidirectional flow
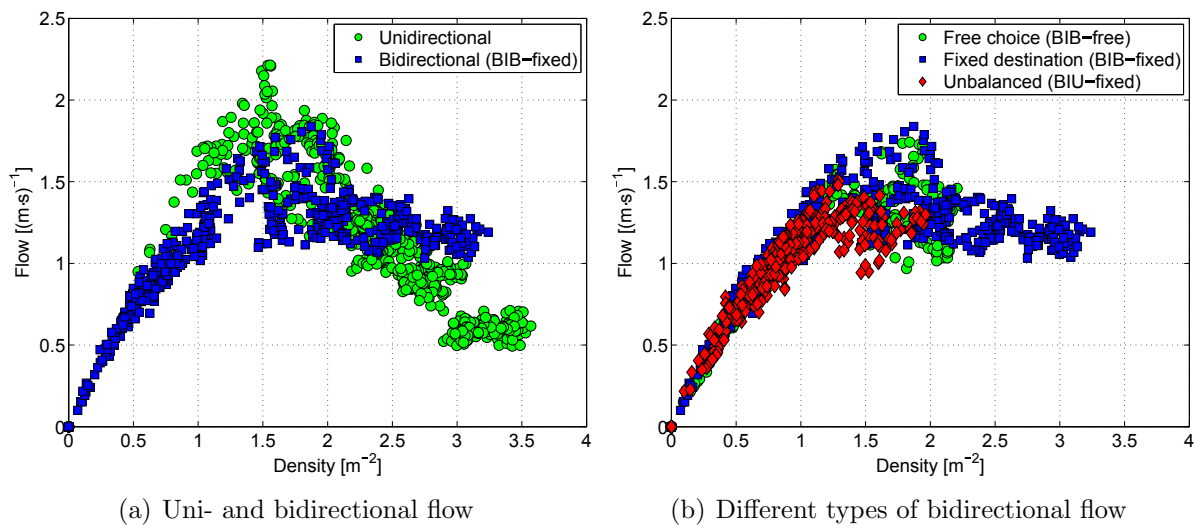
Figure 2.5: Fundamental diagram for the different experiments by Zhang et al.; differences are only found between the uni- and bidirectional case.

pipe flow can be used to describe pedestrian unidirectional motion also, although a slip velocity boundary has to be used. They suggested the following equation to describe the velocity profile in the case of unidirectional motion:

$$\frac{v(y)}{v_0} = 1 - k \left(\frac{y}{w_{corr}} \right)^2 \tag{2.19}$$

with v_0 being the velocity at the centerline (here $y = 0$), w_{corr} the width of the corridor and k an empirical constant.

Saberi and Mahmassani [99] later analyzed two cases (a unidirectional and a bidirectional case [5] respectively) from the experimental campaign by Zhang et al. and came to an entirely opposite conclusion. They found that unidirectional and bidirectional pedestrian streams indeed behave similarly to fluids but the velocity profile has an inverted shape with the minimum found in the centerline and the maximum close to the walls. However, when the analysis was extended to the whole dataset by Zhang et al., Saberi et al. [66] found that the velocity profile is highly dependent on the configuration of the lanes formed and that does not necessarily follow a hyperbolic form.

In the analysis considering the whole dataset by Zhang et al., Saberi et al. also computed the velocity distributions for both x and y directions (in other words main direction of motion and lateral motion). They found that the x-velocity can be described using a sum of four Gaussian distributions:

$$p(v_x) = \sum_{i=1}^{4} \alpha_i e^{\left(\frac{v_x - \beta_i}{\gamma_i} \right)^2} \tag{2.20}$$

with v_x being the x-velocity and α_i, β_i and γ_i experimentally determined parameters (respectively the amplitude of the distribution, the median velocity and the width of the distribution). The first two Gaussian distributions $i = 1, 2$ were found necessary to describe the velocity profile of each group, since pedestrians moving from left to right have positive velocities and negative velocities are found for pedestrians moving in the opposite direction. The remaining two distributions $i = 3, 4$ are used to consider non-steady state conditions, such for pedestrians at the front and at the end of the corridor who were walking faster until reaching a steady-state velocity. For the distribution of the y-velocity, Saberi et al. found that a single Gaussian distribution would be sufficient since effect of non-steady state conditions is smaller. Distributions for the four cases considered here (whose trajectories are illustrated in Figure 2.4) are given in Figure 2.6. The transient effects can be easily noticed for the x-distribution.

Interestingly, Saberi et al. found that for both x and y-distributions the width did not change when the experimental settings were varied (or the change is not significant). Neither the transition from the free choice to the fixed destination setup nor the increase in number of participants had an influence on the width of the distributions. When the median is considered, the relationship between median x-velocity and pedestrian crowd was found being linear (basically in line with the principles of the fundamental diagram). However, median y-velocity did not change throughout the several configurations and was nearly 0 for all the cases.

---

[5]The absolute velocity is used for the bidirectional case.
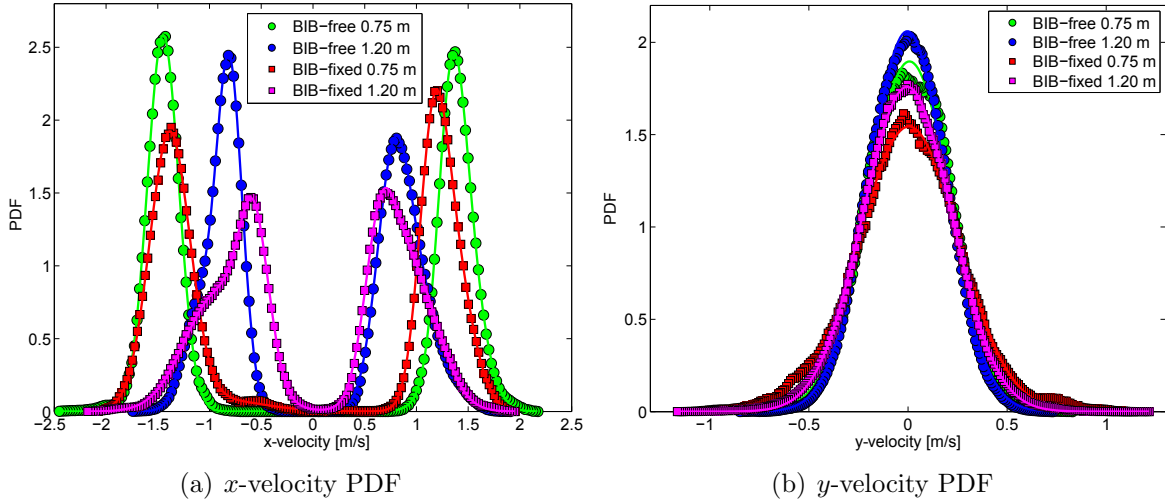
(a) x-velocity PDF

(b) y-velocity PDF

Figure 2.6: Velocity distributions for four cases in the experimental campaign by Zhang et al.; PDF stands for Probability Distribution Function.

Lane structure and order parameter

To detect self-organization in pedestrian flows different methods have been proposed; here we will focus on lane detection in bidirectional streams. On this purpose the bond index method by Yamori [101] or the cluster analysis method proposed by Hoogendoorn and Daamen [102] can be used. Also, the velocity profile previously discussed clearly display the formation of lanes if nominal velocity is considered (not the absolute value) and Zhang et al. [97] originally considered this approach. But here we will focus on the concept of order parameter which is very convenient for the particular case the bidirectional flow. The order parameter was originally introduced for driven colloidal systems [103] and it can be used to measure the degree of alignment between different horizontal layers.

To compute the order parameter it is necessary to divide the considered surface in several cells, similarly to the approach used in numerical simulation (and schematically presented in Figure 1.15(a)). The size of the mesh need to be chosen considering pedestrian size and density. Saberi et al. (who took a similar approach but did not compute the order parameter) used cells having a length (relative to the flow direction in the corridor) of 0.4 m and 0.3 m in width. After considering different sizes we found 0.2 m × 0.2 m more appropriate and this dimension will be used throughout the whole study when space is divided using a computational grid (in empirical analysis).

In each cell the average horizontal velocity (x-direction here) is computed over a time period. Figure 2.7 show the cases considered earlier for the data by Zhang et al. in which the time interval considered is the whole length of the experiment. The (global) order parameter can be computed applying the following equations. First, the local order parameter ϕ_j is computed for each row according to:

$$\phi_j = \left(\frac{n_j^L - n_j^R}{n_j^L + n_j^R} \right)^2 \tag{2.21}$$

where n_j^L and n_j^R represent the number of cells having positive and negative velocities in the jth row (L and R stand for left and right walkers). Finally, the global order parameter Φ can be computed as:

(a) BIB-free for $w_{left} = w_{right}$=0.75 m

(b) BIB-free for $w_{left} = w_{right}$=1.20 m

(c) BIB-fixed for $w_{left} = w_{right}$=0.75 m

(d) BIB-fixed for $w_{left} = w_{right}$=1.20 m

Figure 2.7: Velocities inside the corridor for the experiments by Zhang et al. over the total time of execution. Positive velocities are relative to the left-to-right motion, red ones to the opposite direction. Clearly for the experiments with fixed destination and with many participants the velocities are lower. Mesh size is 0.2 m × 0.2 m.

$$\Phi = \frac{1}{N} \sum_{j=1}^{N} \phi_j \qquad (2.22)$$

where N is the total number of rows. The order parameter is by definition never negative and it is generally always bigger than zero also in the extreme case of complete chaos (or random walk) [6]. The lowest value which the order parameter takes in the case of random walk, depending on the total size of the grid considered, can be computed as:

$$\Phi_{min} = \frac{1}{N} \qquad (2.23)$$

The length of the grid does not play any role in determining the minimum value. It is now possible to compute the order parameter for the cases considered so far using the data by Zhang et al. and the results are shown in Table 2.4.

It can be seen that the case in which pedestrians were allowed to freely choose their path shows an higher order parameter as lanes are clearly separated. On the other hand, the case with fixed destination and a relatively high density (BIB-fixed 1.20 m) had the lowest order parameter among the configurations considered. It is also worth noticing that the configuration with free path and a door opening of 0.75 m has an order parameter lower than the configuration with 1.20 m width. This is related to the fact that lanes are well organized but the division line between lanes is not perfectly horizontal.

Different authors also investigated the number of lanes formed in bidirectional flow. Kaufman [104] considered one supervised experiment (the one also analyzed by Kretz et al.

---

[6]The order parameter becomes 0 when walkers are aligned vertically, with each column represented by a class of pedestrian. However this condition never happen in real situations and random walk is considered the most disorganized state.

Table 2.4: Order parameters for some configurations tested by Zhang et al. and given in Figure 2.7. Differences in lane alignment between the free-choice case and the one with fixed destinations are evident.

Codename	$w_{left} = w_{right}$	Order parameter
BIB-free	0.75 m	0.893
BIB-free	1.20 m	0.964
BIB-fixed	0.75 m	0.469
BIU-fixed	1.20 m	0.272

(a) Number of lanes   (b) Lane width
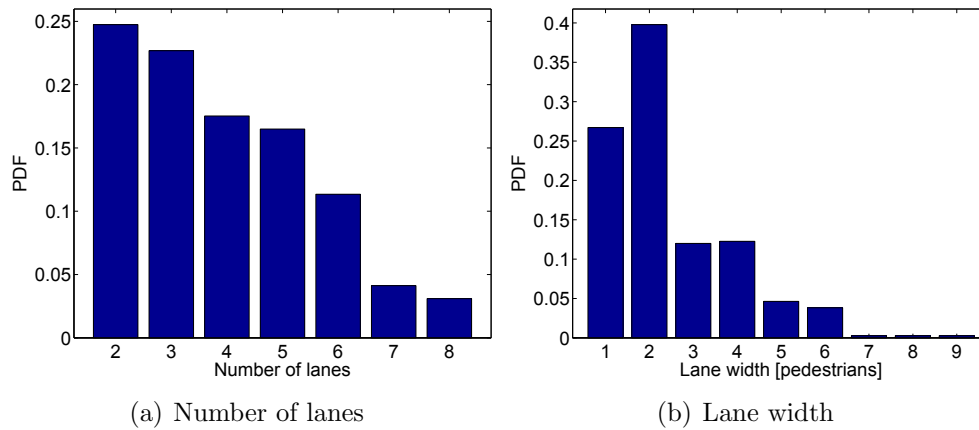
Figure 2.8: Number of lanes and lane width for bidirectional pedestrian flow [104].

[92]) and two on-field observations. In the supervised experiments 2 or 3 lanes have been the most common configurations and when the lane number of was even, people always took the right side. Later, pedestrians assisting a large festival were observed. It was found that when people were overtaking the left direction was preferred, but sidestepping was mostly performed on the right side. In the third case considered, Kaufman reported that the most common number of lanes was 2 and the probability decreased as the number of lanes increased. The conclusions on the number of lanes considering all scenarios are given in Figure 2.8. Also, Kaufman noted that the number of lanes observed for stable conditions is different from the one observed during short-term situations.

Extreme conditions

In general, supervised experiments tend to have low densities because safety has to be guaranteed. Studies considering high densities are usually relative to on-field observations and there is a modest literature on the subject.
AlGadhi et al. [105] analyzed motion of pedestrians during the Mecca pilgrimage and developed a bidirectional speed concentration relation taking into account crowd movements with strong interactions in opposite directions. The model proposed by AlGadhi et al. is quite simple and it is based on a linear relationship between walking speed and density; which may not be appropriate for high densities as we have discussed earlier. However, the context analyzed is rather unique since the densities observed are particularly high. AlGadhi et al. reported that there is a minimum speed (which they called "shuffling speed") of about 0.14 m/s which is maintained even at very high densities. Also, they came to the conclusion that "the impedance exerted on the average speed of a stream of

pilgrims by pilgrims moving in the same direction is more than twice that of those moving in the opposing one".

Helbing et al. [16] also investigated the motion of pilgrims in Mecca and used an algorithm to gain data for velocity and density over a large surface in front of the Jamarat bridge (their results are given in Figure 3.26(a) and will be discussed also in Chapter 3.5.3). They also observed that a minimum non-zero velocity is kept at very high densities over 9 m^{-2} and that the velocity drops from about 5 m^{-2}. However, they found that at about 9 m^{-2} an increase in velocity causes a second peak. The cause for this peak was found being the onset of shockwaves through the crowd. Helbing et al. noticed that at very high densities the transition from stop-and-go waves to the so-called "turbulent flow" occurs. Helbing at al. reported that at those conditions "people were so densely packed that they were moved involuntarily by the crowd". This resulted in random displacements into all possible directions and Helbing et al. created the concept of "crowd turbulence" to describe this phenomenon.

Bidirectional flow with bottleneck

To conclude this experimental overview it is worth mentioning the work by Liu et al. [106], in which the authors studied a bidirectional flow through a bottleneck. A mock corridor 3.2 m in width has been built and flow without bottleneck and with different bottleneck widths (2.4, 1.6 and 1.0 m) has been studied. The authors also tested a unidirectional configuration and two bidirectional configurations with flow ratios of 0.25 (unbalanced) and 0.5 (balanced). Each configuration was tested only once, limiting the universality of their conclusions. Participants trajectories were extracted and analysis has been mostly based on the fundamental diagram and transient changes in flow properties (flow, density and speed). The authors found that in narrow bottleneck pedestrians form a zipper-system, where in each side of the bottleneck a larger amount of space is taken by pedestrian waiting to cross it compared to those who just passed it. Liu et al. also noticed that pedestrians interaction with the counter flow mostly started only when each group encountered in the middle of the corridor. Furthermore, the authors noticed that the flow ratio has an influence also for bottleneck as the differences between different widths got larger for the balanced configuration. However, Liu et al. concluded that the process of lane formation is related with bottleneck width and no clear relation is found with flow ratio. Nonetheless, they observed that flow ratio had an influence on the time evolution of density and flow. As a final remark, Liu et al. concluded that using a wide corridor does not necessarily improve the safety and narrow design may be better instead.

2.3.3   Theoretical studies

As we have seen in the introduction, only simple cases for pedestrian motion can be solved analytically and therefore the theoretical literature on bidirectional flow is rather limited. There is however one study which is worth mentioning as it covers important aspects found in bidirectional streams. Flötteröd and Lämmel [107] were able to introduce a theoretical treatment which allowed them to obtain a universal function for the fundamental diagram and draw a general chart predicting maximum flow (or capacity) in relation with the density of the group in each direction.

Flötteröd and Lämmel introduced the so-called counter flow constrained sending and receiving functions which define a general form of the fundamental diagram for bidirectional flow indicated in Figure 2.9(a). In Figure 2.9(a) "S" and "R" refers to the sending and

receiving functions respectively and are purely theoretical representations (based on a model which was designed to reproduce properties of bidirectional streams).
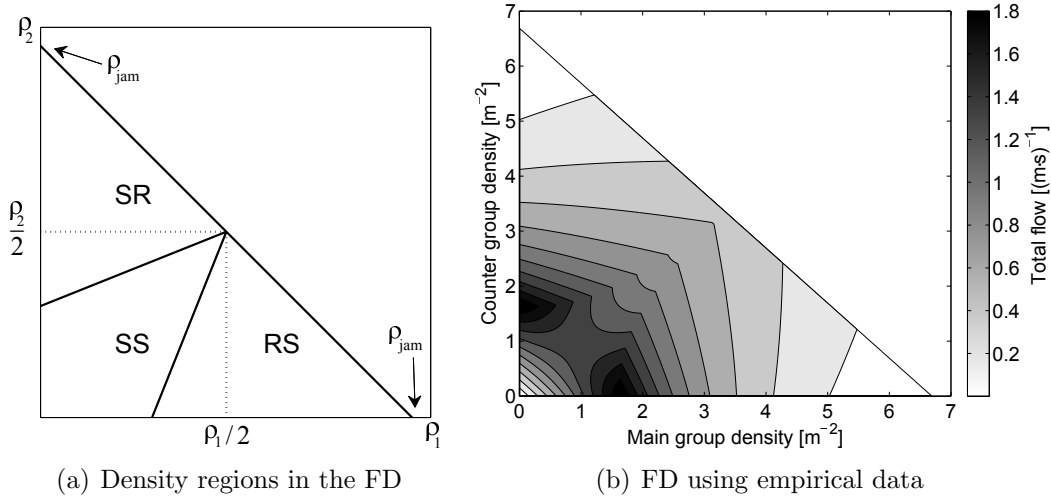

(a) Density regions in the FD

(b) FD using empirical data

Figure 2.9: Semi-theoretical bidirectional flow fundamental diagram by Flötteröd and Lämmel [107]. In (b) values used for plotting are ρ_{jam}=6.69 m^{-2}, v_{free}=1.27 m/s, b=0.61 m, $\alpha = 0$, $\beta = 0.61$ and $\gamma = 1.43$.

However, Flötteröd and Lämmel also managed to adapt their model allowing a calibration using experimental data. The fundamental diagram is defined in the SS regime using the following function:

$$\begin{pmatrix} q_1 \\ q_2 \end{pmatrix} = \frac{v_{free}}{1 + D \cdot v_{free} \ (\rho_1 + \rho_2) \ b} \begin{pmatrix} \rho_1 \ [1 + D \cdot v_{free} \ (\rho_1 - \rho_2) \ b] \\ \rho_2 \ [1 + D \cdot v_{free} \ (\rho_2 - \rho_1) \ b] \end{pmatrix} \quad (2.24)$$

which holds valid if $\rho_2 \leq \rho_1 \frac{2 + D \ v_{free} \ \rho_{jam} \ b}{D \ v_{free} \ \rho_{jam} \ b} - \frac{1}{D \ v_{free} \ b}$. In the previous equations q_1 and q_2 are the flows in the two directions of the bidirectional flow and ρ_1 and ρ_2 the respective densities. v_{free} is the free walking speed, ρ_{jam} the jam density (the density at which the flow becomes zero) and b is a characteristic length for pedestrian width. D is a general-purpose function which will be discussed later. In the RS regime the flows q_1 and q_2 are defined as:

$$\begin{pmatrix} q_1 \\ q_2 \end{pmatrix} = \frac{v_{free}}{1 + D \cdot v_{free} \cdot \rho_{jam} \cdot b} \begin{pmatrix} \rho_{jam} - \rho_1 \\ \rho_2 \end{pmatrix} \quad (2.25)$$

which holds valid for the range not defined by the SS regime. It should be noted that in each case the model is defined for $\rho_1 \in (0, \rho_{jam}]$ and $\rho_2 \in (0, \rho_1]$ due to the symmetry of the bidirectional flow. Function D is defined as:

$$D(\rho_1, \rho_2) = \alpha + \beta \left(\frac{b\rho_1 + b\rho_2}{1\mathrm{m}^{-1}} \right)^{\gamma} \quad (2.26)$$

where α, β and γ are experimentally determined parameters. Flötteröd and Lämmel also used the data by Zhang et al. (more precisely what we defined as UNI and BIB-fixed here) to calibrate their functions and the fundamental diagram for the total flow ($q_1 + q_2$) obtained by using their approach is given in Figure 2.9(b).

2.3.4   Simulation models and related studies

Simulation models for bidirectional flows are conceptually identical to the approach discussed in the introduction. The only particularity of the bidirectional flow (and more in general of complex scenarios) is that the destination changes for each class of pedestrians and this lead to some considerations that are discussed in this section. In the literature review of simulation models we will focus on the Cellular Automata approach, which will be used as the main numerical tool in this study.

If a discrete approach is taken and the Floor Field model is used, two different static floor fields will have to be applied depending if one pedestrian is walking in the right or in the left direction. An illustrative example for the static floor fields of left and right walkers is given in Figure 2.10.

(a) Right walkers   (b) Left walkers
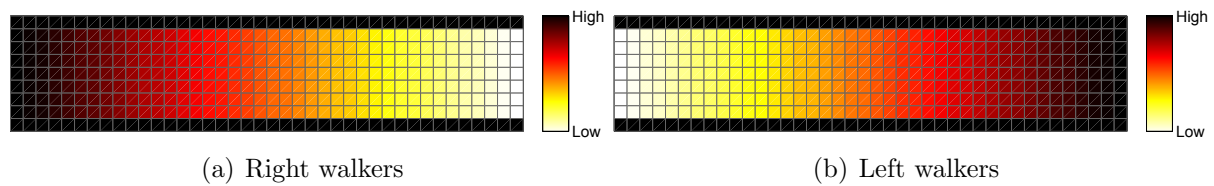
Figure 2.10: Static floor field for pedestrians in a corridor. Left and right walkers are assigned different static floor fields to match their destinations.

In general, the literature on simulation models for the bidirectional flow is mostly related to the approach taken in developing more sophisticated models able to consider the particularity of pedestrian crowds. There is however one particular aspect which has been often studied in the past and it is related with the concept of deadlock. Deadlock (also referred as gridlock) occurs when a complete stop is observed and pedestrians from both directions are unable to cross the corridor (or the scenario) considered. Deadlocks occurs very easily if the most standard form of the Cellular Automata (the approach described so far with only static and dynamic floor field) is employed. In contrast, complete deadlocks almost never occurs in reality and from the previous experimental discussion we know that pedestrian crowds show small velocities ever at extremely high densities.

Head-on conflict and sidestepping

At low densities, when only a small number of cells is occupied, deadlock occurrence probability is quite low. However, when the density is increased, deadlocks occur relatively easily. From a microscopic point of view deadlocks occur because two pedestrians moving in opposite directions and staying in front of each others are unable to move as both destinations are occupied by them (as shown in Figure 2.11). When densities are low sidestepping is a possible solution to resolve the conflict, but when densities grow side cells may be also occupied and pedestrians get stuck.

Figure 2.11: Position exchange to avoid head-on collisions.

Blue and Adler [108] proposed to introduce an exchange probability under which head-on conflicts (like the one shown in Figure 2.11) are resolved by exchanging the position of

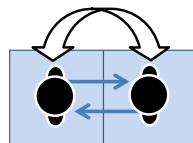both pedestrians with a probability p_E at each time step. When p_E is set equal 0 the basic Floor Field model is obtained and deadlocks are possible and common. By setting p_E equal 1 deadlocks never occurs but interaction between pedestrians is drastically reduced. Jian et al. [109] build a similar model to the one proposed by Blue and Adler and after performing a series of simulations with different parameters concluded that setting p_E equal 0.2 is a reasonable choice.

Blue and Adler [110] later also introduced a lane changing rule to allow pedestrians to laterally move into a different lane to either increase their walking speed or avoid head-on conflicts. A similar approach has also been recently taken by Xue et al. [111], who developed a model with the specific aim to consider lane formation and to reduce the deadlock probability. They introduced the principle of dominant lanes which are attract-ing pedestrians moving in a specific direction, effectively making deadlock formation more difficult.

High density applications

Cell size for CA simulations is typically chosen as 0.4 m in width, representing the average size of human body reported by Weidmann [21]. The maximum density allowed under this setting is rather low, corresponding to 6.25 m^{-2} (as we have seen, densities close to 10 m^{-2} are extremely dangerous but physically possible). To increase the maximum density and at the same time also reduce the deadlock probability several authors proposed different solutions. Bandini et al. [112] proposed to allow more than one pedestrian in a single cell (with a maximum of two in their approach), thus doubling the maximum density reached. Other authors [113, 114] considered the use of a finer mesh to accurately reproduce the shape of human body, an approach which can also be used to increase the density depending on the setup. Bandini et al. also considered a combination of both methods, i.e. a finer mesh with partially overlapping pedestrians. Finally, an alternative approach has been taken by Henein and White [57] who used the standard mesh with only one pedestrian per cell, but introduced a force field which can account for the pressure felt by people in heavily packed crowds. The method proposed by Henein and White does not directly considers dense crowds but allow to estimate their effects, thus making an indirect assessment possible.

Flow regimes and phase transition

There is also a number of studies which aimed at finding criteria and limits for phase transition in bidirectional flows. One of the most complete studies on the subject has been presented by Nowak et al. [63], who have used a common CA Floor Field model to assess the stability of lanes and study more in detail the transition between different flow regimes. In their study, four different regimes are considered: free flow, disorder, (stable) lanes and gridlock. In their analysis on phase transition Nowak et al. mostly considered periodic boundary conditions (i.e. pedestrians leaving from one side are reintroduced on the opposite side), but Weng et al. [68] also extended the analysis to the case of open boundary conditions (pedestrians leave from the respective side and vanish from the sys-tem). For the latter case they concluded that for certain densities, only two regimes are observed: free flow and perfectly stopped phase (or deadlock). Transition is driven by spontaneous fluctuations which turn the first metastable regime into congestion.

When alternative approaches are considered (other than CA), there is an additional num-ber of studies which considered phase transition. Muramatsu et al. used a lattice gas

model with periodic [115] and open boundary [62] conditions to determine the density at which the low density free flow changes into an high density deadlock. However, in contrast to Nowak et al. and Weng et al., in their model the transition did not include an organized regime with stable lanes and is therefore not representative of real conditions. Tajima et al. [116] employed a similar model with open boundary conditions to also study the jamming transition (or deadlock formation). In the case of Tajima et al. there is an abrupt transition from motion in lanes to deadlock and free flow is not considered.

Alonso et al. [117] created an original continuous model which calculates pedestrian motion from Newton's second law, taking into account viscoelastic contact forces, contact friction, and ground-reaction forces. Their model focus on extreme phenomena and takes therefore into account three different regimes which are identified as lane formation, avalanches and clogging. Based on the results of their simulations, Alonso et al. concluded that phase transition should occur earlier, or at lower densities, for the balanced case (flow ratio of 0.5).

Other aspects

In this final section we will discuss various models which have been developed for specific purposes and summarize relevant results on numerical studies on bidirectional flows.

A number of studies employed special models to limit some of disadvantages related to the use of a discrete space in CA. Weng et al. [68] developed a model which can simulate pedestrian walking with different velocities by updating at different time-step intervals. Weng et al. used their model to study phase transition with different boundary conditions as discussed earlier. The different velocities allowed them to notice that "in the stage of lane formation, the phenomenon that pedestrians exceed those with lower walk velocity through a narrow walkway can be found". There is also a number of studies which employed special geometries like hexagonal cells [118] or a real-coded lattice gas scheme [119] to overcome the limitations in diagonal motion, but they focused on evacuations and the specific case of bidirectional motion was not considered.

By using a uni-dimensional CA model, Yanagisawa [120] studied swerving behavior in bidirectional flows. In his model, pedestrians have the memory about which swerving direction resulted in an effective avoidance of the counter flow and memory-loss effect was also considered. If memory-loss is weak swerving direction tends to get unified in each direction, while under strong memory-loss conditions chaotic scenarios form (right and left swerving with equal probability). Yanagisawa was however unable to discuss correlations with lanes, since his model is only one cell in width.

Although based on the social force model, it is worth mentioning the study by Oliveira et al. [121], who showed that, under particular conditions, the use of asymmetrically profiled walls can help in the formation of lanes. However, their model employed periodic boundary conditions and a large number of steps was required to see the influence of profiled walls on lane formation.

Finally, although not considering pedestrians, the work by Ikeda and Kim [122] can be mentioned here. In their study, they proposed a simulation model for self-driven binary particles and studied the effects of density and system size on the lane formation. Although binary particle fluids are investigated, some of the aspects considered in their study (such as density and number of lanes) are directly correlated with pedestrian crowds.

2.3.5 Summary

As we have seen in this literature review, bidirectional flow has been extensively studied in the past and it can be considered as one of the most common scenarios treated in pedestrian dynamics (possibly together with the bottleneck/evacuation scenario). There are however some limitations which can be found in the literature overall:

1. While a large number of observations have been performed for crosswalks, sidewalks and corridors they all referred to low density scenarios or extremely high chaotic cases involving accidents. Also, most of the cases did not consider transient effects and basically focused on obtaining capacity or quantities related with the fundamental diagram.

2. Most studies consider the bidirectional flow as an extension of the uni-dimensional case. While there certainly are some similarities, the bidimensional nature of the bidirectional flow requires the introduction of new quantities which should also take into account lateral displacement. Some attempts to investigate lateral motion already existed but nobody tried to combine forward and lateral motion in a single measure.

3. Theoretical studies on the bidirectional flow are limited and are only partially supported by experimental data (mostly to confirm qualitative aspects of the results).

4. Empirical data are available from few sources but experimental conditions are limited and to draw more general conclusions a vast database including a variety of scenarios is required. This could also help validating the theoretical studies presented so far.

5. High density simulation models mostly focused on increasing the maximum density allowed, but behavior in highly packed scenarios is considered in the same manner to low density conditions. Also, the percolation-like behavior sometimes observed in pedestrian crowds seems not to be correctly reproduced in conventional models used for pedestrian traffic.

In the following sections we will present different studies which should partially overcome the limitations listed above.

2.4 On-field observation in Tokyo

To gain transient empirical data for pedestrian crowds in medium to high densities, an observation was carried out in Omote-sando subway station in central Tokyo. This section will describe the characteristics of the selected location and the methods used for data analysis. Results will be also discussed in detail.

2.4.1 Location and technical setup

Omote-sando subway station was chosen for multiple reasons. First, several passengers reported being stuck in a crowd while exchanging line, thus suggesting the formation of jam. Second, the author personally witnessed on several occasions the transition to congestion in a clearly defined space in the reported subway station, thus providing ideal conditions

for the empirical observation of the phenomenon. Lastly, the compact size of the station and its limited number of entrances and exits gives the opportunity to accurately count the passengers moving in each direction.

Omote-sando station has a daily ridership of 174,394 people making it among the 20 most crowded subway stations in Tokyo [123]. As schematically indicated in Figure 2.12, three lines are running through it, namely the Hanzomon and Ginza lines (running parallel in the vertical direction on the diagram) and the Chiyoda line (running horizontally on the diagram). Each train platform is connected with the main floor (located between the three lines) by means of stairs and escalators as indicated in the schematic image. In the main floor a large concourse area connects all the three lines allowing passengers to leave/enter the station and exchange line/platform on the same common floor. When passengers exchange the train from the Chiyoda line and move to the left side of Figure 2.12 to ride either the Ginza or the Hanzomon line, a dense crowd is formed in the narrow region highlighted in gray. Analogously, the same phenomenon happens in the opposite direction, i.e. when passengers move from the left to the right side of the concourse to ride a train on the Chiyoda line. From now on, to simplify the notation, we will refer to the left side of the concourse as concourse "A" and to the right side as concourse "B". The narrow passage on which this study is based lies between both sides of the concourse (thus between A and B).

Cameras were located in each strategic location in order to count the number of people leaving each platform, entering/exiting the station and passing through the narrow section. Cameras numbered from 1 to 4 were placed to count the number of people leaving/entering each platform on concourse A, cameras 7 and 8 to count the people moving in/out concourse B (from/to the corresponding platform) and camera 5, 6 and 9 were placed at the entrance/exit of the station to count the people leaving/entering it. Finally cameras 10 and 11 were used to directly observe the formation of a dense crowd in the narrow section.
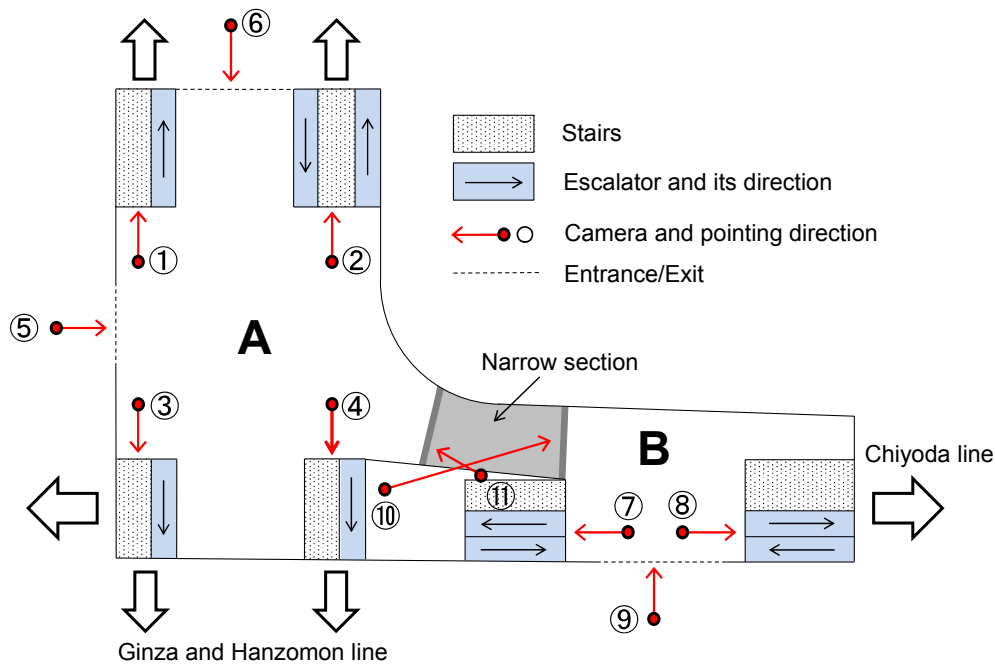

Figure 2.12: Schematic view of the Omote-sando subway station with number and location of each camera and its pointing direction. The narrow section is given in gray [124].

In the morning of December 18th, 2014 (Thursday) the movement of the passengers inside the station was recorded using the 11 cameras from slightly earlier than 7 AM during a roughly 2 hours period (until slightly later than 9 AM). Personnel of the train station supervised the operation to check that each camera was constantly pointing in the predetermined direction and to precisely adjust each camera's time and have a perfect synchronization between them. In addition, detailed information containing the scheduled and effective arrival and departure time for each train on each platform was provided from the operator of the station (Tokyo Metro Co.,Ltd). This allowed us to compute the delay of each train and the arrival delay between trains on different platforms and in particular between both sides of the concourse.

Considering the low ceiling of the subway station (less than 3 m), each camera had to be set at low angle and, in some cases, they were looking frontally to the passengers. This constraint, and the relative long distance from which people were observed, prevented the use of an automated video processing technique to count pedestrians. In addition, because of the time of the day considered, the vast majority of people were commuting to work, most of them wearing black suits. Consequently, because of the low contrast between individuals, an image processing method could have led to uncertain results. Therefore, videos were analyzed manually using the open-source video processing software Kinovea. Given the large number of people involved and the amount of video data to be processed, we decided to focus on the most relevant events during the time considered (for a single operator, analyzing 2 minutes of video for all the cameras required about 1 working day). To select the relevant events, train arrival data provided were particularly useful. Also, it can be easily predicted that in the early morning, when ridership is low and arrivals between both concourses are out of phase, pedestrians can freely move inside the train station. On the other side, a simultaneous arrival of several trains on both concourses during rush hour may quickly result in a congested motion inside the train station. More in general it can be predicted that after 8 AM the station will be more congested as the ridership on all lines is high. Because of the above reasons, out of the 2 hours of video available only about 45 minutes were analyzed, with the selection being based on the train arrival time and a quick analysis of the video recordings obtained.

2.4.2   Data acquisition and treatment

The station selected, having a limited number of exits and a clear division between both concourses, allows to easily guess the direction of each pedestrian based on the images recorded from the cameras on-site. Since both lines connected to concourse A run parallel for a number of stations, passengers are unlikely to exchange line between them. Thus, the most likely options for a passenger getting off a train at this station are: leaving the station from the closest exit or moving from concourse A to B (or in the opposite direction). Entrance to the subway station is restricted by automated gates and thus other transit possibilities (like entering on one side and leaving on the other) are very unlikely (and were observed as a very rare exception to the exchange/enter/exit main rule).

Considering the above facts, the making-up of the inflow for the narrow section in both directions starting from the single flows can be summarized as given in Figure 2.13(a). Each of the flows indicated in Figure 2.13(a) can be easily computed by using the images recorded from each camera. In a similar way the outflow resulting in the narrow section can be obtained by knowing the flow corresponding to each camera in both concourses as

indicated in Figure 2.13(b).

For each camera, the number of people moving in each direction was counted for a 5 s interval. The choice of a 5 s interval is related to practical reasons (passengers were counted manually) and to the fact that macroscopic changes (flow fluctuations in particular) were found having a period longer than 15 s (thus any sampling interval smaller than this would be appropriate). A yellow tactile paving thick line (placed at the ground to allow people with impaired vision recognizing the end of stairs/escalators) was used to clearly count the passengers leaving and entering each platform. For each interval, a raw data matrix contained the number of pedestrians transiting through the camera view, categorized into their direction and the mode used (stairs/escalator) to enter/leave the platform. A sample of the data matrix for some of the cameras is given in Table 2.5.

In this way more than 30'000 people transiting through the subway station during the roughly 45 minutes of analysis have been counted. Constructional setup and safety reasons constrained the position of cameras 10 and 11 (directly observing the crowded narrow section) to unfavorable locations. For these reasons people coming inside this area had to be observed from a very low height (slightly more than 2 m) and a distance of several meters. This perspective, together with the very high flow observed in this location, did not allow using the videos obtained by those cameras even in the case of manual (human operated) analysis.

As given in Figure 2.13(a) the inflow resulting in the narrow section can be obtained by summing up all the flows registered by the different cameras placed at the exit of each platform minus the flow of people leaving from the corresponding exits. Therefore, the total pedestrians' inflow for the narrow section in both directions can be written as:

$$\alpha_{A \to B} = \alpha_1 + \alpha_2 + \alpha_3 + \alpha_4 - \alpha_5 - \alpha_6 \tag{2.27}$$

$$\alpha_{B \to A} = \alpha_7 + \alpha_8 - \alpha_9 \tag{2.28}$$

where $\alpha_{A \to B}$ is the inflow for passengers moving from concourse A to B, $\alpha_{B \to A}$ is the same flow in the opposite direction and α_n is the flow recorded at the different locations $n = [1, 9]$. With Figure 2.13(b) as reference, the outflow resulting from the motion in both directions, from concourse A to B and the opposite, can be written as:

$$\beta_{A \to B} = \beta_1 + \beta_2 + \beta_3 + \beta_4 - \beta_5 - \beta_6 \tag{2.29}$$

$$\beta_{B \to A} = \beta_7 + \beta_8 - \beta_9 \tag{2.30}$$

with β representing the outflow and the subscripts being the same for the inflow [7].

In a second step, because the distances between the narrow section and each camera (platform connection) are different, a further adjustment had to be made to obtain the correct inflow and outflow. When computing the total inflow and outflow, the difference of time required to walk to the different destinations need to be considered. For this purpose, for each route (for example from the left side of the narrow section L to position 4), the time required to cover the distance was obtained by checking at which time a reference person was passing through the cameras located at the corresponding locations. For each of the routes considered, 12 or more people walking at natural velocity (thus not clearly rushing) were chosen and the mean time and the standard deviation (or variance)

---

[7] α and β are used for the flow here to distinguish between inflow and outflow. Although the same notation was used for the theoretical uni-dimensional CA, α and β here are physical quantities expressed in $(m \cdot s)^{-1}$.
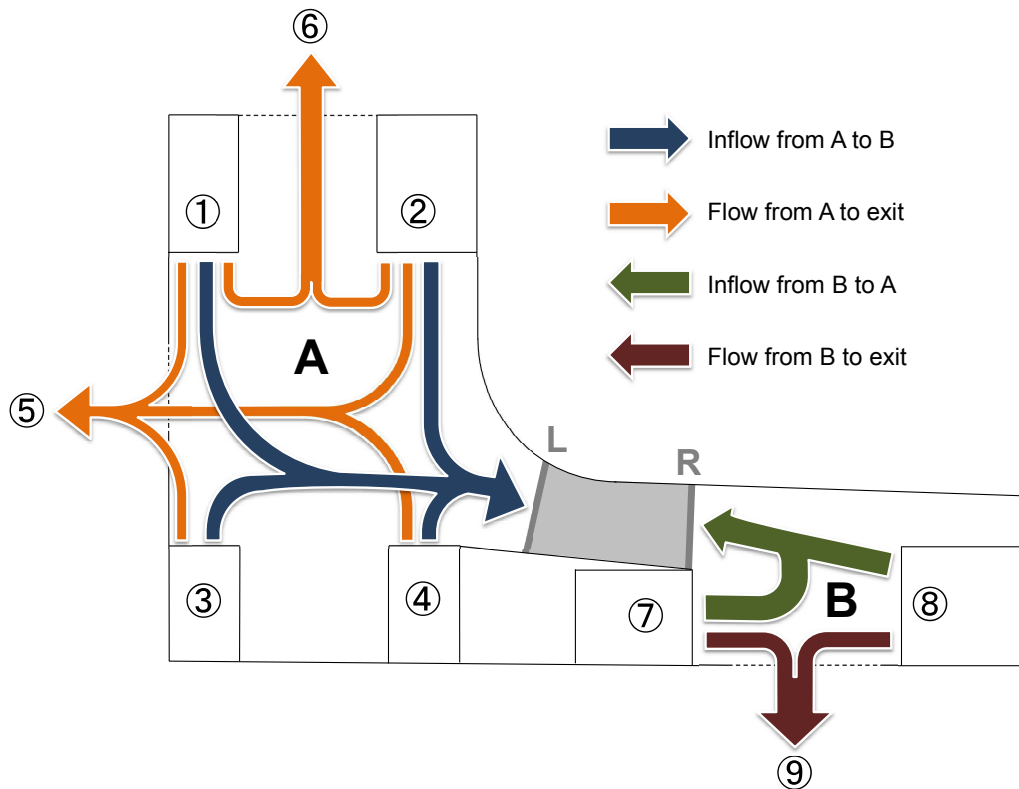
(a) Inflow composition
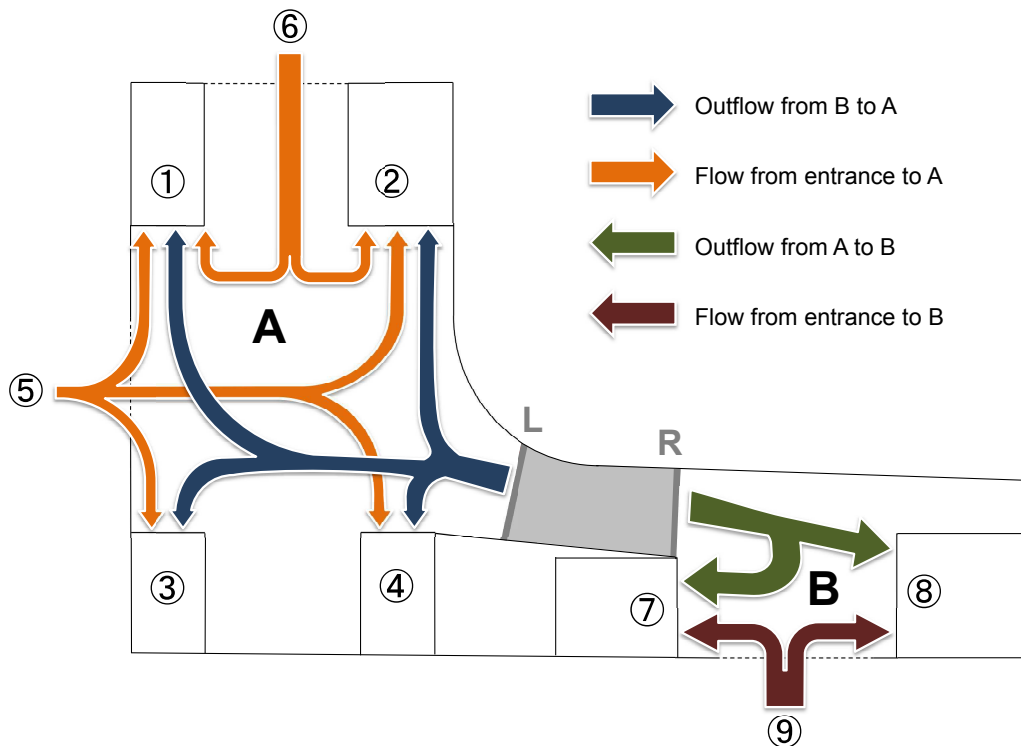
(b) Outflow composition

Figure 2.13: Schematic representation of the composition of the flows resulting in the narrow section in the subway station. Numbers in circles represent the position of the corresponding cameras. "L" and "R" represent the left and right side of the narrow section [124].

Table 2.5: Data matrix containing the number of passenger passing through camera 1, 3, 7, 8 and 9 during the given time period, categorized by their direction and moving mode (ST = stairs, ESC = escalator).

Camera		1			3			9	
Direction		To	From		To	From		In	Out
		Concourse B			Concourse B			Station	
Mode		ST	ST	ESC	ST	ST	ESC	-	
08:00:00	08:00:05	3	0	2	4	0	5	2	3
08:00:05	08:00:10	2	0	4	2	0	3	1	1
08:00:10	08:00:15	0	0	2	0	0	5	1	4
08:00:15	08:00:20	0	1	3	1	0	6	1	1
08:00:20	08:00:25	0	0	4	1	0	8	0	5
08:00:25	08:00:30	0	0	4	1	0	5	0	3
08:00:30	08:00:35	0	0	7	0	0	6	1	5
08:00:35	08:00:40	1	0	3	1	0	8	0	6
08:00:40	08:00:45	0	0	2	0	0	1	0	1
08:00:45	08:00:50	3	0	2	3	0	2	0	3
08:00:50	08:00:55	3	0	2	2	0	2	0	2
08:00:55	08:01:00	3	0	0	3	0	0	0	9

Camera		7				8			
Direction		To		From		To		From	
		Concourse B				Concourse A			
Mode		ST	ESC	ST	ESC	ST	ESC	ST	ESC
08:00:00	08:00:05	13	7	0	1	19	8	0	2
08:00:05	08:00:10	13	9	0	2	18	5	0	6
08:00:10	08:00:15	11	7	0	4	18	9	0	3
08:00:15	08:00:20	9	8	0	4	16	4	0	3
08:00:20	08:00:25	10	8	0	4	13	8	0	2
08:00:25	08:00:30	14	8	0	1	16	10	0	5
08:00:30	08:00:35	8	8	0	1	14	6	0	4
08:00:35	08:00:40	8	2	0	5	11	7	0	3
08:00:40	08:00:45	10	3	0	4	8	6	0	1
08:00:45	08:00:50	7	2	0	4	5	6	0	2
08:00:50	08:00:55	3	0	0	4	5	5	0	3
08:00:55	08:01:00	0	0	1	4	1	2	0	3

were computed as given in Table 2.6. For the routes leading to the exit an average value valid for the whole concourse had to be used, since in some cases passengers would use different exits (such as for position 1 or 4, where exit 5 and 6 are almost at the same distance), resulting in a slightly higher deviation. The walking time values were used to perform the phase shift to adjust the different flows during the total in- and outflow calculations.

Table 2.6: Walking time and average distance/speed for the routes considered [124]. Note that in the case of the entrances/exits it was not possible to determine the one used by each single passenger and therefore an averaged value for the time required to leave the concourse was used. Variance is computed using the standard deviation.

| Route | Walking time | | Average | | Sample size |
	Average	Variance	Distance	Speed	
$1 \leftrightarrow L$	27.3 s	3.9 s	37.9 m	1.39 m/s	12
$2 \leftrightarrow L$	15.3 s	2.3 s	22.2 m	1.46 m/s	12
$3 \leftrightarrow L$	24.9 s	3.5 s	30.7 m	1.23 m/s	12
$4 \leftrightarrow L$	8.7 s	2.2 s	12.4 m	1.43 m/s	12
$5 \leftrightarrow L$	15.4 s	2.6 s	20.2 m	1.32 m/s	24
$6 \leftrightarrow L$	23.0 s	4.2 s	31.4 m	1.36 m/s	24
$7 \leftrightarrow B$	6.4 s	2.5 s	–	–	12
$8 \leftrightarrow A$	15.9 s	4.7 s	–	–	24
$9 \leftrightarrow A$	21.4 s	5.8 s	–	–	24

The walking time obtained from the video analysis was consistent with some simple measurements performed on-site from the author by walking between different locations. In addition, the distance for each route was computed using an accurate map of the station provided by the operator (Tokyo Metro Co.,Ltd). The average walking speed obtained is consistent with the values typically found in the literature, reporting a walking speed in free flow conditions usually between 1.3-1.5 m/s [125, 65, 126]. The walking time between left and right side of the narrow section can be computed using the average walking speed and the length of the section (11.1 m, see Figure 2.14), resulting in about 8 s (because of the limitations imposed by the unfavorable location of cameras 10 and 11, a calculation from video frames was not possible).

To verify the reliability of the data obtained, the total number of people entering and exiting the narrow section between clearly distinct train arrivals was computed using the tabulated data matrix compiled. If people were counted accurately and the flows had been correctly combined, than the number of people entering the narrow section in a given time period must be the same to the people leaving from the opposite side. In fluid-dynamic terms, mass conservation must be satisfied:

$$\int_{t_{start}}^{t_{end}} \alpha_{A \to B} dt dx = \int_{t_{start}}^{t_{end}} \beta_{A \to B} dt dx \tag{2.31}$$

$$\int_{t_{start}}^{t_{end}} \alpha_{B \to A} dt dx = \int_{t_{start}}^{t_{end}} \beta_{B \to A} dt dx \tag{2.32}$$

with α and β being the in- and outflow and t_{start} and t_{end} the start and end time for validation.

A discrepancy of about 2.5% was found for the number of people moving from concourse A to B and about 2.0% for the opposite direction. Considering the large number of people counted (more than 30'000) and the intermediate steps required to obtain the total in- and outflow, the accuracy reached can be considered more than satisfactory.

Finally, the phase-shifted total in- and outflow results were converted from the 5 s interval format used for simple pedestrian counting to the standard $(\text{m}\cdot\text{s})^{-1}$ unit used to indicate pedestrian flow by also using the dimensions of the narrow section given in Figure 2.14.
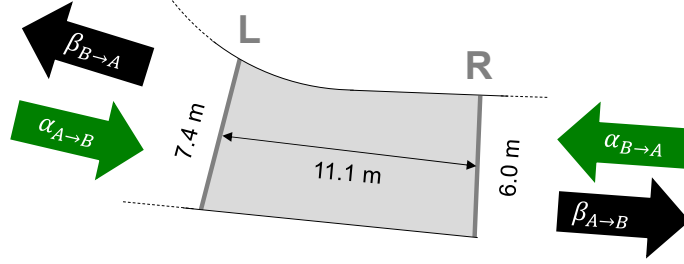

Figure 2.14: Dimensions of the narrow section considered. Surface is about 72 m^2 [124].

In order to obtain clear graphs, the resulting flow was finally filtered using a low pass filter reducing the noise present in the original 5 s resolution data. Choice of the cut frequencies for the low pass filter was based on the simple criteria that noise needs to be reduced to a satisfactory level to make the results easier to read, but, on the other side, important characteristic features present in the signal needs to be preserved to allow an understanding of the phenomena observed.

In addition to the unsteady flow, we computed the cumulative curve of the number of passengers for inflow and outflow in the narrow section. By using the cumulative curve, additional information such as density and average transit time can be obtained. In particular, the vertical difference between cumulative in- and outflow gives the number of people in the narrow section at a given time (thus allowing density calculation). On the other hand, the horizontal difference between cumulative in- and outflow represents the average crossing time when the given cumulative number of people is reached. Additionally, as we discussed earlier, being an important parameter for understanding the formation of congestion, flow ratio was also computed. The inflow ratio (from now on simply flow ratio) used here is defined as:

$$r = \frac{\alpha_{A \to B}}{\alpha_{A \to B} + \alpha_{B \to A}} \tag{2.33}$$

where $\alpha_{A \to B}$ and $\alpha_{B \to A}$ are the inflows on both directions.

2.4.3   Results and discussion

For the most significant moments of the roughly 2 hours considered (and the 45 minutes analyzed) we computed the in- and outflow on both sides of the narrow section, the density and the (in)flow ratio. In this section the most significant results are presented and discussed.

Free flow

In Figure 2.15(a) the in- and outflow for the two directions considered (from concourse A to B and the opposite direction) are represented for a free flow situation. The vertical

lines visible in the figure indicate a train arrival at the given time on the corresponding concourse. As one would expect, after each arrival, there is an increase in the inflow of pedestrians in the narrow section. This is particularly clear in the case of concourse B to A, because the number of arrivals on concourse B is limited and fairly uniformly distributed. In the opposite direction train arrivals are more numerous and it becomes more difficult to distinguish each peak. The in- and outflow peak centers are separated by a 10 s difference, which is approximately the walking time through the narrow section (remember that the original sampling rate was 5 s).

In general it can be stated that the shape of the inflow curve, registered when passengers enter the narrow section, is quite similar to the shape of the outflow registered when they exit from the opposite side. Both can be described in terms of Gaussian distribution. However, looking in detail when comparing the in- and outflow, a reduction in the flow peak height (or amplitude) and a slight increase in the width are observed in both directions. To explain this behavior one need to remember that we combined fluxes in several locations by using the average walking speed (or time, strictly speaking) to adjust the phase shift between the different signals. However, in reality, a Gaussian distribution is observed for the velocity of pedestrians (as we have seen for example in the data by Zhang et al.). In fact, observing the videos, people leaving at first the trains tend to rush toward the destination (running through the narrow section), while people leaving last tend to walk at very low pace. For this reason, even during free flow, a slight change in the flow is observed after entering the narrow section. This is particularly true in the case of movement from concourse B to A, because people leaving the test area on the left side are observed only after 20-30 s in the different cameras.

As a last consideration, it is possible to observe that there is a certain delay between the arrivals on both concourses (simultaneous arrivals are limited and the number of passengers small), thus resulting in a smooth flow during the whole time period considered. Concerning the total flow given in Figure 2.15(b), similar considerations to the above remarks can be made. In particular, about 4 distinct inflow peaks are recognizable, each clearly visible in the total outflow. One can notice that the reduction in the 3rd peak is slightly more accentuated compared to the others. This may suggest some kind of slowing down, which could be linked with a weak congestion. We will discuss about this next.

Organized flow with lanes

Now we will consider a different time period, for which the single and total flows are given in Figure 2.16. Arrivals on both concourses are no longer uniformly dispersed (as observed in the previous case). For both directions it becomes more difficult to relate each outflow peak with the inflow curve which generated it. In particular, by looking at the total flow graph, it seems that there is no relationship between both curves, except the fact that they initially grow starting from a similar time.

During this time period we observed the formation of lanes in the narrow section. In general, compared to the previous case we observed a more constrained and organized flow. People had to consider more carefully their own way, as people coming from the opposite direction were making a sort of resistance to their forward motion. However, we did not observe any complete or partial stop here, as people did not have to significantly slow down to cross the narrow section. It is interesting to notice, that, although slightly higher, for most of the cases the total flow in this period is comparable with the one registered in the free flow case. This suggests that the total flow alone cannot be taken as a single parameter in determining the flow regime which one will observe. Also here
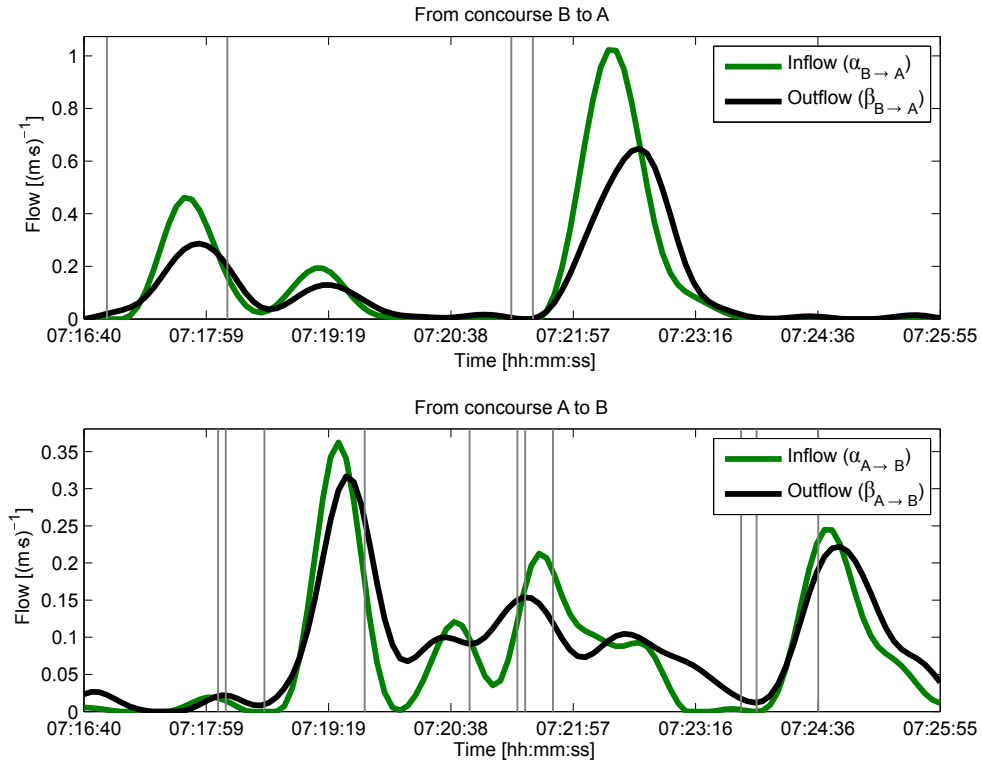
(a) In- and outflow in the different directions
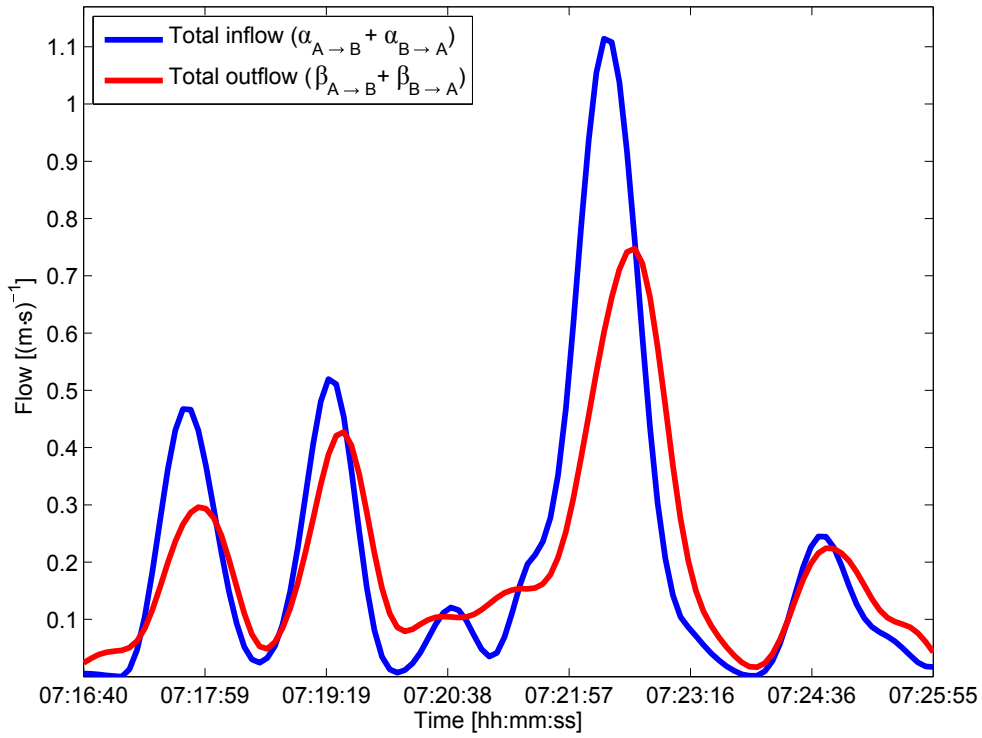
(b) Total in- and outflow in the narrow section

Figure 2.15: Flow in the narrow section when free flow was observed [124].

(as we have seen from the literature), the flow ratio seems to play an additional role.

Congestion and partial deadlock

Finally we will analyze the cases during which congestion and partial deadlocks were observed [8]. The total flow and the flow in both directions are reported in Figure 2.17, 2.18 and 2.19.

In the first case (Figure 2.17(a)), a double train arrival on both tracks connected to concourse B (arrival lines overlaps in Figure 2.17(a) and only a single line is visible) results in a large crowd moving to concourse A to exchange train line. The flow in that direction reaches about 1.5 $(m \cdot s)^{-1}$, more than the total flow measured during free flow. At the same time, an arrival in concourse A creates a flow of passengers moving to concourse B. The resulting inflow in that direction, although smaller than the opposite one, is still remarkable, reaching a maximum of about 0.6 $(m \cdot s)^{-1}$. As a result we saw a large number of people moving simultaneously to the narrow section considered. Congestion (or a partial deadlock) clearly formed, with people in the direction A → B having to significantly slow down and briefly stop because they could not find a way through the larger crowd coming from the opposite side. By looking at both graphs in Figure 2.17(a) it can be noticed that inflow curves clearly grow up and decrease forming a Gaussian shape. However, a different shape is observed in the outflow: the flow first grows, then reaches a local maximum and later slightly decreases. In this portion of time some people had to stop or significantly reduce their speed, especially in the direction A → B. Later, pedestrians can find a way through the crowd, which, by becoming less dense can be penetrated easier (in a sort of percolation-like behavior). This leads to a small increase of the flow in both directions, before finally decreasing as only few passengers still have to cross the narrow section.

The same behavior was observed during another partial deadlock event given in Figure 2.18. In this case, the double peak observed in the total flow during the event is even more evident. In particular, in the lower graph of Figure 2.18(a), it is clear that the sudden increase in the outflow (after reaching a stable value) must be related to some phenomena which happened inside the crowd, as the inflow clearly decreases in the corresponding time period. In both cases the maximum total flow registered was close to 2.0 $(m \cdot s)^{-1}$, clearly higher than the flow we observed in free flow and organized scenarios.

A similar double peak shape was observed in different occasions during the 45 minutes analyzed (like in the time period reported in Figure 2.19 where two characteristic double peaks are recognized). In all the cases, the heavy congestion could be recognized by looking at the cameras capturing the crowd motion in the narrow section. The largest total flow recorded in our study for the time periods considered corresponded to 2.13 $(m \cdot s)^{-1}$ (see Figure 2.19(b)).

Transition to congestion

Coming back to Figure 2.17, it is interesting to notice that the second large peak in the direction B → A (at around 08:03) is not related to any congestion phenomena, although its magnitude is not much different from the first peak. By carefully looking at the corresponding time period (from 08:01) in both graphs in Figure 2.17(a), it can be noticed that crowd motion in both directions is smoothly shifted, thus preventing the formation of a large counter-flow. To better understand this aspect we can compare the

---

[8]Partial deadlock is used here to indicate that some pedestrians had to stop, complete deadlocks almost never appear in reality.
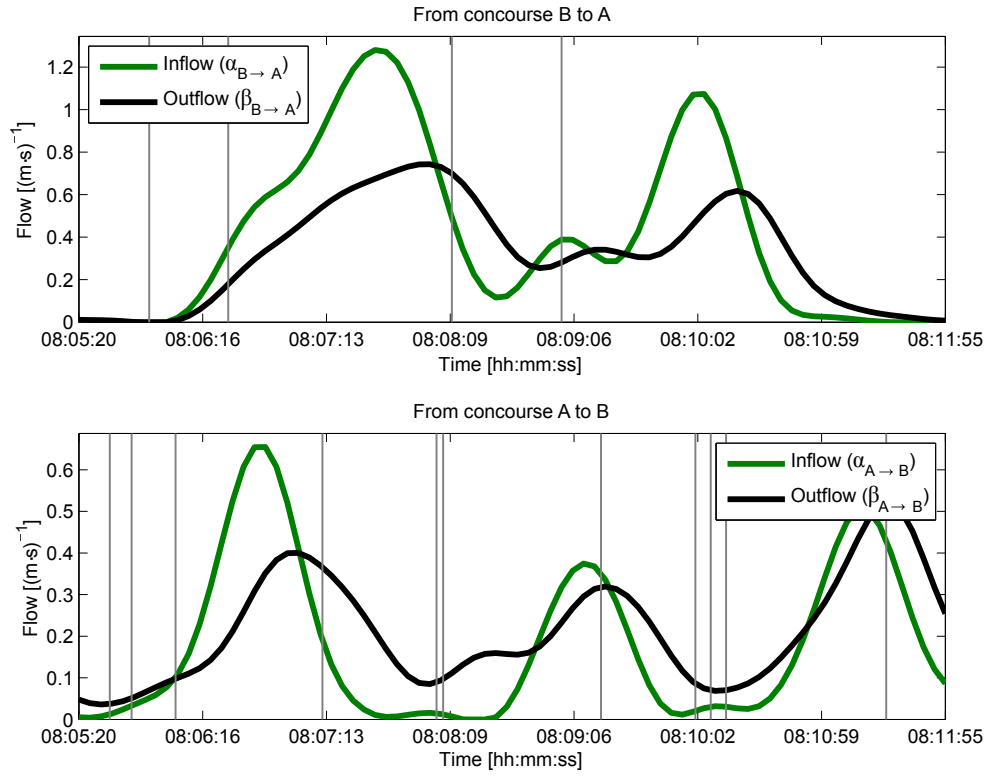
(a) In- and outflow in the different directions
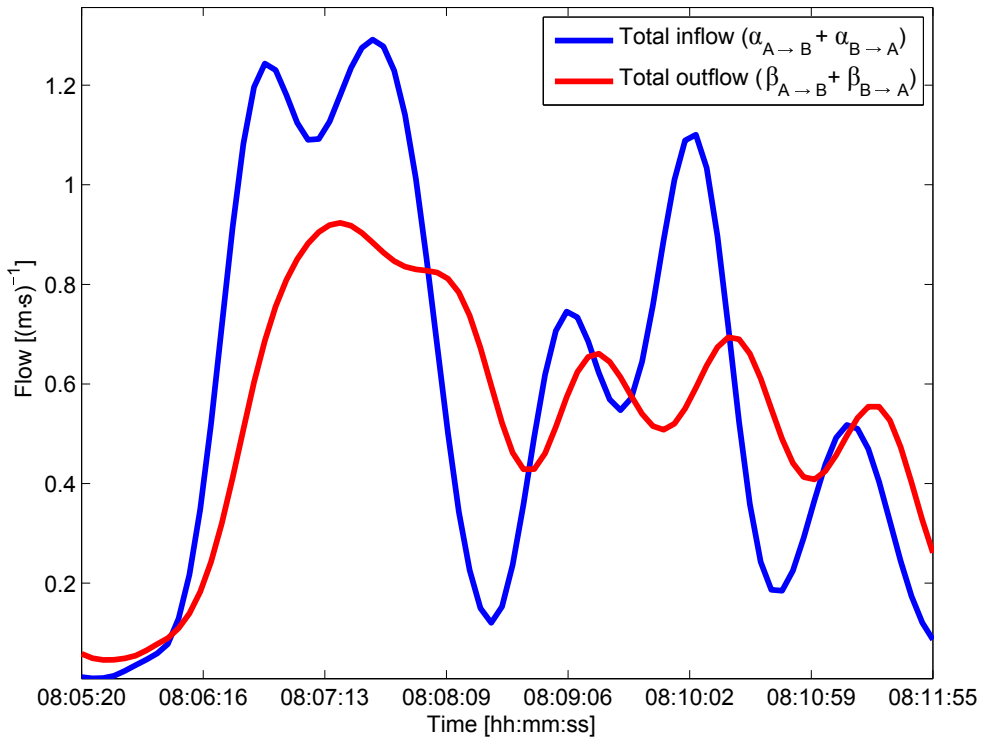
(b) Total in- and outflow in the narrow section

Figure 2.16: Flow in the narrow section when lane formation (organized motion) was observed [124].
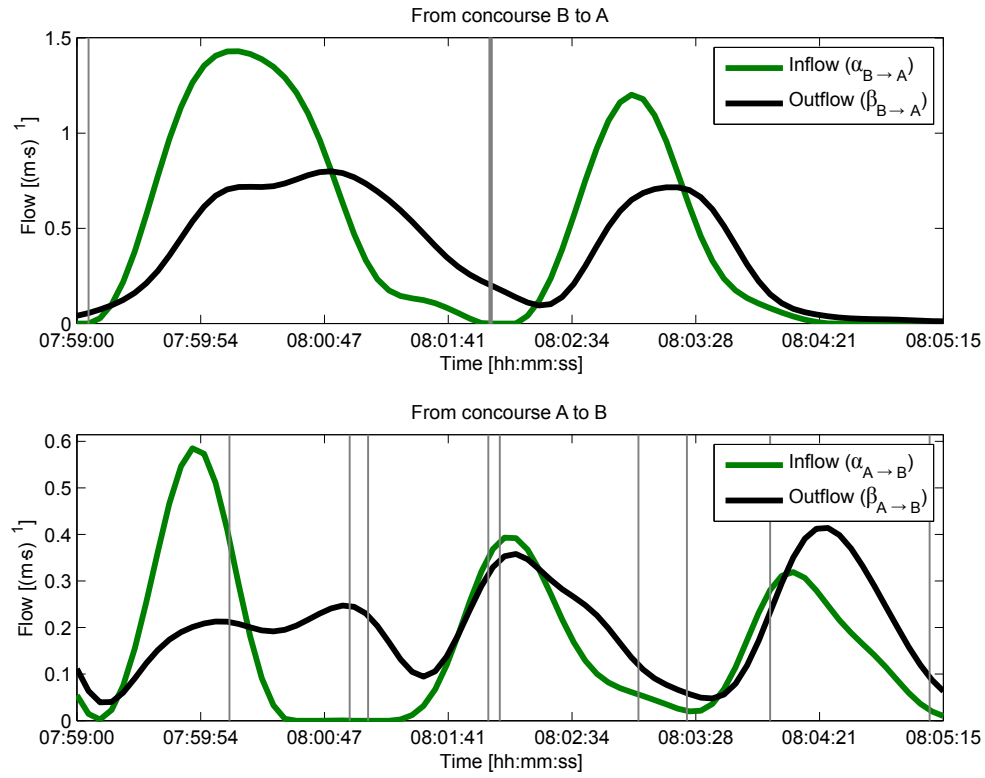
(a) In- and outflow in the different directions
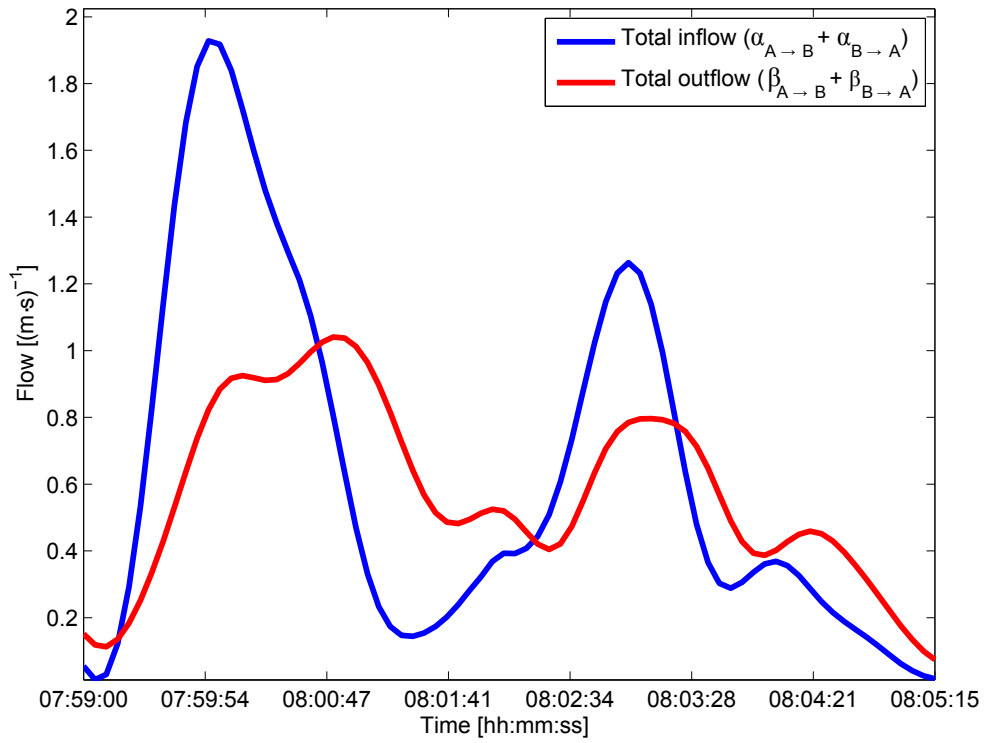
(b) Total in- and outflow in the narrow section

Figure 2.17: Flow in the narrow section when congestion was observed [124].
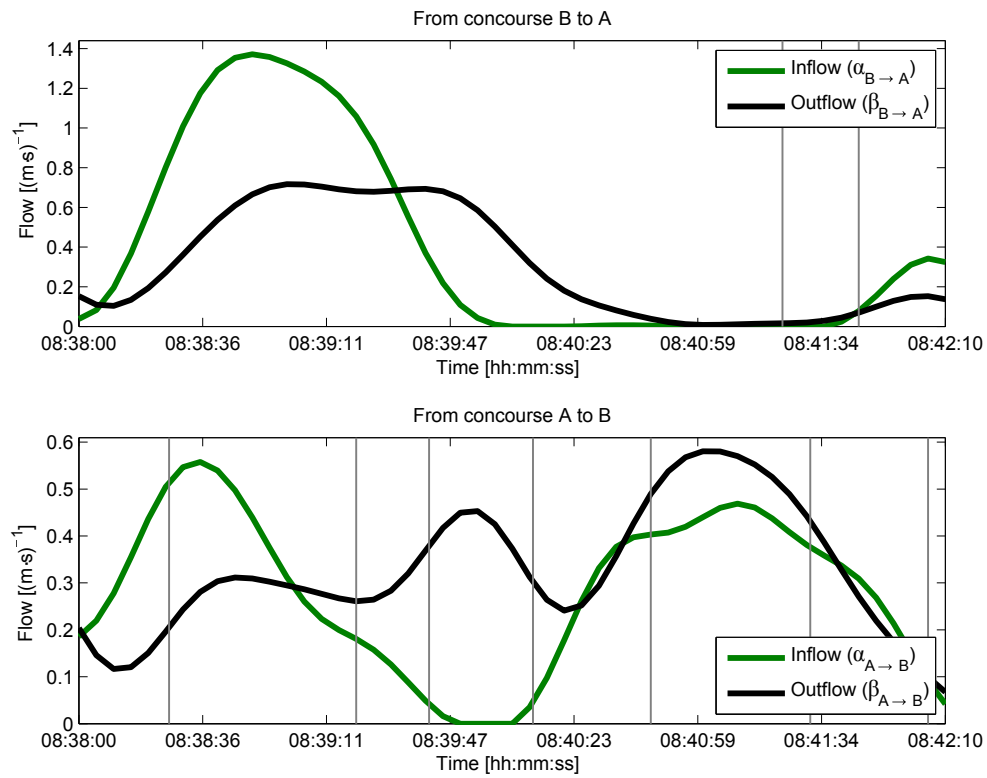
(a) In- and outflow in the different directions

(b) Total in- and outflow in the narrow section

Figure 2.18: Flow in the narrow section when congestion was observed [124].

(a) In- and outflow in the different directions

(b) Total in- and outflow in the narrow section

Figure 2.19: Flow in the narrow section when the maximum inflow was recorded. Congestion resulting in partial deadlocks was observed [124].

flow ratio with the density inside the narrow section at different times. Figure 2.20(a) shows the cumulative number of people entering and leaving the narrow section during the time period corresponding to Figure 2.17. At the beginning th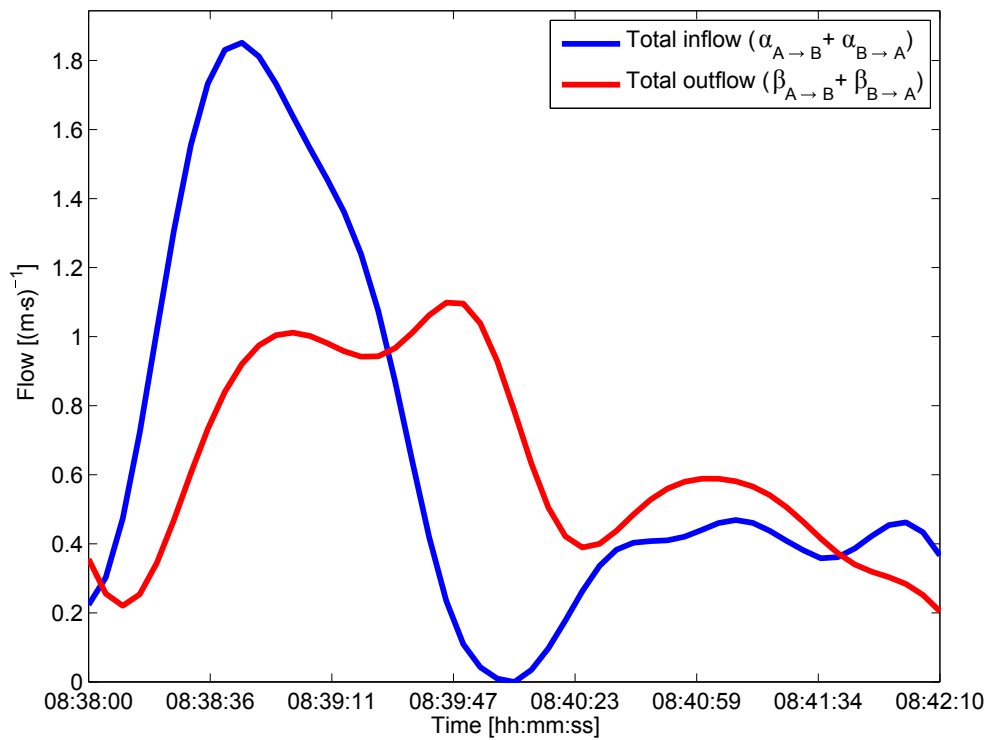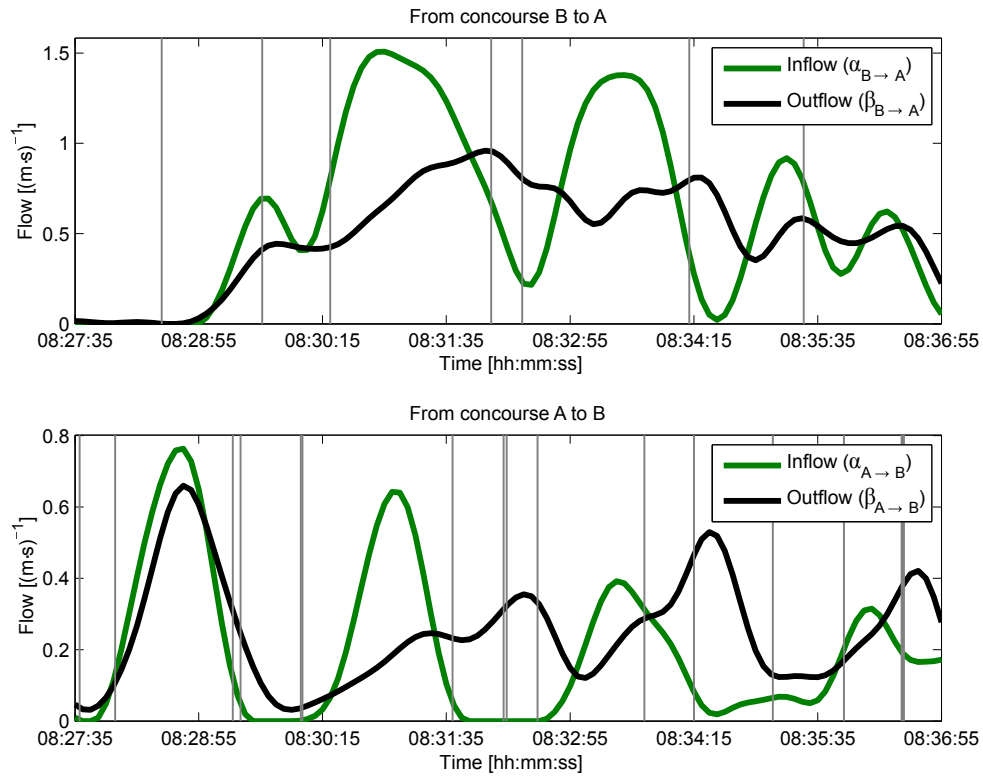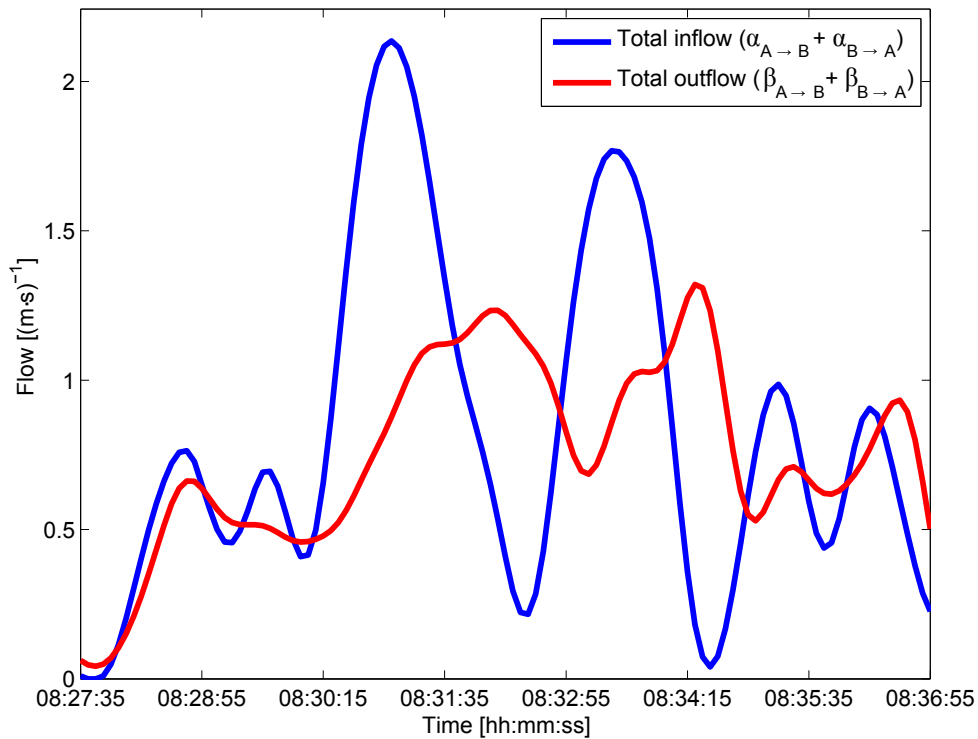e corridor was empty, thus creating the necessary conditions for the analysis based on the cumulative graphs. First, both the cumulative inflow and outflow grow as people enter the narrow section and promptly leave from the opposite side. After a short time cumulative inflow grows more rapidly, therefore indicating that someone needs more time to cross the section and people start to accumulate within it. After a while, both curves become closer again as the flows in both directions approach zero. Later, a new set of train arrivals leads to a new increase of both curves to finally converge again when the corridor empties. The small difference visible at the end of the curves is related to the previously discussed error resulting from manually counting the passengers and combining the data of the different cameras (about 2% here).

The vertical difference of both curves in Figure 2.20(a) gives the number of people in the narrow section at any given time, which, divided by its surface, gives the density indicated in gray in Figure 2.20(b). By comparing this curve with the flow ratio, it can be observed that a steep increase in the density is found when the flow ratio is close to 0.5 (balanced flow). In the first half of the graph it can be noticed that when the flow ratio reaches a value of about 0.3 a steep density increase occurs. In the second peak the flows in both directions are less balanced, thus preventing a sudden increase of the density inside the narrow section. A similar behavior was observed in different time periods corresponding to highly crowded situations. The same type of phenomenon is observed for the time period corresponding to Figure 2.19, for which the cumulative curve, the density and the flow ratio are reported in Figure 2.21. Like in the previous case, even here, the increase in density after 08:30:15 is associated with an increase of the flow ratio, meaning that a counter flow is obstructing the motion of the pedestrians in the main flow. Although the flow is not perfectly balanced in this last example, it seems that under extreme conditions (high monodirectional flow) a small amount of counter flow can quickly lead to a density increase, as pedestrians find it more difficult to pass the incoming crowd. A similar event is observed after 08:32:55 when another partial deadlock event occurred.

Concluding, as previously suggested, we confirmed that the formation of deadlocks is obviously related with the total flow, but flow ratio plays an important role and therefore needs to be considered closely.

Flow regime categorization

Besides the importance of the flow ratio in pedestrian bidirectional flow, we found that there is a connection between the in- and outflow curves and the type of flow observed. In the case a finite crowd crosses a corridor in opposite directions, the type of flow observed can be described by looking at the shape of the recorded outflow, as schematically given in Figure 2.22. In the case of free flow a Gaussian inflow curve will result in a very similar curve in the outflow. In an organized scenario (with lane formation), the shape of the outflow curve will change, but a single peak Gaussian curve is still recognized. When congestion and partial deadlock occurs a curve including a double peak is observed instead.

Because tracking information such as position or speed were not available for each pedestrian, we could not use numerical indexes such as the order parameter to classify each flow regime. Therefore we decided to classify the flow regime for each inflow-outflow combination (which is roughly corresponding to single or very close train arrivals in this study)
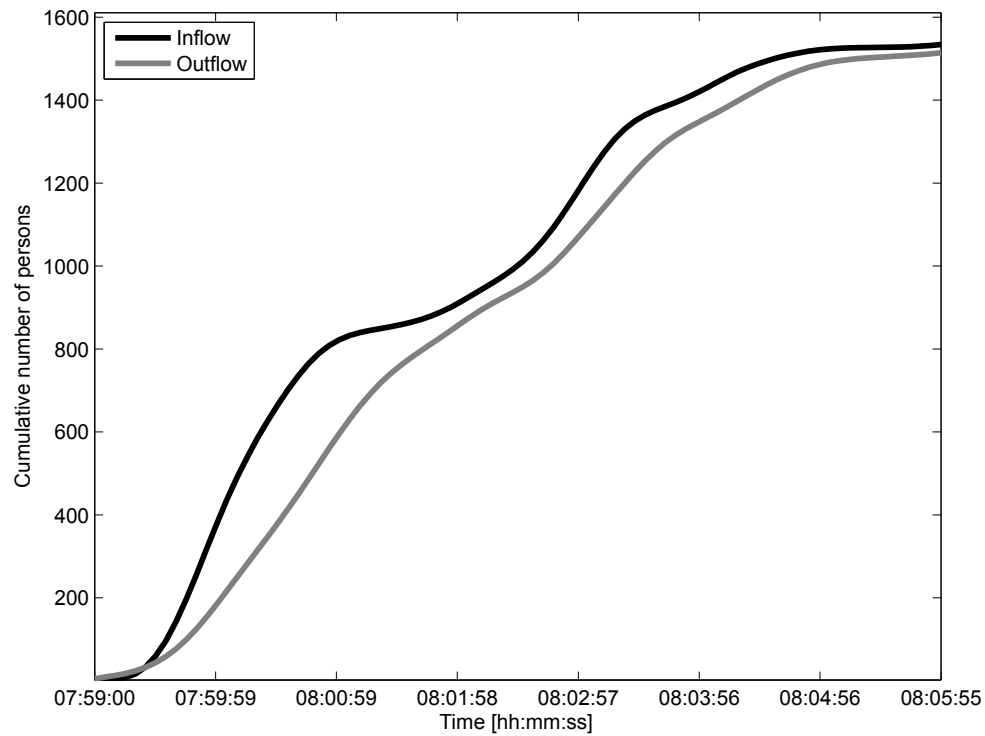
(a) Cumulative number of people in the narrow section
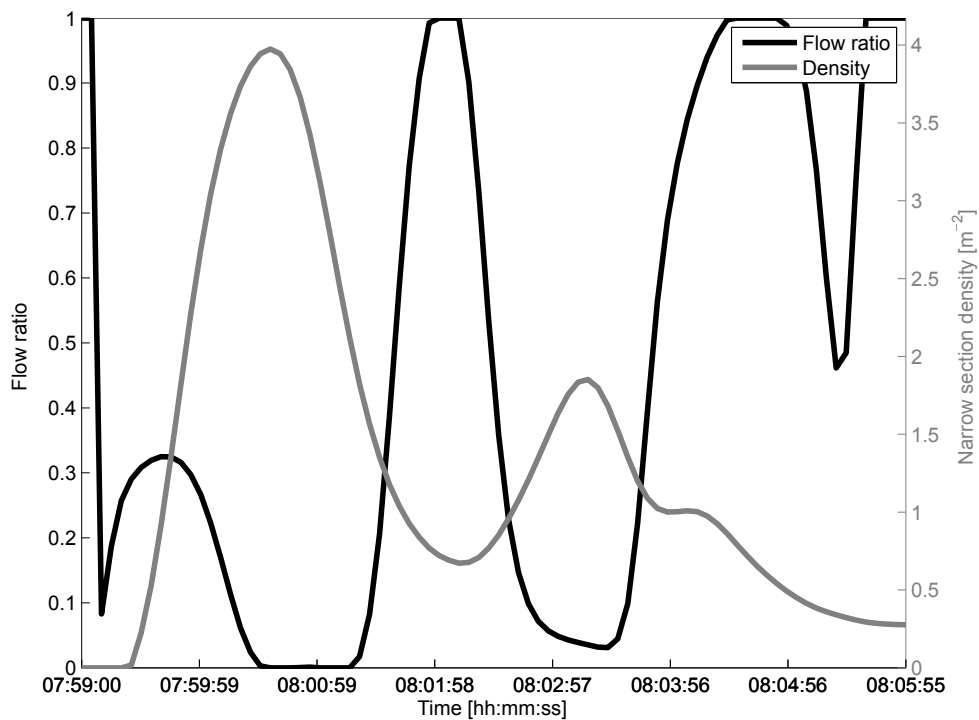
(b) Flow ratio and density in the narrow section

Figure 2.20: Cumulative number of people, flow ratio and density during a partial deadlock event [124].
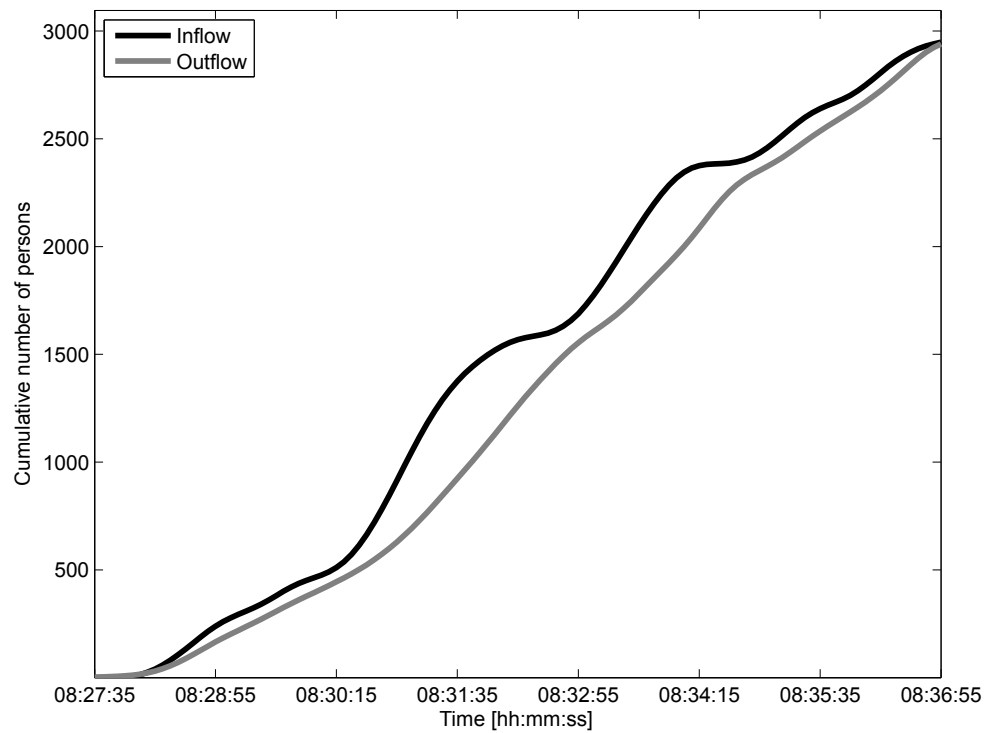
(a) Cumulative number of people in the narrow section
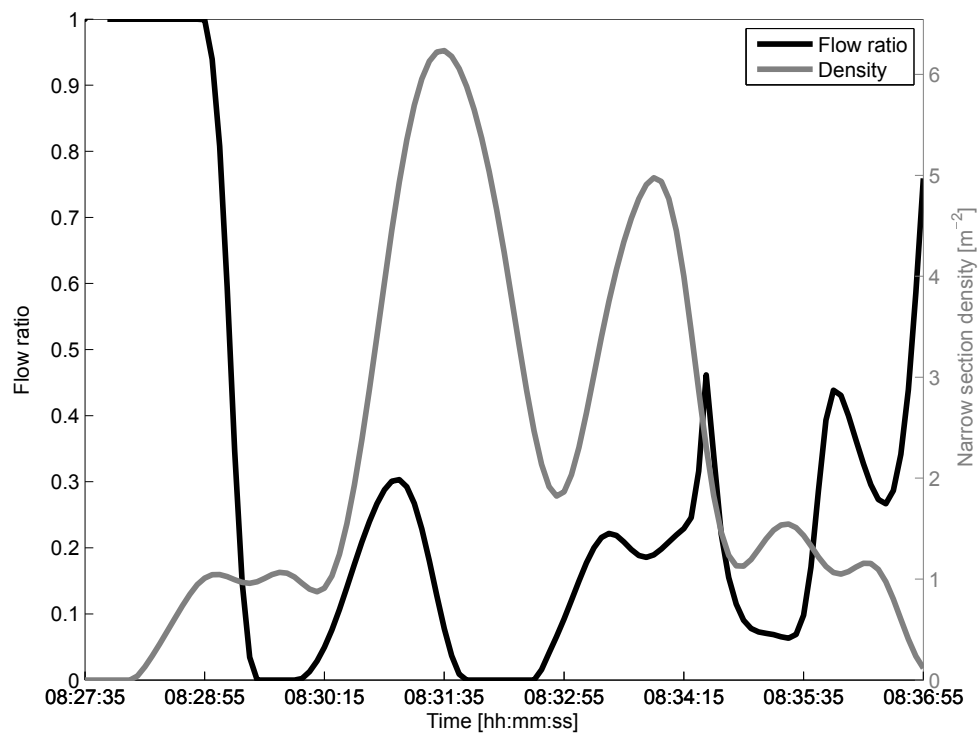
(b) Flow ratio and density in the narrow section

Figure 2.21: Cumulative number of people, flow ratio and density during a partial deadlock event [124].
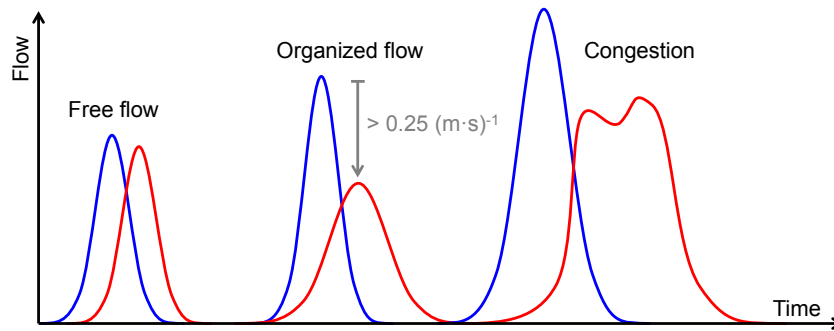
Figure 2.22: Type of flow categorized based on the shape of the in- and outflow [124].

based on the qualitative information contained in the video. Concerning the inspection of the videos, categorization was carried out based on the following qualitative criteria:

- Free flow: pedestrians move in complete freedom and there is no correlation between the movement of the individuals. Distinctive feature of this flow regime is that pedestrians can turn easily because their motion is not constrained by the surrounding crowd.

- Organized flow: some collective behavior is observed in the crowd, the most prominent being the spontaneous formation of lanes. Walking speed in this case is not significantly different from free flow, but lateral movements are constrained.

- Congestion (with partial deadlock): several pedestrians have to stop or significantly slow down because of the large crowd created and the strong counter-flow. The slowing down/stopping behavior is usually observed in the minor flow.

In general we found a good agreement between the criteria based on flow curves and the qualitative recognition. In particular, all the characteristic double peaks were found being related to partial deadlocks, with pedestrians having to stop or significantly slow down. Distinction between free flow and organized flow was more difficult, especially considering that analysis was originally based on qualitative criteria. However, we found that it is possible to set a quantitative criterion to distinguish between free flow and organized flow. In fact, when the difference between the in- and outflow peak was less than 0.25 $(\text{m·s})^{-1}$, free flow was observed. A peak difference larger than 0.25 $(\text{m·s})^{-1}$ with a single peak corresponded to organized flow. The 0.25 $(\text{m·s})^{-1}$ flow drop (difference) criterion is therefore successfully discriminating the categorization based on qualitative aspects.

2.4.4   Summary

As we have seen, most of the articles reported in the literature and considering different flow regimes are either numerical simulation (and therefore difficult to relate with real-life phenomena) or devoted at finding the capacity (i.e. the limit for organized motion). In this study we reported the results of an observation including three different regimes and considering high density crowd.
More in detail, by analyzing the motion of pedestrians crossing a narrow section from opposite directions, we observed characteristic shapes in the curves of total in- and outflow. When a group of pedestrians crossed the test section, a typical Gaussian curve was formed in the total inflow (as a consequence of the velocity distribution being also Gaussian). The outflow curve, however, had different shapes depending on the phenomena which occurred

in the test section. For instance, a Gaussian peak having height and width similar to the one observed for the inflow indicates that free flow occurred. The widening of the width in combination with a reduction of the peak's height signals an organized flow with lanes. The observation of a double peak combination in the outflow (although this characteristic was not present in the inflow curve) points out the emergence of congestion and a partial deadlock during the given time.

In addition, in this on-field study, we confirmed the importance of the flow ratio for determining the flow regime at a given total flow. This study can be relevant for understanding the phenomenological distinction between different flow regimes and can provide important data to validate and develop numerical codes used for the prediction of these phenomena. However, since only time-dependent aggregated quantities are considered, a microscopic description of the phenomena was not possible and trajectories are required on this purpose.

2.5 Supervised experiments

To overcome the limitations found during the empirical observation, in particular regarding the impossibility of obtaining trajectories for pedestrians, different supervised experiments has been performed. Although the general principles are similar to the experiments by Zhang et al. reported in the literature review, objectives and approach taken for data analysis are quite different. In particular, the supervised experiments that will be described in this section deal with low/medium density crowds and the number of participants is lower than the large groups considered by Zhang et al. in their campaign. Here, we will focus on understanding how lanes are formed and why they cannot form in certain conditions. Also, we will consider forward and lateral motion altogether and introduce a more global quantity to be used in bidirectional flows (and more generally in the multidimensional case). In addition, the role of social structures is discussed.

In total, three experimental campaigns were performed using a similar setup but with quite different goals. More precisely these experiments are:

1. A number of experiments involving two groups of pedestrians crossing each other's in a corridor and behaving individually. Technically speaking the term "singleton" can be used to describe this type of social structure. Goal of these experiments was to understand the mechanisms of lane formation and congestion occurrence. This campaign will be referred as "singletons only" (complete individual behavior).

2. The same day, a second set of experiments was performed with the same geometrical setup, but a given portion of the crowd was moving in pairs (some participants were asked to stay close while walking). This is the smallest social group, whose members are only two people and it is referred as "dyad". The goal here was to study the behavior of dyads and understand which impact they have on the performance of the whole group. This second campaign will be referred as "dispersed dyads".

3. A last set of experiments was repeated half a year later with different participants and a slightly changed geometrical setup. This time only singletons were considered (again). The goal of these experiments was to compare and eventually validate the results obtained in the first campaign and see if geometry has an influence. During this last campaign (which will be referred simply as "validation") an innovative method was used to measure body movements (for details see Chapter 3.3.2).

A complete analysis will be presented only for the first set of experiments (the ones with singletons only). For the last two campaigns we will focus on the differences, since many results are the same or very similar (especially for distributions in velocity) to the first case. We will also discuss some differences with the experiments by Zhang et al., but also here the discussion will be limited to analytical techniques introduced here and aspects not reported so far in the literature (conclusions from previous studies were already discussed in the literature review).

2.5.1   Experimental setup

In order to understand qualitatively and quantitatively the influence of flow ratio on bidirectional streams, we used a geometrical setup for the different experiments in which total flow and density are kept at fairly constant level and flow ratio is the only parameter being changed. All experiments were not designed to yield particular results or to confirm some theories developed beforehand (except for the validation experiments), but their main scope was to get as much data as possible (with high accuracy) therefore allowing a critical assessment of the information gained. In this section the details concerning the geometrical layout and the execution of the different experiments are presented and discussed.

Geometrical configuration and technical setup

For all experiments a mock-corridor delimited with band partitions was created on a closed street in front of a tall building (at the university campus). The mock-corridor consisted of three main parts: the measurement area located in the center, two buffer zones located at each side of the central test section and two waiting areas located at both extremes of the buffer zones. A schematic description with dimensions for the whole floor setup is given in Figure 2.23. Sizes given in numbers were constants throughout the different experiments, while w_{corr} and l_{wa} are given in Table 2.7. For corridor width we intend the width of the measurement area and the width of the waiting sections (they are equal).
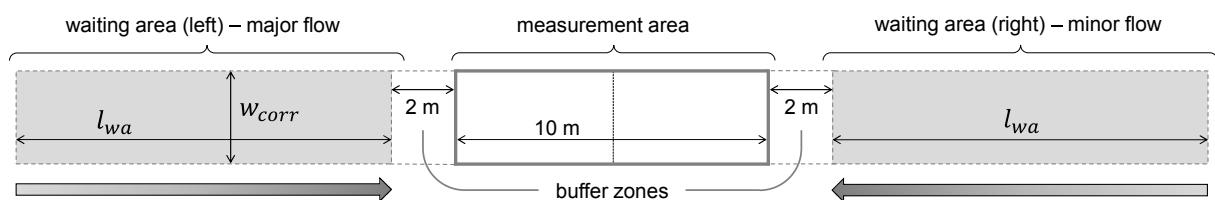
Figure 2.23: Schematic representation and dimensions of the mock corridor used in the different experiments [127].

The buffer zones were used to allow pedestrians reaching a stable speed before entering the measurement area. Although participants were actually already walking when inside the buffer zone, all the results presented in this study only refer to the data gained from the analysis of the measurement area (as the name suggests).

In each waiting area several columns were formed along its length by writing crosses on the ground (see Figure 2.24 and Figure 2.25). The distance between the different columns and the lateral distance between each cross is given in Table 2.7. The first column coincided with the boundary between the waiting area and the buffer zone. The crosses on the ground corresponded with the different starting positions used by the participants during

Table 2.7: Dimensions for the different types of experiment. Mathematical symbols refer to quantities given in Figure 2.23 and Figure 2.24. Singletons only and dispersed dyads experiments use the same configuration (they were performed on the same day).

Campaign	Corridor width w_{corr}	Waiting area length l_{wa}	Start positions (crosses)		
			d_s	d_w	h_d
Singletons only Dispersed dyads	3.0 m	12 m	0.25 m	0.50 m	1.50 m
Validation	2.4 m	13 m	0.30 m	0.60 m	1.00 m
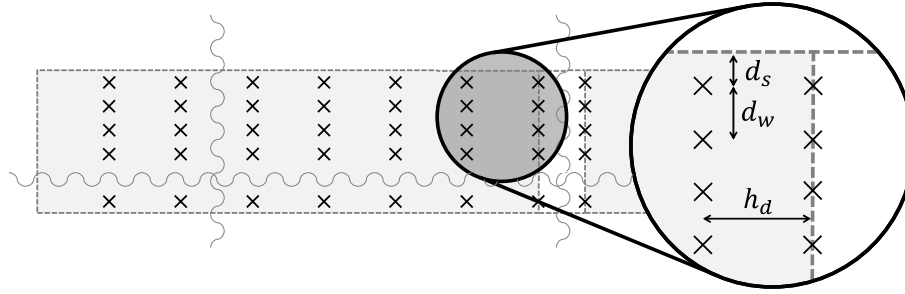
Figure 2.24: Schematic representation of the grid employed in the waiting area [127].

the experiments. In the experiments with singletons only and dispersed dyads the number of positions available matched the number of participants; in the validation experiments the number of position exceeded the number of participants by two.

Three cameras were placed in azimuthal position over the measurement area at an height of 21 m. A high-resolution wide-lens camera was used to record the movements of the pedestrians inside the measurement area. An example for images taken from the central camera is given in Figure 2.25; one may notice that the waiting areas are not covered from the camera's view. The remaining two cameras were pointing to each waiting area to allow keeping a record of the starting positions during each run (for an eventual later exclusion of runs in which participants were taking incorrect starting positions). All the cameras operated at 30 fps (frames per second).

Participants

Participants were recruited among male university students on a voluntary basis and received a fixed compensation for the time spent during the experiments. The participants were given instructions concerning the procedures for the experiments, but they were not aware of the details and the type of measurements which will be gathered. In the singletons/dyads experiments (the first two campaigns performed on the same day) age and free walking speed of participants were obtained. Average age was of 21.03 years and average free walking speed (measured before the experiments started) was found being 1.40 ± 0.10 m/s. In all experiments participants were asked to walk at natural speed, neither rushing nor walking at unnecessary low pace and the obtained free walking speed matches with the values usually obtained for low density urban areas.

All the participants were wearing black T-shirts which were provided at the beginning of the experiments. In addition, depending on the waiting area they occupied and the social group they belonged, different cap colors were used: yellow for the singletons in the left waiting area (composing the major flow) and red for the ones in the right waiting area

(a) Experiment with singletons only

(b) Experiment with dyads and singletons mixed
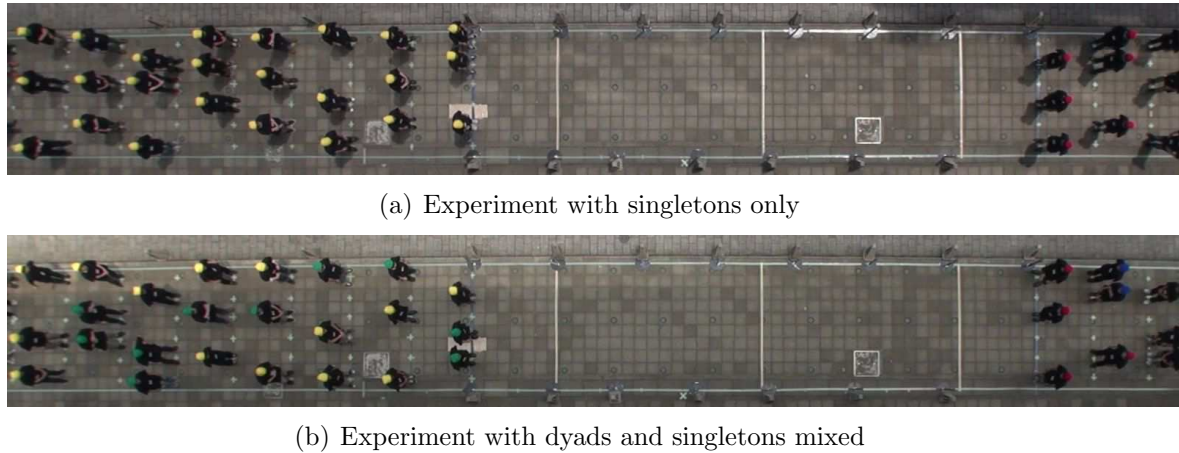
Figure 2.25: Video frames taken before giving the start signal; participants are aligned in the waiting area. Measurement area, buffer zone and waiting area are clearly recognized by white lines. Because of the use of a wide-lens camera, images are distorted at the corners, but distortion in the measurement area is comparatively small. Participants on the left side wear yellow caps (green for dyads), participants on the right side red ones (blue for dyads). In the case of dyads, different starting patterns (line abreast or riverlike) are visible. Configuration for the validation experiment was similar to the singletons only case except for dimensions and number of positions per column.

(composing the minor flow). Dyads in the left waiting area wore green caps and those in the right waiting area wore blue caps.

Table 2.8: Information on participants and weather for the different experiments.

| Campaign | Number of participants | | Date | Weather (temperature) |
	Singletons	Dyads		
Singletons only	54	0	13.06.2015	Partially cloudy (25°C)
Dispersed dyads	30 [9]	24		
Validation	50	0	14.11.2015	Cloudy, light rain (13°C)

During the experiments several breaks were performed to avoid exhaustion of the participants potentially leading to unwanted bias. Weather conditions are given in Table 2.8 with a summary of information regarding participants and social structures. In the validation experiments, it should be noted that although some light rain fell before, during and after the experiments, the results reported here were taken under dry, cloudy weather conditions (breaks were taken when it rained). Finally, it is important to mention that the ratio of dyads (to the total number of participants) was taken to match an empirical value resulting from an observation in a commercial area in Milan, where 42.7% of the pedestrians were found moving in pairs [128] (in the experiment the ratio was 44.4%). Dyads were randomly paired (most of the participants did not known each other's) and asked to walk close to each other's during the experiment reproducing the proxemic behavior of social groups (no instruction was given to them about the spatial pattern to maintain while walking).

---

[9]For the very last procedure with dispersed dyads, only 27 singletons took part since some left earlier.

Execution and instructions

In order to vary the flow ratio, different configurations were tested. We will start the discussion considering the case with only singletons; based on that example the remaining cases can be quickly introduced. In the experiment with singletons a purely unidirectional flow and three different configurations of bidirectional flow were tested. In the unidirectional flow configuration (flow ratio $r = 0$ as minor flow is equal 0) participants in the waiting area took all the available positions provided by the crosses on the ground. Once all participants were waiting in the correct positions a loud oral "start" signal was given and all of them started to walk toward the exit located at the opposite side of the mock-corridor. Participants were asked to start simultaneously at the "start" signal and the distance between them easily allowed such an instruction. After crossing the waiting area located at the opposite side, participants returned to their starting position by walking outside from the measurement area. Participants were asked to keep walking for a long distance after exiting the measurement area to avoid having jam formation at the end of the experiment. A schematic representation of the start positions for this unidirectional configuration is given in Figure 2.26(a). Four different runs were performed in the unidirectional layout and participants were asked to change their starting position on each run. Instructed personnel inspected the waiting area before the start of each run to avoid having the participants in repeating positions (e.g. keeping staying close to a friend/acquaintance or occupying always front/back positions).

In the first bidirectional configuration (see Figure 2.26(b)) 9 participants were moved to the opposite waiting area. Under this configuration some empty places formed in the starting grid of the left waiting area (yellow side). Participants waiting on the left side were asked to take whichever position they liked but to leave one empty spot for each column, while participants on the right side were asked to use one column per person. Supervising staff was present at both left and right waiting areas to avoid participants taking repeating position or starting in a queue configuration (especially in the minor flow). At the "start" signal both groups started walking in opposite directions, thus forming a bidirectional flow inside the measurement area.

Safely assuming that members of the minor flow (right, symbol mn) and major flow (left, symbol mj) have similar free walking speed v_{free}, the flow ratio for this configuration can be computed as:

$$r = \frac{\text{minor flow}}{\text{minor flow} + \text{major flow}} = \frac{v_{free} \cdot \rho_{mn}}{v_{free} \cdot (\rho_{mn} + \rho_{mj})} \tag{2.34}$$

$$= \frac{N_{mn}/A_{\text{wa}}}{(N_{mn} + N_{mj})/A_{\text{wa}}} = \frac{N_{mn}}{N_{tot}} = \frac{9}{54} \approx 0.167 \tag{2.35}$$

where N_{mn} and N_{mj} stand for the number of pedestrians in the minor and major flow respectively (N_{tot} is the total number of participants) and A_{wa} is the surface of the waiting area (same in both directions). Data analysis of the results showed that actual values measured during the experiment are close and in line with the theoretical calculations presented above. This last bidirectional configuration, for which we will refer as 5/1 configuration (figures correspond to the number of persons per column on each side) was repeated four times.

Next, an additional 9 people were moved from the left to the right side, as given in Figure 2.26(c). This time, participants on the right side were asked to leave two spots empty for each column, while participants at the right side took two spots for each column.

Again, this configuration, for which corresponding flow ratio is $r = \frac{2}{6} \approx 0.333$, was repeated four times.

(a) Singletons only unidirectional 6/0 configuration

(b) Singletons only bidirectional 5/1 configuration

(c) Singletons only bidirectional 4/2 configuration

(d) Singletons only bidirectional 3/3 configuration
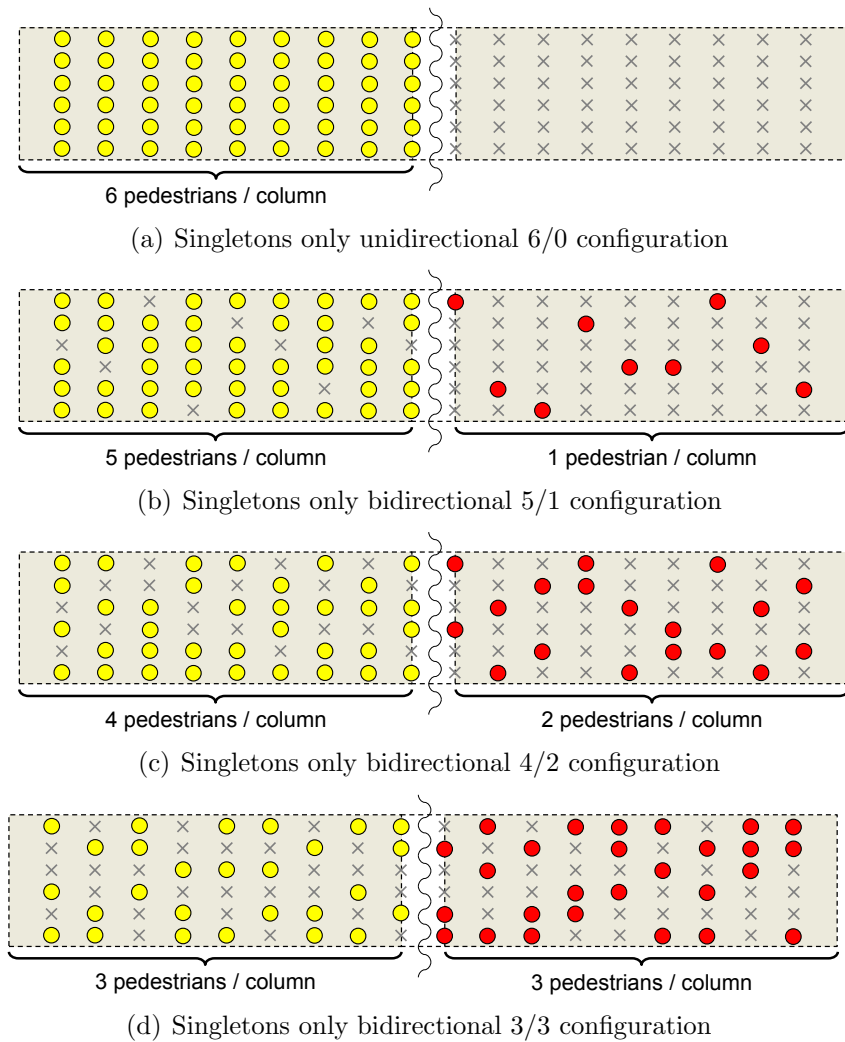
Figure 2.26: Starting positions during the different configurations of the experiment with only singletons [127]. Positions given in the diagram does not necessarily coincide with the actual positions taken by participants during the experiment and are only for illustrative purpose (also, the diagram is not in scale). Crosses represent empty positions, while circles stand for occupied positions. Yellow circles symbolize participants of the major flow and red circles are representative of the minor flow.

Finally, another 9 people were moved from left to right, thus creating the balanced bidirectional flow ($r = \frac{3}{6} = 0.5$) given in Figure 2.26(d). This time both participants on the left and the right side had to take only half of the positions available, leaving three spots empty in each column. Balanced flow configuration was repeated four times also.
After finishing the experiments with singletons a long break was given to participants and dyads (pairs) were randomly formed and instructed for the forthcoming experiments as described earlier. The main concept adopted for the experiments with singletons had been used also for the case with dyads. At first all participants occupied the left waiting area and gradually some of them were moved to the right side to form the minor flow. The main difference in the experiment with dispersed dyads is that members of this social group were asked to form either a line abreast (laterally close) or a riverlike (longitudinal)

pattern already when inside the waiting area. Figure 2.27 illustrates this form of organization by presenting member of dyads connected with a thick line. In the 5/1 configuration because only 1 person per column is allowed in the minor flow only riverlike pattern was possible. Dyads were not given any particular instruction on how to walk but only asked to stay as close as possible, which means that patterns may change during the experiment (as it was observed). Also in the experiment with dyads four repetitions were performed for each configuration.

After testing the different configurations with singletons and dyads uniformly mixed a final special setup was created by having only singletons taking the left waiting area and only dyads taking the right waiting area. Whenever possible, participants were asked to take three positions per column, but in the case of dyads only (right waiting area) it was not always easy to find the right setup allowing a perfect alignment. Therefore in some cases four crosses were occupied and in some other cases only two were used. However, since pedestrians moved after the "start" signal, the singletons vs. dyads case can be considered equivalent to the 3/3 configuration (except the qualitative composition) and in fact measured flow ratio was found being close to 0.5 (balanced flow). This particular configuration was also tested four times. As Figure 2.27(e) shows, only 27 singletons were present in the left waiting area (in the previous trials a total of 30 were present), because some of them left earlier. As we have seen only density is relevant in determining flow ratio, so this small difference was found being irrelevant on the results.

Table 2.9: Experimental configurations and their characteristics during the first two experimental campaigns with only singletons and dispersed dyads (UNI is unidirectional, BI is bidirectional and S/D is the singletons vs. dyads configuration).

		Waiting area			Valid runs	
Case	Type	Major flow	Minor flow	Flow ratio	Singletons only	Dispersed dyads
		[person(s)/column]				
6/0	UNI	6	0	0.000	4	5 [10]
5/1	BI	5	1	0.167	4	4 [11]
4/2	BI	4	2	0.333	4	4
3/3	BI	3	3	0.500	4	4 [11]
S/D	BI	3	3	0.500	-	4

Table 2.9 provides a summary of the procedures previously described with the number of valid runs. As a general rule four runs were performed for each case, but some exceptions exist. The name of the configurations given in Table 2.9 will be later used for discussing the results. We will always refer to each case by using the social group and the corresponding flow ratio configuration. S/D is the singletons (only) vs. dyads (only) configuration given in Figure 2.27(e).

An illustrative example for a video frame taken before the start of the balanced flow experiment is given in Figure 2.25 and Figure 2.28 provides a zoom on the measurement section during the execution of the corresponding experiments.

Finally, the validation experimental campaign is discussed. In this case exactly the same approach taken during the experiments with only singletons was used, except that geo-

---

[10] The very first run was supposed to be a test, but since participants correctly understood the instruction it was also used for data analysis, thus increasing to five the number of runs.

[11] Only three repetitions were considered in part of the analysis, this aspect will be discussed later.

(a) Dispersed dyads unidirectional 6/0 configuration

(b) Dispersed dyads bidirectional 5/1 configuration

(c) Dispersed dyads bidirectional 4/2 configuration

(d) Dispersed dyads bidirectional 3/3 configuration

(e) Singletons only vs. dyads only (S/D) bidirectional configuration
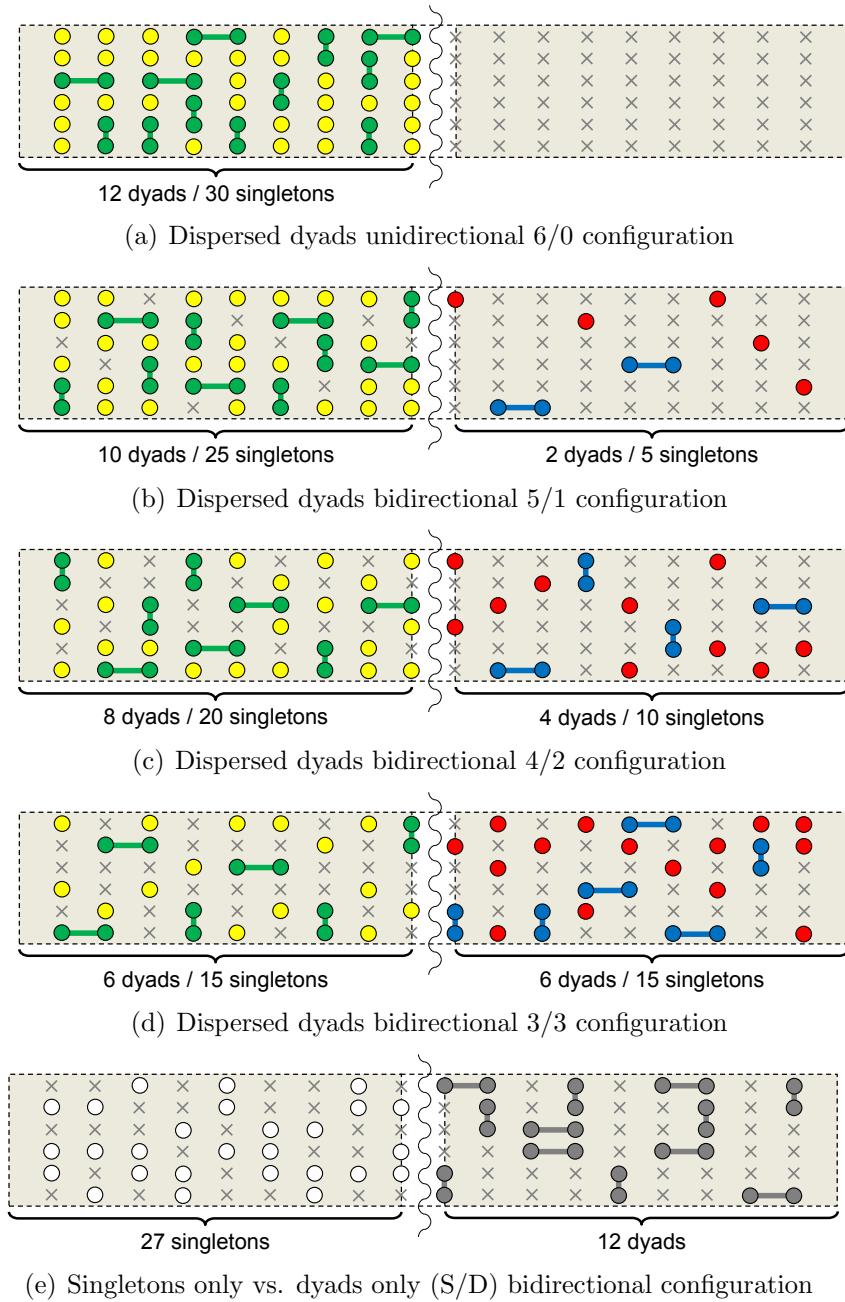
Figure 2.27: Starting positions during the different configurations with dispersed dyads [129]. Image is only for illustrative purpose and not in scale. Dyads are linked with a thick line. Starting positions may form a line abreast or riverlike pattern. In the singletons vs. dyads configuration it was not always possible to exactly having 3 persons/column on the right side, but this case can be considered as a 3/3 configuration and flow ratio was in fact about 0.5. Cap colors for the singletons vs. dyads configuration were mixed and are not given here.

(a) Singletons only BI 3/3 configuration   (b) Dispersed dyads BI 3/3 configuration
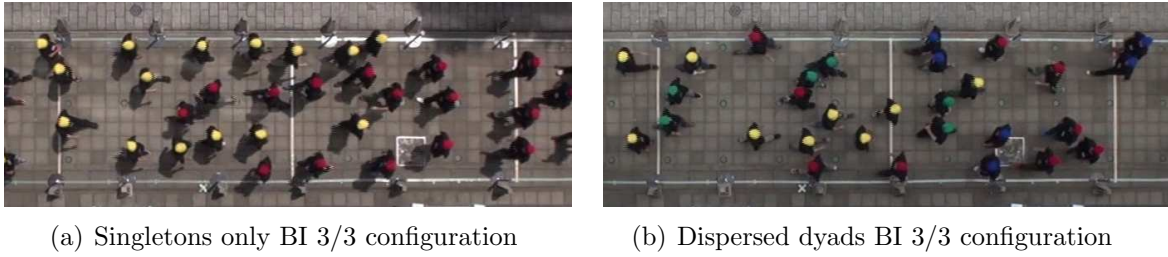
Figure 2.28: Example of video frames taken during the balanced bidirectional flow experiment for singletons and dyads (BI stands for bidirectional). Measurement area is marked with white lines, right walkers (originating from the left waiting area) have yellow or green caps and left walkers (starting in the right waiting area) red or blue caps. Dyads (green and blue caps) can be seen walking close to each others.

(a) Validation unidirectional 4/0 configuration

(b) Validation bidirectional 3/1 configuration

(c) Validation bidirectional 2/2 configuration

Figure 2.29: Starting positions during the different configurations of the validation experiment [130]. Because the number of available starting positions exceeded the number of participants by two (few participants did not show up for the experiment), some crosses are unoccupied also during the unidirectional configuration. Image is only for illustrative purpose and not in scale.

metrical size is slightly changed. Since a narrower corridor was used, only four positions were available in each column and because of time limitations only three configurations were tested. Conceptually the same cases considered in the previous experiments were analyzed since a unidirectional, a balanced and an unbalanced bidirectional flow were tested.

Table 2.10: Experimental configurations and their characteristics in the validation experimental campaign (UNI = unidirectional, BI = bidirectional) [130].

Case	Type	Major flow (left)	Minor flow (right)	Flow ratio	Valid runs
4/0	UNI	4 persons/column	0 persons/column	0.000	4
3/1	BI	3 persons/column	1 persons/column	0.250	4
2/2	BI	2 persons/column	2 persons/column	0.500	3

Table 2.10 provides some summarizing information on the flow ratio and valid runs for the validation campaign. Also here four runs were performed, but one had to be excluded since one participant stopped during the experiment to fix the position of a band partitions.

Video post-processing

The frames obtained from the video recordings of the experiments were first cropped and rotated to contain only the measurement area. Distortion of the lens was found being very limited in the measurement area, but to ensure the qu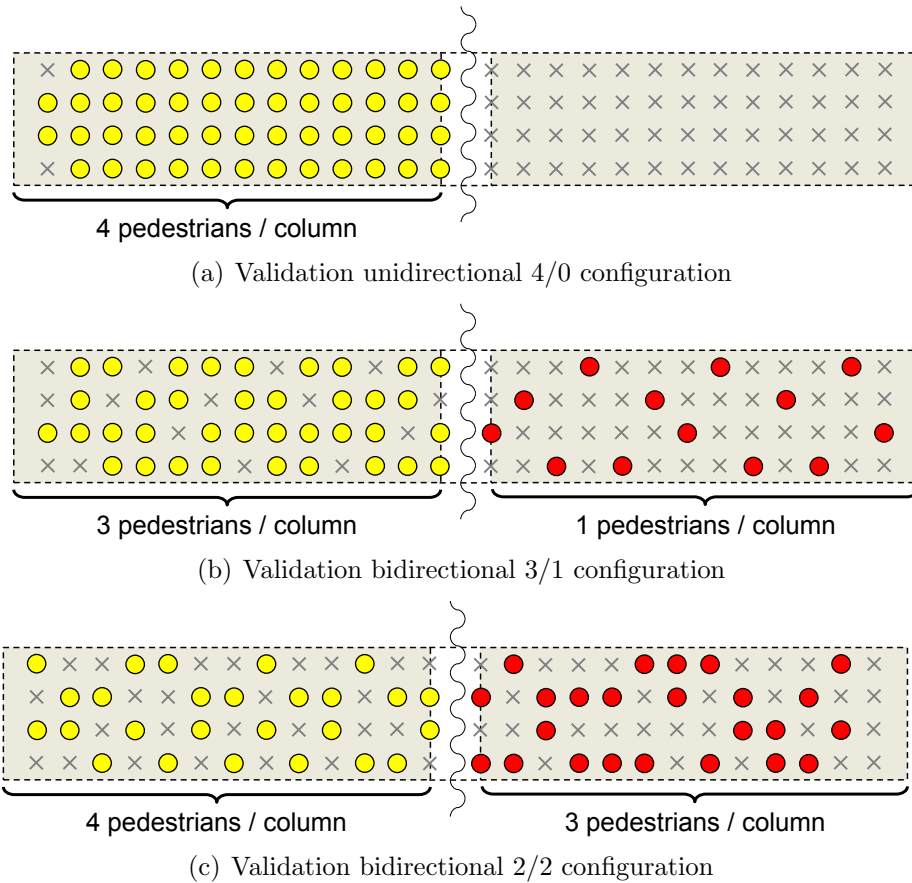ality of the results corrections were taken during the tracking procedure. An example for post-processed video frames taken during the balanced bidirectional flow experiment with singletons and dyads is given in Figure 2.28.
After obtaining the relevant frames centered on the measurement area, images were analyzed using PeTrack [87] software, which allows to obtain the position of each participant for all the time frames considered. Velocities were computed using the position data for each pedestrian, but, in order to remove short-term fluctuations and tracking imperfections a time period of three frames was considered to calculate the average velocity. This means that, given the original video frame rate of 30 fps, a time period of 0.1 s is considered for velocity calculation, sufficiently small to consider rapid changes in trajectory or pace. Densities were computed using the Voronoi cells method [14] to increase the accuracy of the results. Voronoi cells sharing one edge with the entrance/exit of the measurement area were not used for calculation as the "personal space" of the corresponding pedestrian cannot be determined in relation with the ones being behind him.

2.5.2 Singletons only: results and discussion

In this section the main findings of the experiment with only singletons are presented and discussed in detail. The first part includes a general discussion about the qualitative characteristics of the flow observed and an initial analysis using the quantities typically used to analyze pedestrian streams. Later, particular properties and additional quantities are used to describe the main features of the bidirectional flow analyzed.

Speed, flow and density time evolution

By introducing the experimental setup we assumed that flow ratio can be easily computed only considering the density (and ultimately the number of pedestrians) on each waiting area. However, this assumption was based on the prediction that pedestrians composing both the minor and major flow would walk at similar speeds. Before starting detailed data analysis it is therefore convenient giving a look to the profile of speed, density and flow measured during the experiment.

(a) Singletons only unidirectional 6/0 configuration

(b) Singletons only bidirectional 5/1 configuration

(c) Singletons only bidirectional 4/2 configuration

(d) Singletons only bidirectional 3/3 configuration
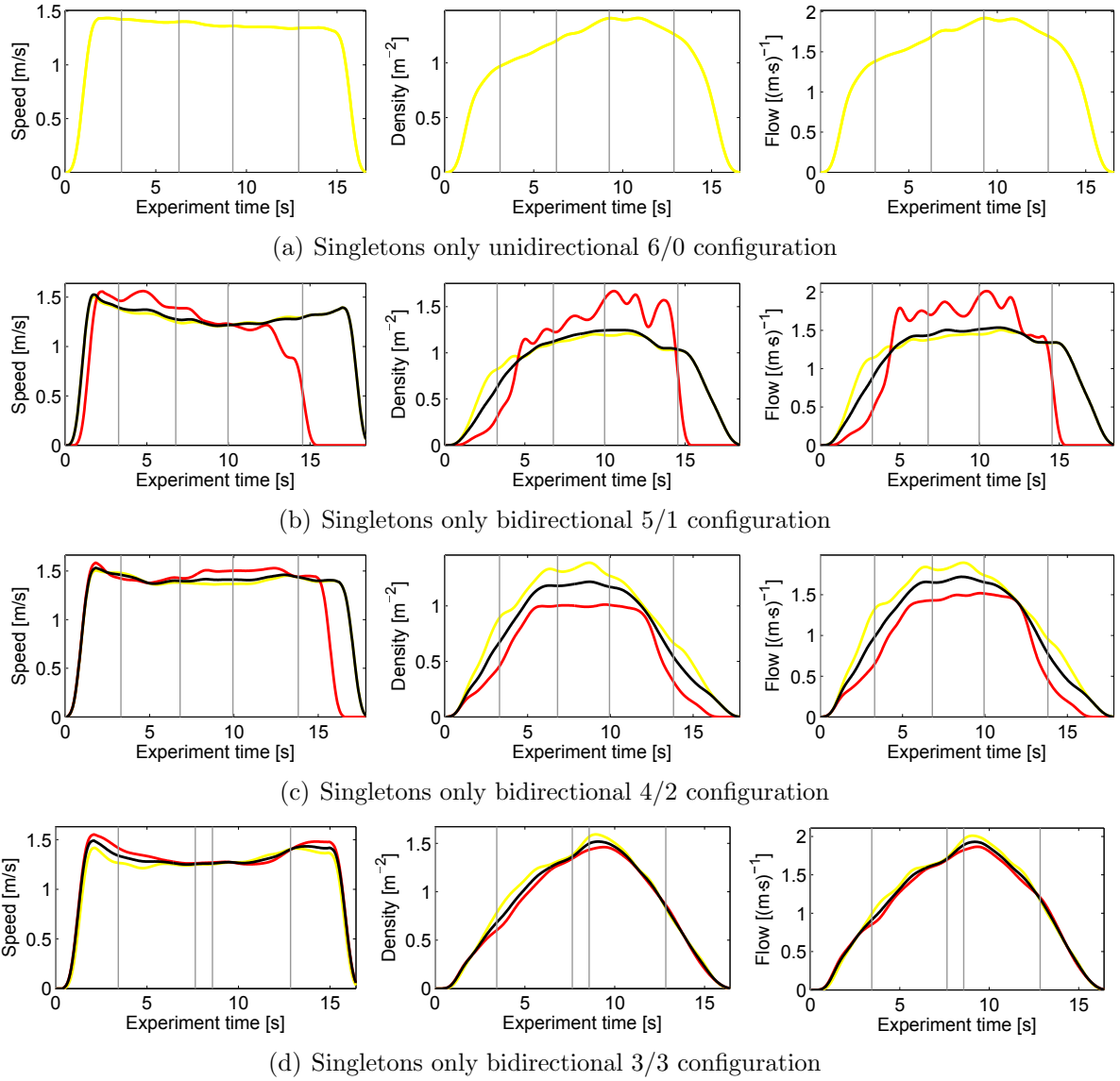
Figure 2.30: Evolution of speed, density and flow for different configurations. It is important to remind that each configuration was repeated four times, so graphs represented here are only for reference (differences between runs were however small). Gray vertical lines represent the boundary between different phases (which will be discussed later).

Figure 2.30 presents average walking speed, density and flow for some representative cases among the four runs of each configuration. Yellow curves are relative to the major flow, red ones to the minor flow and black curves give the average among the whole group. Density is computed using Voronoi cells, which means that starting point for the calculation is the "personal space" of each pedestrian (this explains why differences are not big among both

groups also in the unbalanced cases). Flow is computed using the fundamental relation by combining speed and density.

A comparative analysis of the data obtained showed that, as planned and theoretically predicted, maximum total flow reached comparable levels for all the cases considered (around 1.5–1.8 $(\text{m·s})^{-1}$), while maximum density has been about 1.2–1.3 m^{-2}. Average speed had also a similar profile for all cases with high values recorded at the beginning and the end of the experiment and slightly lower speed when participants were interacting with each others. A quick analysis of the profile for the three quantities considered in Figure 2.30 suggests that congestion did not occur during the experiment (remember also the considerations from the previous on-field observation).

Pedestrians trajectories and crossing time

Next, to get a general idea of the way pedestrians behave inside the mock-corridor it is also convenient considering the trajectories obtained, which are represented in Figure 2.31. The trajectories given in Figure 2.31 correspond to the profiles given in Figure 2.30 and are taken from the beginning to the end of a selected run, i.e. considering the full length of the experiment. The color in each trajectory indicates the horizontal speed (x-velocity) for the given moment/position. It has to be reminded that for each configuration four different runs were performed, so the trajectories given below are only for the most representative example of each configuration and slight differences exist for each run.

(a) Singletons only 6/0 configuration

(b) Singletons only 5/1 configuration

(c) Singletons only 4/2 configuration

(d) Singletons only 3/3 configuration
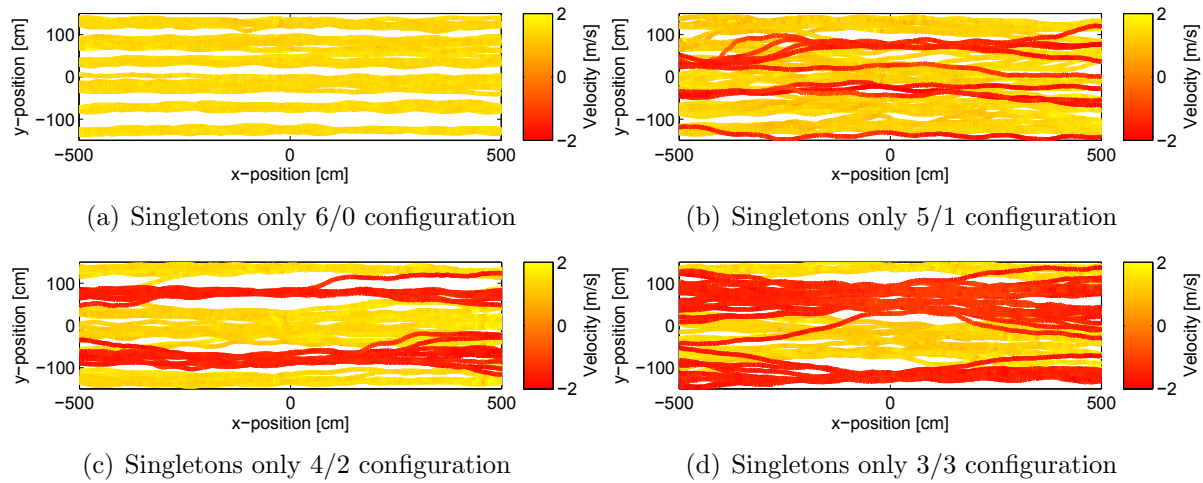
Figure 2.31: Trajectories recorded in a selected run for each of the different configurations. Path color indicates the x-component of the velocity. It is important to remind that each configuration was repeated four times, so the trajectories represented here are only for reference. Major flow (positive velocity, yellow) goes from left to right, minor flow (negative, red) from right to left.

Although Figure 2.31 overlaps different time frames and therefore it is not sufficient for a complete analysis, some aspects which will be discussed later can already be observed here. In particular, in the unidirectional 6/0 case it can be observed that people tend to keep their original position and simply keep going straight. In fact, especially in the left side of Figure 2.31(a), six different lanes are easily recognized, which eventually become slightly mixed at the exit on the right side. In Figure 2.31(b) (bidirectional 5/1 configuration) a more complex flow pattern is observed as pedestrians of the minor flow (having negative red velocity) have to take some deviations to overcome the incoming large counter flow.

Although some stable lanes can be observed (by seeing that at the left side trajectories of the minor flow tend to some extent to occupy an area unused by the major flow), in general the flow behavior can be described as unorganized since trajectories of the major and minor flow overlaps in different locations.

The bidirectional 4/2 case (Figure 2.31(c)) shows a more ordered scenario. Members of the minor flow now tend to organize themselves in groups by forming a more limited number of lanes and taking a defined portion of the corridor. Although in the right side of Figure 2.31(c) pedestrians of the minor flow show some individual behavior, more organized lanes are formed in the center. The emergent lane formation mechanism is particularly recognizable in Figure 2.31(d) (balanced bidirectional flow), where each group (left and right walkers) show a similar behavior by forming two lanes in each direction which takes a very clear amount of space in the corridor (trajectories do not overlap in the central part of the measurement area and some lateral space is left).

We can now consider the crossing time, i.e. the time required to go from one side to the other of the measurement section, given in Table 2.11. For each configuration the crossing time measured for each pedestrian in the four runs was recorded and the corresponding average and 1σ deviation are reported. Separate figures are given for the major, the minor flow and the whole group of pedestrians.

Table 2.11: Average measurement area crossing time for the different configurations (UNI = unidirectional, BI = bidirectional) and the different groups. Uncertainties are 1σ standard deviation [127]. Measurement area length is 10 m.

Case	Type	Flow ratio	Crossing time		
			Complete group	Major flow	Minor flow
6/0	UNI	0.000	7.273 ± 0.319 s	7.273 ± 0.319 s	–
5/1	BI	0.167	7.309 ± 0.561 s	7.398 ± 0.465 s	6.870 ± 0.768 s
4/2	BI	0.333	7.266 ± 0.580 s	7.365 ± 0.573 s	7.070 ± 0.549 s
3/3	BI	0.500	7.326 ± 0.592 s	7.488 ± 0.613 s	7.164 ± 0.525 s

The average crossing time taken from the complete group of pedestrians does not show any significant trend, thus suggesting that average values are inappropriate to describe overall characteristics of pedestrians streams. On the other hand, the dispersion shows a small but clear trend in connection with the flow ratio, with the unidirectional flow case having the most uniform crossing time and the balanced case having the largest dispersion.

When major and minor flows are considered separately it is interesting to notice the opposite trend observed in the variance. While variance of the major flow increases with the flow ratio (similarly to the trend of the complete group), variance of the minor flow has the lowest value in the balanced bidirectional configuration and shows the largest dispersion in the 5/1 configuration. In the case of the minor flow a linear trend is observed in the average value too, while for the major flow it is difficult to recognize a particular pattern, although it appears that, in general, bidirectional cases have higher crossing times compared to the unidirectional case.

Fundamental diagram

Before starting the statistical analysis we wish to give a look to the fundamental diagram to make sure that the different configurations are equivalent in terms of the flow regime

observed and to understand the role of the minor and the major flow. Figure 2.32 shows the fundamental diagrams of the different configurations plotted in the same graph. Diagrams were generated by taking the average density and x-velocity (making up the flow by multiplication) measured during each time frame (i.e. every 0.03 s) from the beginning to the end of each run. Each dot in Figure 2.32 is therefore obtained by considering the average density and x-velocity in a given time frame. Again, density was computed using Voronoi cells and pedestrians entering and leaving the measurement area are excluded. All the four runs of each configuration were used to create a single fundamental diagram.
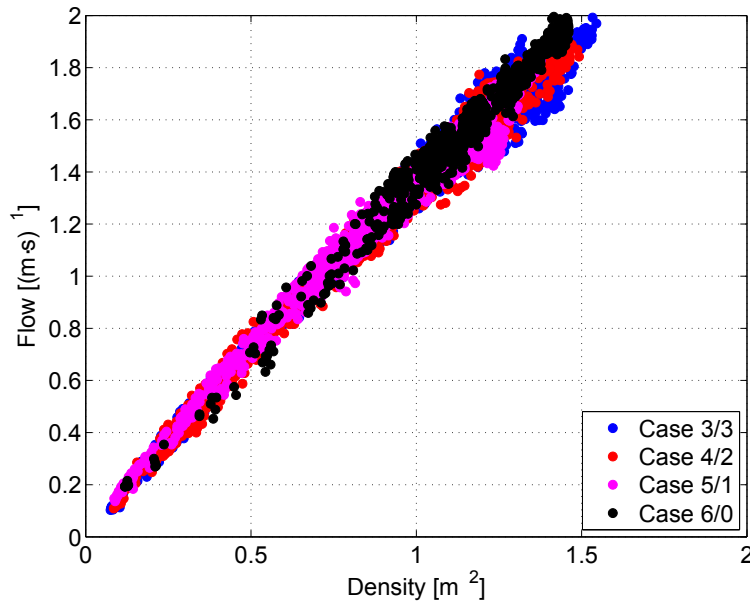
Figure 2.32: Comparison of the different fundamental diagrams; no differentiation is made between minor and major flow. Uncongested, comparable flow was observed in all the cases. Without further investigations differences between the different configurations cannot be easily identified [127].

A first glance clearly reveals that uncongested flow was observed during the experiment. All the graphs show, on average, an almost linear behavior with most of the dots being aligned along a fictional line starting from the origin. By analyzing Figure 2.32 only, one may conclude that all configurations are equivalent, with only a slightly larger dispersion found for the balanced bidirectional flow. These qualitative remarks are supported by numerical evidence obtained by performing a linear regression on the fundamental diagrams and measuring the dispersion resulting from the average slope. Results given in Table 2.12 shows that especially for the bidirectional cases there is no significant difference between the fundamental diagrams. This is in line with the conclusions by Zhang et al., who found that no difference can be found between bidirectional fundamental diagrams.

To grasp any difference between the different configurations we can now compare the fundamental diagrams by considering separately minor and major flow. For each time frame, average density and x-velocity were computed separately for each class of pedestrians and results were plotted using different colors as shown in Figure 2.33. In this case, for each time frame, two dots are generated: one using the density and x-velocity of the major flow and the other one using data of the minor flow. Again, the four runs were combined to obtain a single fundamental diagram for each configuration.

Probably the most relevant feature to be recognized in the fundamental diagrams is the

Table 2.12: Slope resulting from the linear regression of fundamental diagrams given in Figure 2.32 (complete group) and Figure 2.33 (major and minor flow) [127]. Dispersion is measured using the root mean square error.

Case	Velocity		
	Complete group	Major flow	Minor flow
6/0	1.341 ± 0.047 m/s	1.341 ± 0.047 m/s	–
5/1	1.286 ± 0.057 m/s	1.284 ± 0.059 m/s	1.313 ± 0.160 m/s
4/2	1.300 ± 0.059 m/s	1.286 ± 0.067 m/s	1.344 ± 0.077 m/s
3/3	1.267 ± 0.070 m/s	1.237 ± 0.072 m/s	1.300 ± 0.087 m/s

high dispersion of red dots (minor flow) observed in the 5/1 configuration at high densities (see Figure 2.33(b)). This explains the results observed for the crossing time and indicates that members of the minor flow have to continuously slow down/speed up to find their way through the incoming larger major flow. In contrast, the unidirectional case shows a very compact shape, with most of the dots to be found in a limited surface. Interestingly, except for the larger dispersion observed in the 5/1 configuration, minor and major flows show very similar characteristics when compared using the fundamental diagram, suggesting that further investigations are required. The above remarks are reflected by the numerical data given in Table 2.12.

Bidirectional flow mechanisms

Because the fundamental diagram does not give information concerning the mechanisms observed in bidirectional flows, we need to consider different quantities. But before continuing, it is important to define the several steps leading to the formation of lanes in bidirectional streams.

Although two groups of pedestrians are considered, the experiment starts as a combination of unidirectional streams with opposite directions and only later a bidirectional flow is formed. Six different time instants are relevant for the experiment considered (for some of them a representative image is given in Figure 2.34):

- $t_0 = 0$: the first pedestrian (either minor or major flow) enter the measurement area (time measurement starts from here)

- t_1: the leading pedestrians of the major and minor flow cross each other's (see Figure 2.34(a))

- t_2: pedestrians start exiting from both sides (see Figure 2.34(b))

- t_3: the last pedestrian either of the major or the minor flow enters the measurement area (see Figure 2.34(c))

- t_4: the last pedestrians of each group leave behind each other's (see Figure 2.34(d))

- t_5: the last pedestrian leave the measurement area (time is stopped, from now on data are not analyzed).

The processes observed for each interval between the time instants considered above can be described as follows:

(a) 6/0 configuration

(b) 5/1 configuration

(c) 4/2 configuration
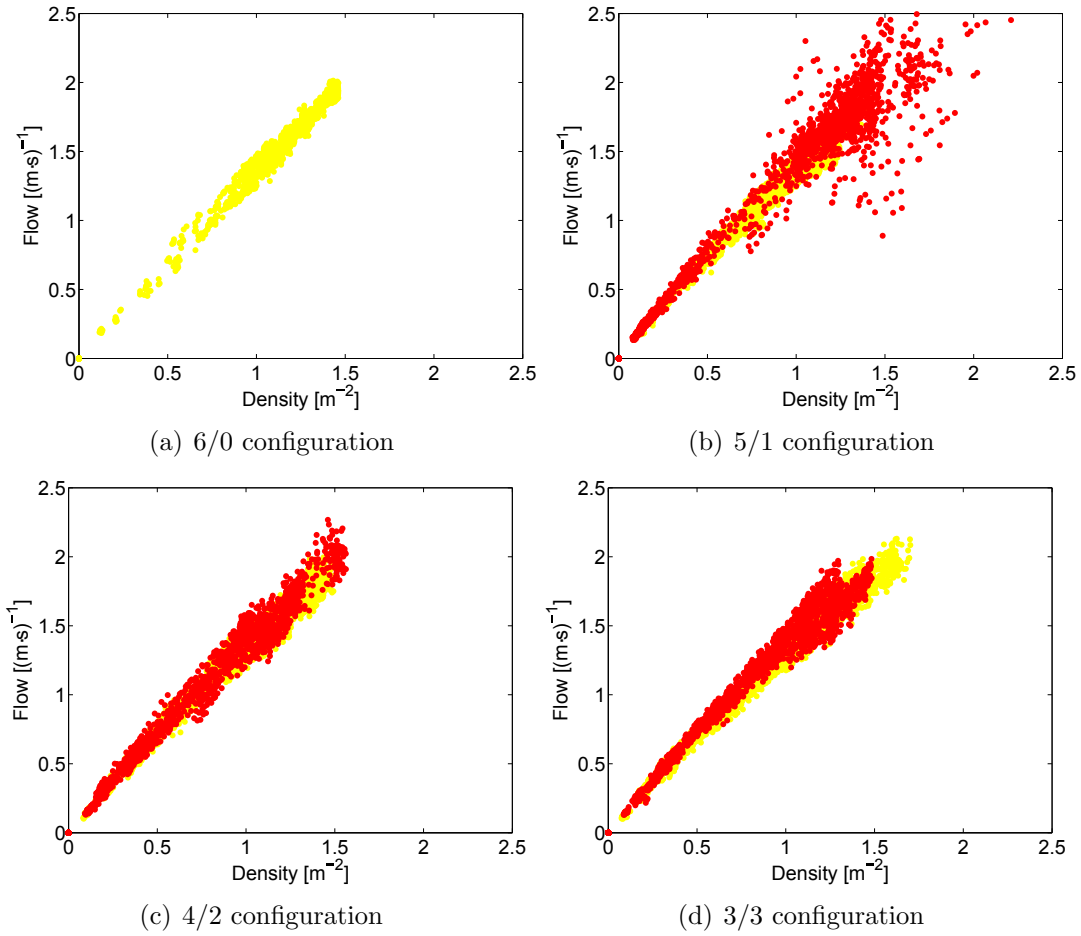
(d) 3/3 configuration

Figure 2.33: Fundamental diagrams for each configuration. Diagrams were obtained by combining the results of the four runs in each case [127]. Dots' color indicates the group considered: yellow stands for major flow and red for minor flow.

(a) Time t_1: beginning of lane formation

(b) Time t_2: beginning of full bidirectional flow

(c) Time t_3: beginning of lane dissolution

(d) Time t_4: end of bidirectional flow

Figure 2.34: Relevant moments during the process of lane formation and dissolution in a balanced bidirectional flow. Major flow pedestrians wear yellow caps, minor flow participants use red caps.

- Phase 1 ($t_0 - t_1$): unidirectional free flow. Major and minor flow can be considered as two separate unidirectional streams, pedestrians have not yet started physically interacting with each other's.

- Phase 2 ($t_1 - t_2$): lane formation. Pedestrians moving in different directions interact with each other's and lanes are formed.

- Phase 3 ($t_2 - t_3$): full bidirectional flow. The whole measurement section is filled with pedestrians of the major and minor flow, a bidirectional stream can be observed in all the x-positions of the section considered.

- Phase 4 ($t_3 - t_4$): lane dissolution. Lanes are being dissolved and in parts of the measurement section unidirectional flow is observed.

- Phase 5 ($t_4 - t_5$): unidirectional free flow. Again, minor and major flows can be regarded as two separate unidirectional streams.

Because each phase is conceptually different, from now on we wish to consider each time interval separately and investigate if there are characteristic features describing the phenomena observed in each of them. To allow a comparison with the quantities observed for unidirectional flow (6/0 configuration), we decided to divide the time interval in a similar way, although the phenomena observed are the same in all the phases. At the scope, instead of considering the incoming counter flow, the centerline ($x = 0$) is used to determine the beginning of a phase and the start of the following one in the case of unidirectional flow.

Velocity distributions

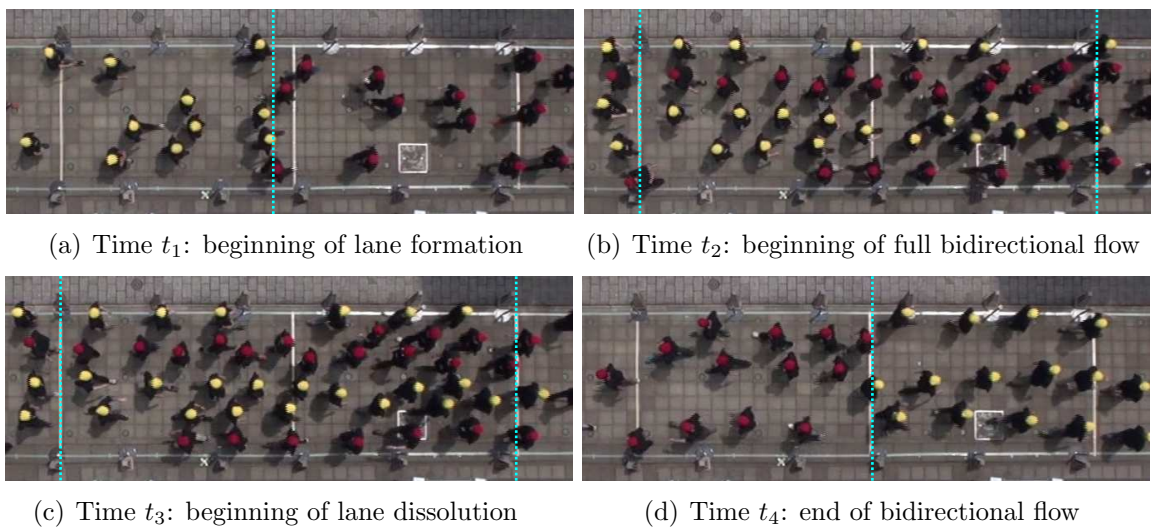First of all it is important to examine the x-velocity, thus the velocity of the forward motion. As we have seen in the literature overview, opinions differ on which distribution is expected along the width of the corridor. However, in our case, possibly because of the low densities considered, x-velocities were found similar everywhere in the $x = 0$ position (center) with no particular distribution observed.

When x-velocity distribution among all participants is concerned, then in all the cases considered a Gauss distribution was observed and confirmed by fitting with the Gaussian function. This is not surprising and it has been often reported in the literature as we have seen before [131, 21, 66]. It is therefore appropriate to measure velocities in terms of average value and 1σ variance. The results for the x-velocity during the different phases and in function of the flow ratio are reported in Figure 2.35; colors refers to the minor and major flow as used for the previous graphs. To make comparison easier, absolute values are used for the average x-velocity.

During the first phase, the minor flow shows a larger average velocity compared to the one of the major flow. The difference is particularly large for low flow ratios. This result should not come as a surprise because, during phase 1, both minor and major flows can be regarded as separated unidirectional flows whose velocities are related with the densities observed. As a consequence, the low density of the minor flow comes with a higher velocity. Variances during phase 1 are comparable and relatively low, showing that pedestrians are moving in a uniform way.

During phase 2 (lane formation) the average x-velocities clearly drop, while there is an increase in the variance observed, especially in the case of the minor flow. Although in
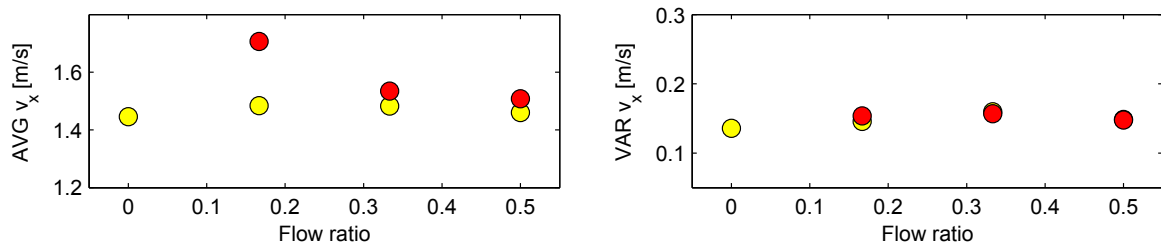
(a) Phase 1: unidirectional free flow
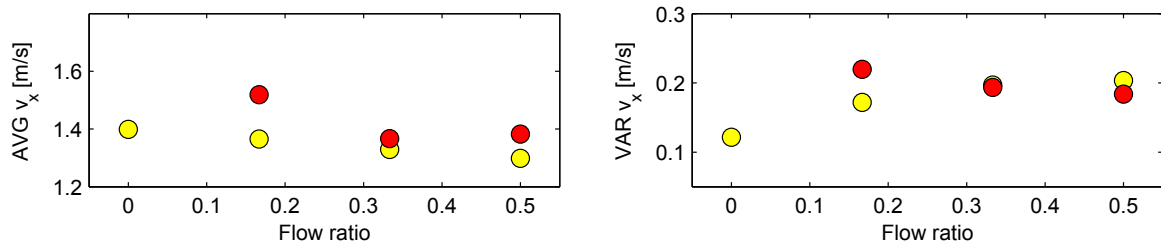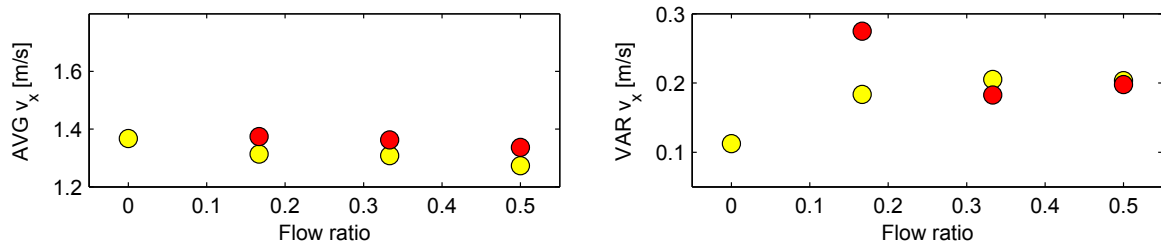
(b) Phase 2: lane formation

(c) Phase 3: full bidirectional flow

(d) Phase 4: lane dissolution

(e) Phase 5: unidirectional free flow

Figure 2.35: x-velocity for the different phases [127]. Yellow dots refer to the major flow and red dots to the minor flow. AVG stands for average, VAR for variance.

general the minor flow still has a higher x-velocity compared to the major flow, a wide range of velocities is observed.

In phase 3 (full bidirectional flow) there is an additional increase in the variance measured, while the average values stay almost constant. Interestingly, the variance of the major flow increases with an increase in flow ratio, with the variance of the minor and major flow being almost identical for balanced bidirectional flow. The difference in variance is particularly clear for the 5/1 configuration (flow ratio = 0.167).

In phase 4 (lane dissolution) the average x-velocity slightly increases and the variance decreases, showing an opposite behavior to the process which led to lane formation.

Finally, in phase 5, as the flow becomes unidirectional, the velocities grow again, while the variance drops, showing again a fairly uniform motion.

Although pedestrians' velocity clearly has a larger x-component, it is important to consider the y-component also, because it accounts for the lateral motion measured during each phase. In presenting the results for the y-velocities (given in Figure 2.36), we used the absolute value to compute the average, while the variance was computed using the nominal value. The absolute value is required to account with the same weight left and right movement, which would result in an average y-velocity close to 0 otherwise.

Phases 1 and 2 show similar profiles concerning both the average and the variance of the y-velocity. In each case, both the average and the variance of the major flow grow with an increase in flow ratio, showing that for the balanced case the major flow requires more lateral adjustments compared to the homogenous unidirectional flow or low flow ratios.

It is interesting to notice how the trend changes when a full bidirectional flow is formed in phase 3. With a partial exception of phase 4, the full bidirectional flow is the only moment in which the y-velocity (both average and variance) decreases with flow ratio. This indicates that the balanced flow is clearly more stable than the cases with low flow ratio and the level of y-velocity reached by the balanced flow is comparable to the one of the unidirectional flow, thus confirming the hypothesis stated by some researchers that once lane are formed, bidirectional flow can be regarded as two unidirectional flows moving in opposite directions and taking different portions of space.

Later, from phase 4 to 5, the behavior observed during lane formation is repeated in the opposite way, restoring the growing y-velocity profile observed for the variance of the major flow in phase 1.

ANOVA test on velocity

A two factors analysis of variance (two-way ANOVA) was conducted to test the combined potential effect of flow ratio and phase on the x- and y-velocity of both the minor and major flows. Statistics have been conducted at the $p < 0.05$ level considering the four repeated runs. Results are presented in Table 2.13, where combinations with a statistically significant outcome are given in bold text.

In general, both flow ratio and phase have a statistically significant effect on the variance of both x- and y-velocity, with the relationship being particularly relevant for the phase factor. Average velocity seems to be less affected by both flow ratio and phase. Generally speaking, although qualitative analysis based on the previous graphs suggested that y-velocity follows a particular pattern, statistical analysis indicates that flow ratio and phase have a more significant effect on x-velocity. Finally a significant interaction among both factors was found on the average x-velocity and the variance of the y-velocity, partially in line with the qualitative remarks from the previous sections. In general, minor and major flow seem to be equally affected by flow ratio and phase.
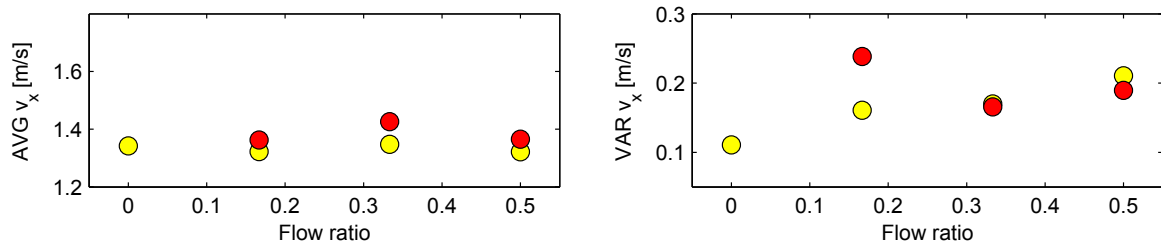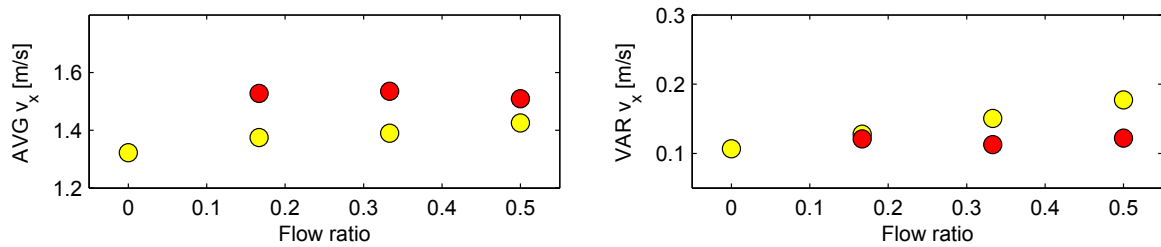
(a) Phase 1: unidirectional free flow

(b) Phase 2: lane formation

(c) Phase 3: full bidirectional flow

(d) Phase 4: lane dissolution
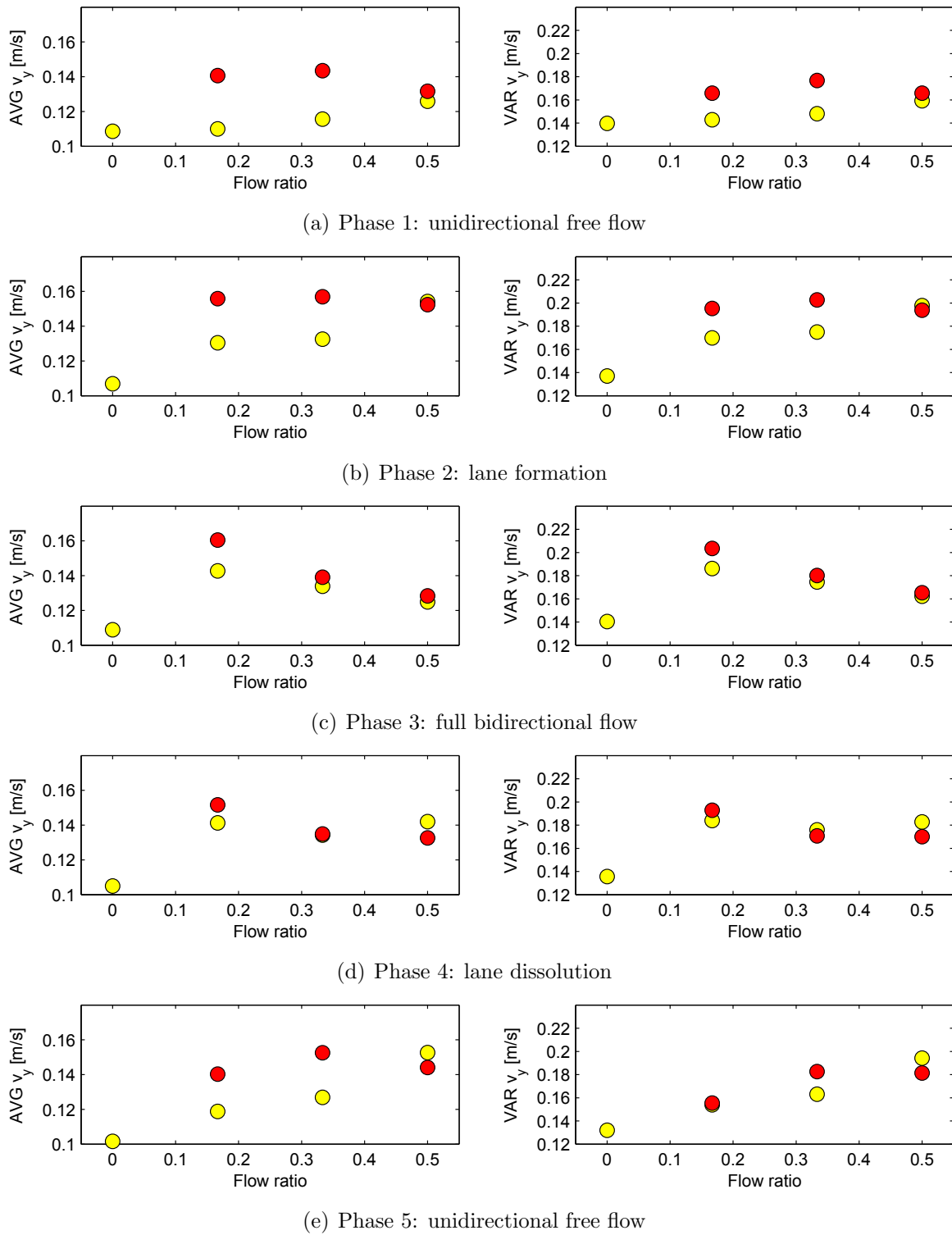

(e) Phase 5: unidirectional free flow

Figure 2.36: y-velocity for the different phases [127]. Yellow dots refer to the major flow and red dots to the minor flow. AVG stands for average, VAR for variance.

Table 2.13: Two-way ANOVA test on the combined potential effect of flow ratio and phase on the different aspects of velocity [127]. Components having a statistically significant effect ($p < 0.05$) are given in bold (AVG = average, VAR = variance).

Flow ratio		Major flow	Minor flow
AVG	x-velocity	$F(3,60) = 0.686, p = 0.564$	$\boldsymbol{F(2,45) = 5.912, p = 0.005}$
	y-velocity	$F(3,60) = 0.469, p = 0.705$	$F(2,45) = 0.214, p = 0.808$
VAR	x-velocity	$\boldsymbol{F(3,60) = 29.80, p < 0.001}$	$\boldsymbol{F(2,45) = 7.005, p = 0.002}$
	y-velocity	$\boldsymbol{F(3,60) = 28.39, p < 0.001}$	$F(2,45) = 1.144, p = 0.328$
Phase		Major flow	Minor flow
AVG	x-velocity	$\boldsymbol{F(4,60) = 25.62, p < 0.001}$	$\boldsymbol{F(4,45) = 20.55, p < 0.001}$
	y-velocity	$F(4,60) = 0.793, p = 0.534$	$F(4,45) = 2.525, p = 0.054$
VAR	x-velocity	$\boldsymbol{F(4,60) = 6.068, p < 0.001}$	$\boldsymbol{F(4,45) = 15.59, p < 0.001}$
	y-velocity	$\boldsymbol{F(4,60) = 6.002, p < 0.001}$	$\boldsymbol{F(4,45) = 4.465, p = 0.004}$
Interaction		Major flow	Minor flow
AVG	x-velocity	$\boldsymbol{F(12,60) = 2.385, p = 0.014}$	$\boldsymbol{F(8,45) = 2.358, p = 0.033}$
	y-velocity	$F(12,60) = 1.059, p = 0.410$	$\boldsymbol{F(8,45) = 2.474, p = 0.026}$
VAR	x-velocity	$F(12,60) = 1.754, p = 0.078$	$F(8,45) = 1.543, p = 0.170$
	y-velocity	$\boldsymbol{F(12,60) = 2.792, p = 0.004}$	$\boldsymbol{F(8,45) = 2.362, p = 0.032}$

Time lapse

We wish to continue the statistical treatment by using a different quantity. Some researchers [132, 133] showed that pedestrians (or animals) interactions are governed by power laws and in particular time lapse distribution (i.e. the time interval resulting from the passage of two consecutive pedestrians through a given position, obtained by measuring the time between consecutive pedestrians passing the same x-location) can be described using a power function. We want therefore to check this hypothesis by using our dataset. Figure 2.37 show the cumulative density function (CDF) obtained for different positions and for the different configurations considered in this experiment. In each case, minor and major flow are considered separately and entrance and exit are relative to the initial position of both groups.

For each case the time lapse distribution fits well with the exponential function given by:

$$\text{CDF}(\Delta t) = \mu e^{\lambda \Delta t} \tag{2.36}$$

where Δt represents the time lapse and μ and λ are parameters to be determined empirically. The wider distribution of the minor flow results from the lower density of the initial group and both distributions become very similar in the case of perfectly balanced flow. The time lapse CDF–flow ratio relationship is summarized in Figure 2.38, where the λ parameter giving the width of the distribution is plotted against the flow ratio for both minor and major flows.

As Figure 2.38 clearly shows, in all positions, the width of time lapse distribution of the minor flow decreases with an increase of flow ratio which is ultimately connected with the density of each group considered separately. The opposite behavior is observed in the major flow, which has its density decreasing with an increase in flow ratio, ultimately leading to a less compact and heterogeneously distributed group. Both major and minor flow lines intersect close to the balanced bidirectional flow, where both densities are equal.
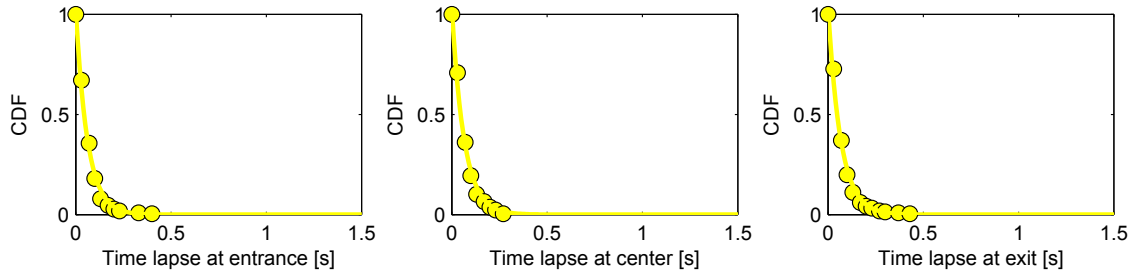
(a) 6/0 configuration
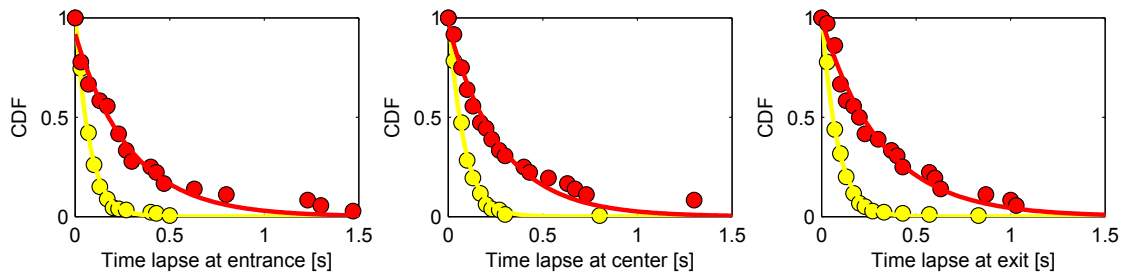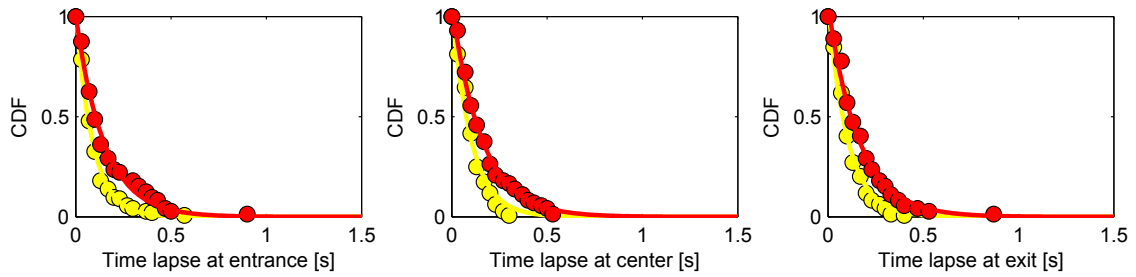
(b) 5/1 configuration
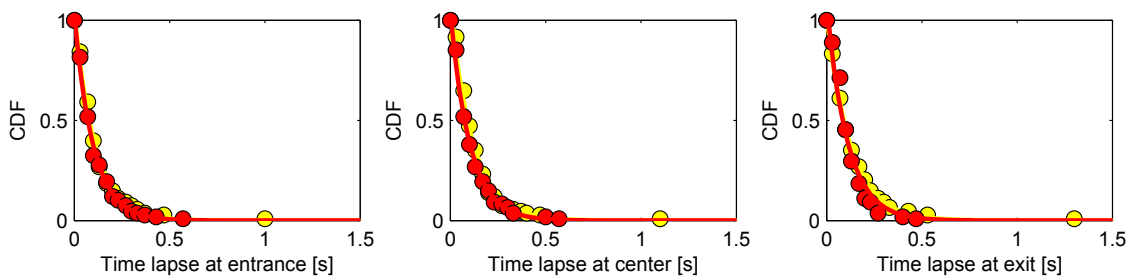
(c) 4/2 configuration

(d) 3/3 configuration

Figure 2.37: Time lapse distribution for the different configurations [127]. Each distribution fits well with the exponential function. Yellow is used for the major flow and red for the minor flow. CFD stands for cumulative density function. Center refers to the $x = 0$ m position.

(a) Entrance   (b) Center ($x = 0$ m)   (c) Exit
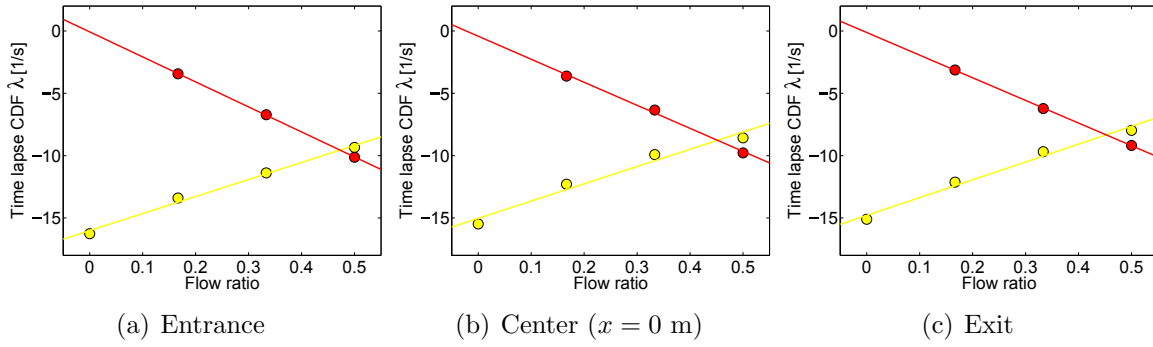
Figure 2.38: Time lapse distribution width in function of the flow ratio for different positions [127]. Yellow is used for the major flow and red for the minor flow.

As Figure 2.37 and Figure 2.38 show, apparently the width of the distribution does not change as pedestrians move across the measurement section. However, because the changes may be quite small, it can be more appropriate to check this behavior by performing a fit with an exponential function at several x-positions of the measurement section. The result of this procedure is given in Figure 2.39.
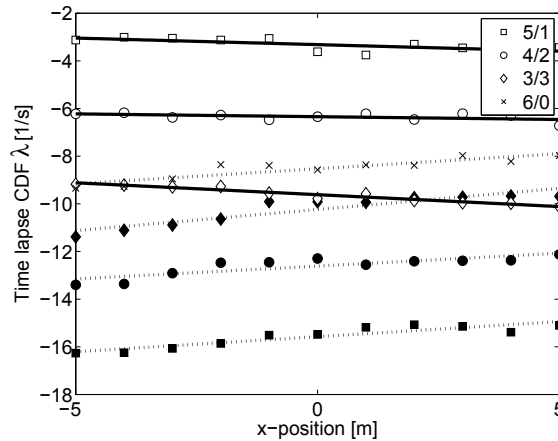
Figure 2.39: Evolution of the time lapse width along the test section depending on the flow ratio. Filled markers fitted using dotted lines belong to the major flow; empty markers fitted using continuous lines to the minor flow. Configurations are distinguished according to the legend provided.

As Figure 2.39 shows, the distributions of the time lapse change as the pedestrians walk along the measurement section and the relationship appears to be linear. Slope for the lines of the minor flow appears to be opposite to the one of the major flow, but this is only because they move in different directions (minor flow pedestrians start from the 5 m x-position and move in the negative x-direction). In both cases, the distributions get wider when pedestrians leave the measurement section. Finally, it can be observed that although both groups start with different distributions in the different configurations, the rate of change seems to be fairly constant. This behavior eventually suggests that, as some researcher suggested, bidirectional flows can be regarded as bottlenecks and, because of the change in distribution width, one may argue that defining them as moving bottlenecks getting narrower can be a more appropriate comparison.

Concluding, we could confirm that time lapse distribution can be described using power laws, but it is difficult to grasp the nature of the phenomena observed only based on this

distribution. In the next sections we will discuss different quantities which may contribute in gaining a wider understanding of the bidirectional flow.

Order parameter

Until now only statistical or one-dimensional quantities have been considered; but we want now to extend the discussion on bidimensional quantities, which may become useful to describe more complex phenomena. First of all, we will use the order parameter. From Chapter 2.3 we know that to compute it a computational grid comprising the average velocity recorded in each location (cell) over a finite time period is required. We can therefore use the data gained in the experiment and discretize the measurement area in cells having a fixed side length. Here, a cell size of 0.2 m was chosen, taking the balance between having a small accurate mesh and filling enough cells to allow a meaningful calculation of the different parameters (in addition, the size chosen is half the typical cell width used in pedestrian simulations). In each cell location, the average velocity is computed for the 5 phases considered so far. As an illustrative example, the velocity grid obtained for a single run of the balanced bidirectional flow is given in given in Figure 2.40 (the case considered here corresponds to the trajectories given in Figure 2.31(d)).

The bar graph on the right side of Figure 2.40 gives the overall velocity profile taken along the whole x-length for the different y-positions (or rows). As shown in Figure 2.40(c), the bar graph helps counting the number of lanes and the direction for each of them.

Given the definition of the order parameter, it is however meaningful to only consider the full bidirectional phase for comparison, since non fully-developed cases would lead to values depending on the number of pedestrians in each group and not representing the nature of the phenomenon being observed. Results for the order parameter computed in the different configurations during phase 3 are given in Table 2.14.

Table 2.14: Order parameter for the different configurations during full bidirectional flow [127]. 6/0 configuration is omitted because order parameter is 1 by definition. Uncertainties are 1σ standard deviation and relative to the various runs.

Configuration	Flow ratio	Order parameter
5/1	0.167	0.824 ± 0.130
4/2	0.333	0.881 ± 0.131
3/3	0.500	0.938 ± 0.105

In Table 2.14 a linear relationship between flow ratio and order parameter is shown, with the order parameter increasing as the flow becomes balanced. However, uncertainties have fairly large values, therefore making it difficult to make clear distinctions. A one-way AREVA analysis on the order parameter confirms that the influence of flow ratio is not significant (F(2,9) = 0.862, p = 0.455).

Still, a qualitative visual analysis of the video recordings suggests that indeed more ordered lanes are observed in the balanced case, where the order parameter is very close to unity. The results suggest that the order parameter might be used to grasp a more general image on bidirectional pedestrian flow, but its accuracy is limited and in absence of large changes (very disorganized scenarios were not considered here) differences can be statistically insignificant. We will later see (in Chapter 2.6.2) that alternative measures can be used to judge the alignment of lanes in bidirectional flows.

(a) Phase 1: unidirectional free flow

(b) Phase 2: lane formation

(c) Phase 3: full bidirectional flow

(d) Phase 4: lane dissolution

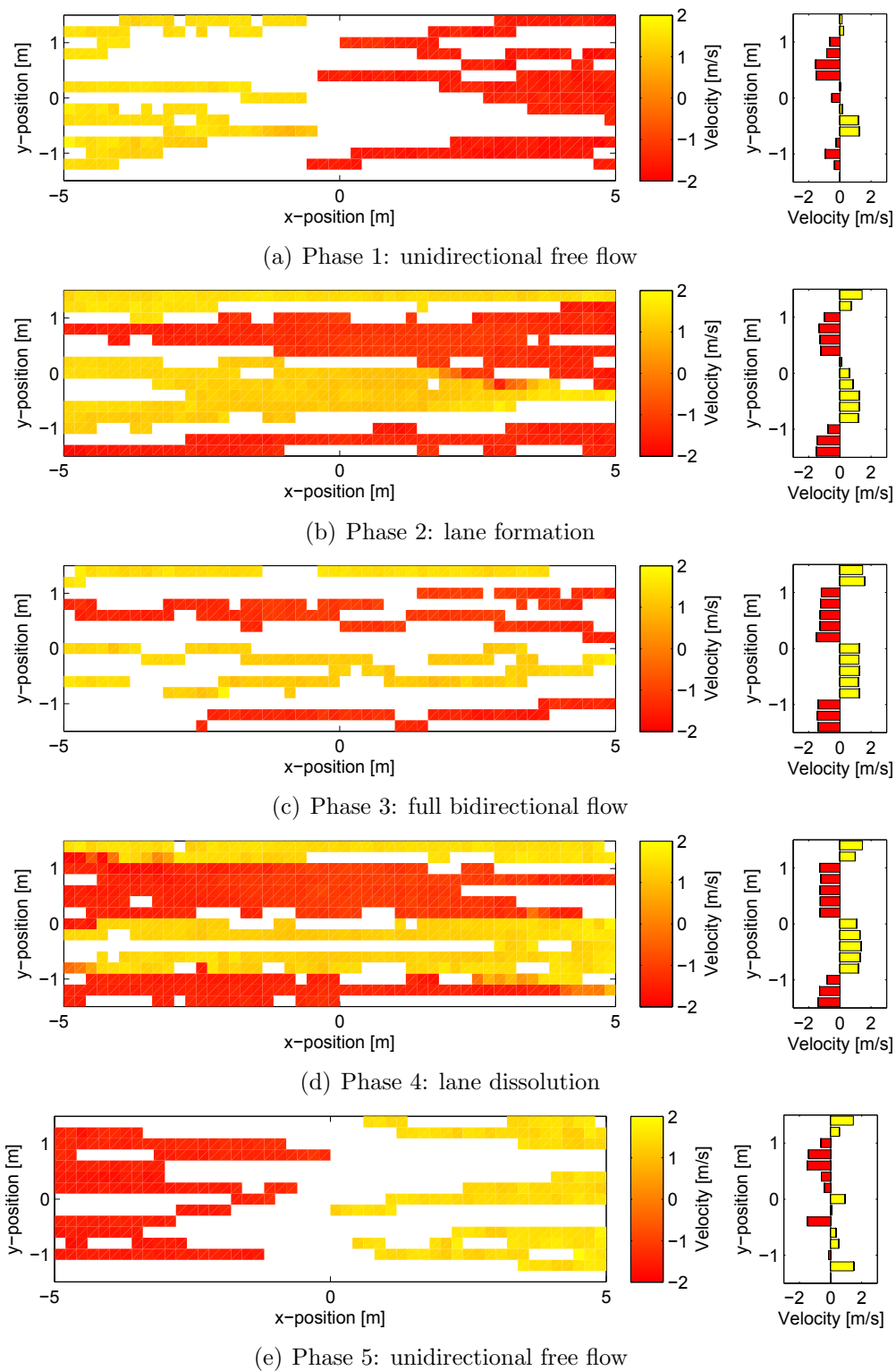
(e) Phase 5: unidirectional free flow

Figure 2.40: 2D plot of the average x-velocity in different locations for each phase. The bar graph on the right side gives the average velocity across the different rows. Grid size is 0.2 m × 0.2 m and white spots indicate unavailable data. Major flow has a yellow gradation and minor flow is represented with red gradation.

Vector field and rotation

To overcome some of the limitations of the order parameter and allowing a combined analysis of both x- and y-velocities, an additional method is proposed.

The concept of rotation (or vorticity, turbulence) is not new in pedestrian dynamics and several authors have used different mathematical methods to analyze crowd using this principle [16, 8, 134].

In this regard, it can be useful to consider the same grid used for the order parameter, but create a vector field by using x- and y-velocities in each cell as shown in the example of Figure 2.41. From the resulting vector field $\vec{V}(x, y)$ the rotation $\vec{R}(x, y)$ can be computed in each position using the following equation:

$$\vec{R}(x, y) = \begin{pmatrix} r_x \\ r_y \\ r_z \end{pmatrix} = \nabla \times \vec{V}(x, y) \tag{2.37}$$

Since only x- and y-values are used, r_x and r_y will be 0 and only r_z can deliver useful information. In addition, since right-hand and left-hand rotations in the vector field result in opposite signed r_z values, to get a measure of the extent of rotational movement in the flow the difference

$$\max(r_z) - \min(r_z) \tag{2.38}$$

may be defined as the rotation range measuring the amount of rotation in pedestrian streams. We can now compute the rotation range for each configuration and analyze the behavior in each of the phases considered so far. The results are given in Figure 2.42.

Clearly, the unidirectional case has a low rotation range during the full length of the experiment. In general, a qualitatively similar behavior is observed in all bidirectional cases with a sort of inverted "W" shape and with rotation peaking during lane formation and dissolution. Overall, the 5/1 configuration shows the largest rotation range throughout the experiment, meaning that bidirectional flow with a small minor flow needs continuous turning to avoid collisions with the counter flow. Although all configurations have similar rotation range values during lane formation, the differences become evident once lanes are formed. In phase 3 (full bidirectional flow), rotation range shows a linear relationship with flow ratio (similar to the order parameter), with the value observed in the balanced case being close to the unidirectional flow. This shows again that the lanes formed in the balanced bidirectional case are very efficient, thus requiring only a very limited degree of lateral adjustments. In the 4/2 case, although the rotation range decreases from phase 2 to 3, the reduction is less marked. Finally, it can be noticed that in phase 1 and 5 all the cases have similar values, indicating that, indeed, only unidirectional flow is observed there. In addition, the low rotation range in phase 1 suggests that only little actions are performed to avoid the counter flow and the main process of lane formation actually starts only once pedestrians are very close to each other's (as already observed by Liu et al. [106]). Although the leaders of each group take some measures to adjust their positions and visual interactions are observed, it is only when pedestrians in the back follow their leaders that clear lanes are formed (in phase 2).

Finally, a two factors analysis of variance was conducted to test the potential combined effect of flow ratio and phase on the rotation range. Results reported in Table 2.15 clearly show that a significant effect is shown for the flow ratio factor and the phase factor. In

(a) Phase 1: unidirectional free flow

(b) Phase 2: lane formation

(c) Phase 3: full bidirectional flow

(d) Phase 4: lane dissolution

(e) Phase 5: unidirectional free flow
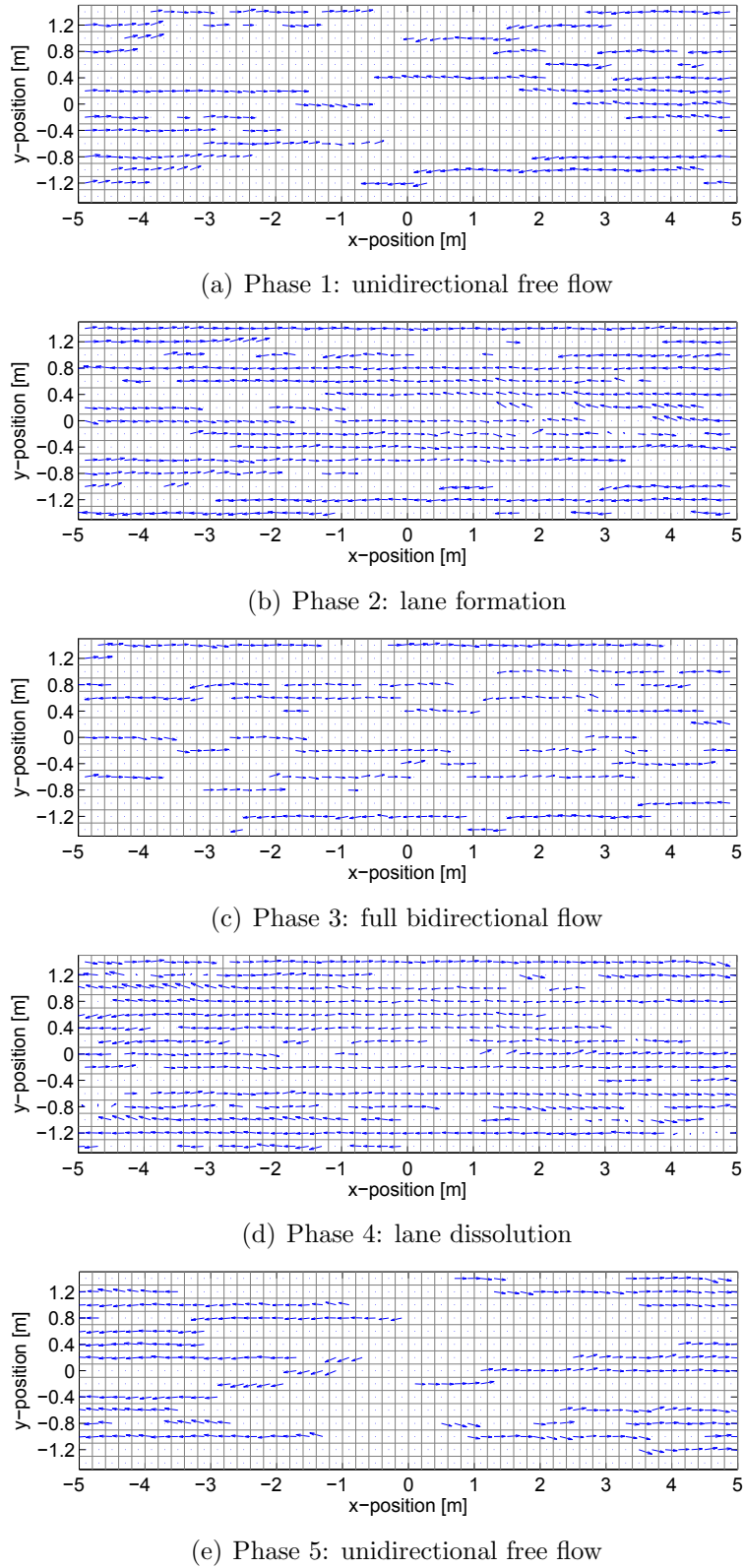
Figure 2.41: Vector field for the different phases of the balanced bidirectional flow. Grid size is 0.2 m × 0.2 m and white spots indicate unavailable data. The case represented here corresponds to the one reported in Figure 2.40.
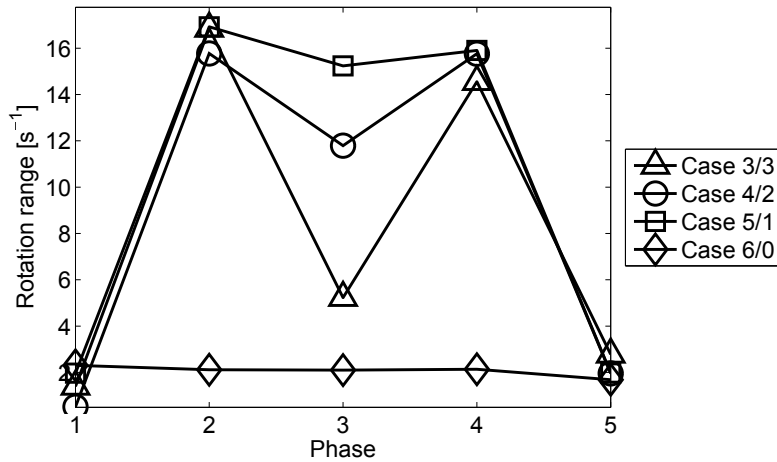
Figure 2.42: Rotation range (from minimum to maximum) during the different phases and for each configuration [127].

Table 2.15: Two-way ANOVA test on the potential combined effect of flow ratio and phase on the rotation range [127]. Statistics have been conducted at the $p < 0.05$ level, relying on repeated measures (four runs per configuration).

Factor	ANOVA test results
Flow ratio	$F(3, 60) = 81.36$, $p < 0.001$
Phase	$F(4, 60) = 139.51$, $p < 0.001$
Interaction	$F(12, 60) = 19.46$, $p < 0.001$

addition, a significant interaction among the two factors (flow ratio and phase) was found, thus justifying the different slope observed in Figure 2.42 for the different flow ratios.

2.5.3   Behavior of dyads and influence on pedestrian flow

Having introduced the various methods to analyze bidirectional flows and in particular the treatment considering phases, we can now apply the same methods on the case with dispersed dyads. In the discussion here we will skip those results which are qualitatively similar to the case with only singletons and we will focus on the differences. Also, we will introduce a particular technique which can be used to analyze the behavior of dyads.

Crossing time and fundamental diagram

To start with, it is convenient considering the crossing time, because it provides general information and it allows a macroscopic comparison between the experiment with only singletons and the one with a portion of dyads discussed here. Like in the previous case Table 2.16 shows the crossing time for the different configurations considering the complete group of pedestrians and the major/minor flow separately.
For the unidirectional case results are in line with the experiment with singletons only which had a crossing time of 7.273 ± 0.319 s. The slightly higher crossing time can be explained considering that experiments with dyads were carried out later and under stronger sun exposure and participants may have been a little bit tired (difference in crossing time is however minimal and within the statistical margins). It is however interesting observing

Table 2.16: Average crossing time for the different configurations (UNI = unidirectional, BI = bidirectional) and the different groups. Uncertainties are 1σ standard deviation.

Case	Type	Flow ratio	Crossing time		
			Complete group	Major flow	Minor flow
6/0	UNI	0.000	7.393 ± 0.574 s	7.393 ± 0.574 s	–
5/1	BI	0.167	8.340 ± 0.961 s	8.305 ± 0.799 s	8.513 ± 1.539 s
4/2	BI	0.333	8.598 ± 0.929 s	8.594 ± 0.917 s	8.606 ± 0.959 s
3/3	BI	0.500	8.579 ± 0.969 s	8.578 ± 1.026 s	8.580 ± 0.915 s

that variance for the unidirectional case is larger when dyads were included, showing that the whole group was less homogeneous.

For the bidirectional configurations the crossing time in the presence of dyads is about one second higher compared to the case with only singletons. Variance of the complete group is also larger, about 0.9 s in the case with dispersed dyads and slightly less than 0.6 s if only singletons are considered. This shows again that dyads contribute in destabilizing the equilibrium and group in the overall is more dispersed. However, when considerations on the flow ratio and differences between minor and major flow are concerned, then the same conclusions for singletons only apply. In particular, there is a clear trend in the variance of both the major and minor flow in regard with flow ratio. Although absolute values are different, the order of magnitude for changes is similar to the singletons only case with the variance of the major group being about double in the balanced case compared to the unidirectional configuration. It is also worth noticing that the 5/1 case is now the fastest bidirectional configuration and the 4/2 case the slowest. This is in contrast with the results reported for the singletons only experiment.

We can now consider more explicitly the particularity of dyads by computing separately the crossing time for dyads and singletons (in the dispersed dyads campaign), as given in Table 2.17.

Table 2.17: Average crossing time for the different configurations (UNI = unidirectional, BI = bidirectional) and the different social structures in the dispersed dyads campaign. Uncertainties are 1σ standard deviation. S/D stands for the singletons (only) vs. dyads (only) experiment.

Case	Type	Flow ratio	Crossing time		
			Complete group	Singletons	Dyads
6/0	UNI	0.000	7.393 ± 0.574 s	7.329 ± 0.609 s	7.472 ± 0.519 s
5/1	BI	0.167	8.340 ± 0.961 s	8.048 ± 0.936 s	8.705 ± 0.866 s
4/2	BI	0.333	8.598 ± 0.929 s	8.429 ± 1.014 s	8.810 ± 0.764 s
3/3	BI	0.500	8.579 ± 0.969 s	8.383 ± 0.980 s	8.825 ± 0.902 s
S/D	BI	0.500	8.221 ± 0.884 s	7.833 ± 0.723 s	8.657 ± 0.847 s

It can be noticed that in every case singletons are faster than dyads (time is smaller). It is also possible to see that the difference in crossing time between singletons and dyads is particularly large for the 5/1 configuration (0.657 s) and the case with singletons and dyads divided in separate groups (0.824 s). The crossing time difference is the smallest in the unidirectional case (0.143 s). When variance is considered, it can be seen that dyads

always have a smallest variance compared to singletons except the S/D case. Although it is quite predictable that members of the same dyad should have very similar crossing time, it is quite surprising that also among different dyads the differences are not large. This could mean that dyads encounter similar difficulties in moving through the counter flow, making differences among them smaller compared to singletons. Finally, it is also remarkable to notice that the relationship between flow ratio and variance observed in major and minor flow is partially lost when singletons and dyads are considered separately. We can now consider the fundamental diagram for the case with dyads, which is given in Figure 2.43. It should be evident that linearity which was observed in the case with only singletons is lost when dyads are included in the group. Although the unidirectional flow still presents a quite clear linearity, the bidirectional cases look more congested.
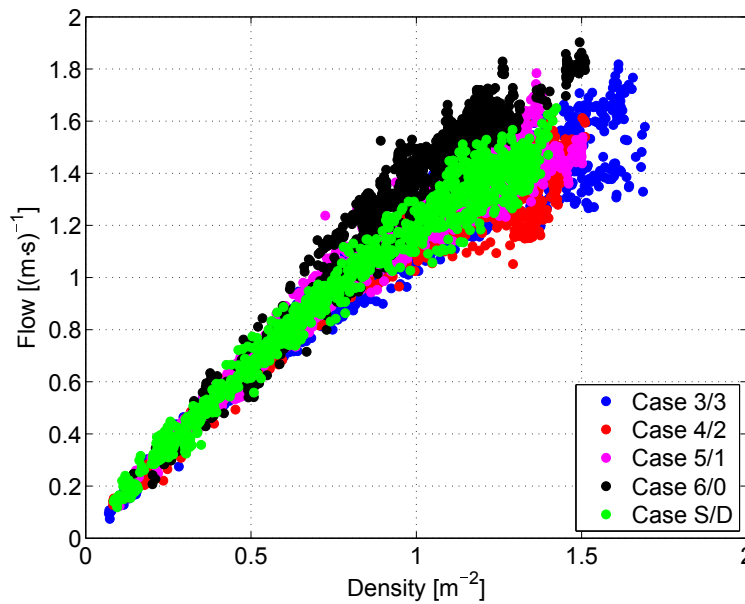
Figure 2.43: Comparison of the different fundamental diagrams for the experiments with dyads; no differentiation is made between minor and major flow [135]. A comparatively congested motion is observed with the FD loosing linearity at densities above $1.0 \, \text{m}^{-2}$.

The case which looks more congested is the 4/2 configuration, which has the lowest flow for a corresponding density of about 1.2–1.3 m^{-2}. In contrast, the S/D configuration which has dyads moving against singletons seems quite stable, probably implying that dyads mainly become an obstacle when are dispersed within the group and if considered separately they may found a way to organize with each other's. The highest density is recorded in the balanced bidirectional flow (3/3 configuration), which starts showing a transition into congestion but not particularly accentuated.

Velocity and time lapse

We can now continue the analysis and consider changes in velocity during the different phases and the time lapse evolution. We have seen for the case with only singletons that the time lapse follow an exponential law. To make comparison easier, we can therefore take the logarithm of the time lapse distribution and plot it for the different configurations and the different social structures as given in Figure 2.44. Especially at the entrance dyads are more dispersed than singletons showing a larger time lapse evolution. At the center

dyads still have larger time lapse but the difference is less marked (and mostly limited to the 5/1 configuration). It is however worth to noticing that at the exit there is an inversion for the 4/2 configuration, with singletons being more dispersed than dyads. It should be reminded that the 4/2 configuration was found being the most congested when the fundamental diagram was analyzed.
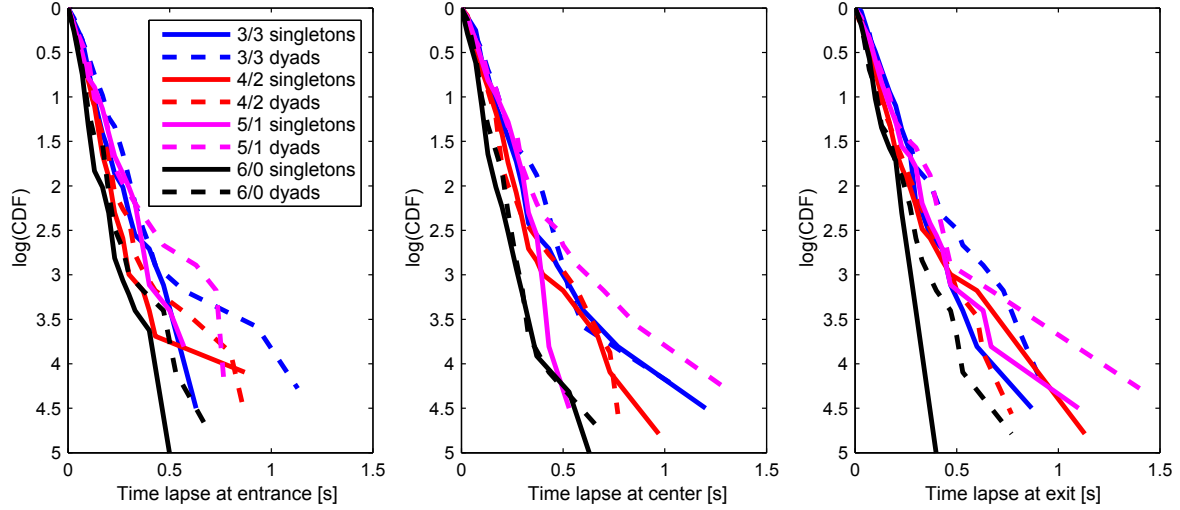
Figure 2.44: Comparison between time lapse for singletons and dyads during the experiment with both social structures. Dyads are slightly more dispersed than singletons; CDF is the cumulative density function.

We can now consider the velocity distribution with the same method used for singletons only. Here we need to remark that to allow an analysis based on the different phases, a few runs had to be excluded (one run for the 5/1 and 3/3 configuration respectively). Also, in the S/D configuration a measurement area of 8.0 m (with the same central location) had to be considered to allow the distinction of the different phases.

Concerning the changes in velocity distribution, the same conclusions obtained for the case with only singletons apply, but reduction observed in lateral motion during full bidirectional flow (phase 3) is much less marked. On the other side, the changes in x-velocity are stronger and during the full bidirectional phase the x-velocity significantly drops. Since conclusions are qualitatively similar to the singletons only case, numerical values and graphs are not provided here.

Order parameter and rotation range

Next, bidimensional properties can be analyzed and we can start the analysis considering the order parameter which is given in Table 2.18 for the full bidirectional flow phase (the only phase which allows a meaningful comparison between the different configurations). It can be noticed that configuration 4/2 appears to be the most organized in terms of alignment of the lanes formed. This is partially in contrast with the image provided from the fundamental diagram, which showed that 4/2 configuration is the one having the most congested condition (also it is the slowest one). It is however important to remark that for all configurations the order parameter for the case with dyads is always lower then the case with singletons only. This shows again that the presence of social groups has an influence on the smoothness of pedestrian streams and lanes are organized less efficiently.

In this regard, it should be remarked that the difference between both experiments in terms of order parameter becomes larger when the flow ratio grows (the highest at $r = 0.5$). This may imply that the presence of dyads does not significantly deteriorate the overall organization if the flow was already relatively disorganized when it was fully composed by singletons. However, quite organized configurations may be destabilized by the the presence of social groups.

Table 2.18: Order parameter for the different configurations during full bidirectional flow with dyads and singletons. 6/0 configuration is omitted because order parameter is 1 by definition. Uncertainties are 1σ standard deviation. Singletons only results are repeated.

Configuration	Flow ratio	Order parameter	
		Dispersed dyads	Singletons only
5/1	0.167	0.784 ± 0.149	0.824 ± 0.130
4/2	0.333	0.831 ± 0.048	0.881 ± 0.131
3/3	0.500	0.734 ± 0.171	0.938 ± 0.105
S/D	0.500	0.803 ± 0.197	–

Partially in line with the previous remarks, it should be noted that the balanced configuration is now showing the least organized lanes despite the fact it was the most organized when only singletons were used in the experiment. When dyads are included the balanced configuration is the one having the lowest order parameter, ever lower than the S/D configuration having the same flow ratio.

Next, we can consider the rotation range, which is depicted in Figure 2.45. Qualitatively it can be observed that the same shape obtained for the case with only singletons reoccurs when dyads are also included. In particular, low rotation ranges are observed in the initial and final phase (1 and 5 respectively) and for the unidirectional case during the full length of the experiment. Lane formation and dissolution (phase 2 and 4) have the highest rotation range for all bidirectional configurations, meaning that the changes in organization are reflected by rotation within the crowd. Also, amount of rotation during lane formation and dissolution seems to be similar for all bidirectional configurations.
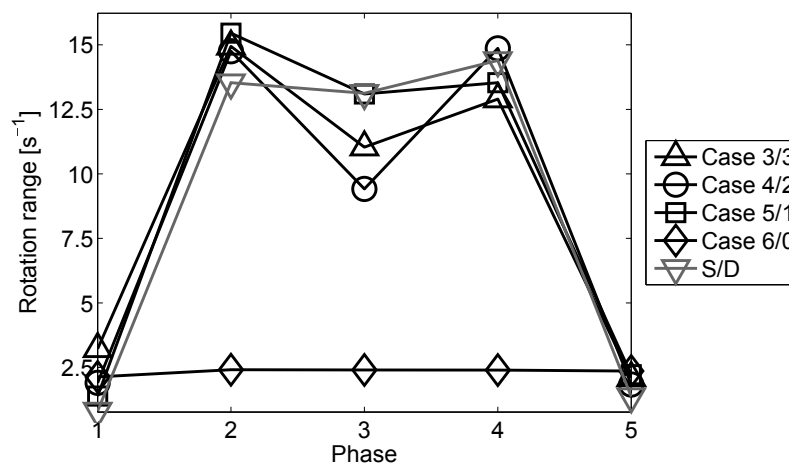
Figure 2.45: Rotation range during the different phases of the experiments involving dyads. S/D configuration is given in gray as it represents a particular case.

During full bidirectional flow (phase 3) a sensible reduction in the rotation range is ob-

served with lanes already formed and moving smoothly (although the amount of reduction changes from case to case). For instance, 4/2 case is the one having the lowest amount of rotation in the full bidirectional phase, which seems to be in line with the remarks done on the order parameter. It is therefore confirmed that the 4/2 case has some peculiarities in the experiment with dyads: crossing time and fundamental diagram implied a comparatively congested motion, but order parameter and rotation range resulted in the opposite interpretation. As a last remark on the rotation range it should be noticed that the S/D configuration does not show the reduction observed in the other cases after lanes are formed: rotation range grows after phase 1 and remains constant between phases 2 and 4. This means that organized lanes actually did not form or were not stable enough to show a significant change in the rotation range.

Dyads behavior

We can conclude the discussion on dyads by considering a particular analysis on the specific behavior of their members. Figure 2.46 and Figure 2.47 show the positions for members of the dyads relative to their center of motion.

(a) 6/0 configuration

(b) 5/1 configuration

(c) 4/2 configuration

(d) 3/3 configuration
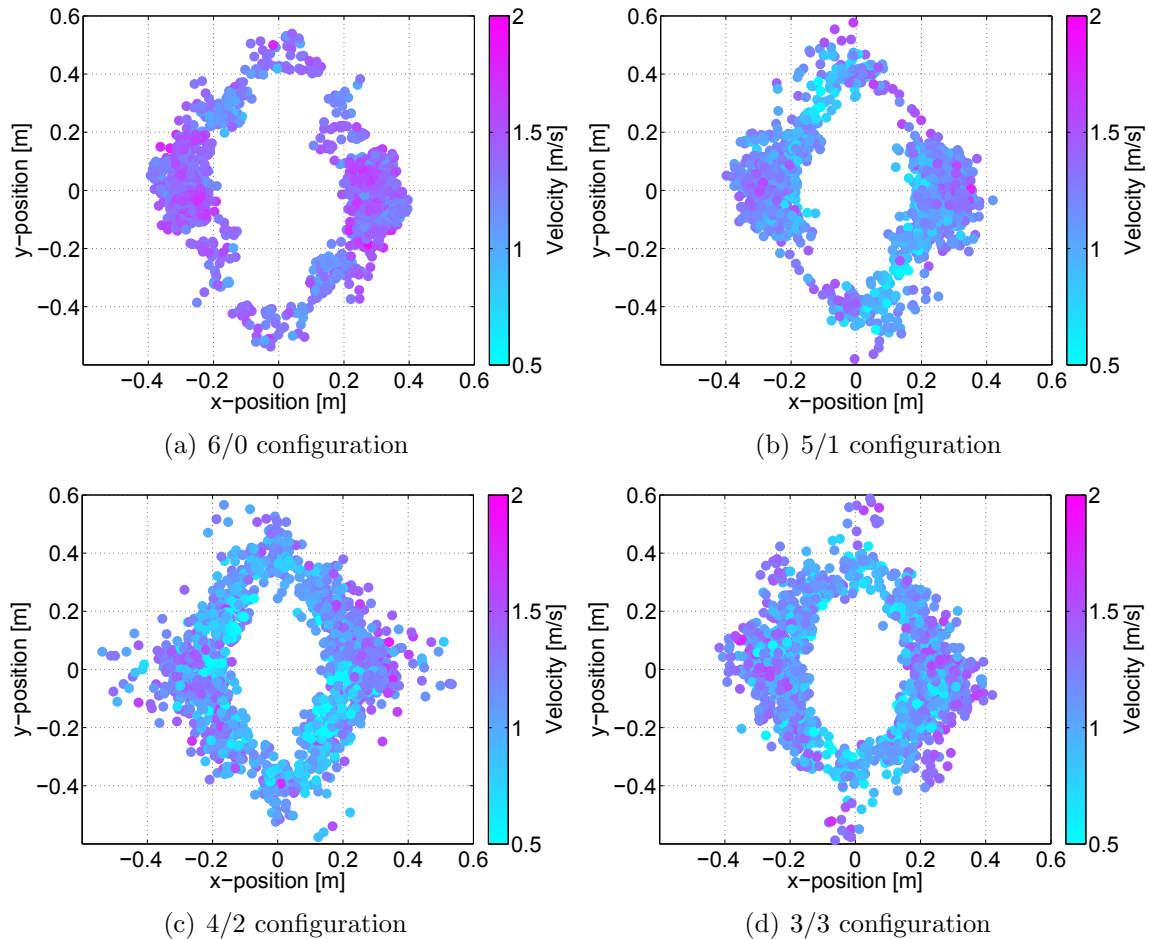
Figure 2.46: Relative position for members of the dyads during the various experimental procedures, colors indicate velocity [135].

For each frame, center of mass of each dyad is computed and the relative position of each member is plotted as a dot in Figure 2.46 and Figure 2.47 (all repetitions and dyads are considered in each plot). Origin is the center of mass and the closest the dots are to

the center the more compact is the shape taken by components of the dyad during the experiment. Dots aligned along the y-axis are representative of the riverlike configuration, while dots aligned along the x-axis are typical of a line abreast configuration. A circular shape means that dyads changed their configuration during the experiment as they walked through the counter flow.

(a) 6/0 configuration

(b) 5/1 configuration

(c) 4/2 configuration

(d) 3/3 configuration
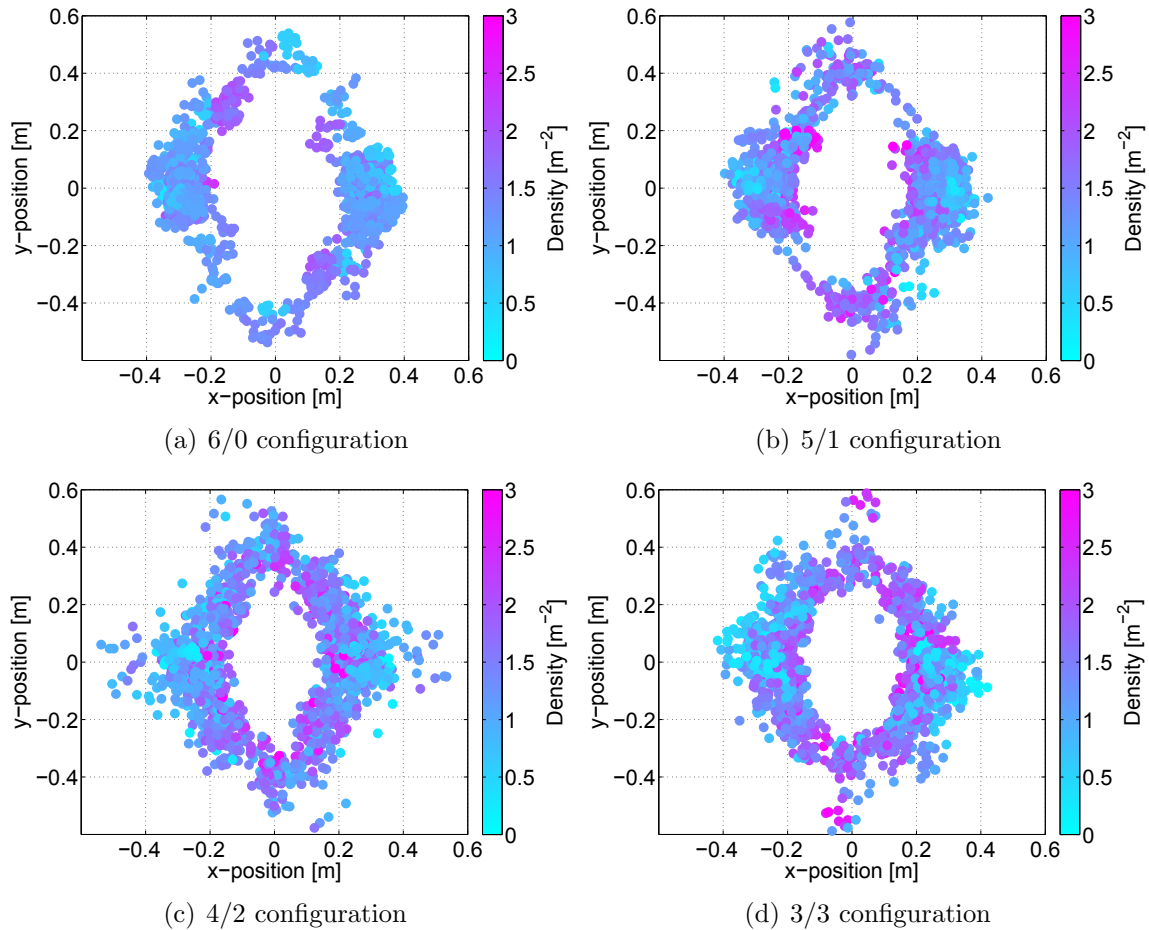
Figure 2.47: Relative position for members of the dyads during the various experimental procedures, colors indicate density generated from the Voronoi cells of the considered participants [135].

From Figure 2.46 and Figure 2.47 it is observed that the closest the members, the highest the density and the lowest the velocity. Concerning the density, it is important to remark that the fact of staying close does not necessarily means higher density as the Voronoi cells are dependent on the other pedestrians lying nearby. The results should be interpreted with the qualitative description that when confronted to a denser crowd, member of the dyads tend to stay closer to reduce their resistance in regard to the counter flow. It can be also noticed that in general the shape taken by dyads can be approximate with one ellipse showing that dyads change from riverlike position to line abreast several times during the experiments, finally resulting in the shapes given in Figure 2.46 and Figure 2.47. It is however necessary to remember that diagrams given are the summary of all dyads during all repetitions and shapes for individual dyads may vary in a certain extent. Finally, we can use the diagrams of Figure 2.46 and Figure 2.47 to understand the differences we observed between the different configurations.

In this regard, it is remarkable to notice that 4/2 configuration is the one having the

widest dispersion (along the x-direction). By considering the resistance in regard to the counter flow created by the largest "cross section" in the 4/2 configuration, it is possible to explain the highest crossing time and the shape of the fundamental diagram observed. On the other side, this largest dispersion could have resulted in a more effective utilization of space which is confirmed by noticing that 4/2 configuration had a number of lanes close to 4, i.e. two lanes for each direction. This can explain the high values obtained in the order parameter and the low level of rotation. Also, from the crossing time, we know that in the 4/2 case dyads have the smallest dispersion among bidirectional configurations, while singletons the highest one. By also visioning the videos of the experiment it can be observed that in the 4/2 configuration dyads took a central role in determining lane structure, which resulted in a ordered flow, but also limited the freedom of motion of singletons.

It can be therefore concluded that, from a microscopic point of view, the coordination between dyads and singletons is beneficial for the overall group and the dispersion of dyads inside the crowd can play an important role in obtaining this form of coordination. However, as we will see later, when a very macroscopic approach is taken in terms of both space and time, then differences may cancel out and different cases have similar probabilities of resulting into jam over the long run.

2.5.4   Results of the validation experiment

The validation experiment was performed with the same modalities as the singletons only experiment, although geometrical dimensions were slightly different (2.4 m corridor instead of 3.0 m) and participants were completely changed (experiment date was in fact 6 months later in respect to the experiments reported above). Since one of the objectives of this experimental campaign was to check the validity of the methods introduced in the previous experiments by employing different participants and making small changes in geometrical setup, it is convenient to limit the discussion to relevant points and skip those aspects which are similar to what reported above.

Crossing time and fundamental diagram

We will start again from the crossing time which is reported in Table 2.19.

Table 2.19: Average crossing time for the different configurations (UNI = unidirectional, BI = bidirectional) in the validation experiment. Uncertainties are 1σ standard deviation.

Case	Type	Flow ratio	Crossing time		
			Complete group	Major flow	Minor flow
4/0	UNI	0.000	6.643 ± 0.258 s	6.643 ± 0.258 s	–
3/1	BI	0.250	7.471 ± 0.803 s	7.787 ± 0.645 s	6.571 ± 0.449 s
2/2	BI	0.500	7.772 ± 0.910 s	8.178 ± 0.945 s	7.332 ± 0.626 s

A first look on Table 2.19 reveals that crossing time are significantly lower than in the first round of experiments (singletons only and dispersed dyads). For the unidirectional case in the first experiment with singletons it was 7.273 s and 7.393 s for the configuration with dyads. The different crossing time was clearly related with the much lower temperature (the relation between walking speed and temperature was already reported by Weidmann).

Apart from the differences in absolute values, the relations observed in the first experiment with singletons concerning flow ratio and crossing time dispersion/average are generally valid. Probably the only difference worth noticing is that the large dispersion in the minor flow is now observed for the balanced case (in the singletons experiment was the 5/1 configuration), although the small number of bidirectional configurations considered here is not enough to allow coming to a conclusion on this aspect.

As usual it is also important considering the fundamental diagram which is given in Figure 2.48.
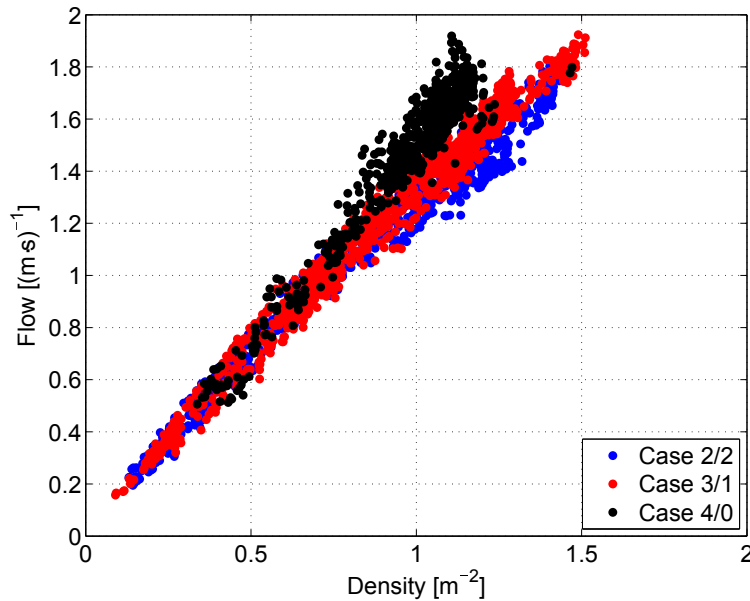
Figure 2.48: Comparison of the different fundamental diagrams for the validation experiment; no differentiation is made between minor and major flow [130].

The three cases considered show a very clear linear relationship meaning that uncongested motion was observed; the three different slopes observed indicate different walking speeds although the differences are not particularly large and are mainly limited to the bidirectional cases. Again, as Zhang et al. observed, the fundamental diagram allows to distinguish uni- and bidirectional flow and to make general considerations, but to understand the details additional analytical tool are required.

Order parameter and rotation range

By considering the order parameter for the full bidirectional flow as reported in Table 2.20 it becomes evident that both bidirectional configurations have almost perfectly aligned lanes, since in both cases the order parameter is very close to unity.

Considering the very close values for the 3/1 and 2/2 configuration and the associated deviations, it is impossible to define which configuration is the most organized. We can use again the rotation range to gain some deeper understanding of the changes occurring during the experiments as given in Figure 2.49. The rotation range of Figure 2.49 partially confirms the qualitative remarks made on the basis of the order parameter, i.e. that differences between both bidirectional cases are minimal. Both configurations clearly show the typical inverted "W" shape observed so far, but in contrast to previous cases they appear to be shifted in magnitude but qualitatively similar in trend.

Table 2.20: Order parameter for the different configurations during full bidirectional flow [130]. 4/0 configuration is omitted because order parameter is 1 by definition. Uncertainties are 1σ standard deviation.

Configuration	Flow ratio	Order parameter
3/1	0.250	0.980 ± 0.040
2/2	0.500	0.958 ± 0.051
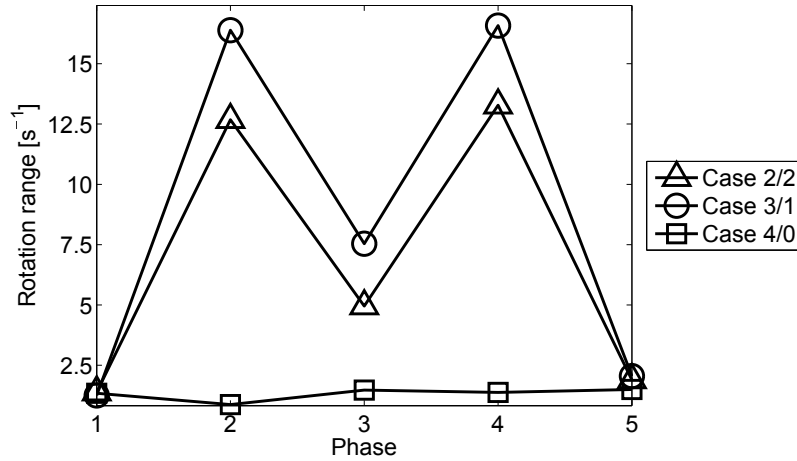
Figure 2.49: Rotation range during the different phases of the validation experiment [130].

In part, the goal of the validation experiment to confirm newly introduces techniqued has been achieved as the rotation range has clearly showed that it is possible to distinguish different phases. Also, the high level of stability reached when lanes are formed is clearly seen. But the validation experiment also showed that the figure on bidirectional streams is more complex, as the differences observed so far partially vanished by using a slightly smaller corridor. The number of lanes observed during the validation experiment was about 0.5–1.0 smaller [12] compared to the first experimental campaign and on average 4 lanes were observed, roughly matching the initial starting configuration. It can be concluded that the smaller corridor led toward a quicker and more efficient organization and the reduced number of starting rows further contributed in this direction. On the other side, in the initial experimental campaign the number of lanes formed is smaller than the number of rows in the starting configuration which means that participants tried to form new structures while crossing the corridor.

2.5.5   Comparison with the experiments by Zhang et al.

Finally, to conclude the part dedicated to the supervised experiments it is worth completing the comparison with the work by Zhang et al. started by introducing the past literature. In the initial discussion we only considered the analytical approach taken by Zhang et al. or other authors analyzing their data. For instance, fundamental diagram and velocity distributions have been discussed and order parameter has been computed while introducing the concept. However, as we have seen in this experimental discussion, the newly introduced rotation range is also relevant and we can therefore use this ap-

---

[12]Number of lanes is averaged over long time and for different configurations, resulting in rational values.

proach on the data by Zhang et al. from their analytical campaign.

Figure 2.50 shows the evolution of the rotation range for the case in which participants were able to choose their destination and the case in which they had assigned destinations (forcing the creation of a congested "cross flow").

(a) Free choice (BIB-free)   (b) Fixed destination (BIB-fixed)

Figure 2.50: Rotation range for the different setups considered by Zhang et al. (data are openly available [98], figure were independently generated). In some points grid cells were not sufficient to compute rotation range. Values given in the legends refer to the waiting rooms doors' width. In some points rotation range could not be computed.

In Figure 2.50(a) it is observed that for small densities, i.e. when the width of the doors in both waiting rooms were small (namely 1 and 1.5 m), rotation range is limited in all phases. Values around 2.5 s^{-1} were typical of unidirectional streams in the cases observed so far and this observation confirms the hypothesis made by some researchers, that, under certain conditions, space is equally used by main and counter flow leading to a level of stability typical of unidirectional flows. It is interesting to notice that when the width of the doors was set at 1.8 m the flow start smoothly in phase 1 and lanes are efficiently formed in phase 2. However, the rotation range keeps growing, meaning that adjustments are required to keep the lanes organized. Still, in the 1.8 m case, the rotation range measured during phase 3 is around 5.0 s^{-1}, a value which was judged as "stable lanes" in the previous cases. When the doors are further opened then lanes do not naturally form from the beginning and significant rotation is required in phase 2 to reach a stable configuration. Also, lanes are increasingly less stable and rotations are necessary to keep them organized in phase 3.

We can now consider the case with fixed destinations for which the rotation range is depicted in Figure 2.50(b). A clearly different image is obtained with the rotation range peaking during phase 3 for narrow door width configurations (1.0, 1.5 and 1.8 m, partially for 3.2 m) and peaking at phase 2 for configurations having large inflows. It should be reminded, that rotation range was first introduced for low density experiments in which velocities do not significantly change in magnitude. However, in the case of Zhang et al. there are significant changes in velocity, since densities are considerably higher. To account for changes in velocity and still being able to consider bidimensional aspects, it is convenient to introduce the relative rotation range [13] obtained by dividing the rotation range with the x-velocity (forward motion) whose results are shown in Figure 2.51.

---

[13]In Chapter 3 we will call the call the relative rotation range as "congestion level".

(a) Free choice (BIB-free)   (b) Fixed destination (BIB-fixed)

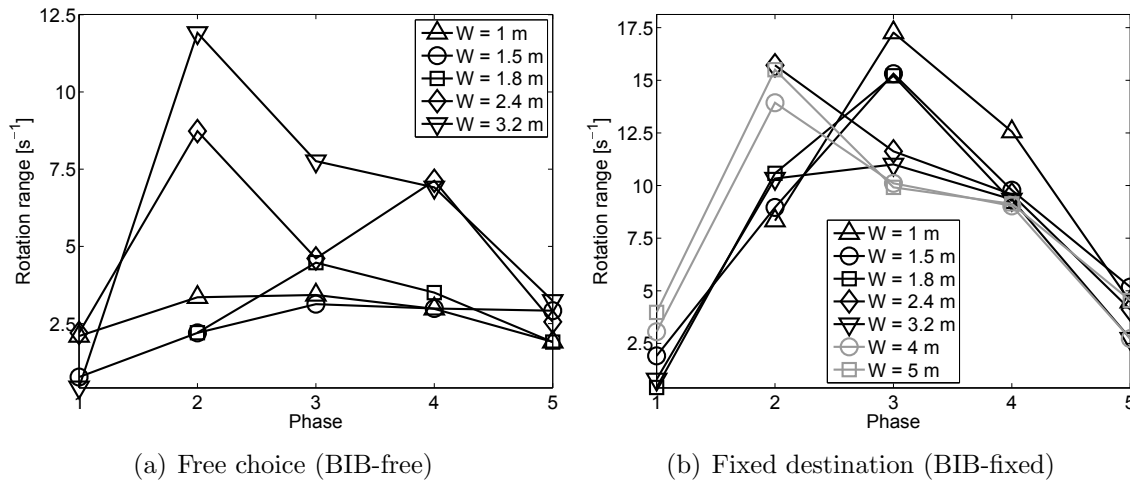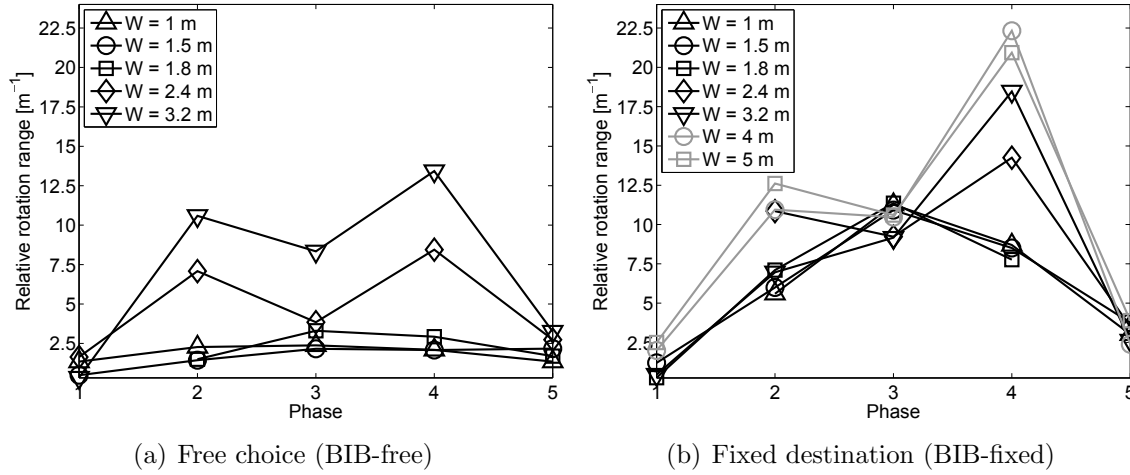Figure 2.51: Relative rotation range (rotation range divided by x-velocity) for the different setups considered by Zhang et al. (data are openly available [98], figure were independently generated). Some points are missing as in Figure 2.50.

From Figure 2.51(b) it can be observed that although qualitative results do not change for phase 2, when velocities are still relatively high, there is a significant change in phase 3 and all cases show similar values of relative rotation range. When both configurations are compared in Figure 2.51(a) and Figure 2.51(b), the differences in phase 3 (full bidirectional flow) become evident. For free destination choice and low densities (up to 2.4 m door width) a low relative rotation range is obtained, meaning that lanes were stable and smooth. At high densities (3.2 m) instabilities arose and in the fixed destination case all configurations resulted in comparatively congested motion due to the experimental setup. It is also interesting to notice that the highest values for relative rotation range are obtained in phase 4 when lanes dissolve, meaning that, in general, dissolution of lanes tend to be more chaotic than their formation, possibly due to the fact that participants did not face a large number of counter flow pedestrians.

Finally, the unbalanced case considered by Zhang et al. is investigated and results for the rotation range and its relative equivalent are given in Figure 2.52.

The general image presented analyzing the unbalanced configuration (with fixed destinations) is not much different from the balanced case with fixed destinations. The reasons for this small differences may be related to the flow ratio adopted by Zhang et. being of about 0.4, i.e. quite close to the balanced case. It is also necessary to remark that experiments by Zhang et. were performed for a relative long time period, so it is possible that some sort of transient effect arose, minimizing the differences between balanced and unbalanced configuration. Nonetheless, it is worth noticing that the several setups considered so far show similar qualitative properties, meaning that the concept of rotation range can successfully grasp changes in bidirectional flows.

2.5.6   Summary

Pedestrian bidirectional flow has been studied by designing a set of experiments in which flow and density have been kept fairly constant and flow ratio was changed to grasp its influence on lane formation and the efficiency of the flow itself. Experimental conditions were chosen considering previous research and characteristic situations observed in reality. Aim of the experiments was to study typical geometrical configurations and social

(a) Rotation range

(b) Relative rotation range
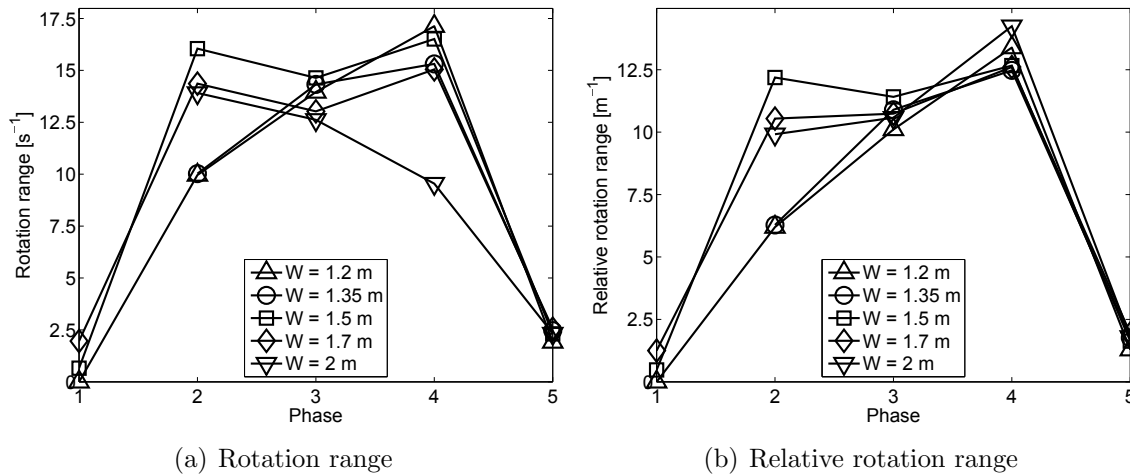
Figure 2.52: Rotation range and relative rotation range for the unbalanced case (with fixed destinations) investigated by Zhang et al. (data are openly available [98], figure were independently generated), flow ratio was set to around 0.4 (small fluctuations can be expected). In some points grid cells were not sufficient to compute rotation range.

structures by collecting a sufficient amount of data using state-of-the-art techniques. Results showed that to understand the phenomena leading to lane formation and to measure the stability of each case, 5 different phases need to be distinguished:

- Phase 1: unidirectional free flow. Both minor and major flow simply keep going straight. Most of pedestrians barely turn in this phase and little anticipating actions are taken to avoid the incoming counter flow.

- Phase 2: lane formation. Pedestrians turn to the left and to the right in a large extent to allow the creation of lanes. The lateral motion is particularly strong in the case of balanced flow. Lanes are formed at the end of this phase.

- Phase 3: full bidirectional flow. Lanes flow separately in a unidirectional manner. At low densities and for individual behavior, the stability is particularly strong in the balanced case, to an extent in which each lane can be considered separately, as if a wall would be placed between them. If the difference between the minor and the major flow is large, lanes tend to be more unstable. Stability during this phase is also affected by the presence of dyads or aspects related to density and route choice.

- Phase 4: lane dissolution. As the flow becomes partly unidirectional in portions of the surface, lanes are dissolved. Large lateral movements are observed resulting in an high rotation range because pedestrians take advantage of the reduced density while leaving the measurement section.

- Phase 5: unidirectional free flow. Only unidirectional streams are observed. Again, pedestrians simply keep going straight toward the destination. Rotation is very limited here.

In addition, we showed that statistical quantities are required to analyze pedestrian streams and simple average values are not sufficient to grasp the fundamental characteristics. In this regard, the use of bidimensional quantities can help understanding some of the behaviors observed and, in particular, the rotation applied to the velocity vector

field has shown being of particular importance. Concerning social structures we showed that coordination between different entities becomes relevant to assure a smooth flow and the dispersion of groups inside the crowd plays an important role in this regard.

Finally, this experimental part allowed advancing some initial guess on the virtually different conclusions concerning balanced bidirectional flow. It is possible to summarize all experiments by noticing that once lanes are formed, the balanced bidirectional flow is the most efficient. However, the relatively large extent of lateral motion required to create lanes can lead to jam formation when the density increases. This explains why, besides the higher efficiency at low densities, balanced bidirectional flow results in partial deadlocks earlier compared to low flow ratio cases at high densities as we have seen in the on-field observation.

2.6 Theoretical description of phase transitions and comparison with experimental data

In the previous experimental part we have seen that there are several flow regimes which can be distinguished in bidirectional flows. So far, our focus has been mostly set in understanding microscopic mechanisms with a particular regard on lane formation and its connection with the formation/dissolution of congestion. We want to continue this type of analysis but extend it to a larger database of experimental data and verify if and to which extent the analysis presented so far can be applied to more real situations. In addition, we also want to move into a macroscopic scale and investigate how the transition from different states can be described mathematically.

Concerning this last aspect; in the literature overview we have seen that several functions have been defined to quantify capacity of bidirectional flows. Here, we want to find a way to understand the differences and potentially unify them. In this regard, we need to remember that transition to congestion may depend on a number of factors: flow ratio, overall group size, density, social group composition, route choice and surrounding environment just to mention few. We will see which one is relevant and what are the most important quantities describing stability and efficiency of bidirectional flows.

Becoming able to quantify the capacity of bidirectional flows and define the different phase transitions is important because it means predicting incoming congestion at the early stages. As we have seen in Chapter 2.3, phase transition in bidirectional flow has been often studied by means of simulation and some theoretical approaches have been used in particular to obtain the fundamental diagrams of CA systems. However, descriptions based on experimental data are not common and the approach presented in Chapter 2.4 (on-field observation) had the disadvantage of relying on transient data, meaning that congestion can be only recognized after it already occurred.

Therefore, in addition to the above goal of obtaining a mathematical description for capacity, we also want to define a method to compute the probability of a given configuration to turn into congestion if the observed condition should continue for a long time.

2.6.1 Experimental database

To investigate more in detail properties of bidirectional flow with a particular regard to phase transition we created a database consisting of different experiments and observations performed by several researchers. This section will be devoted in explaining those

experiments and the way in which are categorized into different groups.

Table 2.21 and Table 2.22 present some of the characteristics of the experiments included in our database. Most of the experiments were described in the previous sections (Chapter 2.3, 2.4 and 2.5), so here we will focus on the ones being newly introduced.

Except for dataset G (on-site observation of Omote-sando subway station), they all consists of a collection of pedestrians' trajectories gained in controlled conditions or during observations. Dataset G was created by analyzing the flow data obtained from the 45 minutes observation and categorizing each peak according to the discrimination technique introduced earlier (in Chapter 2.4) [14]. The dataset for case G contains inflow in each direction and the flow regime observed chosen among free flow, organized motion in lanes and congestion.

In most of the cases pedestrians trajectories were obtained using an image processing software (mostly PeTrack [86, 87]), although in F pedestrians trajectories were automatically computed using an algorithm analyzing data gained from several laser finder sensors. In the experiments by Zhang et al. (D & E) images from two different cameras were combined to cover the full length of the corridor. As shown in Table 2.22, many studies specifically considered the balanced bidirectional flow, so most of the data regard cases with a flow ratio close to 0.5. The number of pedestrians involved also varies greatly from study to study, with the lowest figure being of 50 participants for the controlled experiment in B (validation experiment) and empirical observations combining results from more than 1000 pedestrians. Most of the studies (observations included) focused on pedestrians behaving individually (singletons), with the exception of the experiments with dyads in which about 40% of the participants behaved in pairs. One of the most distinguishing element between the different cases concerns the destination choice. For the cases A–D participants to the experiments were able to choice freely the direction from which leave the corridor after traversing it (either right, left or straight). As seen previously, under this condition, lanes can easily form and tend to be stable.

In E–G pedestrians were aiming to a particular destination and had therefore to cross the corridor in a specific direction (or angle). As a reminder, in the particular case of the dataset provided in E, half of the participants were asked to leave the corridor from the left side and the other half from the right side (thus creating a sort of cross-flow inside the corridor). Datasets F–G refer to observations and it is more difficult to determine if pedestrians were aiming at a particular destination or just intended to cross the corridor. However, considering that both cases refer to subway stations it is possible to guess that pedestrians were aiming to a particular exit/platform, thus limiting their freedom of choice. As a consequence, we overall observed for the datasets E–G that some sort of lanes actually formed, but tended to be unstable since pedestrians needed to cross the corridor with different angles.

Finally, it is also important to remember that geometries were not the same for all the experiments and different strategies were used to calibrate the flow ratio when needed. Since these points were previously discussed in detail, the diagrams provided in Figure 2.53 should be sufficient for understating the differences.

On the overall, the database created allows to study the dynamics of bidirectional flow from a density of about 0.1 m^{-2} up to a maximum of 6 m^{-2} (or 3 m^{-2} if only datasets including trajectories are considered). Pedestrian flow also covers the range of values typically reported in the literature, with a maximum value of about 2 (m·s)$^{-1}$. Geometrical

---

[14]As a reminder, flow regime was categorized using the difference between in- and outflow. Inflow peak will be taken here as the flow in each direction corresponding to the observed flow regime.

Table 2.21: Experiments and observations considered in the empirical database [95]. Except for F, all the cases have been discussed in detail before. In some cases data are openly available and provided in the references. Total time refers to the total length of the experiment/observation (excluding breaks); time considered refers to the portion of time used for data analysis here. With the exception of G, data obtained are pedestrians' individual trajectories.

#	Experiment/observation name	Type of study	Sensor	Data extraction	Recorded time Total	Considered
A	Singletons only	Controlled experiment	Single camera	Tracking software	12 min	12 min
B	Validation experiment	Controlled experiment	Single camera	Tracking software	8.5 min	8.5 min
C	Dispersed dyads	Controlled experiment	Single camera	Tracking software	11 min	11 min
D & E	Campaign by Zhang et al. [98]	Controlled experiment	2 cameras	Tracking software	25 min	25 min
F	Data by Zanlungo et al. [136, 137]	On field observation	Laser finder	Automated algorithm	1 day	60 min
G	Omote-sando subway station	On field observation	9 cameras	Manual counting	2 h	45 min

Table 2.22: Scenario dimensions, crowd properties and social structure for the considered cases [95]. Destination refers to the condition if pedestrians were aiming to a particular destination or just intended to cross the corridor (direction irrelevant).

#	Destination	Social group	Corridor size Length	Width	Maximum Density	Flow	Flow ratio	Pedestrians
A	Free choice	Singletons	10 m	3.0 m	≈ 1.5 m^{-2}	≈ 2 (m·s)$^{-1}$	0, 0.17, 0.33, 0.50	54
B	Free choice	Singletons	10 m	2.4 m	≈ 1.5 m^{-2}	≈ 2 (m·s)$^{-1}$	0, 0.25, 0.50	50
C	Free choice	Dyads and singletons	10 m	3.0 m	≈ 1.7 m^{-2}	≈ 2 (m·s)$^{-1}$	0, 0.17, 0.33, 0.50	54
D	Free choice	Singletons	8 m	3.6 m	≈ 2 m^{-2}	≈ 1.7 (m·s)$^{-1}$	0.4, 0.5	≈ 300
E	Fixed	Singletons	8 m	3.0 m & 3.6 m	≈ 3 m^{-2}	≈ 1.8 (m·s)$^{-1}$	0.5	≈ 300
F	Fixed?	Various	20 m	8.0 m	≈ 0.1 m^{-2}	≈ 0.1 (m·s)$^{-1}$	0–0.5	>1100
G	Fixed?	Various	11.1 m	6.0–7.4 m	≈ 6 m^{-2}	≈ 2.1 (m·s)$^{-1}$	0–0.5	>8700

(a) Experimental configuration in A–C   (b) Experimental configuration in D & E
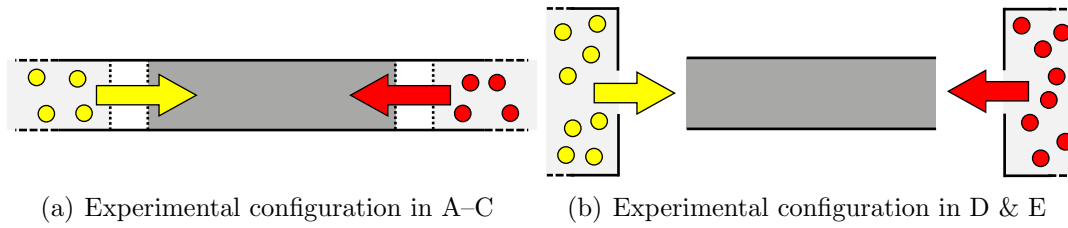
Figure 2.53: Test section (central corridor) and waiting (starting) areas for different types of experiment [95].

dimensions of the corridors also show some variation with the aspect ratio (length divided by the width) ranging from 1.5 to slightly more than 4. As we will see later, it is however convenient to group the different studies in 4 categories as shown in Table 2.23.

Table 2.23: Grouping of datasets with similar properties and possibility to learn from experience [95].

#	Case study	Dataset(s)	Learning possible?
(a)	Natural small group interaction	A & B & C	No?
(b)	Continuous flow forced direction	E	No
(c)	Repeated configuration free choice	D	Yes
(d)	Empirical observations	F & G	No?

The categories reported in Table 2.23 are not relative to geometrical or "fluid-dynamic" properties (flow, density and speed), but they rather refer to conditions at which the experiments (observations) were performed. Datasets A–C consists of experiments with a relatively small number of pedestrians walking in a more or less natural environment and without any specific indication on destination or behavior to be followed. In those cases groups were shuffled during each execution and therefore participants were not able to get any advantage from the multiple repetitions. It is therefore excluded (or very unlikely) that participants were able to develop some form of organization evolving over the time of the experiment (i.e. a long term cognitive process).

In the experiment of E each pedestrian was asked to leave the corridor from a different location (half left and half right). Therefore, although experiments were repeated under similar conditions, pedestrians did not get any advantage by knowing the experimental setup. This was not the case for the experiment described in D, where participants had the freedom to choose from which side of the corridor to leave. After the first low density execution, two lanes clearly formed dividing both flows. At the second execution, participants already learned that forming two lanes would make crossing of the corridor easier and they continued showing this behavior until the last repetition. The case reported in D is therefore different from the cases usually considered in traffic engineering (or binary particle systems), since it represents a situation which rarely forms in reality. As will see later, it is however interesting to study this specific case. Finally, we decided to consider F & G together since are both relative to empirical observations. In addition, density and flow observed in both cases are very different and it is therefore possible to distinguish both cases also when plotted in the same graph.

To consider cognitive aspects more consistently we also evaluated the Performance Shaping Factors (PSF) for each group of experiments. Results are given in Table 2.24 where the

Table 2.24: Human Reliability Analysis (HRA) based on the SPAR-H method [138, 139, 95]. Multipliers refer to each Performance Shaping Factor (PFS) and the product of them is given as a measure relative to the probability to fail in the task (translated into passing the corridor here). Ergonomics and human machine interaction has been omitted as experiments did not include handling machines.

Case study	(a)	(c)	(b)	(d)
Free choice?	Yes	Yes	No	No?
Available time		Nominal = 1		Scarce = 10
Stress and stressors	Nominal = 1		High = 2	
Complexity			Obvious = 0.1	
Experience and training			High = 0.1	
Procedure		Nominal = 1		Poor = 5
Fitness for duty			Degraded fitness = 5	
Work process			Good = 0.8	
Product	0.04	0.08	0.4	5

different cases have been sorted based on the overall score resulting from the product of the various factors. In each case the task which is analyzed is constituted by the crossing of the corridor (therefore an action in the SPAR-H approach for the Human Reliability Analysis). For all experiments analyzed (A–E) time was sufficient to perform the task (and participants were paid for it), but in the observations considered here pedestrians were in a train station and time factor was surely more relevant (probably more in G than F). This explains the different choices in Table 2.24. The different levels of stress considered in the PFSs are related with crowd density, which clearly has a contribution. Finally, we distinguished two cases each on the procedure PFS. Observations in which pedestrians did not had a preferential way are considered at the same level of the experiment in which destinations were mixed, i.e. existing but poor procedure. Experimental cases with freedom of choose and no crossing paths have a nominal value for the procedure PSF. The remaining PFSs have been set equal for all the cases.

Results show that natural small group interaction have a small overall coefficient, followed by the free choice configuration and the one with forced directions. Empirical observations have the highest value mostly due to time constraint and crowd density. This type of categorization allows to objectively see the discrepancies between each case and it is clear that the empirical cases in particular need to be considered with special regard. In addition, we can predict that choice of direction could have an influence on the results.

2.6.2   Analysis results and discussion

This section will present the analysis of the database introduced above and the results obtained from it. Figure 2.54 should be used as a reference in the following discussion. The overall process for analyzing pedestrians' trajectories can be summarized as follows. Each case will be divided into small time intervals and for each interval flow regime, degree of (self) organization, flow and density will be computed. To determine the flow regime, the correlation coefficient and the obstruction index (which will be introduced hereafter) are used. The level of organization is typically computed using the order parameter, but we will use another approach (lane variance) to avoid issues related to the relation
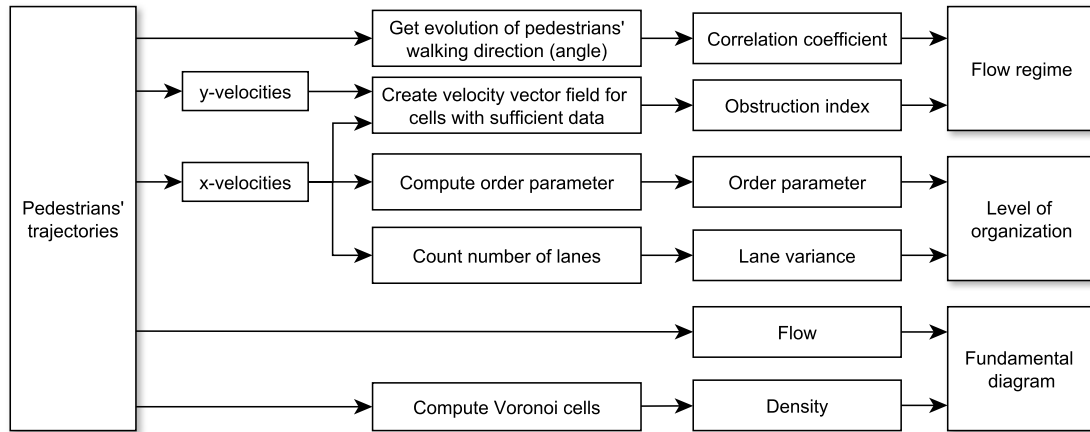
Figure 2.54: Summary of the quantities considered in this study and methods used to compute them [95].

between order parameter and flow ratio. After presenting the results for flow regime we will propose a model which can be used to describe phase transition (and capacity in particular) in relation with flow ratio.

Flow regime

To start with, we will present the procedure used to obtain the flow regime at different moments. The underlying principle is the same to the one presented in Chapter 2.5.2, i.e. the corridor is divided into a mesh in which the average velocity is computed to create a vector field representing the overall crowd movement. Also here, a mesh size of 0.2 m is used, equivalent to half the mesh size usually employed in CA simulations, i.e. 0.4 m. In addition, the use of a mesh composed of 0.2 m cells allows to consider crowds up to 25 m^{-2}, well beyond the physical limits for human crowds.

The different cases considered in the database have been divided into time intervals ranging from 3 to 4 s and in each interval average velocity was computed for each cell. A variable time interval was used because some of the experiments are relatively short (between 10 and 20 s) and by fixing a time interval, some part of them would get lost. Applying this method on the whole database resulted in a time interval of 3.35 ± 0.13 s, showing that, besides the relatively large variation allowed, time intervals were relatively similar from case to case.

To characterize the flow regime (and subsequently phase transition) obstruction index and (trajectories) correlation coefficient have been used. The obstruction index is a measure based on our previous observation that lateral movements have an important role in bidirectional flows and also supported by the conclusions from Weng et al. [68], who, working on a simulation model, concluded that phase transition is triggered by "spontaneous fluctuations". We can simply assume that congestion will form easily if the number of lanes is high and pedestrians move laterally to a large extent. The obstruction index is therefore the product of the average number of lanes and the y-velocity [15] over the time interval considered and the whole surface of the corridor. In mathematical terms:

---

[15]Absolute value is used to account for lateral motion and oscillations on the left and right side altogether and in the same measure.

$$\mu = \frac{N_{lanes}}{w_{corr}} \cdot \overline{|v_y|} \tag{2.39}$$

where N_{lanes} is the average number of lanes, w_{corr} the width of the corridor and $|v_y|$ the average (absolute) y-velocity (μ was chosen due to the similarity with the friction coefficient). The relative rotation range has been also tentatively used to define phase transition, but the approach using the obstruction index was found more effective and stable as we will discuss later.

The (trajectories) correlation coefficient was introduced to detect the formation of lanes. This approach is not new and has been already used to detect collective motion in birds [140]. By noting pedestrian position with $\vec{p} = (x(t), y(t))$ we can quickly compute the velocity as:

$$\vec{v} = (v_x(t), v_y(t)) = \frac{d\vec{p}}{dt} = \left(\frac{dx(t)}{dt}, \frac{dy(t)}{dt} \right) \tag{2.40}$$

with dt being the time interval used for differentiation (3 video frames or about 0.1 s here). The evolution of the walking direction $\theta(t)$ can be computed according to:

$$\theta(t) = \tan^{-1} \left(\frac{v_y(t)}{v_x(t)} \right) \tag{2.41}$$

resulting in a single quantity function (only time). This procedure can be applied for all pedestrians detected in a specific time interval. Finally it is possible to compute the correlation coefficient between the various pedestrians. Assuming that pedestrian i moves according to $\theta_i(t)$ and pedestrian j according to $\theta_j(t)$ we can define the correlation coefficient between both pedestrians as R_{ij}. When all pedestrians are considered this will result into the symmetric matrix:

$$\mathbf{R} = \begin{bmatrix} 1 & R_{12} & R_{13} & \dots & R_{1N} \\ R_{12} & 1 & R_{23} & \dots & R_{2N} \\ R_{13} & R_{23} & 1 & \dots & R_{2N} \\ \vdots & \vdots & \vdots & \ddots & \vdots \\ R_{1N} & R_{2N} & R_{3N} & \dots & 1 \end{bmatrix} \tag{2.42}$$

where N is the number of pedestrians. The overall correlation coefficient can be obtained by taking the average of the absolute value of either the upper or lower triangular matrix (excluding the diagonal elements). In case only one pedestrian is detected an overall correlation coefficient of 0 is assigned (calculation is obviously not possible in this case). When pedestrians move in a lane, motion among them is "synchronized" and therefore the correlation coefficient can be used to judge the existence of lanes.

The two quantities presented above has been used to discriminate between different flow regimes in each time interval and the threshold values has been defined as follows:

- Congestion: obstruction index bigger than 0.1 s^{-1} and density bigger than 0.30 m^{-2}.

- Organized flow (lanes): average correlation coefficient larger than 0.1 and density bigger than 0.15 m^{-2}.

- Free flow: none of the above conditions.

Density has been used in the above discrimination to exclude exceptional cases which could lead to erroneous categorization. A typical case is represented by a pair of pedestrians walking close to each others' in an empty corridor. This would lead to an high correlation coefficient at very low densities and therefore a threshold value for density is required. Analogously few pedestrians walking in the vertical direction in an almost empty corridor would result in a relatively high obstruction index and to exclude this case a threshold value for density is required. As a final remark it should be noted that dataset G is not based on pedestrians trajectories but the categorization was possible using an alternative method (as discussed earlier in Chapter 2.4).
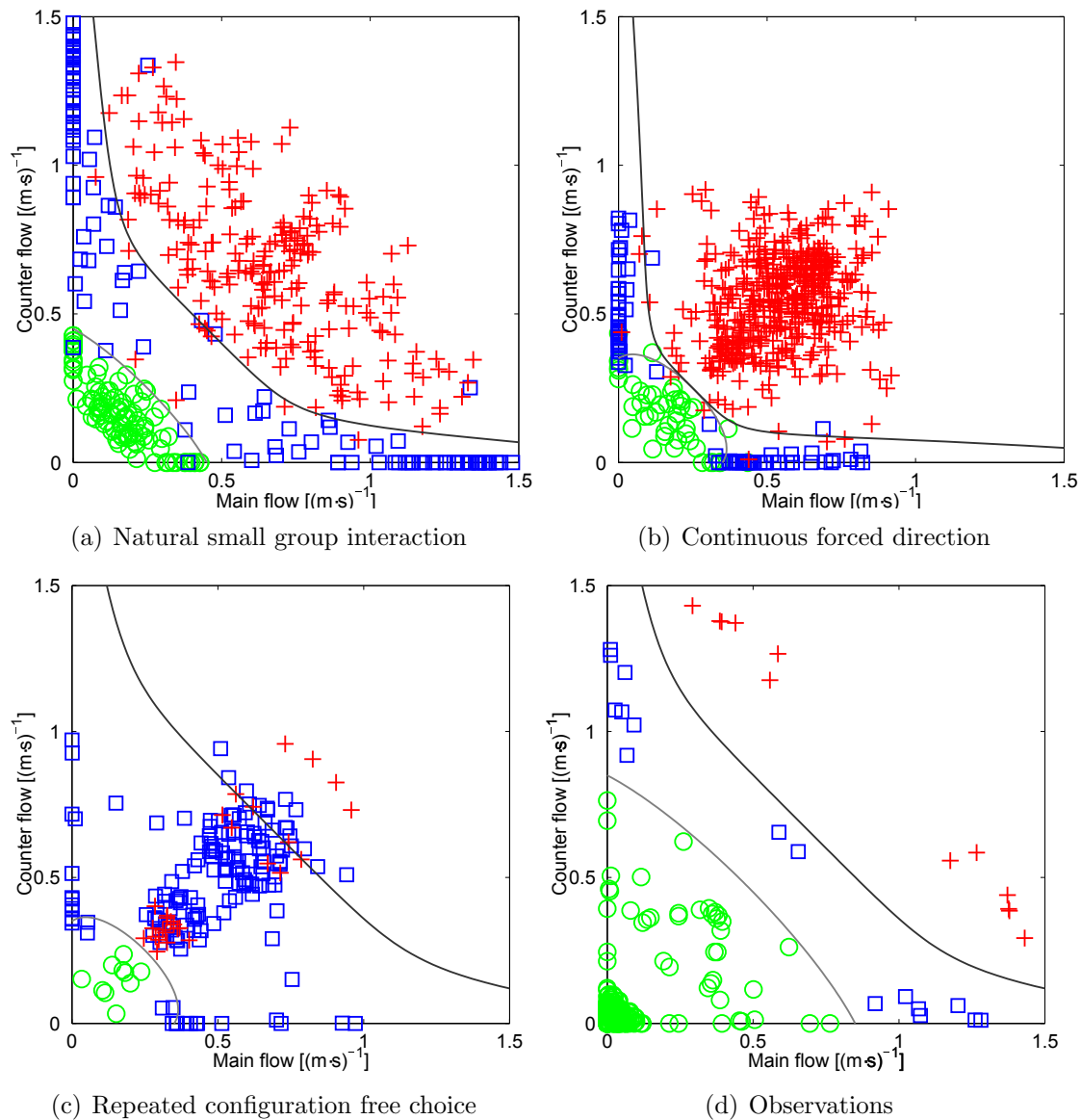
Figure 2.55: Flow regime and phase transition for the different cases considered in Table 2.23. Crosses represent congestion, squares organized flow and circles free flow [95].

We can now use the above discrimination mechanism and plot each case by using its corresponding amount of flow in each direction. Figure 2.55 presents the results where crosses are used for the congested flow regime, squares for the organized flow and circles for free flow. In the experiment involving a small group of participants (Figure 2.55(a)) a clear phase transition is shown when going from free flow to organized lanes and when

changing into a congested motion. The transition is still clear but less sharp for the case involving forced direction (Figure 2.55(b)) and is somehow vague for the series of experiment involving a learning process (Figure 2.55(c)). In the case of the observations (Figure 2.55(d)) clear transitions are also observed, but the number of points is rather limited and results could change when more data becomes available. It is also interesting to notice that in the case with forced direction a direct transition from free flow to congestion is observed for the balanced case.

(a) Small group interaction   (b) Forced direction   (c) Free choice with learning process
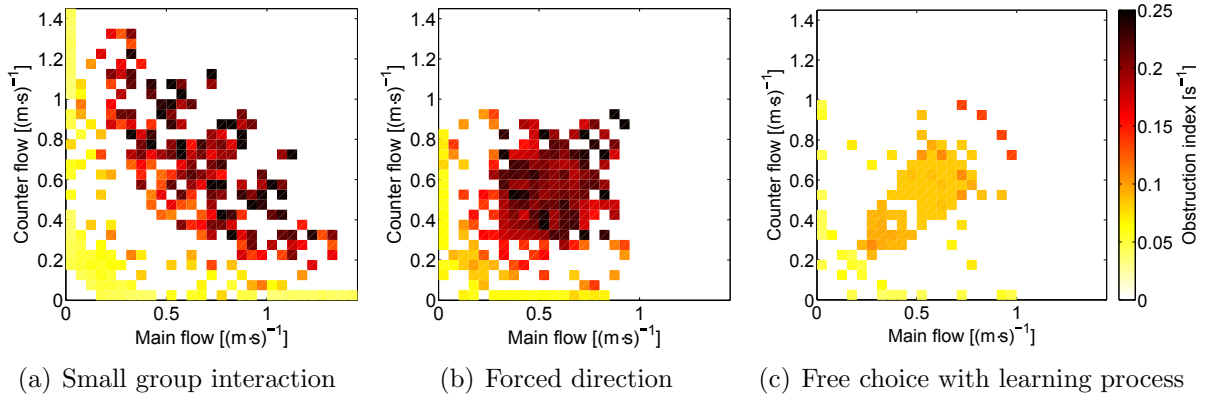
Figure 2.56: Obstruction index for the cases given in Table 2.23 (except observations) [95]. Results are averaged for equivalent combinations of main flow and counter flow.

Figure 2.56 presents an alternative representation where average values for the obstruction index are plotted for the different configuration of main flow and counter flow. From Figure 2.56 it is seen that there are clearly different zones related to the division lines presented in Figure 2.55. It is also seen that the choice of 0.1 s^{-1} as boundary value allows to set a clear separation between zones characterized by low obstruction index and zones with relatively high values.

(a) Small group interaction   (b) Forced direction   (c) Free choice with learning process
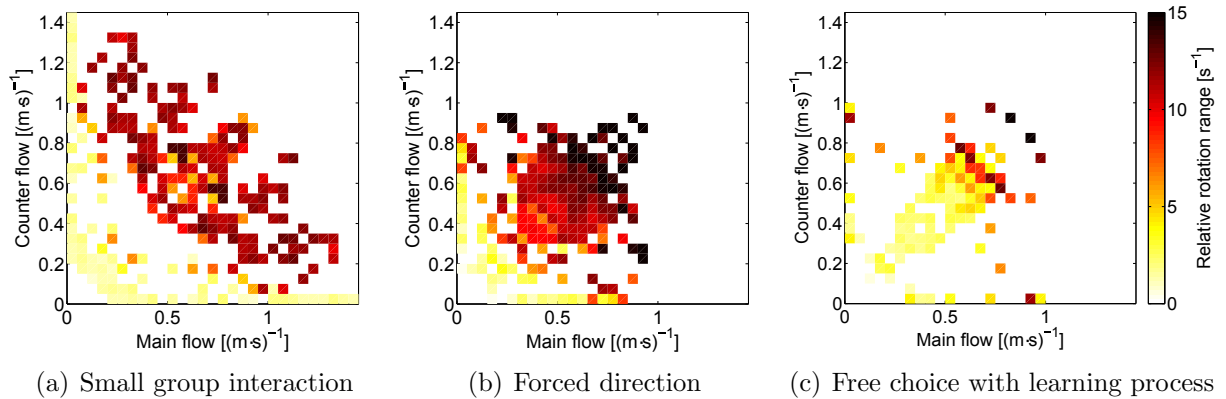
Figure 2.57: Relative rotation range for the cases given in Table 2.23 (except observations) [95]. Results are averaged for equivalent combinations of main flow and counter flow. Qualitative results are the same as the ones obtained using the obstruction index.

In Figure 2.57 an approach using the relative rotation range presented earlier is also given and it is noticed that results are fairly similar to the ones obtained using the obstruction index. This shows that the relative rotation range can be also used to judge the level of

congestion of bidirectional streams. However, when plotted using single points (and not averaged values), the relative rotation range was found being more noisy and therefore we opted for the obstruction index in the visualization of Figure 2.55.

In general, results were robust against moderate changes in threshold values. In particular we found that results did not particularly change when the density condition was neglected showing that the classification using the obstruction index and the correlation coefficient could be sufficient. However, we found that for extreme situation like the ones discussed earlier the density consideration is preferable. Discrimination results changed in certain extent when the obstruction index was varied, but as Figure 2.56 shows the choice of threshold values cannot be arbitrary and valid values need to be considered carefully. On the other side, few changes were noticed by changing the value of the correlation coefficient from 0.05 to 0.2. Also, we found that grid size had an influence on the results, but its choice is related to dimensions of human body and when chosen within reasonable limits the effects of grid size were minimal or absent. More specifically, results obtained by using a mesh of 0.3 and 0.4 m looked similar to the case presented here for 0.2 m. However, results drastically changed when the size was decreased to 0.1 m, showing that the order of magnitude needs to be in line with dimensions of human body (and maximum density).

Phase transition

As Figure 2.55 shows, transition from one flow regime to another seems to be clearly defined. In this section we will present a simple model which can be used to mathematically describe the relationship between phase transition and flow ratio. The function describing transition into congestion can be also used to asses capacity of bidirectional flows.

To start with, we can consider a model consisting of $n \times m$ cells as the one shown in Figure 2.58. The theoretical model discussed here is conceptually similar (and inspired) from the grid considered in the above experimental discussion, although cell size is irrelevant here and only their number is considered [16]. We will define the main (or front) flow as moving from left to right (white cells in Figure 2.58) and the counter flow moving in the opposite direction (gray cells). In each cell a pedestrian is assigned to the counter flow with a probability r (the probability of belonging to the main flow is therefore $1 - r$). In more practical terms (and to link it with the previous discussion) we can call r the flow ratio.

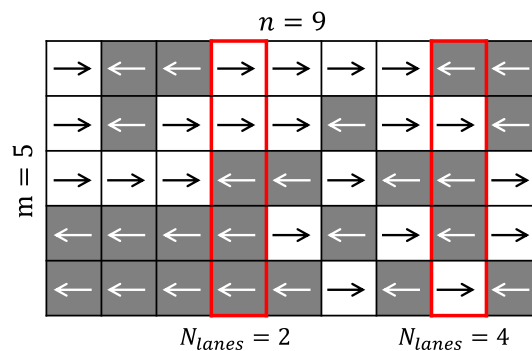Figure 2.58: Bidimensional grid representing pedestrians moving in opposite directions in a counter flow. Lanes are counted for the two selected boxes.

At first, we can consider the number of lanes. A lane is typically defined as a group of

---

[16]Although the model presented here has some similarities with the Ising model used for ferromagnetism, both approaches are different and cells are independent in our model.

people walking in the same direction. When a corridor is very long it is possible that the number of lanes change in each location, although in general it may not vary to a large extent. If a grid like the one presented in Figure 2.58 is provided, it is possible to compute the number of lanes in each n-location (or cross section) by counting the number of subset of adjacent cells moving in the same direction. The two examples provided should help understanding the concept. In the worst (or least organized) case the number of lanes correspond to the number of cells. Under perfect alignment a minimum of two lanes is formed (excluding unidirectional flow). It can be shown that the expected value for the number of lanes in function of the flow ratio is:

$$N_{lanes}(r, m) = 2 \cdot (1 - m) \cdot r \cdot (r - 1) + 1 \qquad (2.43)$$

where m is the width of the corridor as indicated in Figure 2.58. The relative number of lanes, which is the number of lanes divided by the number of cells, will result in the following equation:

$$\widetilde{N}_{lanes}(r, m) = \frac{N_{lanes}(r, m)}{m} = 2 \cdot \frac{1 - m}{m} \cdot r \cdot (r - 1) + \frac{1}{m} \qquad (2.44)$$

The above equation can be written into a general form equation $a \cdot r \cdot (r-1) + b$ which can be used to describe real data. Figure 2.59 shows the relationship between the number of lanes and the flow ratio. Figure 2.59(a) displays the number of lanes for different values of m, while Figure 2.59(b) provides the number of lanes per meter width [17] obtained by analyzing the whole database of experimental data. It can be seen that the general form for the relative number of lanes fits well with experimental data ($R^2 = 0.953$), showing that the above model can be used to describe simple properties of bidirectional streams from a macroscopic perspective (considering the statistical nature of the model large database like the one presented here needs to be analyzed).

(a) Expected number of lanes (b) Relative number of lanes in A–F
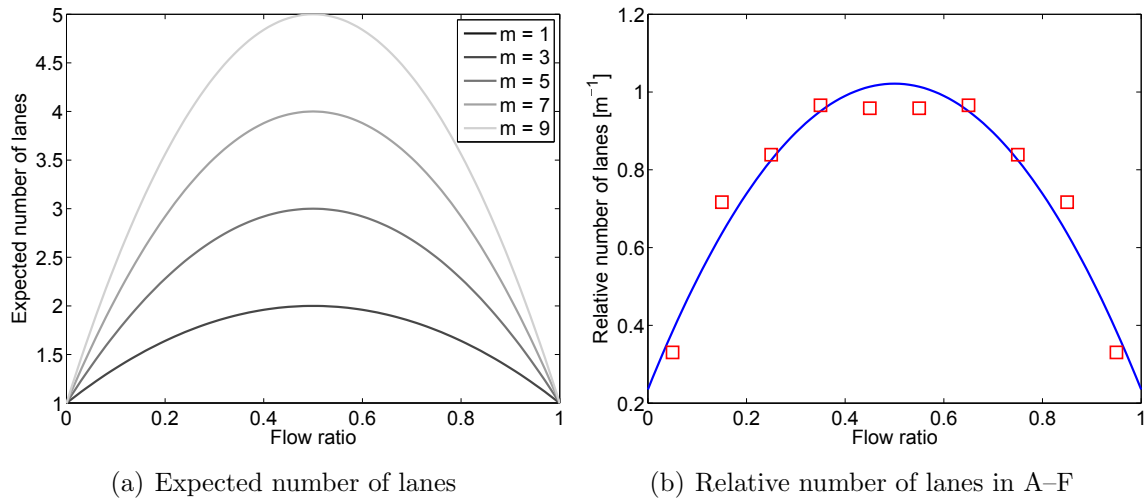
Figure 2.59: Number of lanes in bidirectional streams from a theoretical and an experimental perspective. In (b) fitting parameters are $a = -3.146$ m^{-1} and $b = 0.235$ m^{-1}.

From the above discussion it is learned that the balanced configuration results in the highest number of lanes. This discussion can be related with the transition from free flow

---

[17]Each configuration considered has different corridor widths, so the relative number of lanes is required to merge the different cases altogether.

to organized flow and we can guess that this transition will be related with the mechanism of lane formation. The hypothesis is that the highest the number of lanes the later (in term of total flow) will be the transition, because pedestrians need time (and space) to organize themselves. We can therefore use the general form for the relative number of lanes $\widetilde{N}_{lanes} = a \cdot r \cdot (r-1) + b$ to describe phase transition to organized flow.

To fit with the experimental values we need to define the minimum flow q_{min}^* (when transition is easier), which will corresponds to unidirectional flow (with a flow ratio of 0 or 1). We can also expect the maximum flow for transition q_{max}^* to correspond to the balanced case having flow ratio equal $\frac{1}{2}$. The parameters a and b can therefore be obtained as:

$$q_{lanes}(r) = a \cdot r \cdot (r-1) + b \tag{2.45}$$
$$a = 4 \cdot (q_{min}^* - q_{max}^*) \tag{2.46}$$
$$b = q_{min}^* \tag{2.47}$$

with $q_{lanes}(r)$ being the function describing the flow at which transition from free flow to organized flow occurs. In Table 2.25 the numerical values for q_{min}^* and q_{max}^* used in the plots of Figure 2.55 are provided. In general, the function proposed fits well with the transition from one set of points to the other, with the partial exception of the case with forced directions (Figure 2.55(b)) where the passage is less sharp (especially for unidirectional flow) and finding appropriate parameters becomes more difficult.

Table 2.25: Parameters used for the free flow–organized flow transition [95].

Case	Qualitative type of flow	q_{min}^*	q_{max}^*
(a)	Natural small group interaction	0.45 $(m \cdot s)^{-1}$	0.50 $(m \cdot s)^{-1}$
(b)	Continuous forced direction	0.35 $(m \cdot s)^{-1}$	0.50 $(m \cdot s)^{-1}$
(c)	Learning process possible	0.35 $(m \cdot s)^{-1}$	0.50 $(m \cdot s)^{-1}$
(d)	Observations	0.85 $(m \cdot s)^{-1}$	0.95 $(m \cdot s)^{-1}$

From Table 2.25 it can be also noticed that q_{min}^* and q_{max}^* are quite similar for the three cases considering controlled experiments (a–c), meaning that the transition from free flow to organized lanes occurs at similar flow levels although the composition of the crowd and their destinations are different. The difference observed for the observations may be related to the different approach used to determine the flow regime used in G (data from F are relative to very small densities and appear in the lower-left part of the graph).

Next, we can try to describe the transition from organized flow to congestion (i.e. the capacity). Some authors described the motion of pedestrians in packed conditions as a percolation process in which pedestrians "diffuse" through the counter flow [112, 124]. Although the densities relative the to transition into congestion are not extremely high we can assume that similarities exist when it comes to the formation of congestion and its relation with flow ratio. We can therefore consider again the model of Figure 2.58 and this time compute the probability of having an "open path", i.e. all the cells pointing in the same direction. Figure 2.60 shows different examples for possible configurations in a single row: obstructed path, open path from left-to-right and right-to-left.

For a single row, it can be shown that the probability of having an "open path" in either direction is:

$$n = 9$$
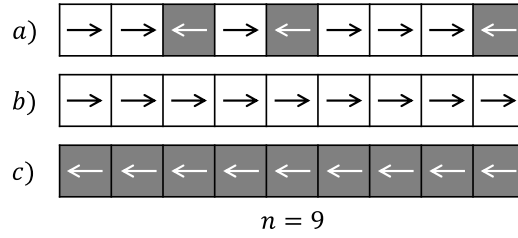
Figure 2.60: Example for row configurations with $n = 9$ cells, gray cell indicate counter flow. In case (a) it is not possible to pass from one side to the other in neither direction. Case (b) and (c) represents "open" cases in the right and left direction respectively.

$$p_{open\,path}(r, n) = (-1)^n \cdot [(r-1)^n + (-r)^n] \tag{2.48}$$

and the probability for a system composed of multiple rows like in the example of Figure 2.58 is:

$$p_{open\,path}(r, m, n) = 1 - \left(1 - \left\{(-1)^n \cdot [(r-1)^n + (-r)^n]\right\}\right)^m \tag{2.49}$$

with m and n being respectively the number of rows and columns. Figure 2.61 shows the plot of (2.49) for $m = 1, 3$ and $n = [1, 9]$. The biggest difference between both functions lies in the slope for unidirectional configurations ($r = 0, 1$), which is zero for the case $m = 3$ and takes different values for $m = 1$. However, for all combinations of m and n, the minimum is found at $\frac{1}{2}$ (i.e. balanced bidirectional flow).

(a) $m = 1$

(b) $m = 3$
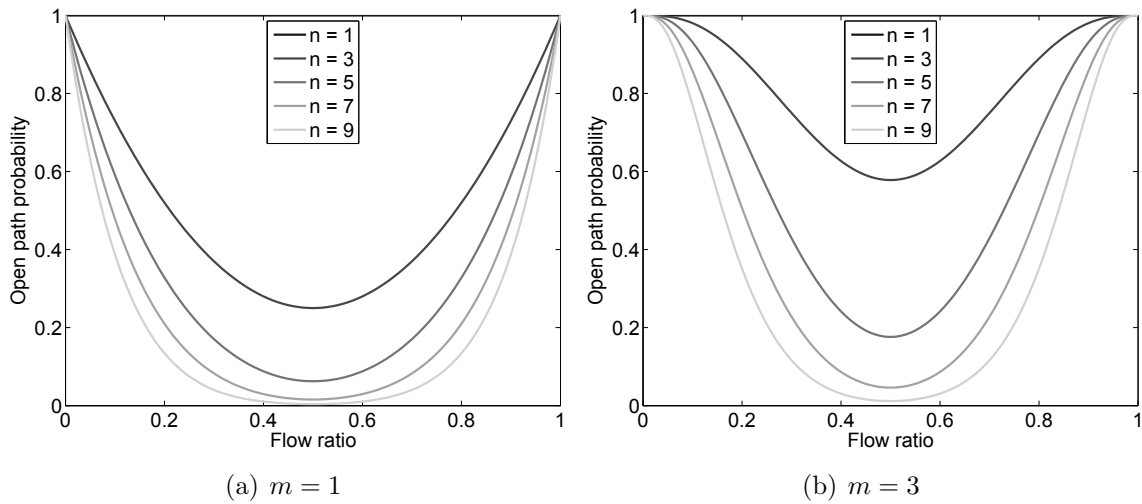
Figure 2.61: Open path probability for different grid sizes.

We can now consider the applicability of $p_{open\,path}$ to real data, but similarly to the previous case we need to adapt the function to the physical values corresponding to pedestrian flow. We can therefore define as q_{max} the maximum flow for transition into congestion and this will be equal to the capacity for unidirectional pedestrian flow (2.20 $(m \cdot s)^{-1}$ will be used here). The "quickest" transition is happening at the balanced flow configuration and as a consequence the value q_{min} will be assigned to a flow ratio $\frac{1}{2}$. This leads to the following form of the function describing phase transition to congestion (or capacity):

$$q_{cong}(r, m, n) = [1 - p_{open\,path}(r, m, n)] \cdot \alpha + \beta \qquad (2.50)$$

$$\beta = \frac{q_{min} - p_{min} \cdot q_{max}}{1 - p_{min}} \qquad (2.51)$$

$$\alpha = q_{max} - \beta \qquad (2.52)$$

where p_{min} is equal to $p_{open\,path}(\frac{1}{2}, m, n)$ and corresponds to the minimum value of $p_{open\,path}$. The numerical values used for q_{min}, q_{max}, m and n are provided in Table 2.26. Since the capacity for unidirectional flow is a universal value all the cases make use of the same parameter for q_{max}. In addition, it is remarkable noticing that the same value of m and n can be used for all the cases, thus suggesting that they can be used as universal values for pedestrian crowds. Also, since $m = 1$ it is shown that the unidimensional model is sufficient to describe this aspect of bidirectional flows.

Table 2.26: Parameters used for the organized flow–congestion transition [95].

Case	Qualitative type of flow	q_{min}	q_{max}	m	n
(a)	Natural small group interaction	0.90 $(\mathrm{m} \cdot \mathrm{s})^{-1}$	2.20 $(\mathrm{m} \cdot \mathrm{s})^{-1}$	1	15
(b)	Continuous forced direction	0.50 $(\mathrm{m} \cdot \mathrm{s})^{-1}$	2.20 $(\mathrm{m} \cdot \mathrm{s})^{-1}$	1	15
(c)	Learning process possible	1.35 $(\mathrm{m} \cdot \mathrm{s})^{-1}$	2.20 $(\mathrm{m} \cdot \mathrm{s})^{-1}$	1	15
(d)	Observations	1.35 $(\mathrm{m} \cdot \mathrm{s})^{-1}$	2.20 $(\mathrm{m} \cdot \mathrm{s})^{-1}$	1	15

Concerning the minimum flow for transition q_{min} it is clearly seen that the case with forced directions has the lowest value and in fact in the balanced case transition to congestion appears directly from free flow. The case with repeated runs showing a learning process has the highest value, showing that trained pedestrians behave in a more efficient way compared to normal crowd. The differences observed here highlight the benefits in defining flow regimes with the approach presented here against the use of the fundamental diagram. As we have seen earlier in Chapter 2.3.2 the fundamental diagram for bidirectional flow is similar although differences in the behavior of pedestrians are clearly observed. As already discussed, transition to congestion is mostly related with the concept of stability. Therefore, if two groups of pedestrians pass through each other's quickly forming lanes it does not necessarily mean that the given configuration is stable. In other words, the discrimination in flow regimes presented here can be used as an early warning signal showing that the given configuration could turn into a jam on the long run.

Classically, the definition of stability for pedestrian streams was based on the capacity function as seen in the literature review. However, the results presented here show that an univocal definition of capacity is not possible since there are factors related with cognition and perception which can influence the behavior of a crowd. Several authors found that during the pilgrimage in Mecca abnormal types of fundamental diagrams are obtained for people moving around the Kaaba [16, 36]. The same authors suggested that pilgrims are prepared to endeavor the dense crowd and motion among them is synchronized in some extent, thus preventing the occurrence of accidents despite the extremely high densities in most of the situations (although some fatal exceptions exist).

For the cases considered here, the influence of cognitive aspects is evident in the series of experiment with a learning process (Figure 2.55(c)) where the transition to congestion appears at higher values of flow. Also in the observations (Figure 2.55(d)) similar values

are found (high flow data refers to G) and this could be related to the fact that some of the pedestrians observed are frequent users of the subway station, meaning that organizational strategies could form over the long term [18].

Transient effects

Having presented a method to define flow regimes and described the relation between capacity and flow ratio we can now analyze the mechanisms leading to congestion and try to understand the reasons behind the different shapes for capacity presented in the literature review (mostly "U" and "W" shape).

In the previous discussion we have seen that the balanced case has the highest number of lanes and the obstruction index is also higher. We have also seen that in the case examined a "U" shape was observed for capacity (although a different representation was used in Figure 2.55). But still, we haven't discussed the organization of lanes yet. In general a statistical/probabilistic analysis was performed so far which was based on the fact that lateral motion combined with a high number of lanes have a higher probability of leading to congestion. However, if lanes are separated and well organized the effect of obstruction is minimized. To understand the reasons leading to the "W" shape the organization of lanes need to be considered.

In this regard, the order parameter presented earlier has been often used to assess the stratification of systems composed of lanes, with applications ranging from colloidal fluids [103] or chemical processes [122] to also include the case of pedestrians [63]. However, despites its practical aspects and the widespread use in the literature, the application of the order parameter to this study is limited by the fact that it is related with flow ratio. For instance, it can be shown that the expected value for the order parameter in a random configuration having flow ratio r is:

$$\Phi_{expected} = 4 \left(1 - \frac{1}{n}\right) \cdot r \cdot (r - 1) + 1 \tag{2.53}$$

where n is the number of columns as given in Figure 2.58. This clearly shows that there is a dependance between the order parameter and the value we can get for a particular configuration.

As a consequence we decided to take an alternative approach to analyze the organization of lanes. Using the principles presented in Figure 2.58 we can compute the number of lanes in each column and to assess the degree of organization the variance (in terms of the standard deviation) among the several columns is obtained. Results for this analysis are presented in Figure 2.62 for the three cases considered so far and the full database as a whole.

In all the three cases it is clearly shown that lanes tend to be more organized in the balanced configuration with the most disorganized lanes found for flow ratio around 0.2 (or 0.8 in the opposite direction). Also, it is clearly seen that when cognitive aspects become dominant (in the case showing a learning process) lanes get more organized at any flow ratio. When these considerations on lanes are combined with the mechanisms related with congestion described earlier, it can be concluded that strong lateral motion and multiple lanes can lead to congestion. However, if lanes are clearly defined and well

---

[18]In addition, it should be reminded that only few points are available for defining transition to congestion in Figure 2.55(d) and classification method for the flow regime is partially different from the other cases.

(a) Experimental cases   (b) Full database
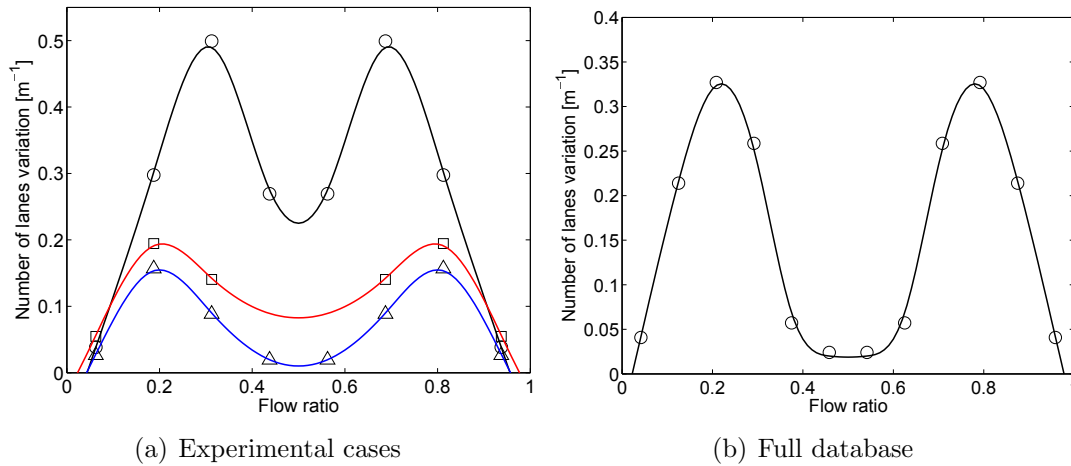
Figure 2.62: Variation for the relative number of lanes in the cases given in Table 2.23 during organized flow (except observations) [95]. In (a) circles represents the case with natural small group interaction, squares the forced direction case and triangles the case with free choice involving a learning process.

organized, then the balanced configuration sees an increase in capacity, eventually leading to the "W" shape observed under stable conditions.

We can therefore derive a modified version of q_{cong} taking into account the formation of organized structures over the long run around a balanced configuration. This function can be obtained by summing up q_{cong} with a transient term derived from the relative number of lanes (the transient mechanism is related to the formation of lanes), leading to the following form:

$$q_{cong}(r, m, n, \tau) = q_{cong}(r, m, n) + k \cdot r \cdot (r - 1) \cdot \tau \qquad (2.54)$$

where τ is a transient term representing (a relative) time and k is a scaling factor to be determined using empirical data. By setting the minimum at a flow ratio of $\frac{1}{2}$ and the maximum for the unidirectional cases (and leaving $\tau = 0$) it can be obtained $k = 4 \cdot (q_{min} - q_{max})$.
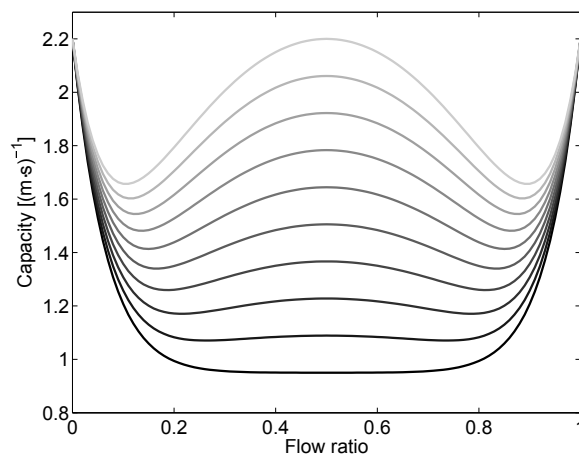
Figure 2.63: Example for the changes in capacity over a time period. Values used here are $m = 1$, $n = 15$, $q_{min} = 0.95$ (m·s)$^{-1}$, $q_{max} = 2.2$ (m·s)$^{-1}$ and $\tau = [0, 1]$ (0 being the darkest line and 1 the lightest).

Figure 2.63 shows the unsteady form of q_{cong} plotted using typical values for m, n, q_{min} and q_{max} and letting the transient term τ vary from 0 to 1. It can be seen that the function proposed here allows to reproduce most of the equations reported in the literature. Understanding under which conditions the transient term starts playing an important role and how to predict if the flow will result into an organized form around the balanced configuration, could be an interesting topic for future research.

Bidirectional flow fundamental diagram

Finally, we want to conclude our discussion on the results by comparing a particular form of the fundamental diagram (FD) resulting from the complete analysis of our database with the one provided by Flötteröd and Lämmel [107]. In their study (whose details are given in [107] and Chapter 2.3.3), a theoretical FD for the bidirectional flow was derived and experimental data (roughly corresponding to our dataset E) were used to derive the parameters defined in their functions. Figure 2.64 presents both the FD by Flötteröd and Lämmel and the one resulting from our database.

(a) Semi-theoretical FD [107]   (b) Experimentally derived FD
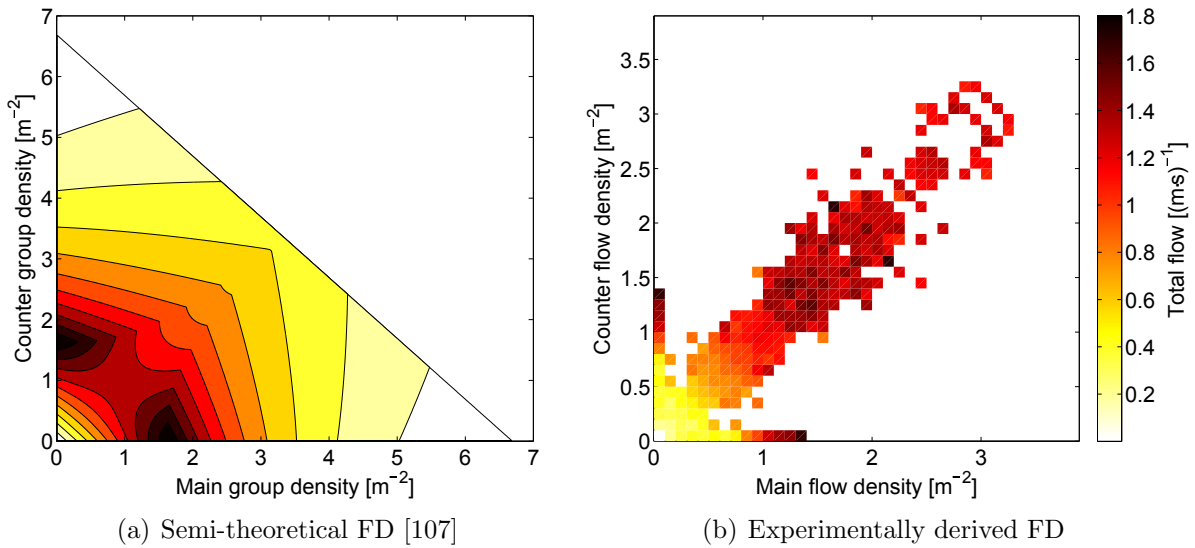
Figure 2.64: Comparison between experimentally obtained data and the FD by Flötteröd and Lämmel. The whole database is used to create the experimental fundamental diagram.

Although the number of points not covered by the analysis discussed here is rather large, it can be noted that, in general, the FD by Flötteröd and Lämmel reproduce well the characteristics of bidirectional flows. In particular, the maximum flow for the unidirectional case is correctly predicted being at about 1.5 m^{-2} and the change in flow along the symmetry line is also well depicted until the same density (1.5 m^{-2}). However, when the density grows above 1.5 m^{-2}, Flötteröd and Lämmel predict that over the symmetry line a somewhat linear drop in flow should occur, but this behavior is not observed in the FD resulting from our database. This can be related to the fact that Flötteröd and Lämmel used a limited number of experimental data to calibrate their model and therefore it becomes specific of the dataset used. Since, in general, qualitative features seems to be well described in their model, on-purpose experimental data could help increasing the reliability of the their bidirectional flow FD.

2.6.3   Summary

A method to categorize flow regimes in bidirectional pedestrian streams based on information gained from their trajectories has been presented. We showed that following behavior is related with organized motion in lanes, while the newly defined obstruction index can be used as a signal relating to the presence of congestion. This discrimination method has been used to analyze a large database of pedestrian trajectories from several researchers around the globe which were divided into four groups based on qualitative aspects relating with conditions under which observations/experiments were performed. We showed that the method proposed here allows to create three regions (free flow, organized flow and congestion) characterizing levels of flow under which a particular flow regime is expected. To describe the phase transition between different flow regime and characterize its relation with flow ratio we proposed a statistical model based on properties of bidirectional streams. Relative number of lanes predicted with our model matched with the values obtained from experimental data showing the validity of the model proposed. We consequently proposed a function describing transition from free flow to organized flow and another one describing the transition to congestion, otherwise referred as capacity. Both functions were fitting comparatively well with experimental data although some discrepancies existed in the region characterized by balanced flow. Besides some universal nature found in the parameters used to fit the several cases, we also found clear differences which could be partially explained considering cognitive aspects relating to conditions under which experiments/observations were performed.

Furthermore, we analyzed more in detail specific aspects related to stabilization of bidirectional streams. In particular, we tried to understand the reasons leading some authors to consider the balanced configuration as one of the most efficient and some others considering it as the less efficient. Our analysis suggests that congestion is caused when opposite moving lanes obstruct each other's due to lateral motion. In the balanced configuration the "friction" exerted between lanes is larger because more lanes are generally formed and pedestrians tend to waive more than in the unidirectional configuration. However, when lanes are uniformly spatially distributed then the balanced case becomes more efficient since interactions among lanes are strongly reduced. Situations leading to this condition could be a topic for future research, but our analysis suggests that cognitive aspects like the training process observed in some cases analyzed here contribute in making bidirectional flow more efficient.

Overall, this study allowed to define some methods which can be used to analyze bidirectional pedestrian flows and partially fill the gap between different equivalent studies found in the literature. We provided some initial evidence to conclude that the balanced case of the bidirectional flow requires a larger corridor width because congestion occurs at lower total flow values. However, as stated above, the more efficient organization in lanes allows it to become more smooth and, over the long run, when transient effects occur, balanced case may not be very different from parallel unidirectional streams as some authors reported. These considerations highlight the necessity to provide sufficient (but not redundant) guidance in pedestrians facilities, thus allowing a natural and smooth formation of lanes under changing conditions.

Finally, our study suggested that it is not yet possible generalize pedestrian flows into universal criteria determining human motion, since cognitive processes largely determine the results in pedestrian behavior. Relationship between people and the environment cannot be only based on geometrical features and although we showed that the categorization method allows to distinguish flow regime, functions for phase transition had to be derived

on a case-by-case basis. In the future, with more data being acquired, creating a database containing pedestrians parameters for different situations can contribute in making design of pedestrian facilities more accurate and simulations more reliable.

2.7   High density crowd model

In the previous sections several experimental aspects of the bidirectional flow have been studied. By using the knowledge gained so far it is now possible to propose a new simulation model which comprise qualitative characteristic of pedestrians moving in a counter flow. Also, the transient flow measured in Omote-sando station can be used as a valuable dataset to validate the simulation model, since this type of data are not available in the literature and/or their range of application is limited. The proposed model employes a particular mesh system, dubbed as sub-mesh, which allows to mimic rotation and percolation-like movement in high density crowd.

2.7.1   Model description

In this section the sub-mesh system and the basic transition rules are described and discussed. The fundamental rules of the sub-mesh model (transition probabilities, update sequence, conflict resolution...) are based on the classic Floor Field model (which has been already discussed in Chapter 1.2.5). This section will focus on the peculiarities of the sub-mesh concept and show the differences with similar approaches which appeared in the past.

Computational mesh

In the case of pedestrian bidirectional flow, the use of a discrete mesh in CA models results in a limited mobility for colliding pedestrians. As a consequence, even at low flows, a complete stop may be observed when pedestrians coming from both directions encounter. To avoid this problem, as discussed earlier in Chapter 2.3.4, some authors proposed to introduce an exchange probability to avoid head-on conflicts. This solution works well in a way that pedestrians are less likely to get stuck in front of each other's. However, if the exchange probability is set too high, the model tends to overestimate the capability of pedestrians to get through a crowd coming from the opposite direction. On the other hand, when set too low, the full stop may easily occur.

In addition to the above discussion, it should be reminded that, although most of the rules governing pedestrian motion in simulations are typically independent on the local environment [19], the very limited visibility found in dense crowds strongly affects pedestrians' mobility, thus requiring a different treatment compared to free flow conditions. In particular, we want to reproduce the pushing-like behavior usually observed when congestion is formed in bidirectional flow. As discussed in Chapter 2.4, in reality we observed that people usually stop once they are not able to continue further, but, after a while, they try to find out a route through the opposite coming crowd. By doing so, they move through the dense crowd frequently rotating their body hoping to get out from the opposite side as soon as possible. To overcome the limitations of the exchange probability and to correctly reproduce the behavior observed in dense crowds, we decided to introduce some changes

---

[19]Considering the relationship with the overall surrounding environment (e.g. signals, lights or indications) is also important but it is not the main scope of this study.

to the original CA mesh. In our model, we gave therefore pedestrians the possibility to find a way through the crowd by using some additional positions created in the mid of adjacent cells.

Geometrical configuration of the model proposed is given in Figure 2.65, where a comparison with the standard mesh used in CA is possible. In Figure 2.65(a) the center of each cell is given in dark large dots and each cell is delimited by border lines. In the standard model only one pedestrian per cell is allowed and thus each cell can be empty or occupied by only one pedestrian at its center. In our sub-mesh implementation (represented in Figure 2.65(b)) we introduced additional nodes (given as small dots) located in the middle and at the corners of adjacent cells. Even in the sub-mesh implementation only one pedestrian per position (not cell) is allowed. By using the improved model a maximum number of 4 pedestrians per cell is theoretically allowed (one at the center and a total of 3 at the sub-mesh boundaries [20]).

(a) Conventional   (b) Sub-mesh
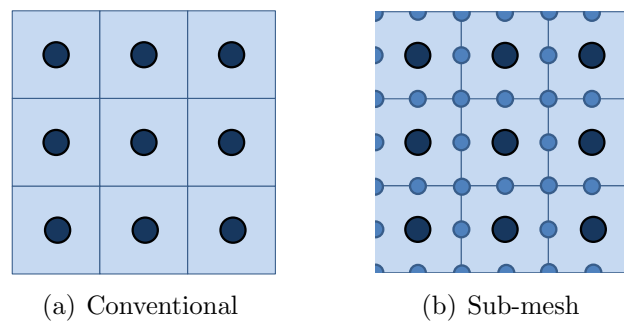
Figure 2.65: Comparison between the conventional and the sub-mesh approach. Sub-mesh locations are indicated with small circles [141].

In the way it has been introduced so far, this approach is not different than having a CA model with finer mesh (as proposed by different authors) and the maximum allowed density would reach 25 m^{-2} (4 times the normal density of 6.25 persons m^{-2} in the case of a 0.4 m squared mesh). However, we want to set the maximum density allowed in our model to about 10 persons m^{-2}, avoiding unrealistically high densities, and keeping the standard size of 0.4 m for each cell. This would not be possible in a standard CA model without changing the mesh size.

In this regard, it is important to notice that, in our model, while center positions are all equivalent, there exist two types of sub-mesh positions depending on the number of cells which they share. Specifically, sub-mesh positions being located at the edges share their location with two adjacent cells, while sub-mesh positions being located at the corners share their location with four neighbor cells. We can therefore assume that pedestrians occupying an edge sub-mesh position are half in one cell and half in the adjacent one. A similar argument can be used for corner pedestrians, but the shared value will be one quarter in this case.

We can now introduce the concept of occupancy which we will use to count the number of pedestrians for each cell. Considering the above arguments the occupancy [21] for each cell can be defined as:

---

[20]Pedestrians lying at the boundaries are shared with neighbor cells: one half for edge positions and one quarter for corner positions as we will see later on.

[21]This is different from the occupancy parameter ϕ which was introduced by presenting the classic Floor Field model.

$$n_{cell} = n_{center} + \frac{1}{2} \cdot n_{edge} + \frac{1}{4} \cdot n_{corner} \qquad (2.55)$$

where $n_{center} \in \{0,1\}$, $n_{edge} \in \{0,1,2,3,4\}$ and $n_{corner} \in \{0,1,2,3,4\}$ represent the number of pedestrians in the center, the edges and the corners respectively. n_{cell} is 0 when the cell is completely empty and 4 when all the positions are occupied. The maximum density allowed in the model can therefore be calibrated by fixing a maximum value of n_{cell}, defined as n_{max} (or maximum occupancy), above which motion to any position of the given cell is not allowed. If n_{max} is set to 1, it is possible to have the standard CA model (only one pedestrian per cell allowed in the center). In our model we also allowed the use of non-integer numbers for n_{max}. This was made possible by creating a floor in which the average n_{max} value corresponded to the sought setting, while each cell takes individual integer values randomly chosen between the upper and lower integer close to n_{max}. This occupancy approach, besides limiting the maximum density to reasonable values, it allows to recreate the percolation-like behavior because different cells may reach maximum occupancy showing different configurations. From this point of view the sub-mesh approach differs from a grid-scaling approach in which at maximum density all cells are equally occupied.

Transition rules

As introduced above, the motivation in using the sub-mesh structure is not only about increasing the maximum density, but we also want to account for the different behavior found in low and high density crowds. Inside a dense crowd the type of motion usually observed in free flow cannot be recognized anymore and in fact after entering it, pedestrians simply try to move to the exit in a sort of zigzag motion, without any preference on turning left or right, but only taking any free space they spot nearby.

Therefore, while high density may be simply obtained by scaling the size of the mesh (although not appropriate as discussed above), a more comprehensive approach is required if behavior of the crowd in dense crowd has to be considered. This particular behavior is reproduced by using some special transition rules which determine under which conditions the sub-mesh positions can be used.

(a) Free flow   (b) Enter crowd   (c) Move in crowd   (d) Leave crowd

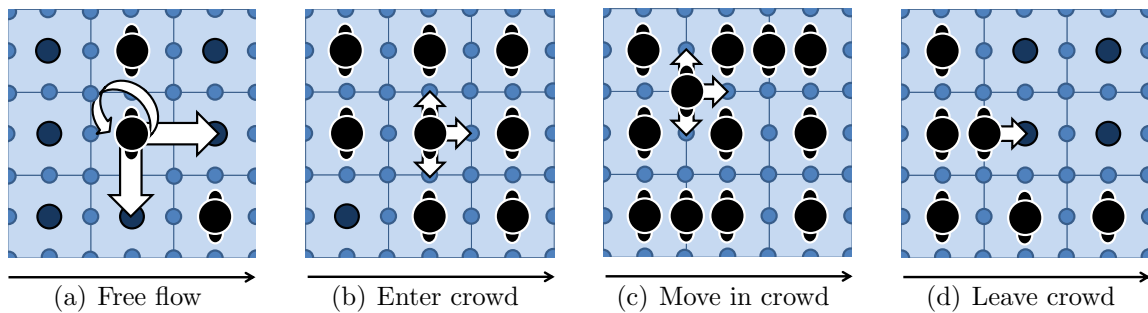Figure 2.66: Different scenarios for a right-walking pedestrian [141].

Figure 2.66 illustrates some typical situations which may be encountered in simulation. Two cases need to be distinguished: motion to a cell center and motion to a sub-mesh position (either edge or corner). The former case will be used to reproduce phenomena observed during free flow or low density conditions, while the sub-mesh will be dedicated

to high-density considerations. The different rules applying to free flow and congested motion are summarized as follows:

1. During free flow (in case one or more of the neighbor cell are free) pedestrians will move from one center to the other (as schematically illustrated in Figure 2.66(a)). In the case of the right walking individual (thus moving from left to right) given in Figure 2.66(a), that specific pedestrian may move forward, turn right or stay in the same position [22]. Pedestrians select the target cell (forward, left, right or wait/stay) according to the transition which has the highest probability (calculation of this probability for the sub-mesh environment will be described later).

2. After having waited a time larger or equal to the maximum waiting time t_{wait} in the same position, if free flow movement from center to center is not yet possible, pedestrians are allowed to move to one of the neighbor sub-mesh locations (see Figure 2.66(b)). In reality, in this case, a dense crowd has already formed thus limiting the motion of the pedestrians. By giving them the alternative of the sub-mesh, an improved mobility can be achieved. However, it is important to remember that one pedestrian is allowed to move to a sub-mesh if and only if the occupancy n_{cell} for the given cell will not go beyond the maximum occupancy n_{max}.
   The introduction of the waiting time t_{wait} allows to reduce the walking speed when entering and moving inside a dense crowd (by decreasing the moving frequency, speed is also decreased). In fact, since the waiting time before making the next step must be larger or equal to t_{wait}, by setting $t_{wait} \geq 1$ pedestrians have to wait at least one step before moving to each sub-mesh location. In addition, since sub-mesh to center distance is half the distance from center to center, even by setting $t_{wait} = 0$ the overall walking speed in dense crowd is halved.

3. After having moved in a sub-mesh position (corresponding to a dense crowd in reality), pedestrians can move from sub-mesh to sub-mesh (see Figure 2.66(c)) by respecting the two rules introduced earlier (i.e. moving only after having waited t_{wait} time steps or more and only if the target cell has occupancy lower than n_{max}).

4. If an empty cell center is spotted, pedestrians can choose to move there directly (without waiting) as in the case of free flow (see Figure 2.66(d)). Again, as in all the other cases, the maximum occupancy per cell n_{max} cannot be exceeded. In case both a sub-mesh and a cell center pedestrians aim to move to a free cell center, priority is given to the sub-mesh pedestrian. This is related with the observation that pedestrians leaving a dense crowd tend to be more motivated in moving forward compared to pedestrians which are just trying to enter the crowd.
   As an exceptional case, a back-step is allowed in this case, but only after waiting longer than $t_{wait} + 1$ time steps. We found this necessary to avoid the formation of local jam clusters, which require the half back-step to dissolve. However, even in

---

[22]In the previous literature some discussion has been made about the necessity to include the back step in bidirectional flow models. Some authors [68, 142, 62] argue that because of the intrinsic nature of bidirectional flow, back stepping has to be avoided and some showed that the use of back stepping will have little influence on the results [109]. On the other side, some authors [143] stressed on the importance of the use of back step to make the model more reasonable. Although experimental observation and personal experience suggest that back stepping should not be required, we decided to introduce it at first. However, we found its influence not significant (or negative) and therefore we excluded back stepping in the final model presented here.

the most congested situation, the use of this option accounted for about 2% of the total distance traveled. After re-entering a low density region by moving to a cell center, pedestrians can move again in a free flow motion by walking from center to center during each time step.

The transition rules given above are schematically summarized in Figure 2.67.
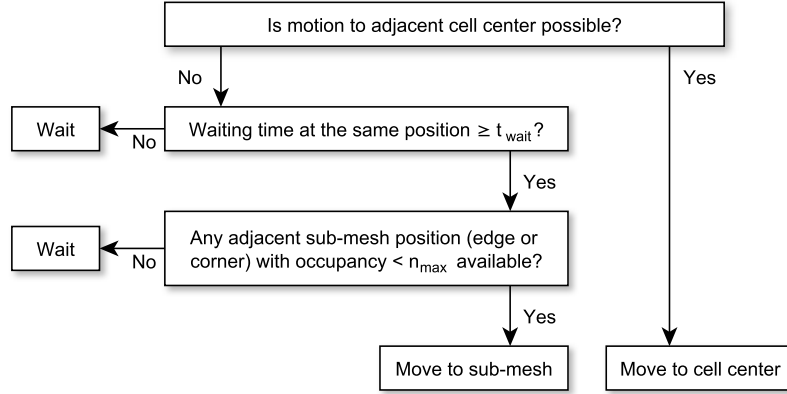
Figure 2.67: Transition rules for cell center and sub-mesh positions summarized.

Calculation of the transition probability is performed based on the Floor Field model and, in addition to the classical static and dynamic floor fields, to increase the accuracy of our model, we used the anticipation [55] and the wall [56] floor fields. Therefore, by considering the different floor fields and the exclusion rule (maximum one pedestrian per position), the transition probability for a cell (center) at position i, j can be computed as:

$$
\begin{aligned}
p_{i,j} =& N\xi_{i,j}\exp(-k_S S_{i,j})\exp(k_D D_{i,j})\exp(-k_A A_{i,j}) \\
& \exp(k_W W_{i,j})(1-\phi_{i,j})
\end{aligned}
\tag{2.56}
$$

with N being the normalization parameter, $\xi_{i,j}$ the obstacle parameter (0 if cell i, j is a wall or obstacle cell, 1 otherwise), $S_{i,j}$, $D_{i,j}$, $A_{i,j}$, $W_{i,j}$ the values of the static, dynamic, anticipation and wall floor fields, k_S, k_D, k_A, k_W their corresponding sensitivity parameters and $\phi_{i,j}$ the occupancy parameter. In the case of the sub-mesh implementation the occupancy parameter will be 0 if occupancy in cell i, j is less then n_{max} and 1 otherwise. In mathematical notation:

$$
\phi_{i,j} = \begin{cases} 0, & n_{cell}(i,j) < n_{max} \\ 1, & \text{otherwise} \end{cases}
\tag{2.57}
$$

In the case of sub-mesh, the transition probability is a combination of the floor field values of the adjacent cells.

Considering Figure 2.68 with a right walker in the center, the transition probability for a left turn can be computed as:

$$
\begin{aligned}
p_{i,j+\frac{1}{2}} =& N\xi_{i,j+\frac{1}{2}}\exp(-k_S\frac{S_{i,j}+S_{i,j+1}}{2}) \\
& \exp(k_D\frac{D_{i,j}+D_{i,j+1}}{2})\exp(k_W\frac{W_{i,j}+W_{i,j+1}}{2}) \\
& (1-\phi_{i,j+1})
\end{aligned}
\tag{2.58}
$$

Figure 2.68: Transition probability in the case of sub-mesh motion.

with the notation being the same of the previous equation and index $\frac{1}{2}$ indicating the position of the sub-mesh location. This means that the transition probability for a left turn to the left sub-mesh will be given by the transition probability computed by using the average value of the different floor fields in the current and the left target cell. The same applies to the right and the forward sub-c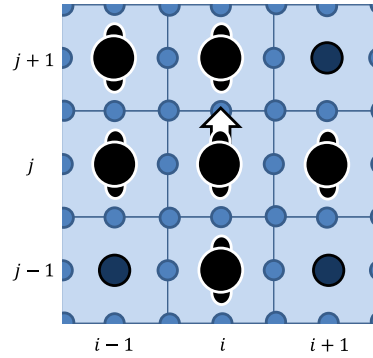ells and the corner positions (in this case 4 neighboring cells are used). In other words, the pedestrian will move to the sub-mesh closest to the cell that would have the highest transition probability if empty. It has to be remarked that the anticipation floor field was omitted in the above equation; the obvious reason being that the anticipation of movements for the pedestrians coming in the opposite direction makes no sense in a dense crowd with very limited visibility.

Finally, we decided to keep the exchange probability used in some CA models. However, to adapt it to our model, we used the following special rules:

1. A pair of pedestrians heading to opposite destinations (here left and right walkers) may choose to exchange their position (see Figure 2.11) with a probability $p_E \in \{0, 1\}$ only after having waited at the same position a total time greater than $2 \cdot t_{wait}$ time steps. For this reason, the exchange probability used here is different from the one previously used in other studies. Here, even setting an exchange probability equal to 1 will not result in an instantaneous exchange, because a pair of pedestrians will have to wait more than $2 \cdot t_{wait}$ time steps before being allowed to consider an exchange (the value of 2 has been chosen intuitively based on the fact that two pedestrians are involved). By setting t_{wait} relatively large, pedestrians are likely to move to alternative locations before considering a position exchange.

2. Position exchange can take place for a pair of opposite walking pedestrians which are both at the center or alternatively in the center and in one sub-mesh position. In case three pedestrians are aligned in both cells' center and the middle sub-mesh, then exchange takes place only for the pairs located at minimum distance (cell center/sub-mesh pair).

The use of the position exchange rule may seem in contrast with the sub-mesh system presented here. In fact, setting n_{max} sufficiently high, complete stops are very unlikely to occur. However, we observed that adding the exchange probability to our sub-mesh model can increase the accuracy of the results, both from a qualitative and quantitative point of view. This can be explained considering the fact that the sub-mesh implementation allow a temporary increase in local density and enhance the mobility in dense crowd, but it is

a relatively slow process acting as a buffer accumulating pedestrians coming from opposite directions. A combination with the position exchange allows keeping the maximum density to reasonable limits while providing a solution to quickly dissolve the crowd.

Update procedure is performed using the parallel update rule, i.e. target position is reserved before actually moving each pedestrian. In case of conflict, i.e. multiple pedestrians wishing to move to the same position, one of the pedestrians targeting that position will be chosen with equal probability. The scheme followed in the simulation process is the same presented in the introduction describing CA simulations and given in Figure 1.17(a).

2.7.2   Results

Calibration and validation

A bidirectional flow model using the rules described above was implemented in the NetLogo open source software [144]. The model consisted of an horizontal corridor 6.2 m in width and 12.2 m in length. Pedestrians can enter on one side of the corridor and leave from the other side, thus forming either unidirectional (when pedestrians enter only from one side) or bidirectional flow. Because two kind of walkers are present in the model, namely left- and right-walkers, two different static fields were used. Dynamic field is also specific to each type of walker, reproducing the fact that pedestrians going in one direction follow only other pedestrians walking in the same direction. On the other side, the anticipation field acts between the two different kind of pedestrians, with left-walkers trying to avoid collisions with right-walkers and the opposite situation. Finally, the wall field is the same for both type of walkers, as both left- and right-walkers try to avoid being too close to the wall.

In order to estimate the parameters to be used in the model, data obtained from the empirical observation described in Chapter 2.4 were employed for calibration [23]. A small difference exists between the geometry of the corridor from the on-field observation and the model used for simulation, with the corridor referring to experimental data being slightly larger on the left side. However, since congestion was observed in the right side of the corridor (where the width is the same in both experimental and numerical cases), the approximation used in the numerical model (with both sides having equal width) can be considered accurate enough to correctly reproduce the phenomena observed in reality. To estimate the parameters to be used in the numerical simulation model, we used the experimental inflow on each side of the corridor as simulation input and we computed the outflow resulting in the exit located at the opposite side. Results for the total in- and outflow and the density under normal (free flow or organized lanes) and crowded conditions (congestion) are given in Figure 2.69. A density map for the average density obtained throughout the simulation length is also provided to show where most of the crowd concentrate.

In density and flow evolution, the dotted line represents the average simulation result, with the region along it giving the standard deviation resulting from the several simulation runs (500 for each case). The bold line is the experimental result recorded during observation. Simulated density here is defined as the overall number of pedestrians in the corridor section divided by the total surface of the corridor itself; in- and outflow is intended as the sum of each quantity on both sides of the corridor (i.e. total flow).

---

[23]Not all the results presented in the on-field study could be used for comparison with simulation, because, in some cases, lanes partially formed before the entrance of the corridor, thus making the setup of boundary conditions unfeasible.

(a) Flow under normal conditions

(b) Flow under crowded conditions

(c) Density under normal conditions

(d) Density under crowded conditions

(e) Density map under normal conditions

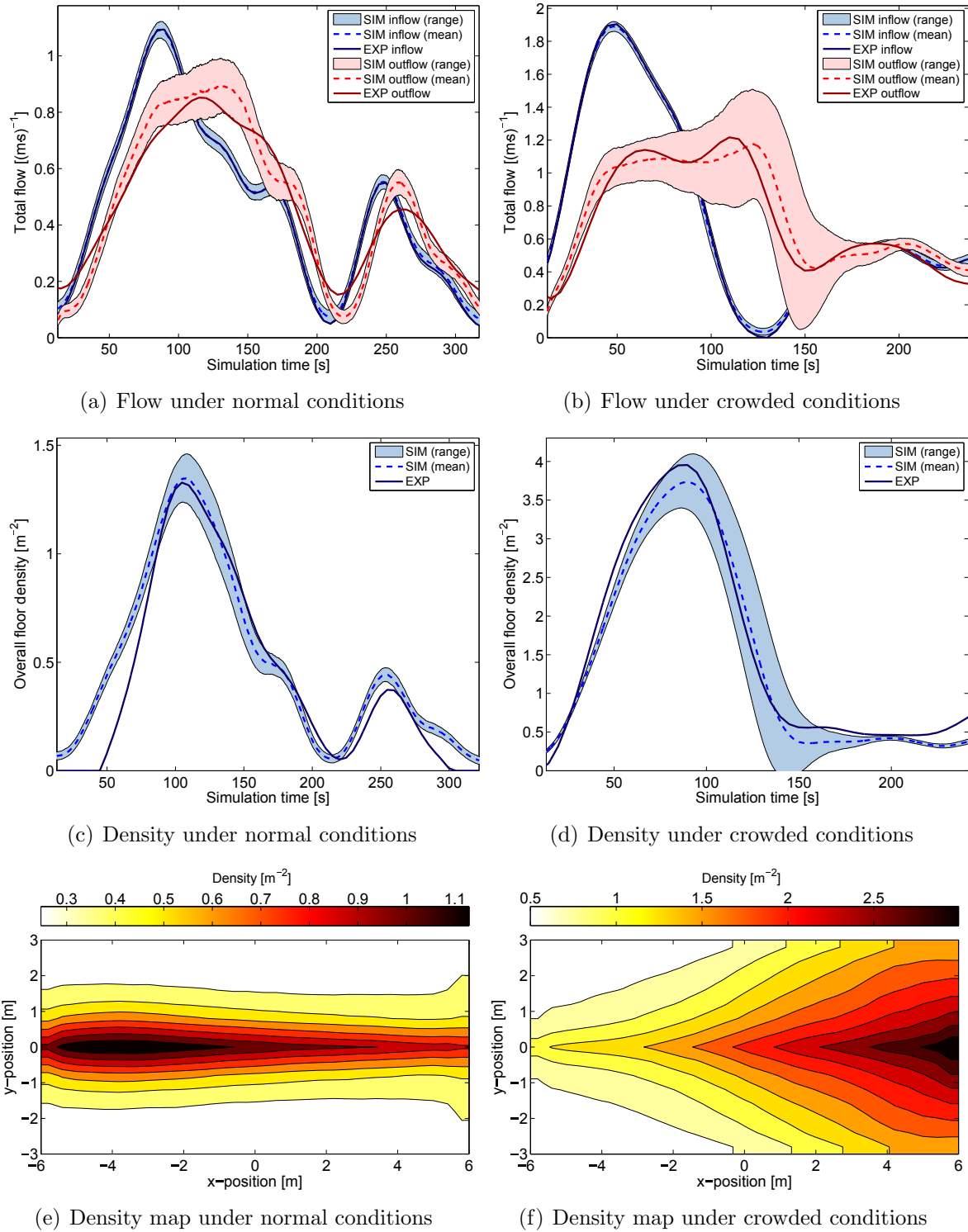(f) Density map under crowded conditions

Figure 2.69: Comparison between experimental and simulated results. SIM stands for simulation and EXP for experimental data.

In the case of flow results, it is important to remark that although the experimental inflow is taken as input for the simulation, some small differences exist between the inflow actually achieved during simulation and the one expected. This can be explained considering the fact that experimental flow curve was filtered to remove sampling noise, thus resulting in a continuous graph. In the numerical model, to reproduce a given flow, a discrete number of pedestrians need to be introduced, which may result in small differences between expected and obtained curves. This is particularly visible for sudden inflow changes, such between consecutive peaks. In general, however, differences between the cumulative must-be inflow and the one obtained accounted for less than 1–2%.

As shown in Figure 2.69, in general, a relatively good agreement is found between experimental and simulation results, with agreement of the density curves being particularly good. Qualitatively the most relevant changes are correctly reproduced in all the cases, with the quantitative values being also in satisfactory agreement. In particular, the double peak observed during the formation of congestion is reproduced in the numerical simulation (see Figure 2.69(b)), although the changes between both peaks appear smaller compared to the experimental result (especially concerning the decrease of the outflow, which, although observed in simulation, is much smaller compared to the experimental result). This characteristic could be reproduced due to the higher mobility given by the sub-mesh model presented here. In this regard, it is observed that, although overall density reaches about 4 persons m^{-2} during the formation of congestion (see Figure 2.69(d)), local densities were higher than 6 persons m^{-2}. We can conclude that the sub-mesh implementation was found being a useful method to allow motion under dense crowd conditions, although its efficiency for higher densities (above 6 persons m^{-2}) or different geometrical configurations has to be checked if new experimental data for those conditions will become available in the future.

Finally, it is worth mentioning that, although a comparison is not possible, the density map obtained from simulation in the crowded scenario reflects the qualitative observation that the densest crowd formed at the right side of the corridor.

It is however important to remark that a slightly different set of parameters had to be used for the two cases, whose numeric values are given in Table 2.27. Free walking velocity was set at 1.4 m/s to correspond with the measurement performed during the observation.

Table 2.27: Model parameters calibrated using different scenarios. k_S, k_D, k_A and k_W are the values of the static, dynamic, anticipation and wall floor field respectively; α_D and β_D are the diffusion and decay of the dynamic field and d_A is the anticipation distance. Walking velocity is set at 1.4 m/s.

Parameter	Normal	Congested	Parameter	Normal	Congested
k_S	8.0	12.5	k_A	8.0	12.5
k_W	0.75		d_A	4	
k_D	6.0		α_D	0.25	
p_E	0.275		β_D	0.25	
n_{max}	2		t_{wait}	1	

In Table 2.27 k_S, k_D, k_A, k_W, p_E, n_{max} and t_{wait} are the model's parameters described in the previous section, while α_D and β_D are respectively the diffusion and decay of the dynamic field and d_A is the anticipation distance (for details refer to [55]).

The parameters which had to be adapted depending on the situation are all related to

the way pedestrians behave under different conditions. In particular, it can be observed that a large k_S had to be used in dense crowd (when a congestion was formed). This can be explained by considering the fact that in order to cross the corridor, pedestrians need to counteract the pressure formed by the large counter flow. In other words, more efforts are required to cross the corridor under congested dense crowd compared to normal conditions. However, it can be observed, that the required increase of k_S is related with the maximum observed inflow (the peak in the crowded scenario is about 1.6 times the one under normal conditions). In this sense, linking the parameter k_S with the incoming flow may be useful in obtaining a model capable of accurately simulate different scenarios. Parameter k_A, related with the anticipation floor field, had to be adapted to the different flow conditions as well. Interestingly, we found that, by setting k_A equal to k_S, besides obtaining quantitative good results, a fairly natural behavior can be observed during simulation by following the motion of pedestrians. In this regard, the sensitivity parameters which need to be adjusted can be reduced to one, since k_A can be safely set equal to k_S.

Comparison with the conventional model

To grasp the fundamental differences with the conventional model we performed the congested case simulation using the standard CA mesh by setting $n_{max} = 1$ and $t_{wait} = 0$. Two different values for p_E were used as given in Figure 2.70 which presents the results.

(a) $p_E = 0.15$ (b) $p_E = 0.40$
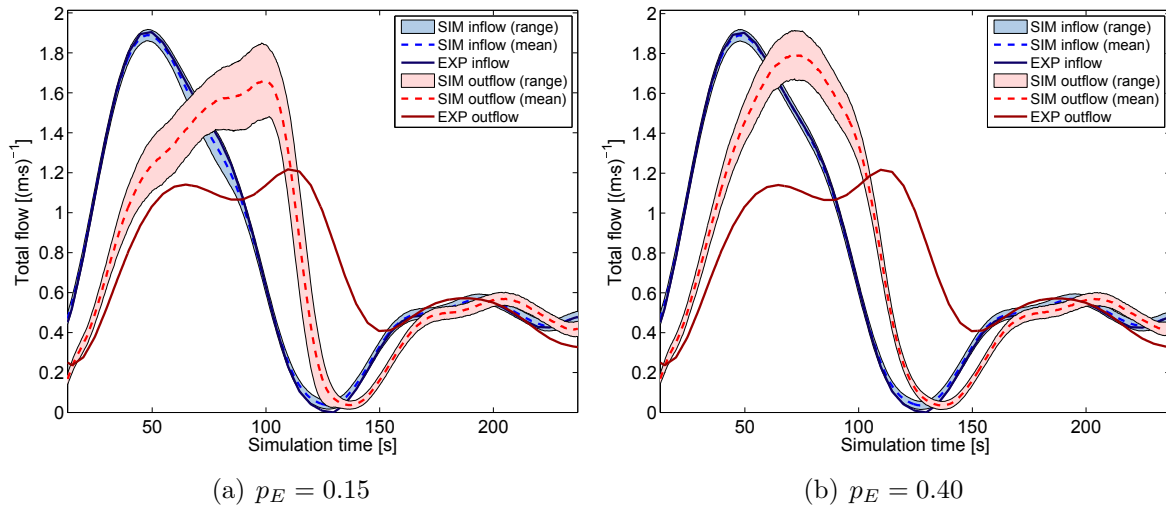
Figure 2.70: Measured and simulated flow in the congested case using the standard mesh ($n_{max} = 1$ and $t_{wait} = 0$). p_E acts as a sort of filter blocking part of the incoming flow. When set too low (in this case about < 0.10), in most of the simulations a complete stop occurred.

In none of the two cases the double peak (or similar shapes) observed in reality is correctly reproduced. In addition, low values for p_E (generally < 0.10) resulted almost constantly in a complete gridlock as both groups of pedestrians had to stop in front of each other's (simulations were aborted when the given inflow couldn't be reached). This shows that, while the exchange probability has an effect in avoiding head-on collisions, its role is similar to a filter which regulates how much counter flow is allowed to pass through a crowd. The waiting time and the sub-mesh introduced here create a sort of buffer allowing a temporary increase in density which enhances the permeability of the crowd.

Pedestrian behavior

We can now look more in detail into the behavior of pedestrians in the different situations. Considering that the simulation is performed stepwise, the movement at each iteration can be categorized as follows:

1. Forward motion: direction did not change from the previous iteration.

2. Waiting: position has not changed since the previous iteration.

3. Rotating: position and direction are different compared to the last moving iteration.

4. Position exchange: pedestrian changed its position with someone else.

When a pedestrian leaves the corridor the number of steps for each action are converted into time and those figures are combined with other pedestrians leaving at the same time. Figure 2.71 represents the average time required to cross the corridor from side to side divided into the different actions given above. The scenario with normal conditions (whose flow was given in Figure 2.69(a)) is depicted in Figure 2.71(a) and Figure 2.71(b) considers the case with a dense congested crowd (flow was given in Figure 2.69(b)).

(a) Normal conditions (free flow or lanes)   (b) Dense crowd (congestion)
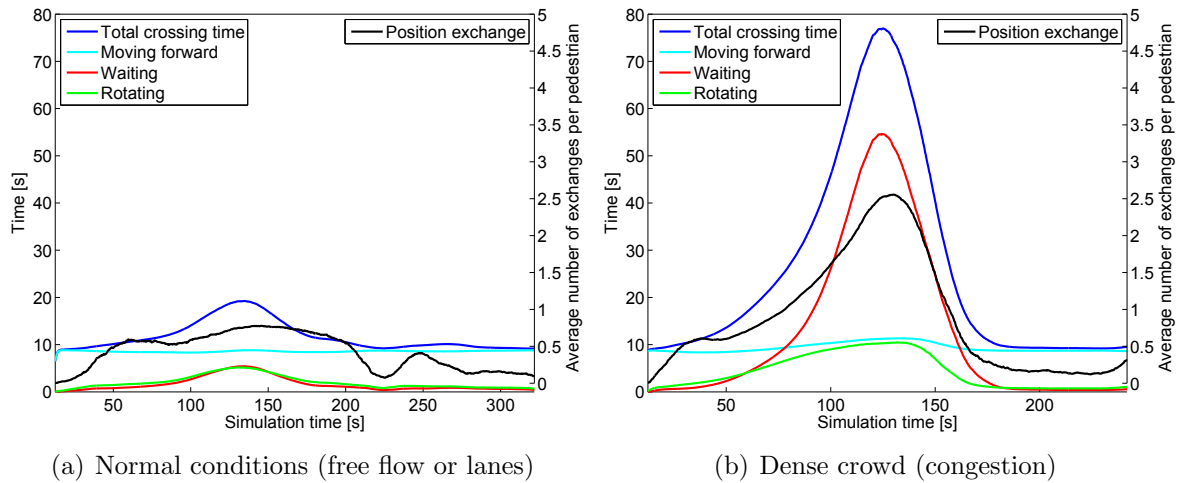
Figure 2.71: Average time required for different actions while crossing the corridor.

The total crossing time is the average time required to cross the corridor from side to side and can be obtained by summing up the time necessary for the different actions. It clearly grows when a large counter flow is encountered. The time spent moving forward is almost constant in both cases because most of the pedestrians move forward for a distance which is close to the horizontal distance of the corridor (free walking speed is constant in our model). Small variations can be observed in case one pedestrian will have to walk for a short distance toward the wall to a avoid a collision, thus walking forward for a longer distance compared to the minimum required to cross the corridor.

Concerning the waiting and rotation times, in Figure 2.71(a) it can be observed that they both follow a common path by peaking in the most crowded moment. The increase in overall crossing time can therefore be attributed to an increase of both values. We also wish to consider the average number of position exchanges required to cross the corridor for each pedestrian, given by the the black line in Figure 2.71(a) (with the corresponding scale given on the right side). Clearly, during normal conditions, position exchange is not

a relevant phenomenon (less than one position exchange is observed on average).

We can now analyze more in detail the crowded scenario of Figure 2.71(b). As one would expect, during congestion the overall crossing time grows, eventually requiring more than one minute to cover the corridor distance in the worst situation. It is interesting to notice that there is a substantial difference between the scenario illustrated in Figure 2.71(a) and Figure 2.71(b). In fact, during congestion, waiting time and rotation time are not coupled anymore. As indicated in Figure 2.71(b), at first there is a steep increase of the waiting time, which later eventually decreases. On the other side the rotation time slowly grows from the beginning of the congestion throughout the whole duration, until finally quickly dropping when the scenario gets less crowded. This indicates that the dissolution of a dense crowds is related to an increased mobility of the pedestrians, while its formation is connected with a large number of people having to stop to avoid collisions. Consequently, guiding pedestrians along preferential directions may be useful in avoiding the initial stop created by the incoming large counter flow and indications or signs play an important role here (as already suggested in the experimental analysis).

In the dense crowd situation, position exchange plays a more important role (compared to the previous case), with a maximum value of about 3 position exchanges reached during the maximum flow. This shows that although the increased mobility given by our model, exchange probability cannot be completely ruled out. From a more broad perspective these results show that indeed, as we have seen for the experimental case, using rotation-like mechanisms is also important for simulation models.

Extended bidirectional flow fundamental diagram

We will now use the simulation model developed here to obtain some complex fundamental diagrams for bidirectional flow (in the experiments high densities were not possible). First, we wish to compare the fundamental diagram obtained by simulation with experimental results from the literature. By using the model described above we performed simulations for a balanced bidirectional flow by changing the inflow setting from 0.05 $(\text{m·s})^{-1}$ to 2.50 $(\text{m·s})^{-1}$ (in 0.05 $(\text{m·s})^{-1}$ steps). Parameters for the dense crowd were used and simulations were each performed for a total time corresponding to 5 minutes in reality (with computational time being clearly much shorter). Resulting total outflow and density were recorded in the fundamental diagram and simulation results were compared with the semi-experimental data provided by Weidmann [21] in his meta-study (see Figure 2.72) [24].

The fundamental diagram of Weidmann has been chosen among the several ones available in the literature because of the following reasons:

1. It is one of the few which provides data for relatively high densities, i.e. above 4–5 m^{-2}, while most of the experimental studies are limited to free flow scenarios with densities below 2–3 m^{-2}.

2. It has been widely used in the literature as reference and, although its accuracy has been debated, its widespread use allows a prompt comparison with results from different studies.

A good agreement between both datasets is found for densities below about 5 m^{-2}, with the results from simulation being slightly higher than the data by Weidmann. For higher

---

[24]Data used for comparison refer to the semi-empirical results reported by Weidmann and not the equation which fits those data. Flow is obtained by multiplying density with velocity.
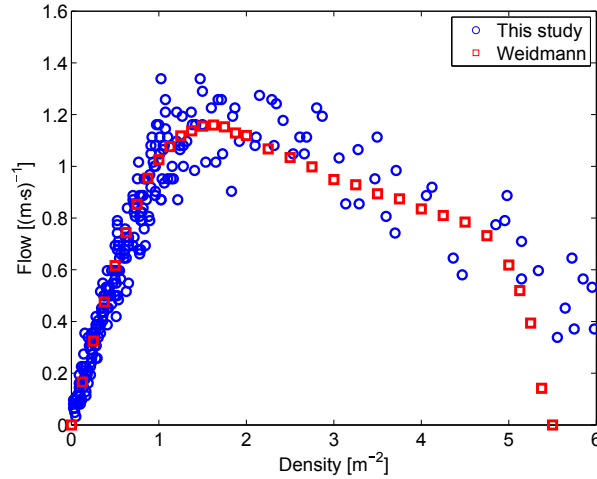
Figure 2.72: Comparison of the numerically simulated bidirectional flow fundamental diagram with the data by Weidmann [37].

densities the flow given by Weidmann quickly drops to 0, while the simulation's results only slightly decreases keeping a moderate flow even under high density conditions. We will discuss about this aspect below, but it is important to remember that the result given by Weidmann is based on a collection of experimental data and it is assumed (without being strictly verified) that for densities above around 5 m^{-2} motion is not possible (as we have seen in the introduction this may not be completely correct).

Finally, we computed the fundamental diagram by changing the flow ratio of bidirectional flow from 0 to 1 in steps of 0.1 (total inflow values were the same as above, from 0.05 (m·s)$^{-1}$ to 2.50 (m·s)$^{-1}$). Since flow ratio is symmetric around 0.5 we decided to summarize all results in a 0 to 0.5 scale. For example, a 0.6 flow ratio used in the simulation is represented together with the results of the 0.4-case. This approach also helps making visualization clearer. Results for the flow ratio dependent bidirectional flow fundamental diagram are given in Figure 2.73.

The fundamental diagram presented here shows a qualitatively and quantitatively good agreement with the one reported by Zhang et al. for their experimental campaign (see Figure 2.5). Clearly, balanced bidirectional flow is the one performing the worst, reaching a lower maximum flow and appearing at very high densities. Unidirectional flow shows a stronger stability, without decaying into congested motion for the 5 minutes duration of the simulations. In general, as the flow ratio approaches 0.5, instability grows, with congestion occurring earlier.

As Figure 2.73 shows, a very small outflow is recorded even in extremely dense crowd (above 6 m^{-2}). This is a consequence of the fact that p_E is small, but still larger than 0 in our model, thus allowing few pedestrians to cross the corridor even during very crowded scenarios. During the simulation a percolation-like behavior was observed for such densities, with a limited number of people being able to cross the corridor after a long time. The fact that results can be produced even for such high densities clearly shows the theoretical capability of our model to deal with very dense crowd.

However, it has to be remarked that over the long run, if densities keep being above around 6 m^{-2}, more complex psychological phenomena are expected such as frustration, panic or desperation, making an accurate prediction an even more challenging task. In addition, pedestrians may fall down and pile on top of each other's, thus creating an extremely dangerous scenario going beyond the modeling capabilities.
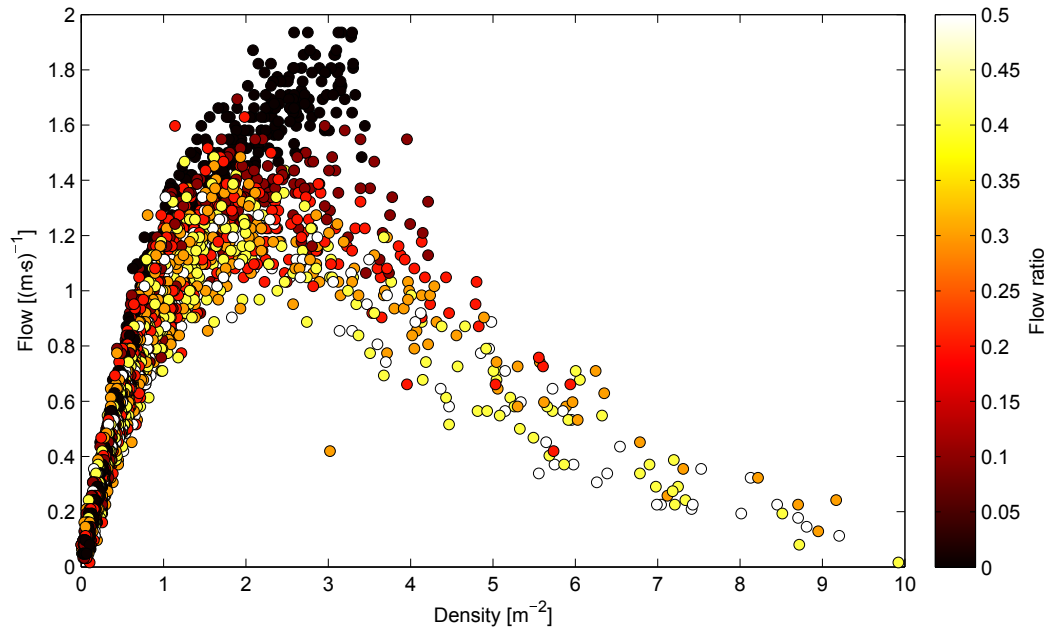
Figure 2.73: Bidirectional flow fundamental diagram and its relationship with flow ratio [37]. Comparable experimental results are given in Figure 2.5.

Nonetheless, the model presented here gives the possibility to investigate if such high densities may actually occur (even for a short time) and to investigate with higher accuracy accidents which already occurred in the past. From this point of view the high density allowed by the sub-mesh model gives a deeper insight into the formation of dangerous crowd phenomena, thus possibly allowing preventing them in the future.

Accuracy of diagonal motion

Finally, considering the geometrical configuration of the sub-mesh model it is important to verify if diagonal motion is correctly accounted for and what is the error in such cases. We consequently simulated the case of two equally large groups of pedestrians entering a corridor (width 5 m, length 15 m) from both sides. Each group consisted of 200 people and we tested different densities by changing the total flow (from both sides) at the entrance from 1.0 $(m{\cdot}s)^{-1}$ to 2.0 $(m{\cdot}s)^{-1}$. To assess the effect of geometrical configuration we changed the angle of the corridor from 0° (horizontal) to 26.56° and finally 45° by keeping the dimensions constant. The parameter-set for the normal case was used and 50 simulations were run for each configuration.

Figure 2.74 shows the average density from the beginning (first pedestrian enters the corridor) to the end (last pedestrian leaves) of the simulation for the case with a total flow of 1.0 $(m{\cdot}s)^{-1}$ and 2.0 $(m{\cdot}s)^{-1}$.

As it can be easily predicted, the highest density is found in the center of the corridor, around 4.0 m^{-2} for the case with a flow of 2.0 $(m{\cdot}s)^{-1}$. In general, the density maps are quite similar for the three angles considered, although it appears that in both models the geometry tends to change the distribution of crowd in the center. As it can be observed (especially in the high flow case), in the horizontal case the highest density region is elongated by reproducing the shape of the corridor. However, in the 45° case, a more concentric configuration is observed. Concerning the absolute values, it has to be remarked that an higher maximum density is found in the 45° case compared the other
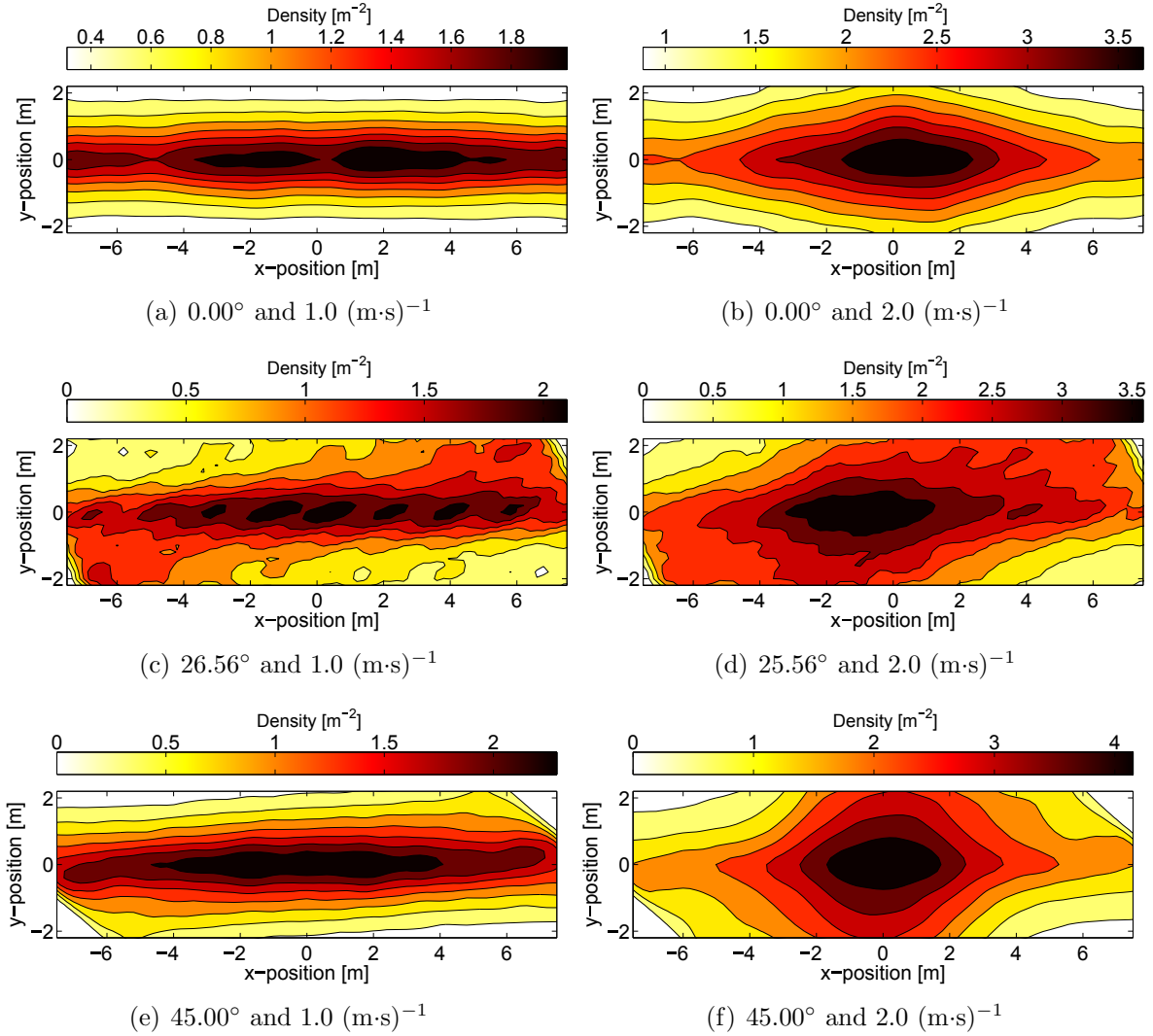
Figure 2.74: Average density in the different regions of the corridor for the case with a total flow of 1.0 (m·s)$^{-1}$ and 2.0 (m·s)$^{-1}$. All the cases have been rotated to facilitate visualization and comparison. In the 26.56° case the discrete configuration used in the model results in a light distortion.

two cases. This behavior can be understood considering the group crossing time (the time required by the crowd to completely leave the corridor) given in Table 2.28.

Table 2.28: Group crossing time depending on the total flow and the geometrical configuration used. Although differences are not large, diagonal geometries have partially different results compared to the horizontal equivalent.

Geometry angle	Total flow	
	1.0 $(m \cdot s)^{-1}$	2.0 $(m \cdot s)^{-1}$
0.00°	104.91 ± 1.72 s	96.31 ± 4.92 s
26.56°	111.13 ± 2.42 s	103.86 ± 6.12 s
45.00°	109.84 ± 1.35 s	107.62 ± 12.33 s

As Table 2.28 shows, while in the low density scenario effect of geometry change is low, for the in 2.0 $(m \cdot s)^{-1}$ case, in the 45° configuration a longer crossing time is required, which creates a denser crowd in the center of the corridor. In the high density case the group crossing time increases slightly more than 10% in the 45° case. Although the change is acceptable, this shows that geometry do have an effect on simulation results and the orientation choice is important for obtaining accurate and reliable results.

2.7.3   Summary

One of the limitations of the Cellular Automata has traditionally been its discrete mesh and the relatively low maximum density associated with it. In this study we presented a modified version of the Floor Field model making use of a sub-mesh system to allow simulations of very dense crowd and account for the behavior found in such situations. A sub-mesh position located between adjacent cells is added and may be used by pedestrians in dense crowd under particular conditions. As a consequence, maximum densities reached can be higher than the ones obtained in conventional Cellular Automata models. At the same time, dense crowd phenomena can be simulated more accurately.

Comparison between simulation results and experimental data from empirical observations showed a satisfactory agreement both under a qualitative and a quantitative aspect. In particular, the characteristic double peak observed in congested dense crowd could be reproduced using a numerical model, allowing a further investigation into the reasons leading to this phenomenon. In this regard, we confirmed the remarks from the on-field observation discussed earlier, i.e. that partial deadlocks form because pedestrians tend to stop in front of a large counter flow. On the other hand, an increased mobility and body rotation inside the dense crowd is associated with the dissolution of partial deadlocks.

The high density framework has been used to generate an extended fundamental diagram for bidirectional flow, showing that dense crowd simulations are actually possible and confirming the instability of the balanced flow compared to unidirectional motion for large disorganized crowds. However, reliable experimental data for high density crowd are required to validate the model under such conditions and/or perform a re-calibration of the parameters used. Finally, we showed that the sub-mesh employed had not a significant effect on geometry changes with a particular regard to diagonal motion. With that said, some improvements may be required if complex structures involving motion at different angles and directions are to be considered.

Direct applications of this model can be accident prevention and/or investigation of ac-

cidents which already occurred in the past. Additionally, the framework presented here may be adapted for a use in different disciplines, with granular and active matter physics, material engineering (for example to simulate conductive properties in fiber-reinforced materials) or fluid dynamic (for porous medium in particular) being potential candidates. In the future, new implementations may be required to further increase the accuracy obtained in simulations, for example by considering the distribution of the walking speed.

2.8   Conclusions and discussion

Having discussed specific aspects of bidirectional flow in each section, the conclusions here will try to summarize the common points and the most important lessons gained from this multi-perspective approach.

Overall, this study on bidirectional pedestrian flow allowed to define some methods which can be used in the analysis and partially fill the gaps between several studies found in the literature. We showed that, to understand the mechanisms occurring in the process of lane formation and later in transition to congestion, several phases have to be considered and mathematical techniques allow to identity them. The experimental cases considered were particularly simple from both a geometrical and an operational level. In particular, in our experiments we could exclude interactions with the environment and long term psychological aspects related with stress. In reality, people have to deal with complex geometries and the environment influences their motion. In addition, psychological effects may become dominant, especially in the case of evacuations. Under such circumstances, it is therefore possible that the different phases described here cannot be found and/or the order in which they appear may be different. Nonetheless, the approach presented allows to form a methodological basis to analyze experimental data and we believe the methods proposed can be applied to real situations, although, as said, the results may be different from the one obtained here by considering supervised experiments.

From a broader perspective, this study showed that laws derived from fluid-dynamics or more generally physics can be used to measure properties of crowds and partially describe their motion. However, as shown in our analysis, as soon as cognitive aspects arise, those descriptions fail in predicting future developments. This fact may lead to erroneous conclusions. If physical (or numerical) descriptions of crowds are correct in certain conditions but fail in others is neither a proof that humans behave like particles nor a reason to show that this approach is wrong. Instead, this contrast can be used to grasp the moment when a given crowd start behaving in a different way, therefore allowing to signalize that attention is needed in dealing with it (especially when crowd control is concerned). Therefore, the specific conclusions on the bidirectional flow reported here need to be considered in the context of this research and future studies can use them as a starting point to show the limit of validity and in which extent psychological/cognitive aspects can contribute in changing them.

With this said on the limitations of this study, we can summarize the lessons learned on the bidirectional pedestrian flow for the case of "standard" interactions, i.e. people following their primitive instinct of achieving their goal (i.e. crossing the specific path here) while minimizing the penalties in the execution of the task (in this case avoiding collisions).

In the specific, it has been shown that three typical states are found in human crowds: free flow, organized motion and congestion. Jam could be also added to describe a crowd barely moving, in particular for very dense, dangerous situations, although we could not

study it neither in the on-field observation nor in the supervised experiments. Transition from one state to another can be described with a probabilistic approach, grouping several types of crowd into a single entity. Although microscopic interactions may change, for example if social structures such as dyads are present, in a macroscopic viewpoint those differences are nullified.

About the flow ratio, we found that balanced bidirectional flow is intrinsically more unstable because both groups require lateral adjustments to form organized lanes and the number of lanes is higher compared to unbalanced configurations. Lane formation is however mostly a one-time process, since, after lanes are formed, interactions with the counter flow are greatly reduced if not canceled. As a consequence, over the long term, balanced bidirectional flow can achieve greater stability and reach a similar efficiency compared to the unidirectional case. The condition for reaching stability is given by the density and cognitive aspects. When density is low, balanced bidirectional flow quickly forms stable lanes and capacity is increased. However, when density is high, stable lanes are more hard to form and both groups continuously work on forming lanes which are soon dissolved. Unbalanced configurations are inherently more unstable, with density having a smaller influence on the level of stability (and influencing capacity to a lesser extent). Trained or "experienced" crowds can form lanes faster, thus showing the relation with cognitive aspects.

From a practical perspective the above conclusions translate into the requirement to have larger infrastructures if balanced flow is expected and design should be based on this conservative assumption to allow a smooth and safe operation. Also, flow separation is fundamental and the formation of lanes should be enforced by means of sufficient (but not redundant) guidance in pedestrians facilities. Our research also provided important numerical values gained from empirical and experimental evidence and those values may become useful for designing pedestrian facilities.

Finally, our research on the bidirectional flow allowed to introduce bidimensional quantities in pedestrian dynamics and to show that rotation, lateral motion and imitation are fundamental actions to describe crowd behavior. The work presented here on the bidirectional flow may be useful for researchers who sought a comprehensive treatment of this specific aspect considering theoretical, experimental and modeling (simulation) approaches. The extensive literature overview should also allow finding interesting and specific readings for those interested in more specific and specialized aspects.

Chapter 3

Measurement of pedestrian crowds in complex environments

3.1   Introduction

In the previous chapter we have seen that the fundamental diagram had a limited validity in allowing to distinguish different bidirectional flow configurations. On the other side, the relative rotation range allowed to highlight some differences and distinguish between different phases. However, the overall discussion so far has been limited to the bidirectional flow, which, although showing a bidimensional motion, does not differ in a large extent to the simple unidimensional case (this is also why we defined it as a "bridge" between the unidimensional and multidimensional treatment).

In this chapter, we want to continue the discussion relative to methods for analyzing and measuring pedestrians crowds, but we wish to gradually increase the degree of complexity to finally include multidimensional cases in which each pedestrian move in a different direction, thus requiring the use of bidimensional quantities. In addition, we want to move to a more practical perspective and also consider the way in which trajectories are gained and which alternative methods are available to physically measure the crowd.

For instance, in all the experiments described so far videos were analyzed using a specialized software (PeTrack) which is designed to recognize motion of pedestrians wearing specific caps (this is the reason why participants were wearing colorful caps). However, in real scenarios, it is more difficult to detect pedestrian motion since conditions may change day by day and hair's color mixes with the surrounding environment. Also, differently from the azimuthal view adopted in the supervised experiments, security cameras in transportation infrastructures are usually placed at low angle positions, with the crowd being seen from a rather front perspective. This makes detection even more difficult and taking into account the geometrical laws of perspective becomes an additional task to be considered. To avoid the problems related with privacy issues, technologies not making use of images from cameras have been developed with laser range sensors being among the most widespread. However, especially in the case of evacuations from fire in the presence of smoke, also technologies based on distance measurement can fail. Assessment of crowd condition becomes even more difficult if sprinkles will set on, creating a physical obstacle to the use of optical sensors.

An additional problem related with the general approach of detecting and counting people is that exact values are required to get an accurate image. Especially when density is concerned, failing to detect a small number of people may result in an incorrect estimation

of density, which could be particularly significant at medium densities when small fluctuations determine rapid changes in crowd behavior. As a consequence, density estimation based on computer vision is only correct when all pedestrians are detected and with the actual technology this is not always possible [145, 146]. On the other hand, estimation of velocity is more accurate and more robust in relation with changes in lighting conditions and crowd composition. Estimating crowd properties based on velocity information is therefore more robust and reliable. Ideally, both information are required to get a complete image of the situation being monitored, but velocity detection may be more meaningful for a numerical analysis and allows to compute more complex information which would be difficult to assess by visioning videos. Density is clearly important, but, in general, a rapid look on footage from security cameras allows to determine if a low or a high density crowd is being observed.

With that said, we need to remind that, as it was already discussed in the introduction, density alone is not sufficient to determine the danger of a specific crowd. So, if a particularly high density is observed (for example using a security camera monitoring the crowd in a transportation facility), the next step should be on determining the way in which people move to assess if it is an organized motion or a chaotic dangerous one.

To summarize, there are two important aspects which are relevant in determining crowd organization and smoothness: define a universal quantity measuring that condition numerically and consider how data are obtained to compute this quantity. In regard to the latter aspect, technologies not relying on computer vision are preferred and, if unavoidable, then velocities should be prioritized toward density.

This chapter will deal with the above two aspects, therefore helping to bridge the knowledge learned in the bidirectional case with more realistic scenarios. More specifically, there are two objectives which represent the core of this chapter:

1. Define a method to measure congestion in complex geometries and for multidimensional motion. This part should also include the definition of one or more threshold values defining phase transitions from different flow regimes or forms of organization.

2. Consider the application of the above method with existing technologies to detect and/or sense pedestrian motion. In this regard, limitations of the existing technologies should be taken into account and if required, new methods should be proposed.

As it will be presented in this chapter, we will move toward the first objective by introducing an alternative approach assessing crowd condition. The relative rotation range introduced for the bidirectional flow will be extended for multidimensional complex environments determining a so-called congestion level measuring the smoothness of motion in pedestrian crowds [1]. In addition, in relation with the second objective, we will use inertial sensors contained in commercial electronic devices to sense the movements of pedestrians and estimate crowd properties. This approach allows to overcome the "perfect-detection" requirements found in the case of computer vision, because with inertial sensors few dozens of pedestrians can be used as a sample representative of the behavior of the whole crowd. Consequently, by sensing them, overall crowd quantities are obtained.

This chapter is organized as follows: at first a brief introduction on methods used to measure pedestrian crowds is given, later we will extend the discussion started for the bidirectional case to more complex environments and also consider the motion of pedestrians sensed using inertial sensors. Overall conclusions and discussion are given at the end of this chapter.

---

[1]To simplify notation we will refer to the relative rotation range as congestion level in this chapter.

3.2   Existing methods to measure crowd properties

In the previous chapters, pedestrian trajectories were considered as given and no details have been provided on the methods used to extract them (except providing the name of the software used). In this chapter, we will discuss more deeply aspects related to crowd measurement and sensing and consequently a concise background on existing technologies is required. In introducing those topics, our aim is not on giving an exhaustive literature review but only on presenting common knowledge related to computer vision technologies and alternative methods used in pedestrian dynamics.

3.2.1   Computer vision

Computer vision is the most common method used to obtain pedestrian trajectories in public spaces. Applications and specific algorithms are numerous and it is beyond the goal of this text to list all of them. The review by Kok et al. [147] covers many aspects related with computer vision while also discussing important topics in pedestrian dynamics and interested readers are referred to their text for more details. Here, we will divide computer vision algorithms into two main categories: optical flow and recognition/tracking methods (alternative subdivisions are however possible based on applications).
Junior et al. [148] noted that techniques working in non-crowded conditions may fail for packed crowds, with the opposite case being also true. In general, it can be stated that technologies based on the optical flow works well for high density scenarios, while recognition and tracking is more suitable for low density scenarios. Both approaches will be presented in this section.

Optical flow

Optical flow is a general technique used in different disciplines and it is commonly employed in fluid-dynamics to detect the motion of fluids. On that purpose, small particles are injected inside a fluid and consequently move following its streamlines. The area to be studied is exposed to strong light exposure by flashing it at constant intervals. Pictures are taken when the flash is on allowing to keep a track of the particles moving inside the fluid. In the case of pedestrians, the head of people already constitute the "particles" immersed inside the fluid and therefore frames from videos can be directly analyzed. More in general, the optical flow technique can be applied to any type of image sequence, but knowing the size of the particles to be studied help improving the accuracy of the results.
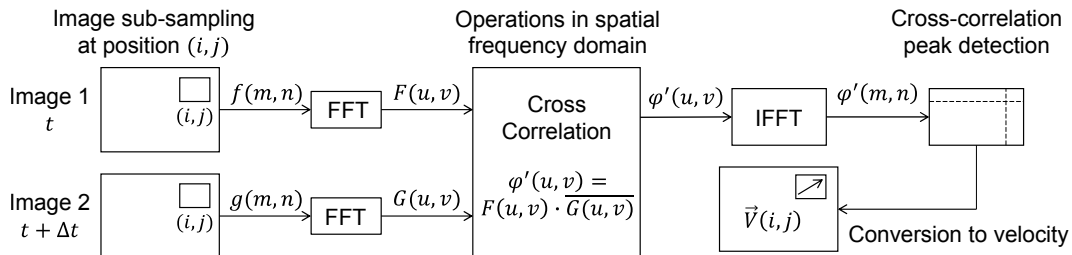

Figure 3.1: Computational process to get a velocity vector field from video frames [49].

Once an image sequence is obtained the process given in Figure 3.1 is used to get velocity information. Two successive images are selected and analyzed in the interrogation area (usually in the order of few or a dozens of pixels). Each interrogation area corresponds to a

vector in the final vector field and therefore interrogation area is moved along the image to analyze it completely (possibly overlapping them to obtain more accurate results). A Fast Fourier Transform (FFT) is performed for each interrogation area and a cross-correlation is computed among interrogation areas corresponding to both images. The location of the peak resulting in the cross correlation function allows to determine magnitude and direction for the velocity vector inside the interrogation area. When the process is applied on the whole image a vector field is obtained. Figure 3.2 provides the example of a generic optical flow algorithm applied on the video from the unidirectional flow experiment of Chapter 2. Since the whole calculation is based on digital images divided into pixels, a calibration is required to convert pixel units into physical units used in the analysis.
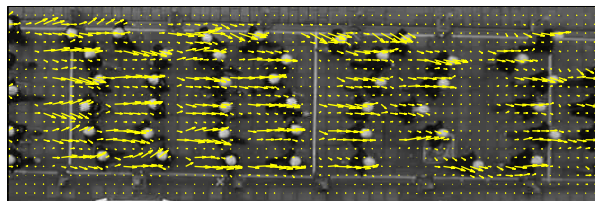

Figure 3.2: Example of an optical flow algorithm applied on the unidirectional flow experiment; direction of motion is clearly recognizable (image is only representative and units are unspecified).

Calibration can be performed by measuring walking speed of pedestrians being analyzed or comparing the motion seen in video with architectural features of known size (time required to cross a road for example). The optical flow can be applied to any type of image and applications also include detection of speed of vehicles or particles as in the case of fluid-dynamics. Under packed conditions, when the whole image is covered by pedestrians or the part occupied by them is clearly defined, optical flow provides an accurate description of the velocities in the different regions. However, for non-crowded scenarios the optical flow may result in some noise created by changes in exposure conditions not related with motion of pedestrians. This is seen for example in the upper-left side of Figure 3.2, where velocity vectors are created from a line drawn on the ground. Under low density conditions, detection and tracking of single pedestrians may result more accurate.

Pedestrian recognition and tracking

If density is relatively low and pedestrians are clearly distinguishable one by one, then individual recognition and tracking may be more suitable. The software used to gain trajectories in the controlled experiments of Chapter 2 is also based on this technique. Trajectory extraction by having participants wearing colored caps is a well established technique for supervised experiments which started more than ten years ago [149].
In contrast to the optical flow approach which provides a general vector field for the whole crowd without distinguishing individuals, the recognition technique allows to obtain single trajectories. The process is divided into two phases: recognition and tracking. The recognition part allows to recognize shapes belonging to individuals. The algorithms used for recognition are more complex than the ones used in the optical flow and they aim at finding typical features of people. Recognition algorithms are typically focused on looking for specific aspects, also depending on the intended applications. If cameras are looking at the crowd from a azimuthal perspective then recognizing the shape of the head may be more efficient. Applications based on security cameras looking frontally to people in

very low densities conditions are searching for full body silhouette. Figure 3.3(a) shows
an example of pedestrians detected using PeTrack software [88].

(a) PeTrack example
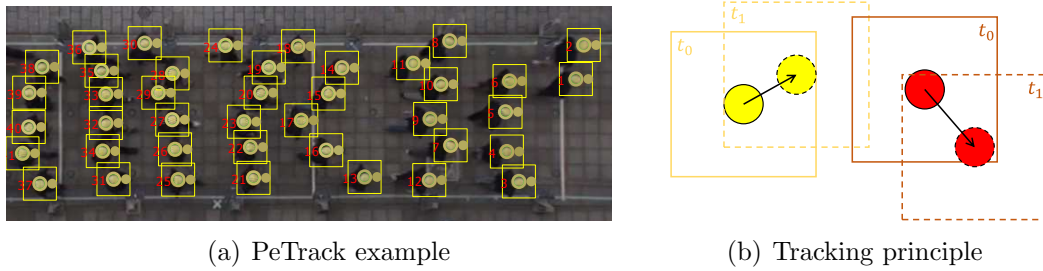
(b) Tracking principle

Figure 3.3: Left: example of pedestrians detected and tracked using PeTrack software [88]
in the unidirectional flow experiment of Chapter 2. Search region is indicated as a square
surrounding participants' caps. Right: principles for tracking between two consecutive
frames t_0 and t_1.

To construct pedestrians' trajectories tracking is necessary, since detection alone cannot
link positions found in one frame with the ones corresponding to the previous frame. The
tracking algorithm has therefore the aim to link pedestrians and positions and build a
unique trajectory composed by the positions occupied from a given pedestrian in all the
frames considered. On this purpose a search region is usually employed which defines the
maximum distance traveled by one pedestrian between two frames. Like in the example
of Figure 3.3(b), if one pedestrian is found at frame t_1 inside the search region of a pedes-
trian at frame t_0 then both positions are associated to the same person. In Figure 3.3(b)
the yellow and red trajectories are relative to two different pedestrians. More complex
algorithms can be used to allow, for example, taking into account rapid acceleration of
pedestrians leaving to a certain degree the search region, but the underlying principle
remains the same.
This technique has the clear advantage of defining accurate positions, thus allowing com-
plex analysis taking into account pedestrian distance, density and calculations not possible
using the optical flow. However, when densities get high, recognizing single individual fea-
tures inside the crowd may become difficult. Also, when large crowds need to be tracked,
the computational requirements rapidly grow and search regions get filled with several
people thus making difficult linking positions with individuals. Under these conditions
one may have to renounce to the accuracy given by trajectory extraction and opt for the
more general but reliable approach of the optical flow.

3.2.2   Laser and distance sensors

Detection of pedestrians based on images from surveillance camera has the disadvantage
that adequate lighting conditions are required. For instance, detection under darkness
is not possible or special cameras are required (e.g. infrared cameras). An alternative
method to detect pedestrian motion in public spaces is the use of laser or distance sensors.
Distance sensors allow to determine a bidimensional map including the distance between
the sensor and objects lying nearby. If a distance sensor is placed in azimuthal position
above a crowd it allows to distinguish standing people from the ground lying at a larger
and uniform distance. Figure 3.4(a) provides a representation for a hypothetical distance
map obtained by using a distance sensor.

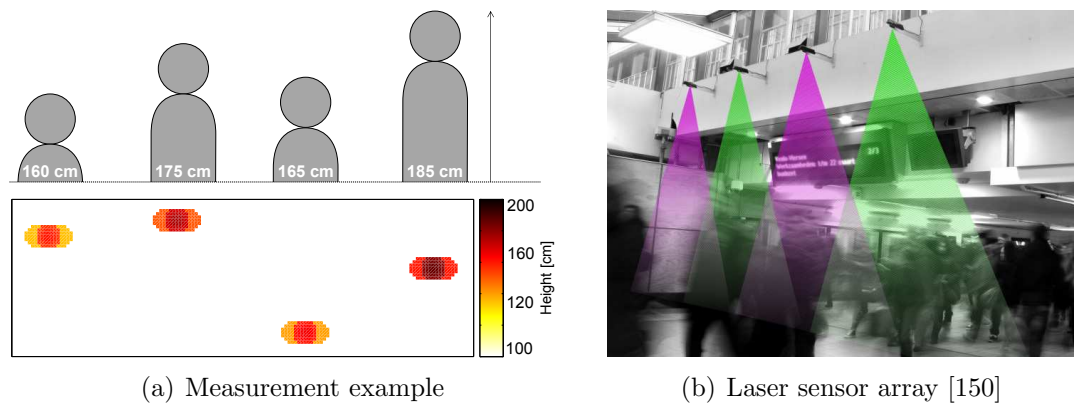(a) Measurement example   (b) Laser sensor array [150]

Figure 3.4: Left: example for persons detected using a distance sensor which also allows to measure height of people; ground is given in white color. Right: example of laser sensor arrays used in a train station (reproduced with permission from the author).

In Figure 3.4(a) it is seen that height of detected people can be measured also allowing to distinguish between adults and children. Once a distance map is generated, then, algorithms similar to the ones for computer vision are used to distinguish single individuals and continuously track their position. One advantage in the use of distance sensors is that privacy sensitive information are not gathered and they can operate under different lighting conditions without any influence on the detection accuracy. However, their range of detection (in terms of surface) is usually limited (typically an area of few meters in width [150]) and for large scale applications an array of distance sensors is used as shown in Figure 3.4(b). The availability of commercial equipment at low cost has seen an increase in the use of this technology and several applications has been reported including single sensors and arrays connecting several ones [151, 150]. In general, distance sensors are suitable to gain microscopic information and when used on a large scale require important computational power. It is however possible to distribute the different tasks by having some computations performed directly on each sensor, thus collecting only the summarized information for large scale processing.

3.2.3 Alternative methods

The methods presented above are mostly focusing on microscopic aspects in the measurement of crowd, with the aim of obtaining velocity and/or density in a building and/or for a festival ground. Computer vision is already a well-established technology and systems based on laser sensors are also finding an increasing number of applications. There are however alternative methods which allow to gain approximate information on different scales ranging from small neighborhood to whole cities or large regions. Although the research described in this work is mostly dealing with microscopic aspects, it is worth mentioning macroscopic scale measurement methods and, as we will see later, some of them can be applied on multiple scales.

WiFi or Bluetooth sensors are used to estimate the travel time between different points on a given route [152]. MAC (Media Access Control) scanners are used to detect the presence of electronic devices in the proximity of the sensor. By having several scanners in a limited area it is possible to reconstruct the route of each person by looking for the same MAC address in each scanner's position. In general, only approximate information

are gained (such as the average time required to cross a bridge [152]), but in complex environments this approach allows to get a general picture of which is the preferred route and how do the travel time change during a whole day. Also, it is worth mentioning that although nowadays many people make use of electronic devices, the efficiency of this type of sensors is related with the amount of people using them. In addition, the use of WiFi and Bluetooth sensors may become difficult in the presence of many antennas and fixed devices, where considerable noise is created by the different equipments [152].

An alternative approach to gain information on pedestrian position and travel path is represented by the use of inertial sensors. Inertial sensors are devices capable of measuring changes in velocity and orientation in terms of acceleration and angular velocity. By integrating the signal gained from the measurement of the acceleration it is possible to obtain the velocity, which by further integration provides the position. If initial position, velocity and orientation are known it is possible to compute the trajectory for one pedestrian by continuously measuring acceleration and angular velocity. In general, devices using inertial sensors also have GPS (Global Positioning System) and compass capabilities, so the initial position can be obtained by one of them or a combination of both. Feliz et al. [153] showed that inertial sensors can be efficiently used to obtain pedestrian trajectories also inside buildings without GPS coverage (always provided that initial position is known). In their study, participants had an inertial sensor mounted on their foot registering (three-dimensional) acceleration, angular velocity, magnetic field, air pressure (used to estimate altitude) and GPS position. Despite the good results Feliz et al. also noted that because of the integration steps required to gain position and orientation, errors accumulate over time and particular measures are required to reduce these effects.

Mori et al. [154] also used inertial sensors, but their focus has been on emergency situations and in particular they investigated if it is possible to distinguish between moving behaviors based on the oscillations of the body. In their evacuation experiments an inertial sensor measuring different quantities has been used, but in their analysis only vertical acceleration (in the direction of gravity) has been considered. Mori et al. concluded that by using the maximum of the vertical acceleration of the body it is possible to distinguish between three states typically found in evacuations: stopping, walking or running. The measurement from their sensors were then combined on a large scale approach to detect the outbreak of a disaster.

On very large scales, GPS position is usually used. Although the accuracy of GPS does not allow to use it for building-scale scenarios, the combination with topological information allows to estimate the route taken by people during evacuations from large natural disasters (earthquake, typhoon, flooding...) inside complex metropolitan areas [155]. In these situations evacuations usually occur outdoor and using public roads, so aggregate information are sufficient and are more important, in particular for policy-makers who have to set priorities on emergency strategies.

3.3   Direct measurement of body rotation in bidirectional flow

In the previous discussion we have mentioned that inertial sensors have been successfully used to gain pedestrian trajectories and judge the criticality in emergencies. However, past studies used special sensors making use of professional equipment which was pro-

vided to participants during the experiments. The miniaturization of electronic devices has allowed to include inertial sensors in common devices such as mobile phones or smartphones/tablets carried daily by common people. Accelerometers and gyroscopes are now commonly used in electronic devices to interact with users and perform several tasks such as rotate the screen or simulate the motion of vehicles in video games. In the following sections, we will investigate possible applications of electronic devices (and inertial sensors) for assessing crowd properties such as velocity and density. To link the discussion with the previous analysis on the bidirectional flow, we will start by measuring crowd properties in bidirectional streams and see how quantities gained from video analysis relates with information gained directly by sensing the crowd itself. Since the analysis of the bidirectional flow suggested that rotation is an important aspect to understand several mechanisms, we decided to measure body movement of pedestrians (and in particular their body rotation, sometimes referred as yawing) by using commercial tablets equipped with a digital gyroscope.

3.3.1   Technical equipment and setup

In this part we will start by introducing the equipment used and the technical setup developed to allow an accurate synchronization between the various devices used. In our experiments, Nexus 7 (2013) tablets were chosen because of technical specifications and because of their relative large size and low weight, which allows to accurately follow body movements while having no (or little) influence on the walking behavior. A wearable bib with a zip pocket was used to fix the tablets on the chest of the experiments' participants. After wearing the bib it was tightly tightened (not too tight to still allow natural movements), with the tablets therefore measuring the motion of that portion of body between the chest and the belly. Participants were obviously aware that tablets were used in the experiment, but they were not informed in regard to which data will be extracted from the devices and which kind of sensors are contained within them.

An application reading the values generated from the different sensors was installed on each tablet and sensing rate was set at 50 Hz. Because of the differences in clock time between each tablet a central storage was preferred. Measurements from each tablet were sent over wireless network to a central PC where data were stored. This allowed to obtain the data from each tablet simultaneously, independently on the clock time differences between each tablet.

Inertial sensors and measuring principles

Nexus 7 (2013) devices are equipped with a range of sensors (gyroscope, accelerometer, magnetic field, light sensor and GPS), but only few of them were used in our experiments. In particular, a motion sensor measures three-dimensional angular velocity and acceleration, but it is important to highlight some differences with the inertial sensors used in the experiments described above (Feliz et al. and Mori et al. in particular) and the ones contained in Nexus devices. One scope of the sensors contained in electronic devices is to determined their orientation for mainly two applications: navigation and screen rotation. In the case of navigation, the compass (based on the magnetic field) plays the most important role, since horizontal orientation is the most important to guide users (for example through different roads in a city). To determine the vertical position (and thus rotate the screen if required) the accelerometer is used. The accelerometer needs therefore to determine the direction of gravity by measuring it. As a consequence,

while specialized inertial navigation devices record no acceleration at still, accelerometer contained in tablets measures gravity when not moving.

The Android OS (Operating System) on which Nexus devices are running provides however an additional measures called "linear acceleration" which removes the gravity to give only the acceleration relative to the motion of the device [2]. In other words, by using the "linear acceleration" measure provided from the OS, acceleration is given as zero when the device is at still. However, as we will see later, that are some issues related with this function.

Validation and calibration

It has to be mentioned that, although the inertial sensor contained in tablets is successfully used in a variety of applications, it is not, strictly speaking, a certified scientific instrument. We had therefore to check the accuracy and the precision in the measurement for angular velocity and acceleration.

To verify the accuracy of the gyroscope sensor we took the 10 tablets available, placed them in a tight box not allowing any type of independent movement and rotated them altogether by 360° using a rotating disk. As Figure 3.5 shows, a rotation on the tablet plane corresponds to a rotation in the z-axis relative to the coordinates of the gyroscope sensor. As the tablets are rotated, the angular velocity in the z-direction increases, before setting again to 0 once the rotation is stopped. The differences between the values recorded by each device are minimal (almost indistinguishable), giving an indication on the measurement precision. In addition, by integrating the signal obtained over the whole time period the measured angle can be obtained. In this case the recorded value was 360.53 $\pm$ 1.34° suggesting that both precision and accuracy of the angular velocity measurement can be assessed as below 1%.
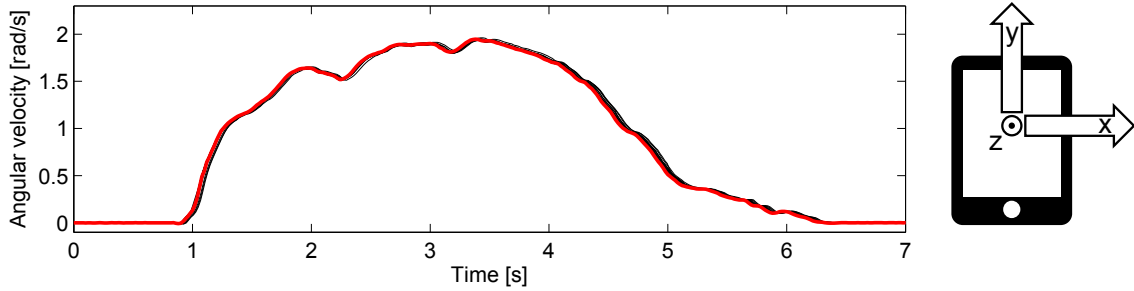
Figure 3.5: Measurement of angular velocity performed using 10 Nexus 7 (2013) tablets. Each line corresponds to a single device, red line is the average among all of them.

What is also important, is that, at still, the signal for the angular velocity oscillates around zero, meaning that integral value should be also close to zero (remember that integral quantities are generally used when dealing with inertial sensors and pedestrians). In addition, we found no significant variation for the angular velocity recorded in the x- and y-direction when the rotation was imposed on the z-axis.

To check the accuracy of the accelerometer we placed all the tablets in the same tight box used in the previous experiment and moved them on a dolly cart for 2.0 m in the y-direction (we made sure that the movement was parallel to the y-direction and perpendicular to

---

[2]It is not clear which algorithm is used to perform this calculation, although it seems (sources are vague here) that a Kalman filter is employed.

both x- and z-directions). During the whole process, z-direction has been measuring the gravity. Figure 3.6 shows the results for this simple experiment in the three axes of the accelerometer.

(a) x-direction   (b) y-direction   (c) z-direction
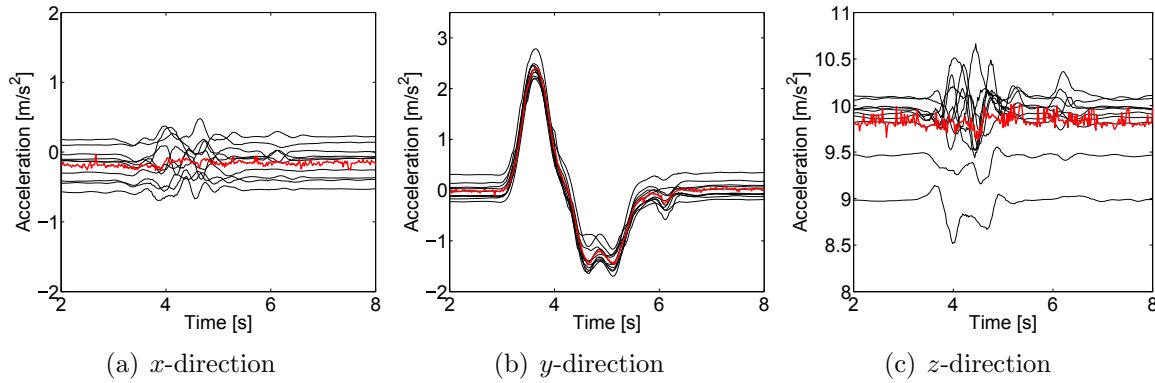
Figure 3.6: Results for the acceleration/deceleration experiment using a dolly cart measured using the accelerometer of Nexus 7 (2013) tablets. Red line correspond to the average result. Time interval has been chosen to cover the most relevant moments.

In the y-direction it is possible to see that a positive acceleration is followed by a deceleration, corresponding to the translation movement performed with the dolly cart. However, what is clear from the three axis is that acceleration at still (i.e. before and after the translation) is not zero and it is not even equal among the different tablets. This does not allow an integration of the signal to obtain more important properties, since the integration would result in a continuous movement although tablets are at still. From the z-direction it is also seen that gravity it is not correctly measured, although most of the tablets are around the correct value (approximately 9.81 m/s^2). In fact, by taking the magnitude at still, the average value among the different tablets was 9.815 ± 0.341 m/s^2, quite consistent with the gravitational acceleration.

As introduced earlier, the Android OS also provides an additional "virtual" measure removing the gravitational component from the acceleration. The results for the "linear acceleration" in the same dolly cart experiment described above are given in Figure 3.7. In the acceleration graph of Figure 3.7(a) is clearly seen that by using the linear acceleration a zero value is reported at still (before and after the experiment). We found similar results in the x- and z-direction, thus confirming that the OS function allows to detect accelerations only when movements are actually performed. However, by integrating the y-acceleration to compute the moving velocity, we found that speed does not return to zero when the cart is at still (this also results in the changing position at the of the experiment). We found that the reason for this fault calculation of velocity (and the distance traveled) is that positive acceleration had been underestimated (compared to deceleration). By increasing the gain for the positive acceleration we were able to obtain the correct distance traveled (2.0 m). However, this "corrective" gain was not constant and it had to be changed each time the experiment was repeated. This shows that reduction of the reported "linear acceleration" may be related to its magnitude and created by the filter applied on raw measurements.

To summarize, the results obtained from these two simple validation experiments are given in Table 3.1.

---

[3]Acceleration magnitude (gravity) measured at still was 9.815 m/s^2, resulting in an accuracy of less than 1%.

(a) Before calibration

(b) After calibration
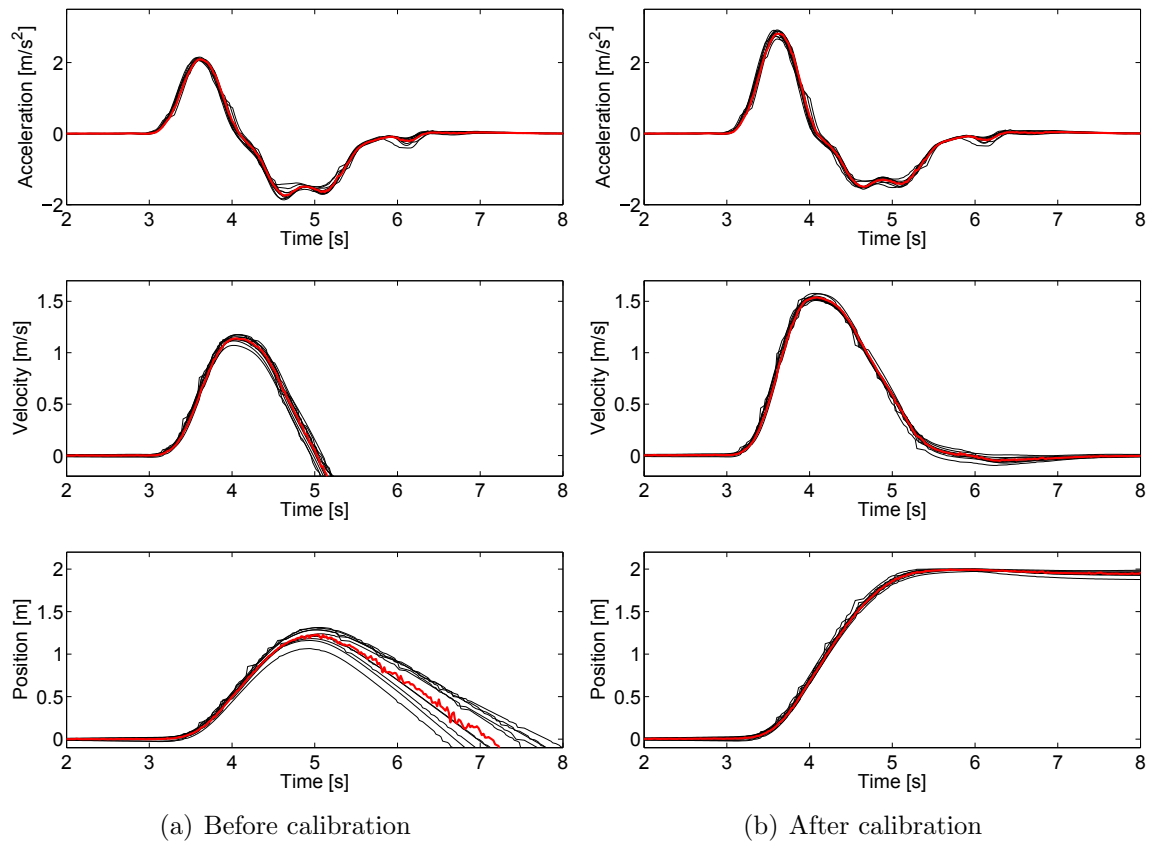
Figure 3.7: Acceleration, velocity and position for the dolly cart experiment to test the accelerometer. Velocity and position are obtained by successive integration of the acceleration signal. All graphs refer to the y-direction.

Table 3.1: Inertial sensors available in Nexus 7 (2013) devices and their characteristics. Conclusion refers to their potential use for estimating pedestrian properties.

Sensor	Gyroscope	Accelerometer	
Measure	Angular velocity	Acceleration	Linear acceleration
Type	Sensor reading	Sensor reading	OS generated
Maximum rate	200 Hz	200 Hz	50 Hz
Precision	$< 1\%$	$< 5\%$	$< 10\%$
Accuracy	$\ll 1\%$	Largely inaccurate [3]	Largely inaccurate
Conclusion	Suitable	Unsuitable	Suitable for comparison

The gyroscope has been found being an accurate scientific instrument, with a low precision and very low accuracy. Also, its maximum sampling rate is 200 Hz, safely allowing to record also very fast movements of pedestrians. On the other side, we had to exclude the acceleration (i.e. the reading from the sensor including gravitational acceleration) as a candidate to be used in pedestrian crowds. The main reason for excluding this type of measurement is that we found that acceleration does not return to zero at still, potentially allowing erroneous estimation of crowd state. Also, the subtraction of gravity can be difficult, since values are not constant.

However, we found that the "virtual" linear acceleration can still be useful although we had to conclude that values returned are an estimation of the acceleration and not an accurate measurement. Important for the aim of this research is that integration of linear acceleration signal at still gives zero, thus correctly indicating no movements. In addition, as Figure 3.7 shows, all the tablets recorded a very similar acceleration signal, so although not accurate in absolute (and physical) terms, it still allows a precise estimation of the magnitude of motion.

Synchronization with camera
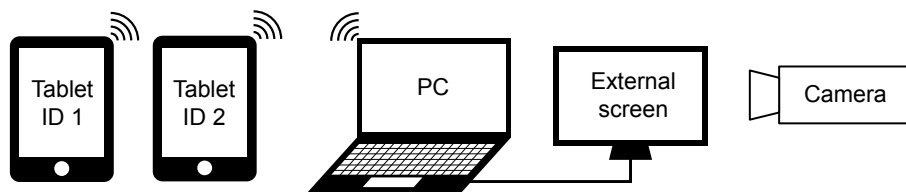
Figure 3.8: Schematic representation of the whole synchronization process [130]. PC is used as reference and central time and inertial data from tablets are sent using a WiFi network. An external screen showing time and changing color regularly is used to synchronize PC with the camera.

So far, we discussed aspects related with inertial measurement, but cameras were also used during the crowd experiments to record pedestrian positions. To allow synchronization between tablets and trajectory data obtained from video recording, an external monitor was connected to the central PC used to store inertial measurements using the WiFi network. Camera's time and PC time were manually synchronized at the beginning of the experiment with an accuracy in the order of few seconds.

Table 3.2: Time synchronization between camera and PC reference time (difference is 2 s in this example). PC is also used to store inertial measurement from tablets. Color change refers to the background color of the external screen in Figure 3.8.

Device	Event	Reference time		Video recording (at 30 fps)	
		Clock format	From midnight	Time	Frame number
PC	Record start	10:27:35	37655 s		–
Camera		10:27:37	37657 s	0.00	1
PC	Color change	10:27:40	37660 s		–
Camera		10:27:42	37662 s	5.00 s	151
	Frame 151 corresponds to 37660 s, so frame 1 must correspond to 37655 s.				

To allow a more accurate synchronization, the time relative to the PC was displayed in the external screen, thus allowing to read that time from the camera monitoring pedestrian motion (an example can be seen in the lower-left side of Figure 3.15). In addition, background color of the external screen was changed every 10 seconds (with the zero reference set at midnight), thus allowing to determine the PC time also from distances where numbers cannot be read clearly (by knowing the approximate time and the frame at which color was changed exact time can be determined). An example for synchronization between PC and camera is given in Table 3.2. As a whole, the synchronization error between the different tablets and the trajectories is of ± 1 frame, equivalent to about 0.03 s. A schematic representation of the technical system used to record, store and synchronize inertial movements measured from tablets is given in Figure 3.8.

3.3.2   Experimental design and procedure

The experiment chosen to test the inertial measurement unit and the system as a whole was the validation experiment presented in Chapter 2.5.1 (whose results are given in Chapter 2.5.4). Since experimental setup and results derived from trajectories have been already discussed, in this part we will focus on the aspects related with the use of tablets. During the validation experiment 10 participants were chosen at random and were assigned the tablets, which were fixed on them with the help from the staff (also checking for the correct orientation). In the unidirectional experiment all participants using tablets belonged to the main (and only) flow, in each bidirectional configuration they were equally split among both groups (i.e. five participants for each direction). In all the cases, staff working for the experiment made sure that tablet-equipped participants were uniformly mixed inside the crowd allowing them to be representative of the collective motion. Also, participants chosen for measurement using tablets were of similar height and average build, making therefore comparison more easy and reliable.

3.3.3   Comparison between direct and indirect measurement of rotation

In this first bidirectional test we focused on body rotation and therefore only data from the gyroscope (which is also the most accurate sensor) were used. We will start the presentation of the results by explaining the analysis method employed to summarize data for this experiment. Figure 3.9 shows an example for the angular velocity measured on the body of a single pedestrian during the balanced bidirectional flow experiment.
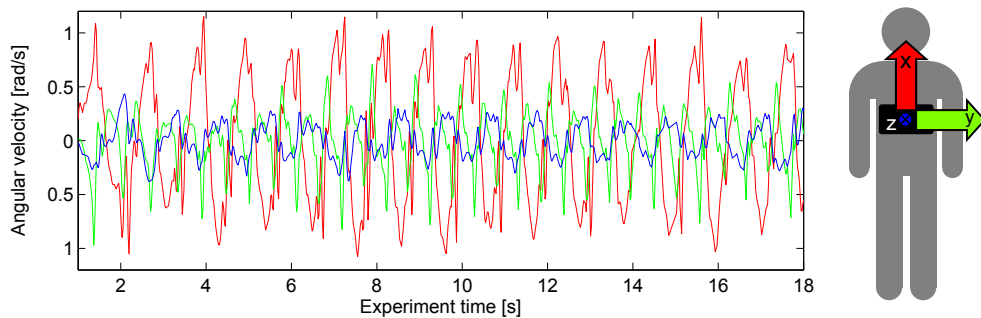

Figure 3.9: Example for the body angular velocity measured on a single pedestrian (balanced bidirectional flow) [130].

As Figure 3.9 shows, some regular patterns are found but it is not easy to summarize the results in a comparative form. Clearly, the alternating movement of legs has an influence in producing maximum and minimum with a characteristic frequency in the x-direction, which could be associated with the walking speed. However, when the three axis are considered together, a more irregular picture is obtained. To simplify the analysis and focus on the most relevant aspects found in bidirectional flows, we limited our considerations to the x-component, which stands for body rotation (or yawing). As Figure 3.9 shows, the x-component is the one having the largest amplitudes and, considering the position of the tablets on the participants' body, it is the one that can provide the most reliable information concerning walking attitude and upper body (shoulder) rotation.

But still, in order to compare the different flow configurations, analyzing the full angular velocity profile as a whole may be a difficult task. Since we are interested in a comparative/qualitative analysis we decided to use an average value defined as follows:

$$\overline{\omega}_x = \frac{\int_{t_0}^{t_1} |\omega_x|}{t_1 - t_0} \tag{3.1}$$

where ω_x represents the angular velocity in x-direction while t_0 and t_1 are the integration limits (start- and end-time considered). In the case of the measured body rotation we were not able to distinguish between the different phases relative to lane formation and dissolution, because we could not determine individually the time at which pedestrians equipped with tablet entered and left the measurement area. Our analysis of the measured body rotation is therefore limited to the average value obtained by all participants equipped with tablets during the whole length of the experiment, defined as the time lasting from the first pedestrian entering the measurement area and the last leaving it. Directly measured body rotation was then compared with the (indirect) flow rotation analysis performed by analyzing trajectories of the pedestrians (and discussed in Chapter 2.5.4). To compare both quantities an average and an integral values are used for the rotation range. In the first, the average value from Figure 2.49 is taken, while for the integral case each value is multiplied by the time length of the corresponding phase. Results are presented in Table 3.3.

Table 3.3: Directly measured body rotation and indirect measurement based on pedestrians' trajectories during the validation bidirectional flow experiment [130].

Configuration	Yawing (gyroscope)	Rotation range	
		Average value	Integral value
4/0 (UNI)	0.363 ± 0.046 rad/s	1.304 ± 0.360 s^{-1}	24.372 ± 7.647
3/1 (BI)	0.430 ± 0.042 rad/s	8.763 ± 1.823 s^{-1}	176.785 ± 23.152
2/2 (BI)	0.390 ± 0.056 rad/s	6.837 ± 2.223 s^{-1}	157.580 ± 48.343

Although measuring principle (and units) are different, rotation measured on pedestrians' body is in agreement with the one estimated using trajectories. Both maximum and minimum values are found for the same configuration, with the unbalanced bidirectional configuration confirmed as rotating the most. While trend is similar, rotation based on trajectories seems more sensible on configuration changes, showing large differences where measured rotation only slightly changes. The relatively large uncertainty found in the balanced configuration may be related with the lowest number of repetitions (3 compared to 4 for the other cases).

3.3.4   Summary

By using the validation experiment as a trial case, the use of commercial tablets to measure pedestrians movements has been tested. To estimate the performance of the sensors used a simple calibration experiment was performed showing that the gyroscope is a reliable sensor which can be used for obtaining comparative and absolute values. Data gained from the accelerometer were less accurate but we concluded that comparative analysis are still possible and reliable.

Results from the bidirectional experiment showed that body rotation measured directly on pedestrians has a similar trend to the amount of rotation estimated using mathematical techniques based on pedestrians' trajectories. This suggests that quantities not directly measurable using image processing and/or tracking systems may be indirectly derived using alternative methods. For instance, body movements can be particularly difficult to estimate based on direct information from video recording, because most of the methods rely on the recognition of pedestrians' head, which cannot provide a complete description of the movement being observed. The method presented in Chapter 2 and based on the rotation range partially allowed to obtain more complex information from trajectories, but results could not be confirmed. The analysis presented here do not only confirm those results, but also constitutes an alternative method to measure pedestrian crowds without having to rely on computer vision or similar techniques.

3.4   Crowd properties in cross flow

In the experiments described so far only bidirectional flow has been considered, which, while common and important, represents only one of the many possible scenario observed in reality. To test both the validity of the rotation range approach and the use of tablets to sense crowd conditions, we designed a cross flow experiment in which participants cross each others' from different directions. This part will be devoted to explaining the experimental setup and the results of the experiment.

3.4.1   Experimental design

On November 14th 2015, after finishing the validation of the bidirectional experiment previously discussed, an intersection as the one shown in Figure 3.10(a) has been constructed by creating 4 paths intersecting each others in a delimited area. A camera (the same used for the bidirectional experiment) placed in azimuthal position 21 m above the ground has been used to record the motion of pedestrians in the intersecting section. Due to space limitations, one leg leading to the intersection had to be bended as shown in Figure 3.10(a) (South leg). Later data analysis (in particular concerning the flow in the 4 different directions) revealed that the bending did not have an influence on people behavior and it has been possible to consider each leg independently. Participants were given caps of different colors allowing to precisely track their position.

Inside each leg, lines at a longitudinal distance of 1 m were drawn on the ground (the first line was 4 m from the center of the intersection). Participants to the experiment were allowed to take any position along the different starting lines, but only one participant per line was allowed. Staff present at the experiment verified that participants did not organize in a single lane and if required some of them were laterally moved from their original position.

(a) General configuration [156]

(b) Detailed dimensions [156]
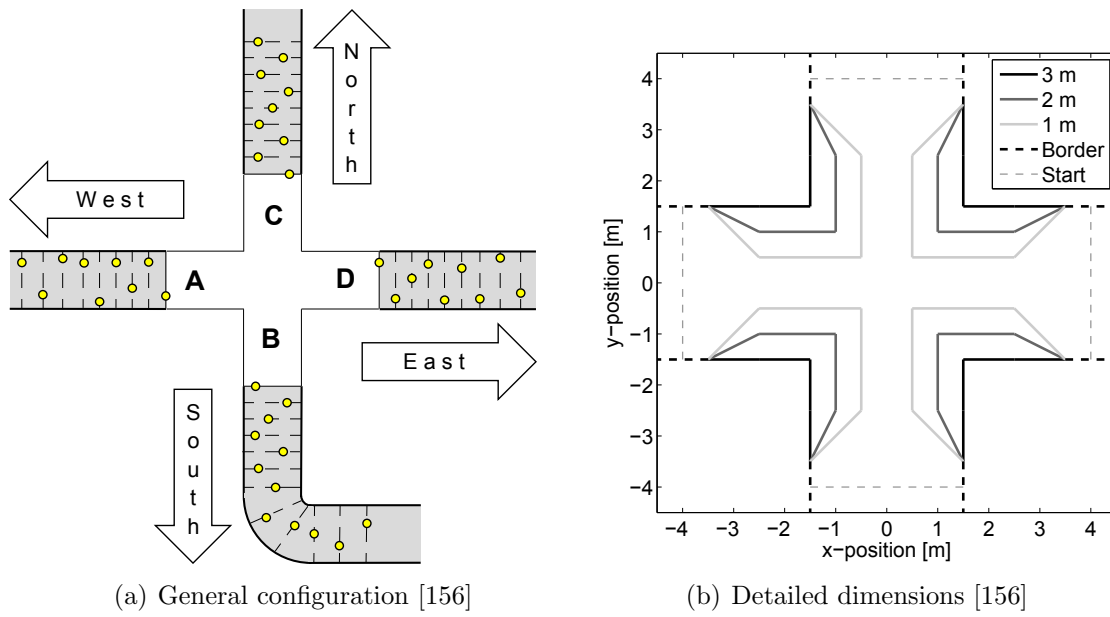
Figure 3.10: Left: geometrical configuration for the cross flow experiment (at the first execution). South leg had to be bended due to space limitations. Starting positions are given as dashed lines along the 4 legs. Participants were allowed to take any position along the line, but only one participant was allowed at each line. Configuration given here is only representative as participants took different positions during each repetition. Right: configuration of the central part of the intersection for the different leg's width. Width of the waiting areas in each legs are kept unchanged, while a bottleneck is created in each entrance to increase the density in the central part. Final section leading to the central area is always straight.

In total 50 male college students took part to the experiment (the same who took part to the bidirectional validation experiment) and were divided into the 4 legs in groups of 12 or 13 people (an exact subdivision was not possible). As a consequence, unaligned lanes of respectively 11 and 12 m formed in the 4 legs. An ID number was assigned to each participant and each one was asked to turn in a different direction at the intersection (details are given in Table 3.4). An almost equal portion of participants had to turn left, right or to go straight (participants going straight were slightly less than the ones turning). The turning direction was given them using a small paper provided at the beginning of the experiment and therefore no-one was aware of the turning direction of others. At a loud "go" signal participants started walking simultaneously toward the intersection and after reaching it they turned to the directions assigned them. After leaving the intersection, participants were asked to walk for a long distance to avoid the formation of congestion close to the exit (after turning).

Table 3.4: ID number and turning direction assigned to each participant. Letters refer to the different legs given in Figure 3.10(a). Participants equipped with tablets are given in bold [156].

Group	Turning right	Turning left	Going straight
A	**1**,4,7,10	**2**,5,8,11	**3**,6,9,12
B	13,15,18,21,**23**	14,16,19,22,**24**	17,20,25
C	26,28,31,**35**,37	27,29,32,**36**	30,33,34
D	39,41,44,**47**,50	38,40,42,45,**48**	43,46,**49**
Total	19 (4 tablets)	18 (4 tablets)	13 (2 tablets)

To avoid any possible learning process (in other words to repeat the experiment under "fresh" conditions), groups were switched after each repetition (details are given in Table 3.5). More precisely, group B in Figure 3.10(a) was switched with group C after the first execution. Later, group A and D were switched. Finally, after the third repetition group B and C were switched again. As one can notice from the right part of Table 3.5, the same configuration was never repeated during the 4 executions, making it very unlikely that participants were able to memorize others' behavior. Also, staff longitudinally switched positions of participants at each repetition to avoid having always the same people at the beginning or at the end of each leg.

Table 3.5: Initial position switching strategy to avoid a learning process resulting from the repeated executions. Cardinal directions refers to Figure 3.10(a). It is important to notice that group locations in Figure 3.10(a) are relative only to the first execution [156].

Execution	Starting configuration	West	South	North	East
1	Initial (Figure 3.10(a))	A	B	C	D
2	Switch B & C (vertical)	A	C	B	D
3	Switch A & D (horizontal)	D	C	B	A
4	Switch B & C (vertical)	D	B	C	A

As shown in Table 3.4, some of the participants (10 in total) were equipped with a tablet to measure their movements and in particular their body rotation as discussed before. Also, the participants equipped with tablets had different hat's color (blue, red or

green) distinguishing them from the rest of the crowd wearing a yellow cap. By knowing the combination of hat's color and starting leg we were able to individually combine data relative to body movements obtained from the tablets and position (or trajectory) obtained from the camera placed above the intersection. This allowed us to precisely determine the time at which a given participant crossed the intersection and analyze the data relative to that particular moment.

Finally, to check the impact of density on the global behavior we investigated 3 different widths for the intersecting legs. On this propose, each final part of the 4 legs was restricted creating a bottleneck before entering the intersection. As shown in Figure 3.10(b), a particular setup was chosen to allow having a straight path before the intersection in each configuration. Starting positions (the lines of Figure 3.10(a)) were not changed and the experimental concepts described so far have been unchanged, the only change performed to reduce the size of the intersection has been in making the entrant bottleneck each time narrower.

Video frames relative to each configuration are shown in Figure 3.11. Inaccessible areas created from the multiple-bottlenecks strategy presented in Figure 3.10(b) are given in gray to make visualization easier.

| (a) Width: 3 m | (b) Width: 2 m | (c) Width: 1 m |
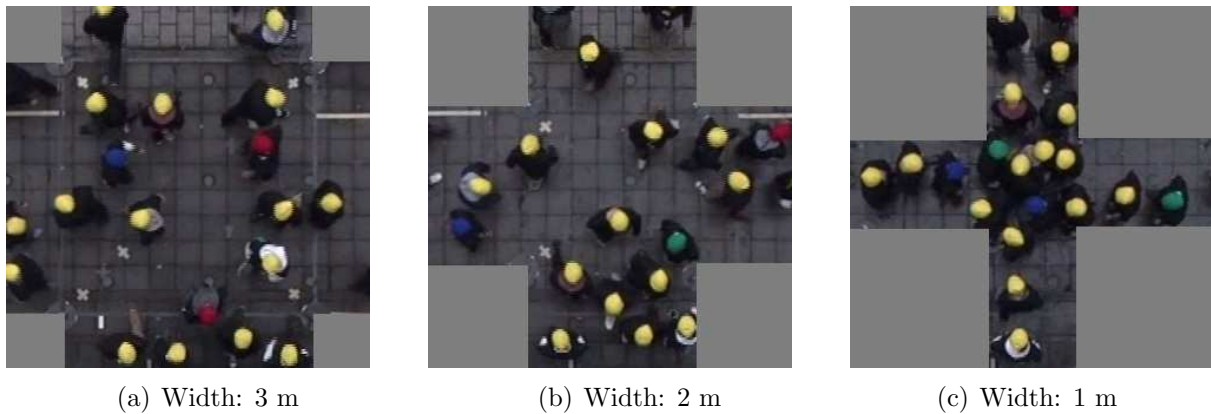
Figure 3.11: Video frames from the three different configurations. To make visualization simpler, inaccessible areas have been cut from the images (and are given in gray). For each configuration 4 executions were performed with the switching strategy described in Table 3.5 repeated each time.

Overall, we can conclude that the experimental setup presented so far allowed us to recreate a fairly natural cross flow in which participants had to consider each situation independently thus creating a new scenario during each execution. The careful planning concerning turning directions and starting positions allowed to consider comparable situations in which only density played an important role.

3.4.2   Results and discussion

As briefly introduced earlier, the particular experimental setup allows to determine individual position of participants equipped with tablets. As a consequence, in the analysis of the results we considered only the region included within 155 cm from the center of the intersection (slightly smaller than the frames provided in Figure 3.11). Also for individuals not equipped with tablets, only trajectories included in this region have been considered. In the case of participants with tablets, we were able to obtain more complex

data combining information from trajectories and measurements from inertial sensors. By using the synchronization system discussed earlier we have been able to relate at each time frame participant position with body motion associated.

Figure 3.12 provides some simple results concerning speed, density (using Voronoi cells) and flow (obtained by multiplication of speed and density) in the central part of the intersection.

(a) Walking speed   (b) Crowd density   (c) Flow (speed · density)
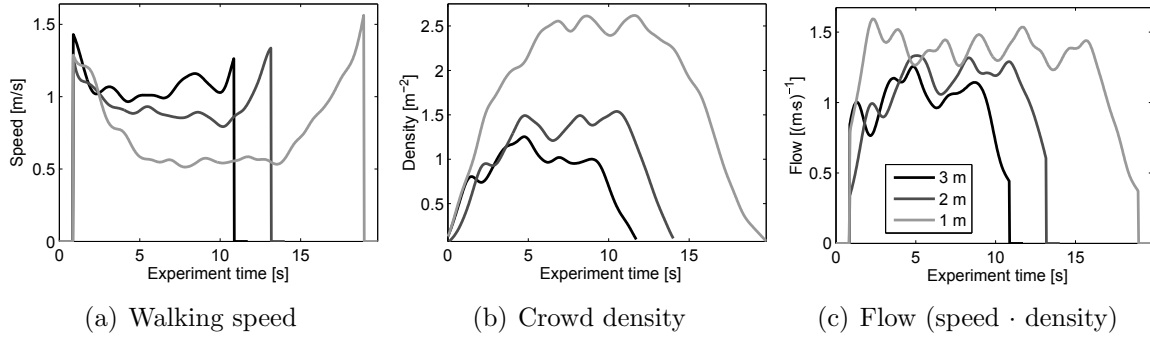
Figure 3.12: Typical speed, density and flow for the three different intersection's widths. Results did not change much among the 4 repetitions. Each case has been filtered to remove noise, which also resulted in the sudden change at the beginning and the end of the experimental time.

We observed that in general a qualitatively similar behavior was observed for the 3 different widths. Density increases as more people move toward the center and at the same time a drop in speed is observed. The combination of both changes lead to a flow with some fluctuations but generally showing no particular trend (although in the 1 m case a light decrease seems to be observed). This similar general behavior allows us to perform a comparative study among the 3 cases. Figure 3.12 also allows to get an idea of the total group crossing time (when velocity drops to zero), which was 10.06 ± 0.25 s, 12.12 ± 0.85 s and 16.73 ± 2.68 s for the 3, 2 and 1 m case respectively.

Average results for the fundamental properties are presented in Table 3.6 and Figure 3.13(a) provides the fundamental diagram of the cross flow studied.

Table 3.6: Fundamental properties and crossing time for the different widths. Deviations refer to the variation of the average values among the 4 repetitions. Crossing time refers to the time required to cross the area considered for analysis, stretching 155 cm from the center of the intersection.

Width	Velocity [m/s]	Density [m^{-2}]	Flow [(m·s)$^{-1}$]	Crossing time [s] Straight	Turn
3 m	1.11 ± 0.01	1.28 ± 0.16	1.37 ± 0.16	2.84 ± 0.67	1.35 ± 1.06
2 m	0.92 ± 0.09	1.46 ± 0.21	1.23 ± 0.05	3.38 ± 0.76	2.27 ± 0.79
1 m	0.74 ± 0.13	2.26 ± 0.25	1.50 ± 0.13	5.11 ± 1.91	4.22 ± 1.62

What is worth noticing is that while density gradually increased when the width was changed, flow had a different trend. In fact, the maximum flow has been observed for the narrowest width and the lowest one for the 2 m experiment. When results are analyzed on the fundamental diagram of Figure 3.13(a) it becomes clear that the narrowest case has been the most congested since a more chaotic dispersion of points is observed. Besides

this qualitative remark, in contrast to the fundamental diagrams previously analyzed for the unidirectional and bidirectional flow (see Figure 2.5), it becomes more difficult to get an idea of the general behavior observed in the case of the cross flow. This shows that while the fundamental diagram provides an accurate picture of the motion observed in the unidirectional case, in multidimensional dynamics interpretation of the results becomes more difficult. A final remark on Table 3.6 concerns the crossing time for the different widths. Although quite obvious, it is interesting to notice that, while crossing time generally increases when density grows, turning time increases faster. This is related to the fact that "shortcuts", which were possible at 3 m width, become meaningless for the narrow passage, where path is more clearly defined.

Concerning the results from inertial sensors, we observed that in the case of turning pedestrians at low densities (3 m width) a clear rotation as the one presented in Figure 3.13(b) was shown in the x-direction also providing evidence of the turning direction.

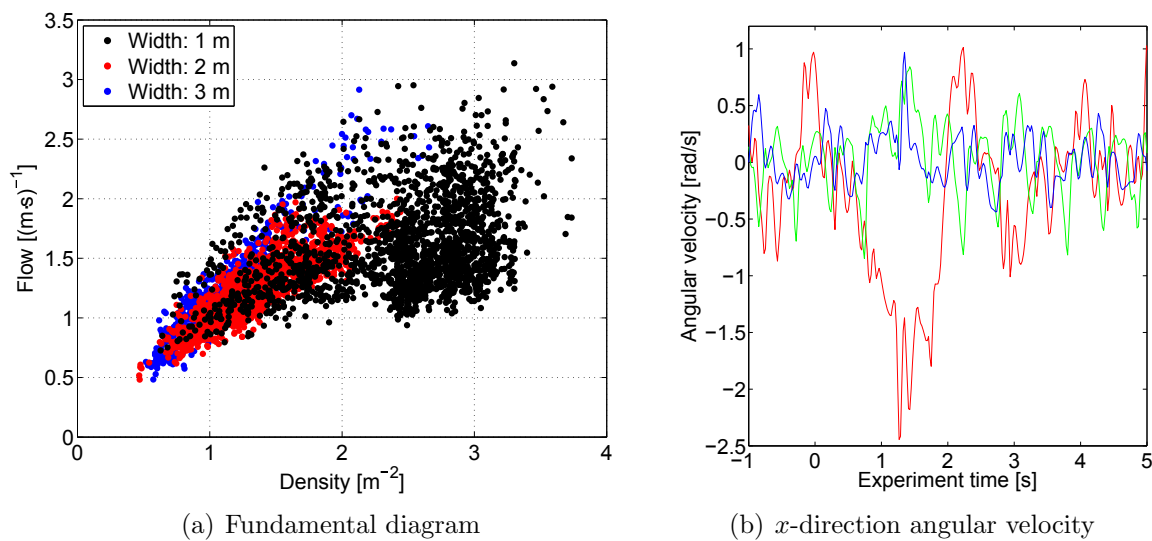(a) Fundamental diagram

(b) x-direction angular velocity

Figure 3.13: Aspects of the cross flow experiment. Left: fundamental diagram for the several widths and repetitions; right: angular velocity (yawing) for a right turning pedestrian.

However, as the density grew we find more difficult to relate movements of the body with trajectories. On the other side, we found that in several occasions direction of the body obtained using inertial data did not match to the direction gained from the trajectories. In the particular case of pedestrians going straight, we often observed that a strong rotation of the body was performed to avoid collisions. While this characteristic is clearly depicted using inertial sensors, trajectories, being based on head positions do not show this behavior. In this sense, we confirmed that considering body rotation and using tablets during the experiments allows to analyze more in detail pedestrian motion and to overcome some of the limitations given by the use of computer vision.

Finally, we applied the concept of rotation range introduced in Chapter 2.5.2 for the case of bidirectional flow to the data gained from the cross flow experiment. In doing so, the velocity vector field has been obtained by dividing the whole area in cells having 0.2 m in width and taking variable time intervals between 2.5 and 3.5 s (on the overall time interval used has been of 3.02 ± 0.22 s). Based on the velocity vector field, rotational has been computed in all valid positions and the difference between the minimum and the maximum value resulted in the rotation range. To account for the changes in absolute

velocity, the rotation range has been divided with the average speed, resulting in what we define as the "congestion level" [4]. In Table 3.7 results for the rotation range and the congestion level are provided along with the average angular velocity measured using the gyroscope (the same integral approach taken in the previous bidirectional experiment is used here). Since the number of turning pedestrians and the ones going straight is constant among all repetitions, average values taken among all participants equipped with tablets are possible and representative of the scenario investigated.

Table 3.7: Properties related with rotation and level of congestion. Note that the congestion level refers to the relative rotation range defined in Chapter 2. Deviations refer to changes among average values in the 4 repetitions.

Width	Rotation range $[s^{-1}]$	Congestion level $[m^{-1}]$	Angular velocity $[rad/s]$
3 m	11.90 ± 0.90	16.55 ± 1.35	0.95 ± 0.07
2 m	7.45 ± 0.20	12.90 ± 0.55	0.99 ± 0.09
1 m	7.05 ± 2.40	17.90 ± 4.25	0.66 ± 0.17

The results of Table 3.7 provides a quite different picture from the interpretation based on the fundamental diagram. The highest congestion level is found in the 1 m case, which is both consistent with the low value found for the angular velocity (indicating slow limited body movements) and the qualitative impression gained by visioning the video recordings. From this point of view the congestion level seems to provide a qualitative good representation of the phenomena observed, since the high flow measured in the 1 m case does not necessarily relate with an efficient and organized motion (as the high crossing times also testify).
When the cases of 2 and 3 m width are considered, then partially contrasting results are obtained. While the minimum congestion level is found for a width of 2 m, the angular velocity relative to body rotation does not differ much. It has to be mentioned, that, in general, the congestion level found for the three cases of cross flow corresponds to a fairly congested motion. In the cases previously considered for the bidirectional flow (see Figure 2.50 and Figure 2.51) values around 2.5 m^{-1} were found for the low density organized motion in lanes and maximum values approached 7.5 m^{-1} at particularly high densities. Also in the cases where organized lanes did not form, during full bidirectional flow values of congestion level never exceeded 10–12.5 m^{-1} and reached 17.5–20.0 m^{-1} only for a limited time during lane dissolution. Therefore, the qualitative picture provided from the congestion level can be considered satisfactory, but still, it is not possible to understand the reason for the low value found in the 2 m configuration and in particular the similar value found for the angular velocity in the configuration with 3 m and 2 m width. Further investigations are required in this regard and the following experiments may provide some possible evidence on this aspect.

3.4.3   Summary

In this cross flow experiment we have tested some methods developed for the bidirectional in a more complex environment. In particular, the rotation range and its related congestion level have been applied on a full bidimensional environment showing that quantitative results are in line with qualitative observations, with some exceptions to be investigated

---

[4]What we called the "relative rotation range" in Chapter 2.

further. We also showed that the fundamental diagram allows to generally grasp the nature of the observed event, but it does not provide a clear picture allowing to distinguish an organized motion from a more chaotic one.

In addition, we also showed that inertial sensors from commercial devices allows to recognize particular features like turning behavior at corners or body orientation adjustments to avoid collisions. However, we found that already at medium densities, body movements become more unpredictable and only aggregated values are useful. Concerning the angular velocity, we found that, while in the most congested case the lowest value was recorded, figures were similar for the two other cases. This aspect need to be studied more in detail.

While the cross flow experiment allowed to successfully consider aspects of multidirectional flows, it had many problems related with the complex setup, especially concerning instructing participants. Changing the start locations after each execution required a moderate time, particularly long when compared to the time used for data analysis which never exceeded 30 s. In addition, data from the tablets had to be analyzed in the intersection area (to allow a coupling with data from trajectories) and in some cases only few seconds were available. Finally, while the transient nature of the experiment provides an interesting perspective, it becomes difficult to summarize results for the different widths.

3.5   Multidimensional chaotic pedestrian crowds

To overcome the limitations found in the cross flow experiment and continue the analysis of multidimensional crowd motion, we designed a new type of experiments. In the previous experiments we tried to increasing the level of complexity by examining increasingly more multidimensional crowds and we moved from the bidirectional case to the cross flow described earlier. However, although the cross flow comprised 4 directions, eventually forcing a complete bidimensional treatment of the phenomena, the experiment was carefully planned, with participants moving along predetermined routes. To move one step forward and consider a fully chaotic multidimensional motion, we designed an experiment in which destinations and routes are not predetermined.

This type of experiment, which will be defined as "chaotic motion" has been repeated on two occasions with similar principles but partially different conditions and equipment. Both experiments are presented separately and a comparative discussion will be provided at the end.

3.5.1   June 2016 experiment

Experimental design

In an attempt to create the most chaotic situation as possible, we designed an experiment in which participants had to keep moving all times, but could not form any organized pattern. On June 11th, 2016 a room whose dimensions are given in Figure 3.14(a) was created using band partitions and participants were asked to walk within it throughout the full length of the experiment.

It has to be remarked that one study [133] found by means of simulation that when people move chaotically in a closed area, over the long term, a rotational motion may form with pedestrians moving around the center. To avoid the formation of this type of self-organization we asked to four or more participants to cross the room in four different

directions, thus creating a chaotic scenario in which emergent structure are not possible or very unlikely. An example for the experiment under low and high densities is given in Figure 3.14(b) and Figure 3.14(c), where participants crossing the room are located outside and arrows describe their passage within it. After passing the room, transiting participants were asked to briefly step out, turn their body and pass it again from the opposite direction.

(a) Scenario dimensions   (b) Low density   (c) Medium density
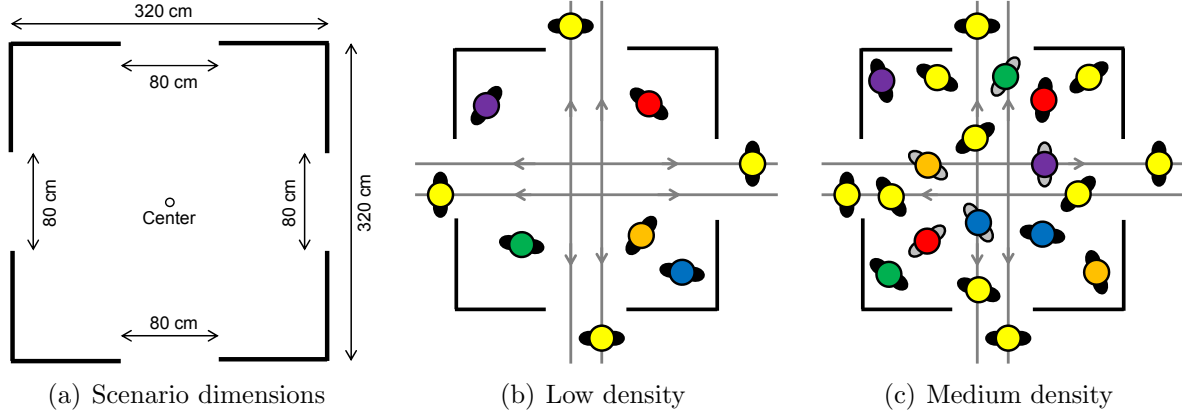
Figure 3.14: Configuration during the chaotic motion experiment for a low density and high density scenario [157, 158]. Participants depicted outside the measurement area were continuously entering and leaving the central section. Participants inside the room had to keep walking for the duration of the experiment without stopping.

Two different patterns (whose details are given in Table 3.8) were tested concerning the number of people crossing the room and the ones randomly moving within it. In the experimental pattern A, the ratio between the number of people staying in the room and the ones passing through it has been kept constant (except the configuration A1 in which only participants moving inside the room were present). At each trial (this experiment was repeated only once for each configuration), the number of crossing people has been increased by 4 (one for each side) and the ones moving inside the room were increased by 5. In total, 5 configurations has been tested in configuration A as given in Table 3.8.

In the experimental patter B the number of crossing people has been kept constant at 4 (except configuration B1) and only the number of people moving inside the room has been changed. In the case of pattern B an higher number of density steps were possible allowing to measure pedestrian motion from a density of about 0.5 m^{-2} up to a maximum of almost 4 m^{-2}.

Finally, to study pedestrian motion at very low densities, we asked to 5 participants to move freely around or inside the experimental area. At that time the remaining participants already left the site so the remaining 5 people could walk without (or with very limited) obstruction. Under these circumstances we were not able to accurately measure density (which has been measured using Voronoi cells for configurations A and B), but we estimated that the 5 people walked in a 50 m^2 surface, thus corresponding to a density of about 0.1 m^{-2}.

A camera was fixed in azimuthal position directly above the center of the room (at an height of 5.5 m) thus recording the movements of pedestrians. Resolution was 1920 × 1080 and 30 frames per second were taken. An example of frames taken during the different configurations is given in Figure 3.15. It can be seen that the wide lens used in the

Table 3.8: Details on the two different configurations tested in the frame of the chaotic motion experiment [157, 158]. In the "free" configuration participants were asked to walk in an undetermined space inside or outside the experimental area (density is an estimation in this case).

#	Participants and role			Density [m^{-2}]
	Moving inside	Passing through	Total	
A1	5	0	5	≈ 0.49
A2	5	4	9	≈ 0.88
A3	10	8	18	≈ 1.76
A4	15	12	27	≈ 2.64
A5	20	16	36	≈ 3.52
B1	5	0	5	≈ 0.49
B2	6	4	10	≈ 0.98
B3	11	4	15	≈ 1.46
B4	16	4	20	≈ 1.95
B5	21	4	25	≈ 2.44
B6	26	4	30	≈ 2.93
B7	31	4	35	≈ 3.42
B8	36	4	40	≈ 3.91
Free	–	–	5	≈ 0.1

recordings [5] creates a rather large distortion which is particularly visible at the corners. Extraction of the trajectories was performed using PeTrack software which allows to fix camera distortion and obtain accurate position of each pedestrian (thus making distortion an irrelevant issue).

(a) Low density (B1)   (b) Medium density (B4)   (c) High density (B8)
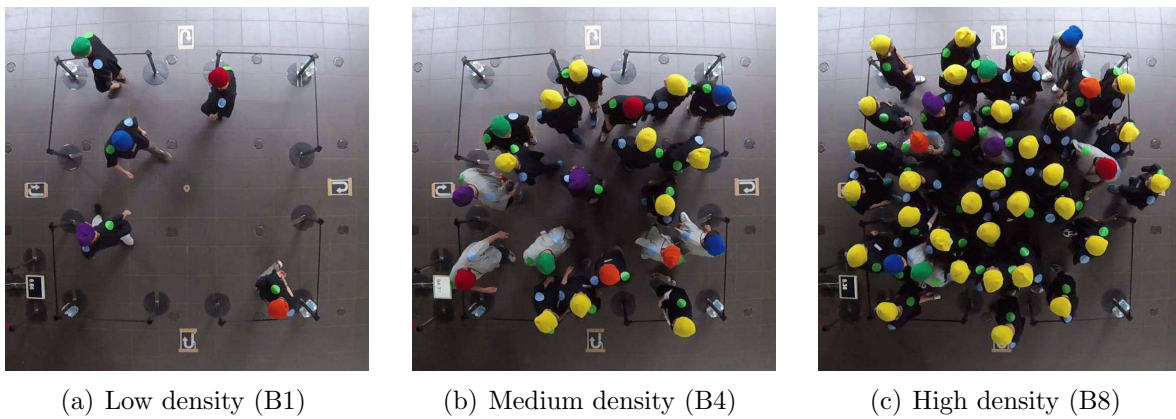
Figure 3.15: Frames taken from videos of the chaotic motion experiment under different densities. Codes refer to the notation of Table 3.8.

From Figure 3.15 it can be seen that participants were wearing caps of different colors. Similarly to the cross flow case, the different colors were used to allow an individual identification of participants wearing caps different from yellow. Like in the previous case, our interest has been on comparing data gained from tracking to those gained from inertial

---

[5]The camera used in these experiments was different from the one used for the bidirectional and cross flow experiments.

sensors on an individual level. Consequently, also in this experiment 10 participants were randomly chosen to carry tablets, which were attached to their chest monitoring central body motion. To link participant ID with the tablet carried by that participant, we used a combination of cap color and T-shirt color as indicated in Table 3.9.

Table 3.9: Combination of colors used to link participant ID with tablet used during the experiment [157]. Participant height is given in bracket. Participants carrying tablets were changed during the break between configurations A and B.

Tablet ID	Color		Participant ID (height)	
	T-shirt	Cap	A-configuration	B-configuration [6]
1		Blue	1 (174 cm)	11 (168 cm)
2		Green	2 (173 cm)	12 (172 cm)
3	Black	Purple	3 (172 cm)	13 (169 cm)
4		Orange	4 (164 cm)	14 (161 cm)
5		Red	5 (174 cm)	15 (182 cm)
6		Blue	6 (180 cm)	16 (162 cm)
7		Green	7 (175 cm)	17 (175 cm)
8	Gray	Purple	8 (167 cm)	18 (173 cm)
9		Orange	9 (177 cm)	19 (167 cm)
10		Red	10 (175 cm)	20 (168 cm)

By taking Table 3.9 as reference it is possible to know that, for example, the purple cap wearing a gray T-shirt in Figure 3.15(b) (experiment B2) uses tablet ID 8 and was the participant having ID 18. In addition, participants were asked to provide their height at the beginning of the experiment, so we can also know that the participant taken as example had an height of 173 cm.

In total 42 male participants were present for the experiment and received a remuneration for the time spent. All of them were university students with the average age being of 20.55 ± 2.10 years. The average height (including those not wearing tablets) was of 170.4 ± 5.5 cm. The experiment was performed outdoor in a covered area ensuring protection from direct light exposure (as seen in Figure 3.15); weather was sunny with a temperature at the time of the experiment of about 25°C. Synchronization between tablets and camera was performed using the method described in Chapter 3.3.1 (the monitor used to check PC time is visible on the lower-left side of Figure 3.15).

Participants were simply asked to walk during the whole length of the experiment without stopping and no additional information were provided on the aim of the experiment or the position of the camera. Start and stop signals were given with a loud oral instruction and participants were asked to start and stop walking simultaneously. Each configuration lasted roughly 2 minutes, time during which participants kept walking continuously. Staff was present at the experiment in particular to avoid that transiting participants would wait too long before re-entering the experimental area after stepping out of the room.

---

[6]During the last free configuration the same setup for B was used concerning tablet numbers and T-shirts/caps color.

Results and discussion

In all the cases, we observed that a stable speed was reached few seconds after the start of the experiment and fairly constant values were recorded until the end when participants were allowed to stop. For this reason, we found appropriate assigning a unique and average value to each experiment concerning speed, density and consequently flow by multiplication (according to the fundamental relation). Results were all analyzed for the time interval during which stable conditions were observed, typically about 10 s after the start of the experiment and 10 s before the end (although more accurate and individual time intervals were used for each single experiment). At first, the fundamental diagram has been obtained by plotting the single values for density (obtained using Voronoi cells) and flow as given in Figure 3.16(a) (excluding the free walk case for which density and flow are not precisely determined).

(a) Density–flow relation

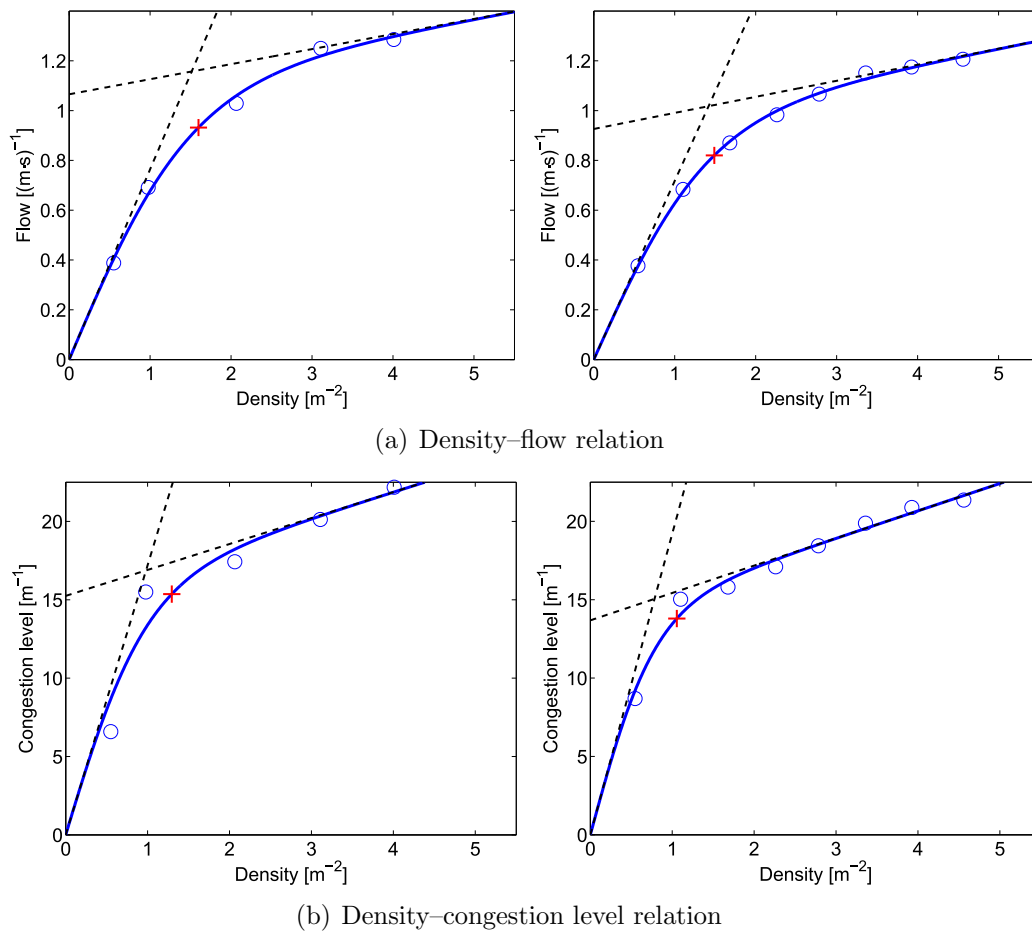(b) Density–congestion level relation

Figure 3.16: Density relationships with flow and congestion level for the two configurations tested [158]. Configuration A is given on the left, B on the right side. All cases fits well with a combination of logistic and linear function. Dotted lines are the two asymptotes found at zero and infinity. Red cross is the "transition point".

It can be seen that in both cases a maximum was not found (at least not in the form of a peak) and the flow kept increasing also at moderately high density. These considerations are in line with the results obtained by Helbing et al. [16] and Dambalmath et al. [36] who studied the motion of the crowd in the Hajj pilgrimage in different years and obtained similar values for the fundamental diagram (this aspect will be also discussed later in

Chapter 3.5.3).
We found that a combination of the logistic and linear function fits well with the results. This function can be written as:

$$y(\rho) = \frac{2a_0}{1 + \exp(-a_1\rho)} + a_2\rho - a_0 \tag{3.2}$$

where y is here the flow, ρ the density and a_0, a_1 and a_2 are fitting parameters (whose values are given in Table 3.10 along with coefficient of determination R^2). This function has two asymptotes found at zero and infinity shown in Figure 3.16 as dotted lines. These functions are defined as $y_1(\rho) = (\frac{1}{2}a_0a_1+a_2)\cdot\rho$ and $y_2(\rho) = a_2\rho+a_0$ for the zero and infinite asymptote respectively. The intersecting point is given by $\rho_{inter} = \frac{2}{a_1}$ and $y_{inter} = 2\frac{a_2}{a_1}+a_0$. By using the line passing through the intersection point and forming the same angle with both asymptotes, it is possible to define a "transition point" which will be the intersection between this line and the fitting function (3.2). Results for this analysis are provided in Table 3.10.

Table 3.10: Fitting parameters for the graphs provided in Figure 3.16 [158]. Units for the fitting parameters have been omitted for simplification and they depend on the quantity considered. R^2 is the coefficient of determination.

Quantity (y)	Setup	Fitting parameters			R^2	Transition point	
		a_0	a_1	a_2		ρ_{trans}	$y(\rho_{trans})$
Flow	A	1.066	1.321	0.061	0.995	1.598 m^{-2}	0.932 (m·s)$^{-1}$
	B	0.926	1.410	0.065	0.998	1.489 m^{-2}	0.820 (m·s)$^{-1}$
Congestion level	A	15.250	2.039	1.665	0.929	1.295 m^{-2}	15.360 m^{-1}
	B	13.680	2.553	1.745	0.984	1.056 m^{-2}	13.795 m^{-1}

The same type of analysis has been also performed by using the congestion level [7] (in this case y becomes the congestion level in (3.2)). Both approaches using the flow and congestion level show qualitatively similar results, although the representation using flow fits better with experimental data. In addition, we found that density relative to the transition point is different depending on the approach used and, also, a moderate gap in transition density is observed between both configurations in the definition based on the congestion level. However, transition point is similar between both configurations when flow and congestion level are employed. For both cases the transition measured in terms of flow and congestion level differs of about 10% (among configuration A and B). In this regard, concerning the difference between configuration A and B, we found that combining both cases only slightly change results, but a separate consideration is more appropriate and accurate at this stage.
Next, we can consider the results gained from the inertial sensors from tablets. In this experiment linear acceleration has been also measured along with the angular velocity gained from the gyroscope. As mentioned in Chapter 3.2.3, Mori et al. [154] used the maximum of the vertical acceleration to determine if people were running, walking or stopped. By combining individual data for body acceleration and speed measured using video recordings we produced the graphs shown in Figure 3.17.

---

[7]Maximum–minimum difference of the rotational from the velocity vector field (used to compute the rotation range and later the congestion level) was taken over the whole room surface. Time interval was chosen between 3 and 4 s, resulting in a used time interval of 3.40 ± 0.03 s.
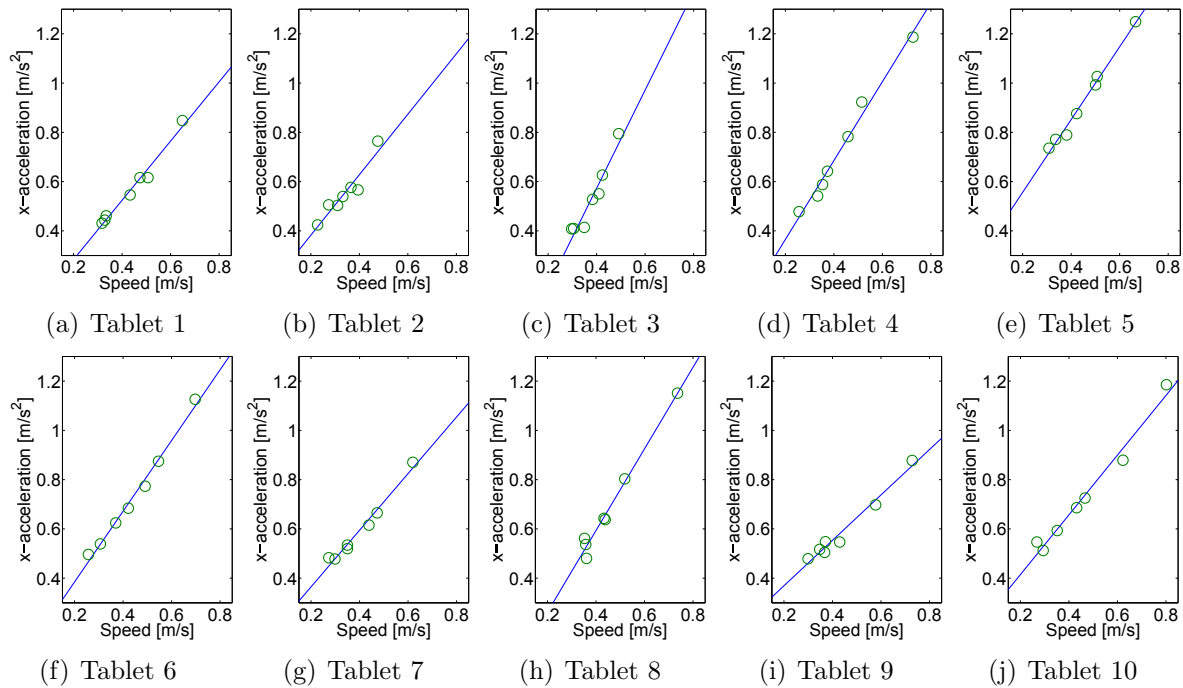
(a) Tablet 1   (b) Tablet 2   (c) Tablet 3   (d) Tablet 4   (e) Tablet 5

(f) Tablet 6   (g) Tablet 7   (h) Tablet 8   (i) Tablet 9   (j) Tablet 10

Figure 3.17: Relationship between individual walking speed and body acceleration in the x-direction (vertical direction) for the B-configuration [157].

A and B configurations are not directly comparable for this type of analysis because different participants wore the tablets and B was chosen since it employs more steps in density. Results for the acceleration were obtained after integration of the signal as given in (3.1). It is seen that walking speed fits comparatively well with the acceleration of the body in the vertical direction, showing that under the experimental conditions tested here a more accurate prediction of velocity is possible compared to the three-states categorization by Mori et al. [154]. Furthermore, we also partially confirmed that linear acceleration can be effectively used despite its limitation in not providing "real" values for acceleration. By checking different quantities such as the angular velocity in x-direction (yawing), we found that similar results are found and a linear trend with speed is seen in all the cases. In addition, we also found that by taking magnitude values (i.e. combining all directions) only minor changes were observed in the results. This observation is important, since in reality it cannot be known where people keep their electronic devices while walking and therefore only magnitude can be used in those cases.

However, from Figure 3.17 it is seen that, although a linear trend is found for all participants, slopes are not equal. In a first guess, trying to understand those differences, we checked the relationship with body height, but we found no significant relation. Interestingly, we found that, when the measurements from the different tablets are combined and compared with crowd quantities such as group average speed and density, then individual differences are not very significant. Figure 3.18 presents the relationship between average crowd walking speed and density toward linear acceleration and angular velocity (magnitudes are used here in all the cases).

In Figure 3.18 we decided to consider both configurations together for two main reasons: (i) because the differences are not large (especially in the case of density) and (ii) because the final aim is to estimate general crowd properties based on inertial measurements. To evaluate speed, a linear function was found fitting well with experimental data, while for

(a) Linear acceleration – speed

(b) Linear acceleration – density

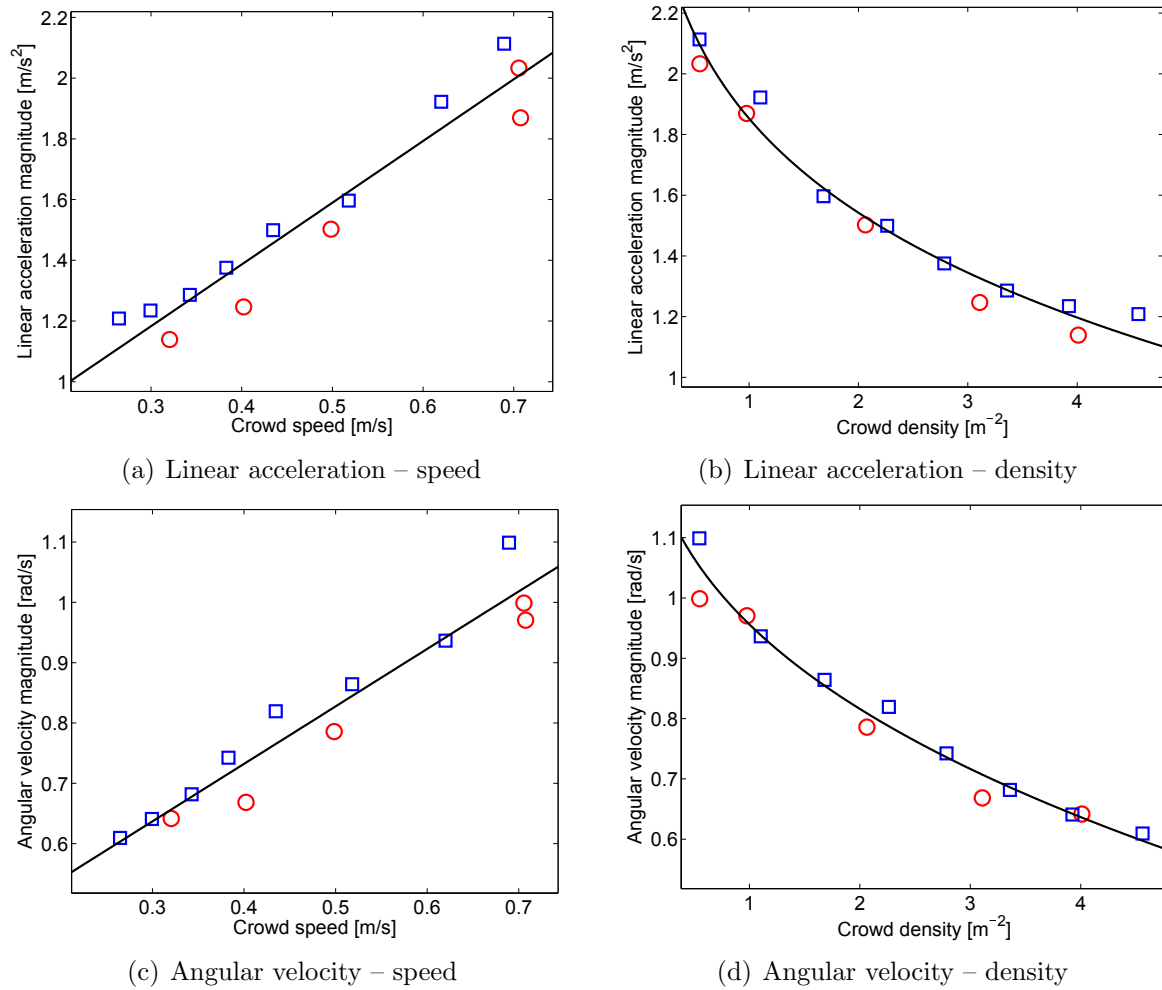(c) Angular velocity – speed

(d) Angular velocity – density

Figure 3.18: Relationship between crowd quantities measured using computer vision and inertial measurements on pedestrians [157]. Circles belong to configuration A, squares to configuration B. Fitting functions and parameters are given in Table 3.11. In all the cases magnitude was used, i.e. the three directions from the inertial unit were combined.

density a power function had to be used.

The fitting values provided in Table 3.11 allow to do some remark on the behavior of crowds at particularly high densities. The function used for speed leads to the conclusion that also when crowd speed is zero, some sort of oscillatory movements are expected from the people since intercept (parameter b_1) for both linear acceleration and angular velocity is positive. The expression for density leads to the same qualitative conclusion, i.e. that at very high densities acceleration and angular velocities are still positive (complete stop is found at a density of 28.32 m^{-2} and 20.04 m^{-2} for acceleration and angular velocity respectively). While the range of speeds and densities considered here may not be sufficient to come to this sort of conclusions, these remarks are in line with observations during accidents which noted that pressure waves occur with people practically staying in the same position all times.

Table 3.11: Fitting parameters for the graphs provided in Figure 3.18 [157]. s refers to the quantity measured from the sensor (magnitude in all cases), x to the crowd measure. Units are omitted in the fitting parameters for convenience. R^2 is the coefficient of determination.

Crowd (x)	Inertial sensor (s)	Function $s = f(x)$	Fitting parameters			R^2
			b_0	b_1	b_2	
Speed	Linear acceleration	$s = b_0 x + b_1$	2.033	0.573	–	0.928
	Angular velocity		0.953	0.351	–	0.927
Density	Linear acceleration	$s = b_0 x^{b_1} + b_2$	-2.750	0.154	4.602	0.975
	Angular velocity		-0.499	0.357	1.455	0.972

In the analysis performed so far the last free walking experiment has not been considered yet. While density could not be measured accurately, we were able to partially measure walking speed in the moments when participants transited below the camera (resulting in a speed of around 1 m/s). Body motion was however accurately measured all the time (tablets continuously streamed inertial measurements even when participants were away from the camera's field of view) and results for both quantities are given in Table 3.12.

Table 3.12: Quantities relative to crowd and body motion during the free walking experiment [157]. Walking speed could somehow be measured, density and congestion level are guessed intuitively. Magnitude values are used for inertial measurements.

Quantity	Result	
	Value	Mode
Walking speed	$\approx$1.0 m/s	
Density	$\approx$0.1 m^{-2}	Estimation
Congestion level	$\approx$0.5 m^{-1}	
Linear acceleration	2.655 m/s^2	Measurement
Angular velocity	0.708 rad/s	

By comparing the results from Table 3.12 with the graphs presented in Figure 3.18 an important consideration has to be made. While the value for the linear acceleration is consistent with the fitting functions obtained, predicting a very low density (0.106 m^{-2}) and a relatively high walking speed (1.086 m/s), the measurement from the gyroscope

seems not to follow the behavior described so far (0.708 rad/s corresponds to about 0.4 m/s). The reason for this prediction failure is that, during the free walking experiment, participants mostly walked straight, turning much less compared to the motion inside the room. This relates to lower values for the angular velocity. A conclusion from this observation is that while both angular velocity and linear acceleration are valid under comparable scenarios, only the linear acceleration is universal in respect to pedestrian crowds and route choice. This could also be the reason which led Mori et al. [154] to focus on the accelerometer in judging moving states during emergencies (although the reason is not clearly stated in their work). For the reasons discussed above, we will focus on the linear acceleration from now on and, considering practical applications, we will always use the magnitude to exclude device orientation issues.

Finally, we can compare the congestion level with the linear acceleration as presented in Figure 3.19. To increase the range of congestion level considered, the result from the free walking experiment has been also used. Although congestion level was not measured there, assuming a low value is a correct a reliable approximation (as it was confirmed in the second experimental campaign of October 2016, see Chapter 3.5.2).

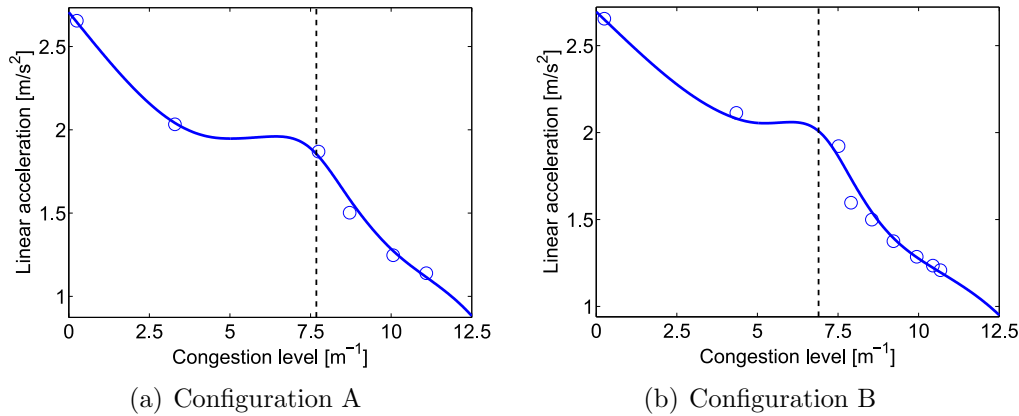(a) Configuration A   (b) Configuration B

Figure 3.19: Relationship between the congestion level and the linear acceleration measured on participants equipped with tablets. Dotted vertical lines represents the "transition point" identified in Table 3.10. Fitting function has been modeled based on the data available and alternative interpretations are possible.

Although a linear equation would be sufficient (and fairly accurate) in fitting the experimental data of Figure 3.19, we believe that a function as the one plotted in Figure 3.19 may be more appropriate. There are mainly two reasons for choosing this particular shape: in both cases the linear behavior seem to be broken around the congestion level that we defined as "transition point" and a similar behavior was observed in the cross flow (although gyroscope was used there and was judged accurate under the experimental circumstances). However, given the limited number of points at low densities and the impossibility in measuring the congestion level in those conditions, further investigations are required on this topic and will be one of the results in the next section.

3.5.2   October 2016 experiment

The experiments presented so far showed that inertial sensors contained in commercial devices allow to get aggregated but yet significant information on crowd motion. However, the methodology tested so far cannot be applied to real conditions, since, in general, it

is not possible to know in advance the position and the orientation of the device used. Also, hardware varies greatly from person to person, with some devices using highly accurate sensors for gaming requirements and others making use of cheap sensors for basic functions only. In addition, in the experiment of June 2016, only densities above 0.5 m^{-2} have been accurately studied. While the overall focus of this work has been on dense crowds, it is also important to notice that most of the public spaces are not extremely crowded. As a consequence of the above discussion, in the experiments of October 2016, we focused on low densities (while also including heavily crowded scenarios) and a part of the participants used their own phones during in an effort to reproduce more realistic conditions.

Experimental design

While in the experiments of June 2016 only the number of people was varied to change the density, in the experimental campaign of October both room size and number of participants were varied. On that purpose mainly two experimental setups were used: a wide room configuration and a narrow room, both given in Figure 3.20. In the wide room configuration we used the entire floor available (with a surface of 96 m^2), while in the narrow configuration different sizes were tested by starting with a side length of 6 m and reducing it until a minimum of 3 m (i.e. a surface of only 9 m^2). The different room sizes also allowed us to study effect of geometry on body movements, which were noticed in the free walk experiment of June 2016.

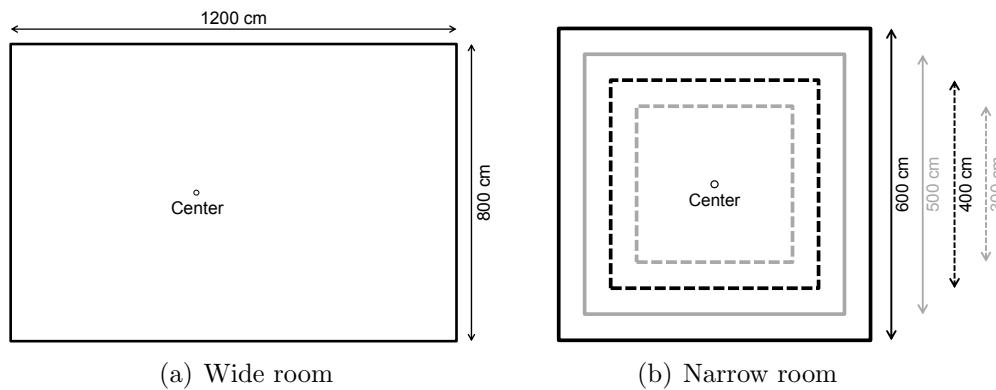(a) Wide room   (b) Narrow room

Figure 3.20: Configuration during the chaotic motion experiment for a low density and high density scenario [157, 158]. In the configuration used for the October 2016 campaign crossing participants were not present.

In the experiments of June 2016 transiting pedestrians were used to avoid the formation of organized structures. However, we found that also when all the people were moving inside the room, emergent phenomena did not form. While we mentioned that some researchers [133] predicted using simulations that circular motion around the center could happen on the long run, the time of our experiments was probably too short to lead to the formation of such structures. As a consequence, we decided to use a simple configuration for the experiments of October 2016 and only motion inside the room was studied.
Participants (university students who voluntarily applied for the experiment) were simply asked to walk inside the room for the whole length of the experiment (also around 2 minutes here) without stopping. The number of participants taking part to each experiment and the room configuration used are given in Table 3.13 (age and height were not

provided in this campaign). At the beginning, the wide room was used and the number of participants gradually increased up to a maximum of 42. Following experiments were performed in the narrow room configuration and the number of participants was kept constant while changing the size of the room. Densities considered ranged from 0.05 m^{-2} up to a maximum of around 4.5 m^{-2}.

Table 3.13: Details on the chaotic motion experiment of October 2016 [157, 158]. 42 participants took part to the experiment and about half of them were equipped with devices measuring their body movements. Tablets were positioned to monitor the motion of the chest as in the previous experiments, position of smartphones are given in Table 3.14.

#	Participants and sensor				Area [m^2]	Density [m^{-2}]
	Smartphone	Tablet	No sensor	Total	Size [m]	
C1	5	0	0	5	96 (12 × 8)	≈ 0.05
C2	10	0	0	10	96 (12 × 8)	≈ 0.10
C3	10	10	0	20	96 (12 × 8)	≈ 0.20
C4	10	10	10	30	96 (12 × 8)	≈ 0.31
C5	10	10	22	42	96 (12 × 8)	≈ 0.44
C6	10	10	22	42	36 (6 × 6)	≈ 1.17
C7	10	10	22	42	25 (5 × 5)	≈ 1.68
C8	10	10	22	42	16 (4 × 4)	≈ 2.63
C9	10	10	22	42	9 (3 × 3)	≈ 4.67

As shown in Table 3.13, 20 participants used electronic devices containing inertial sensors to measure body motion. 10 of them were equipped with Nexus 7 (2013) tablets provided to them for the scope of the experiment. Position and configuration of those tablets has been the same as the experiments presented so far, with the device being positioned around the chest monitoring the motion of the central-upper part of the body. Participants carrying tablets have been the same for the whole length of the experiment (i.e. from C1 to C9).

In addition, to test conditions similar to reality, 10 additional participants gave their consent in using their own smartphones during the experiment. Due to technical limitations, only Android users were selected for this role. Devices were different from person to person and also the position used to keep their smartphone was not the same throughout the volunteers as shown in Table 3.14. To recreate realistic conditions, volunteers using their own smartphones were asked to keep it in the usual position, without giving them particular instructions. At the end of the experiment, the position used to keep their smartphones was asked and is given in Table 3.14. Most of them opted for their pants pocket, although right and left side was almost split in half. Only one participant stored his phone in the pocket of his shirt. Most of the smartphone were equipped with both accelerometer and gyroscope, although ID 10 had only the accelerometer available. This also shows that for practical applications, the accelerometer may be more appropriate. Finally, it should be mentioned that some technical problems occurred to some of the phones limiting their use in some experiments.

Participants using tablets and smartphones were uniformly mixed inside the crowd with

---

[8] Problems with OS generated linear acceleration, which stopped during some of the experiments.

[9] Only acceleration measured, linear acceleration was not provided and could not be used in the analysis.

Table 3.14: Smartphone model, available sensors and place used to keep the phone during the experiment [157]. Except for ID 10 all smartphones were equipped with gyroscope and accelerometer.

| Phone ID | Model | Sensors | | Position |
		Accelerometer	Gyroscope	
1	SO-04G	✓	✓	Pants pocket, right
2	LGV32	✓	✓	Pants pocket, left
3	SO-03H	✓	✓	Pants pocket, left
4	SH-01H	✓	✓	Pants pocket, left
5	F-06E	✓	✓	Pants pocket, right [8]
6	SO-04H	✓	✓	Shirt chest pocket
7	SO-02F	✓	✓	Pants pocket, right
8	F-02G	✓	✓	Pants pocket, right
9	SO-02H	✓	✓	Pants pocket, left
10	HTV31	✓	✗	Pants pocket, right [9]

normal participants not using electronic devices. Different cap colors were used to distinguish each class of participants but we did not focus on individual recognition like in the previous experiments. In particular, blue caps were used for individuals carrying smartphones and green for the ones carrying tablets. Yellow caps were assigned to normal participants not having inertial sensors installed on them.

A camera was fixed right above the center position given in Figure 3.20 at an height of 6.0 m recording the movements of pedestrians. Resolution was 1920×1440 and 30 frames per second were taken. Figure 3.21 shows frames taken for configurations at different densities. As given in Table 3.13, at the beginning only participants with smartphones and tablets took part to the low density experiments and participants with yellow caps were introduced later. For this reason, only blue and green caps are visible in Figure 3.21(a). In Figure 3.21 wide-angle lens distortion has been removed and all images have been corrected showing fairly straight lines delimiting the room. However, distortion effects on body length are evident in particular in Figure 3.21(a). The software used to gain trajectories (PeTrack) allows to correct this distortion and therefore results from trajectories used here are relative to the position of feet. From Figure 3.21(c) it can be seen that maximum densities were particularly high, eventually making motion very difficult.

All experiments were performed indoor in the morning of October 30th, 2016 and participants were paid for the time spent during the different experiments. Participants using their smartphones gave their written permission. Age and height were not measured nor asked during this experiment, but since participants were all male university students recruited with the same procedures of the previous experiments, we can safely assume that experimental conditions were similar to the previous campaigns (June 2016, cross and bidirectional flow). Synchronization between tablets, smartphones and camera was performed using the method described in Chapter 3.3.1 (the external monitor from the PC is visible on the left side of Figure 3.21(a)).

Results and discussion

Analysis of the results has been performed following the same methods presented for the June 2016 experiment presented earlier, although here we set a particular attention in

(a) Low density (C3)   (b) Medium density (C6)   (c) High density (C9)
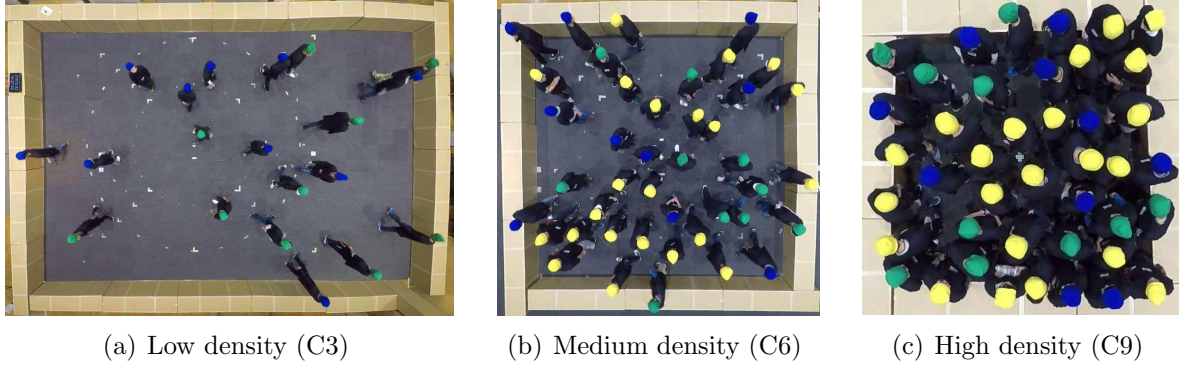
Figure 3.21: Example of frames taken during the chaotic motion experiment of October 2016. Scale of each image is different as it can be guessed from the relative size of each cap.

understanding the influence of the electronic device used on the results. Also in this case, results were only analyzed under stable conditions, i.e. from few moments after the starting signal and few moments before the experiments were stopped. No significant trends were observed for the average velocity during each execution. Densities were individually computed using Voronoi cells although the experimental design used here allow to simply obtain density by dividing number of people and surface.

To start with, the fundamental diagram is considered along with the density – congestion level relationship [10] as given in Figure 3.22.

(a) Density–flow relationship   (b) Density–congestion level relationship
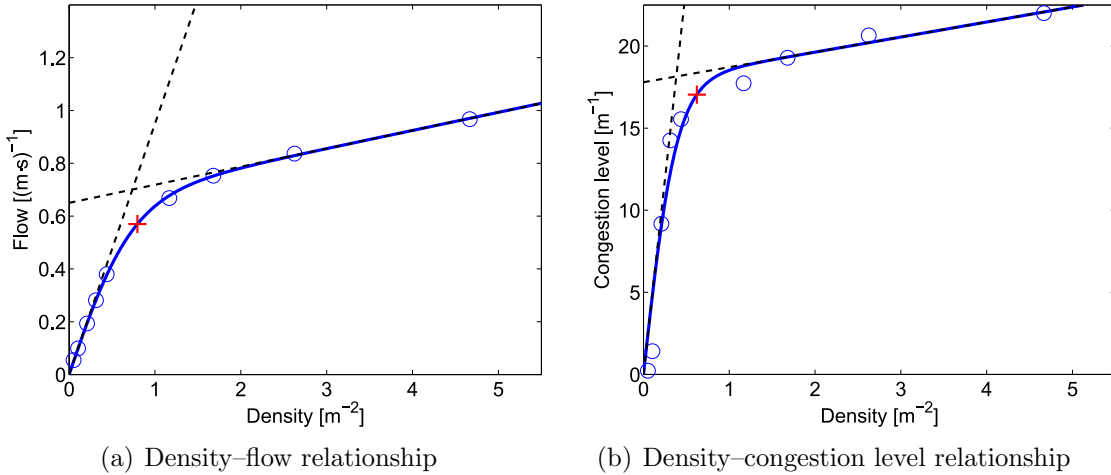
Figure 3.22: Density relationships for flow and congestion level [158]. Equation (3.2) is used for fitting, red cross is the "transition point".

Like in the previous case, we found that equation (3.2) fits well with both datasets, with the flow showing a particularly high coefficient of determination. However, the point of transition determined using the "classical" form of the fundamental diagram results in a flow of 0.572 $(\mathrm{m}\cdot\mathrm{s})^{-1}$ which is quite different from the values found for the June 2016 experiment. On the other side, the transition point in terms of congestion level is in line with the previous values showing that this may be a universal value for pedestrian crowds.

---

[10]Maximum–minimum difference of the rotational from the velocity vector field was taken over the whole room surface. Time interval was chosen between 3 and 4 s, resulting in a used time interval of 3.41 ± 0.02 s.

The different values found for ρ_{trans} (transition densities) compared to the previous case may show that changes in pedestrian crowds are not universal in terms of density, since composition, surrounding environment and geometry could have an influence on critical levels of density.

Table 3.15: Fitting parameters for the graphs provided in Figure 3.22 [158]. Units for the fitting parameters have been omitted for simplification and they depend on the quantity considered. R^2 is the coefficient of determination.

Quantity	Fitting parameters			R^2	Transition point	
	a_0	a_1	a_2		Density	Quantity
Flow	0.650	2.712	0.069	0.999	0.795 m^{-2}	0.570 (m·s)$^{-1}$
Congestion level	17.795	5.226	0.915	0.943	0.622 m^{-2}	17.040 m^{-1}

Having confirmed that results derived from trajectories are analogous to the previous experimental campaign, we can continue the analysis of the results by considering the inertial sensors and the different devices used. Figure 3.23 presents the relationship between (magnitude of) linear acceleration and typical crowd quantities. Graphs are divided into three groups constituting the different types of devices used: tablets only, smartphones only and all devices without distinction. As for the previous case, a linear function was found fitting well data for velocity and a power function the ones for density (fitting parameters and goodness is given in Table 3.16).

(a) Linear acceleration – speed
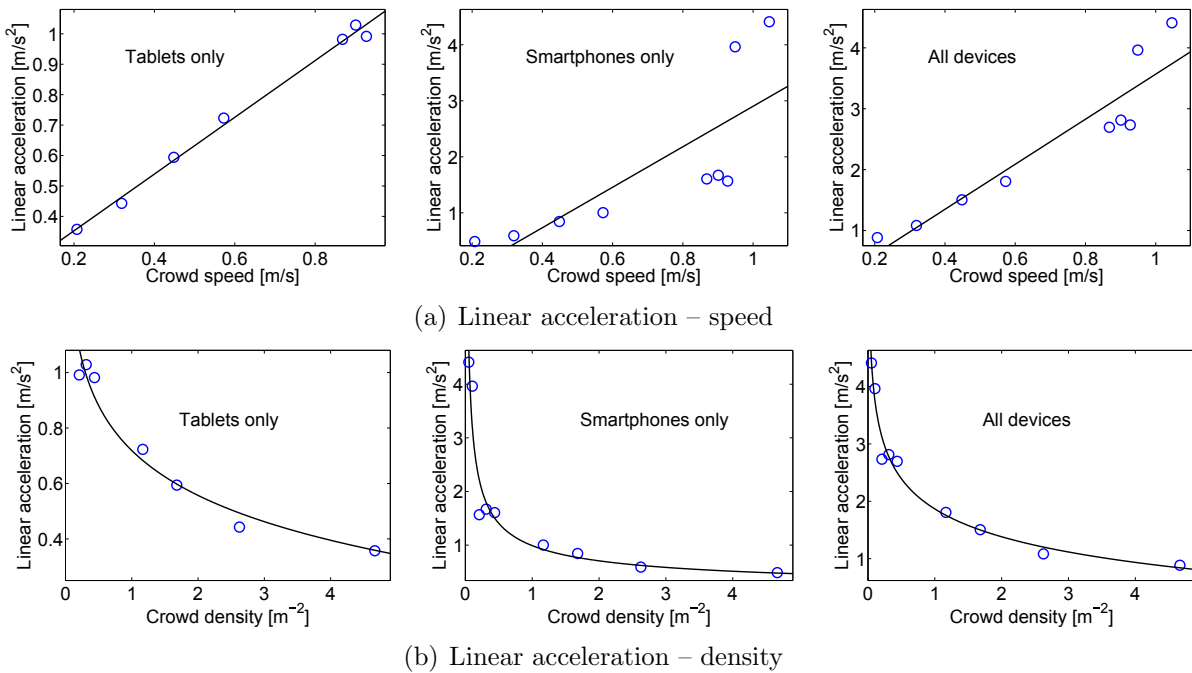

(b) Linear acceleration – density

Figure 3.23: Relationship between crowd quantities measured using computer vision and inertial measurements from portable devices [157] (magnitude is used here). Fitting functions and parameters are given in Table 3.16. The "tablets only" case has less density points available since C1 and C2 configurations only had smartphone participants.

Different observations need to be done here concerning the results reported in Figure 3.23 and Table 3.16.

First of all it was confirmed that the gyroscope cannot provide accurate information since results are dependent on the geometry being tested and the specific position where the device is kept. In Table 3.16 the R^2-value obtained by fitting the given function with magnitude of angular velocity is given in bracket. In all the cases a better fitting is used by using the linear acceleration. More importantly it is seen that when only tablets are considered, which all had the same orientation and position, the worst R^2-values are found for the gyroscope. This is connected to the fact that geometry was changed several times during this experiment and the position of the tablets is very sensitive to this changes. Results get better when smartphones are considered since orientation and position are more randomly distributed among the crowd. To conclude, linear acceleration was confirmed being more accurate and therefore only values relative to the linear acceleration are given for the fitting parameters in Table 3.16 and the graphs in Figure 3.23.

Table 3.16: Fitting parameters for the graphs provided in Figure 3.23 [157]. s refers to the (magnitude) of linear acceleration, x to the crowd measure. Units are omitted in the fitting parameters for convenience. R^2 is the coefficient of determination. Values in bracket are relative to the fitting performed using the angular velocity (whose graphs are not provided here).

Measure (x)	Used devices	Fitting function $s = f(x)$	Fitting parameters			R^2
			b_0	b_1	b_2	
Speed	Tablet		0.933	0.166	–	0.993 (0.500)
	Smartphones	$s = b_0 x + b_1$	3.612	-0.710	–	0.615 (0.584)
	All devices		3.698	-0.131	–	0.875 (0.695)
Density	Tablet		195.6	-0.001	-194.9	0.958 (0.465)
	Smartphones	$s = a_0 x^{b_1} + b_2$	0.896	-0.549	0.095	0.933 (0.928)
	All devices		6.164	-0.118	-4.297	0.979 (0.946)

Concerning the type of device used and the location where is kept, we confirmed that indeed there is an influence on the results. Both speed and density fits well when only tablets are considered, since position and orientation are the same for all devices and hardware/software is also the same (or with very minor differences). When only smartphones are considered, measuring walking speed based on body motion becomes difficult and only a general trend is recognizable to distinguish "fast" or "slow" walking. It should be remarked that, as it was shown in Figure 3.17, walking speed – body motion relationship changes from person to person and the different storing position used by smartphone users can make the difference larger. If walking speed would be evaluated on an individual basis we expect better results, but this may be difficult in a real applications. Also, in this configuration we could not distinguish each individual position to check this hypothesis. However, the power function used for density allows to make a better prediction also when the whole crowd is considered. Although numerical values may not be accurate, distinguish between low and high densities seems possible also for a heterogeneous case like the one considered here with participants using different models of smartphones in different conditions. With this said, it should be remarked that differences in linear acceleration values were particularly large for the case with smartphones and therefore only data gained from real observation could confirm if such an approach is suitable for estimating density in pedestrian crowds.

Finally, we can consider the congestion level – linear acceleration relationship which was
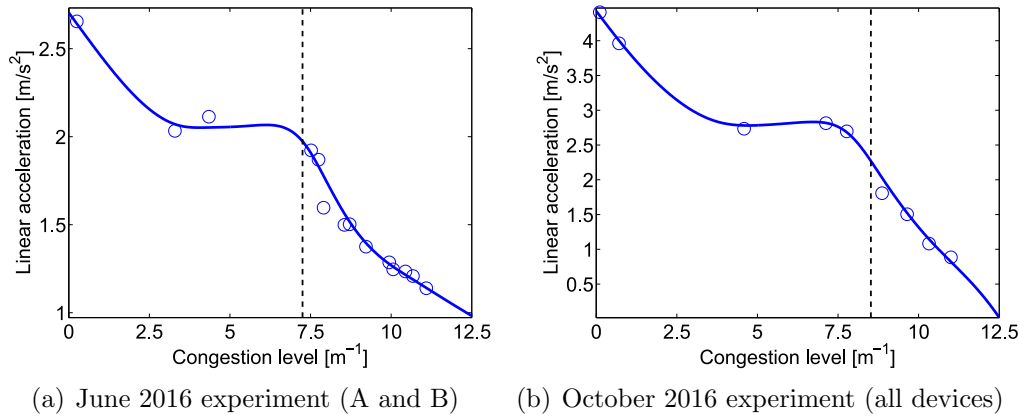
(a) June 2016 experiment (A and B)   (b) October 2016 experiment (all devices)

Figure 3.24: Relationship between the congestion level and the linear acceleration measured on participants. Dotted vertical lines represents the "transition point". Fitting function has been modeled based on the data available and alternative interpretations are possible.

already investigated in the previous case. Results are presented in Figure 3.24, where for comparison the results from the June 2016 experiment are combined in the same graph. In producing the graph for the experiments of October 2016 presented here, all devices were used, but we found that the same qualitative behavior was observed when the different devices were considered separately. Both cases show that some sort of change occurs around the transition point. The number of points available in the latest experiment show that possibly the behavior previously guessed had some validity. In any case, the number of points considered here is still insufficient to come to final conclusions and this behavior require further research. If confirmed, the state occurring before the transition point could translate into some change in the way the crowd behave, possibly failing in forming semi-organized structure to reduce the level of congestion.

Nonetheless, the importance in this result lies in the fact that this behavior could be used to define an acceleration which translates into a transition to congestion. In the cases presented here two different values are observed (around 10 m^{-1} for the experiment of June 2016 and about 15 m^{-1} for the one of October) because of differences in devices used and their position, but with a sufficient large and uniform crowd it could be possible to define more universal values for the transition to congestion in terms of body motion. Such an analysis would not be possible using flow and density, since a continuous power law function was observed (thus making the definition of a threshold not univocal).

However, as already mentioned, there are several factors which can have an influence on these results including technical and cognitive ones (as observed for the bidirectional case earlier). For this reason, the changes occurring in multidimensional pedestrian flows, including the particular shape of the fundamental diagram, can be a topic for future research. The latter aspect will be discussed more in detail in the following section.

3.5.3   Comparison with uni- and bidirectional flow

We want to conclude this discussion on the chaotic crowd experiments by considering the fundamental diagram for pedestrian traffic again and see how it changes when configurations are varied. We will also discuss the validity of the function presented earlier to model the multidimensional fundamental diagram.

To start with, we con consider the fundamental diagrams for the three cases considered up to here: the unidirectional, bidirectional and multidirectional flow (the chaotic scenario). Although different categorizations are possible, we will use this three-stage subdivision to determine the complexity of pedestrian motion. For each type of motion the fundamental diagram for flow and speed is given in Figure 3.25. Data for the unidirectional flow are a combination of the ones provided by Zhang et al. and the ones generated from our experiments. Data from the bidirectional flow are all from Zhang et al. (in our experiments densities were too low and changes in speed minimal), while multidirectional fundamental diagram has been generated using the data from our chaotic experiments (we preferred a dispersed representation here to allow an easy comparison, however it is seen that dots tend to accumulate around specific densities).

As the right side of Figure 3.25 shows, the shape of the density–flow fundamental diagram largely changes depending on the situation considered. In the unidirectional case, a form similar to the one obtained in the theoretical derivation is observed and a qualitative similar shape is seen in the bidirectional case. However, when a complete bidimensional case is considered with multiple directions (the chaotic case of Figure 3.25(c)), then the shape completely changes (as already mentioned earlier). If the density–speed case is considered, the differences appear smaller, but a look on the free walking speed at zero density, should warn that in fact different scenarios are being described.

As presented in the introduction, the equation by Weidmann has been often used to model pedestrian traffic. In the representation for flow, it can be written as:

$$q(\rho) = v_{free} \cdot \rho \left[1 - \exp\left(-k \cdot \left(\frac{1}{\rho} - \frac{1}{\rho_{max}} \right) \right) \right] \tag{3.3}$$

where v_{free} is the free walking velocity, ρ_{max} the maximum density (or the jam density) and k a parameter determining the shape. In addition, also the equation proposed to model the results of the chaotic flow may be used and it takes the form:

$$q(\rho) = \frac{2a_0}{1 + \exp(-a_1\rho)} + a_2\rho - a_0 \tag{3.4}$$

where a_0, a_1 and a_2 are simple parameters which are not directly related to physical quantities. However, with some calculations it is possible to obtain the free walking velocity, which is given by:

$$v_{free} = \frac{1}{2}a_0 \cdot a_1 + a_2 \tag{3.5}$$

The expression for the maximum density can be only obtained implicitly by numerically solving the equation $q(\rho_{max}) = 0$. For both the Weidmann equation and the form proposed in this study, the functions for velocity are simply obtained by dividing by the density (3.3) and (3.4) following the fundamental relation.

As qualitatively seen in Figure 3.25 and numerically provided in Table 3.17, both functions fits well with the experimental data for the three cases (R^2 values are very similar in all cases). To compare some properties of both functions the most important physical quantities relating to each representation have been computed. Free walking velocity (obtained at zero density in the fundamental diagram for speed) is very close between both functions in the bidirectional and multidirectional case and is probably overestimated by using the function proposed here in the unidirectional case (usually walking speed never exceeds 1.5–1.6 m/s except under special conditions). When maximum density

(a) Unidirectional flow [98]

(b) Bidirectional flow [98]
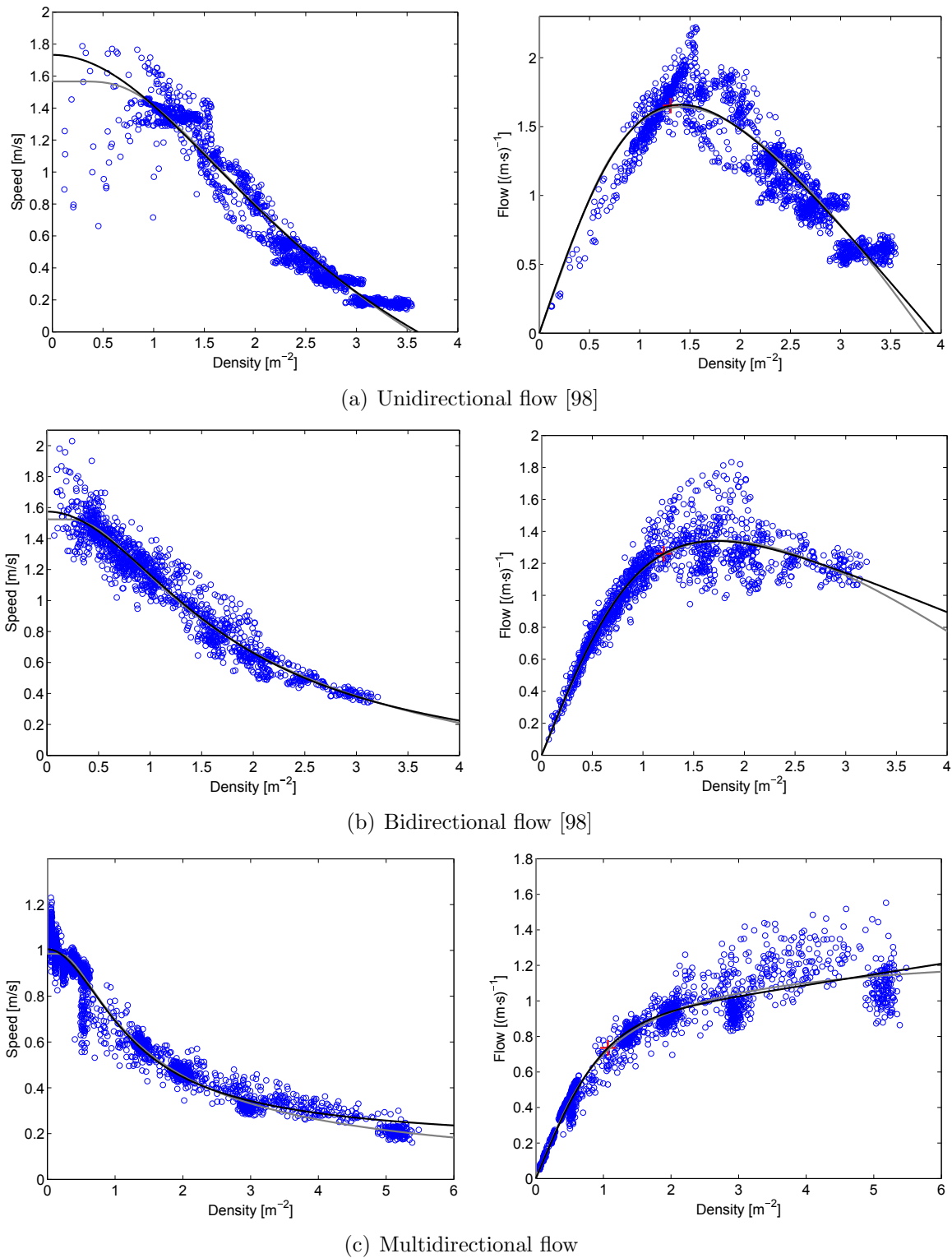

(c) Multidirectional flow

Figure 3.25: Comparison between fundamental diagrams for different types of flow. The Weidmann equation is given in gray, the one proposed in this study in black (relevant values for both are given in Table 3.17). Data from [98] were used in some of the plots (bidirectional and high density unidirectional). The red cross represents the "transition point".

is concerned, the function proposed here seems to yield more plausible values, since we observed densities in excess of 6 m^{-2} during our observation of the bidirectional flow and the maximum density obtained using the equation by Weidmann seems to be relatively low. Quite surprising (although clearly seen in the shape of the graph in Figure 3.25(c)) is the fact that incredibly high densities are predicted in the maximum of the multidirectional case (by using our equation an infinite density is obtained since the function never crosses the abscissa).

Table 3.17: Free walking speed, maximum density and R^2 value for the graph shown in Figure 3.25 [158]. v_{free} is obtained by fitting the speed-density fundamental diagram, ρ_{max} using the expression for flow.

| Function | Flow | Function properties and fitting | | | |
| | | Speed–density | | Flow–density | |
		v_{free}	R^2	ρ_{max}	R^2
This work	Unidirectional	1.733 m/s	0.934	3.929 m^{-2}	0.854
	Bidirectional	1.574 m/s	0.927	7.505 m^{-2}	0.871
	Multidirectional	1.005 m/s	0.959	Infinity	0.959
Weidmann	Unidirectional	1.567 m/s	0.940	3.830 m^{-2}	0.842
	Bidirectional	1.524 m/s	0.924	5.788 m^{-2}	0.869
	Multidirectional	0.985 m/s	0.956	5665.99 m^{-2}	0.962

Although clearly there must be a density at which the flow becomes zero, experimental evidence presented so far also showed that this density is probably much higher than originally predicted.

Figure 3.26(a) shows two fundamental diagrams gained during observations of the Hajj pilgrimage. Helbing at al. [16] analyzed the crowd in a large area in front of the entrance of the Jamarat bridge before and during a deadly accident. Dalmbalmath [36] focused on the circular motion around the Kabaa (without accidents). In both cases, the flow never reached zero even at very high densities. Contrary to what expected, Dambalmath et al. actually noticed that the flow increased at densities above around 5 m^{-2}. Both authors seem to agree that around 5 m^{-2} a sort of transition occurred, although the type of transition may be different in both cases. Helbing et al. actually observed the formation of stop-and-go waves in the densities included between 5.62 and 6.96 m^{-2} [49].

Figure 3.26(a) also provides the data from our chaotic experiment (the compact form summarizing each execution as a single dot has been preferred here) showing that the three datasets have very close similarities for densities below 5 m^{-2}. It can be also seen that our equation fits well with all the cases depicting the (first) transition which has been studied earlier. The equation by Weidmann is also able to describe low and medium densities, but its form does not allow to clearly define the transition appearing when the slope changes around 1–2 m^{-2} (the equation by Weidmann does not present asymptotes). In addition, the shape of both datasets by Helbing et al. and Dambalmath et al. shows that possibly the transitions occurring at high densities can be described with the approach presented here, by defining a stepwise function composed by several asymptotes. It could be possible that, the higher the level of complexity the more transitions are possible. In the unidirectional case, transition from free flow to congestion is observed and for the bidirectional flow we also included organized lanes. However, as the motion becomes complex, more flow regimes could be observed, with transitions depending on the degree

(a) High densities fundamental diagrams

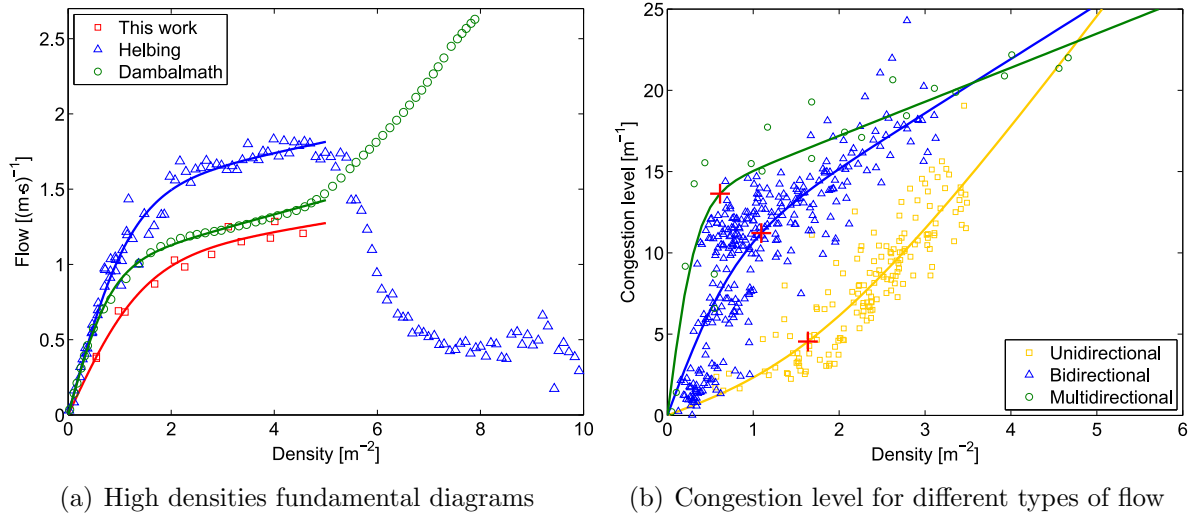(b) Congestion level for different types of flow

Figure 3.26: Comparison between different multidimensional fundamental diagrams [16, 36, 158] (data from Helbing et al. are combined with those from Older [26] at low densities). Fitting function is given in (3.2).

of organization (as discussed in the introduction there are different definitions for flow regimes with Alonso et al. [117] also including avalanches and clogging).

But we will now focus on the first transition, which is the only one for which we possess enough experimental evidence. We will therefore study more in detail the first transition also considering the uni- and bidirectional case. With the same approach described earlier and using the equation presented here it is possible to describe the "transition point" in terms of density and flow. As shown in Figure 3.25 with a red cross, the transition in the unidirectional flow occurs at $\rho_{trans} = 1.308$ m^{-2} and $q_{trans} = 1.652$ (m·s)$^{-1}$. For the bidirectional flow the transition is given by $\rho_{trans} = 1.205$ m^{-2} and $q_{trans} = 1.260$ (m·s)$^{-1}$, while in the multidirectional case (using our dataset) we have $\rho_{trans} = 1.067$ m^{-2} and $q_{trans} = 0.736$ (m·s)$^{-1}$. In other words, when the degree of complexity is increased the transition (as defined using the asymptotes) occurs at lower densities and lower flow. This clearly shows that the transition described in terms of the "classical" fundamental diagram (using density and flow) is not universal. Although there may be alternative approaches to define the transition (our system of using the asymptote is just one), the shapes of the fundamental diagrams given in Figure 3.25 indicate that probably the method used to measure pedestrian crows by flow and density could depend on the scenario considered.

In Figure 3.26(b) the same approach presented earlier (finding the intersection between the midline of the asymptotes and the fitting function) is used on data for the congestion level, but results are even worst than the standard fundamental diagram and transition point largely change when dimensionality is varied. One reason for this large difference could be the high dispersion of dots, not allowing to fit the equation with sufficient accuracy. This aspect was already remarked while examining the data for the chaotic experiment. While we found that the transition in terms of the congestion level was similar among the three cases, they could not be considered altogether. Defining a universal value for the congestion level related to a change in pedestrian motion may be possible, but these results shows that each set of experiments need to be considered separately to allow an accurate determination of this value. This aspect could be a topic for future research.

3.5.4   Summary

In the experiments described in this section the methods and techniques introduced earlier have been taken one step further by considering a type of pedestrian motion without any organized structure. The fundamental diagram obtained for this scenario had a quite different shape from the ones usually observed for the flows considered so far and a specific function was proposed to describe its behavior. We later found that the function proposed here can be used to model also uni- and bidirectional motion and its properties allows to define a transition point.

In the two cases considered here (three if configurations A and B of June 2016 are considered separately), a transition was observed around a congestion level of 15 m^{-1}. The same transition measured in terms of flow seemed to be more dependent on the scenario/geometry considered. We also noticed that shortly before this transition some shift occurred in the way pedestrians behave by changing the motion of their body. However, changes were not large and, considering the different uncertainties related to the analysis, this hypothesis need to be checked by further research. Investigating the reasons leading to this transition could be also a topic for future research.

We found that commercial devices containing inertial sensors can be used to grasp collective properties of the crowd. We found, however, that movements measured from the gyroscope tend to be related with the specific environment and a comparative analysis using this measurement is possible only under the same environment. On the other side, the linear acceleration (beside being inaccurate from a physical perspective) can be successfully used to estimate velocity and under particular conditions also density can be estimated (since they are both related).

From a technical perspective we found that equipment (tablet or smartphone in this study) used and position where it is kept from pedestrians can have an influence on the results, but this influence may become minimal when a sufficiently large number of devices is considered. Our results show that with 10 people it is already possible to distinguish scenarios in terms of low and high speed, although individual differences would need to be accounted to perform precise measurements.

Finally, we compared the results for this multidirectional analysis with those for the uni- and bidirectional flow considered earlier and concluded that the fundamental diagram does not allow a universal determination of relevant transitions (between different flow regimes). Possibly, also here cognitive aspects may play an important role in changing the form of organization within the crowd and determine the numerical outcome represented in the shape of the fundamental diagram. While the congestion level introduced here may help in moving toward a more universal definition, we also showed that its relative high level of noise could limit its applicability to real scenarios.

3.6   Transient scenarios

In all the situations considered so far we investigated steady state scenarios or cases in which pedestrians were uniformly distributed inside the experimental area. While in the bidirectional case of Chapter 2 a transient mechanism was considered in which lanes form and dissolve, the type of analysis performed in that context aimed at defining equivalent phases among several repetitions, thus limiting the analysis to few dots plotted in a single graph (the rotation range – phase diagram for instance). Also in the cross flow scenario, results were reduced to single data points and the very short experimental time did not

allow to analyze the changes occurring in detail.

To overcome the above limitations and study changes of the quantities presented in this work in space and time, we designed two experiments in which pedestrians properties change over space and time. We will present the results of those experiments in this section. Note that both experiments presented here were performed after the chaotic flow experiment of October 2016, so for details on participants and environmental conditions readers are referred to Chapter 3.5.2.

3.6.1   Evacuation through single door (bottleneck)

Experimental design

In all the analyses performed so far a single congestion level was taken to represent the whole situation observed in the experimental area. In the previous contexts, such an approach was valid since differences in space were minimal and irrelevant. Here, we want to check the accuracy of the congestion level in detecting congestion in an heterogeneous scenario while also testing the estimation of velocity based on inertial sensors. For this purpose, we designed an experiment in which congestion and walking velocities changes with a predictable pattern. A bottleneck experiment reproducing an evacuation from a single exit was judged as the most appropriate.

Using the same technical equipment employed for the chaotic flow experiment of October 2016 a room 7 m in side and 4 m in width was set up. An exit 80 cm in width was placed in the middle of the longest edge. The camera was placed right above the exit, thus allowing to track exiting pedestrians with the highest accuracy (distortion is minimal around the center). Images of the room occupied by participants are given in Figure 3.27.
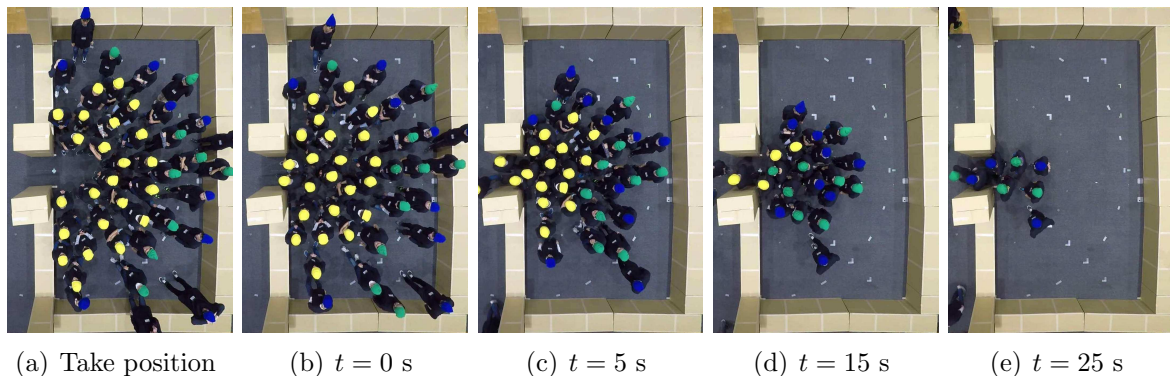

| (a) Take position | (b) $t = 0$ s | (c) $t = 5$ s | (d) $t = 15$ s | (e) $t = 25$ s |

Figure 3.27: Frames taken from the bottleneck experiment at medium density (43 participants). "Take position" refers to the initial positions taken from participants before the start signal was given. Time $t = 0$ is set when the first participant crosses the exit position. Participants with blue and green caps were equipped with inertial sensors.

Participants were asked to enter the room and place themselves concentrically around the exit. In most of the cases we tried to have pedestrians not equipped with sensors taking the positions closer to the exit, but in many cases those demands were not followed by participants (frames from Figure 3.27 show a scenario in which participants followed the orders accurately). No particular instructions were given on how close to position or what side to take, but we simply asked them to dispose in a uniform way.

After the "start" order was given, pedestrians started exiting the room and moved away from the exit on the left and right direction to avoid forming an obstructing crowd near the

exit (the whole experimental area was big enough to avoid an accumulation of participants in front or near the exit). Participants were asked not to rush and walk at normal speed (on the other side, we also asked them to avoid taking too long before leaving and simply move toward the exit). Figure 3.28 shows an example for trajectories gained during the experiment for two different configurations; it is clearly seen that velocities increase after exiting the room. The frames provided in Figure 3.27 should also help gaining an idea on the execution of the experiment.

(a) 25 participants, run 1   (b) 43 participants, run 5
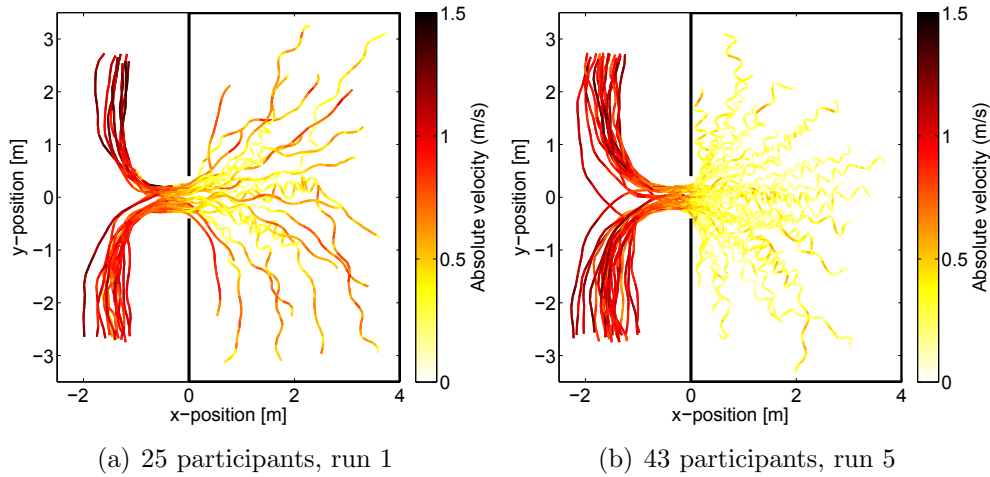
Figure 3.28: Trajectories for the evacuation experiment under low and medium density conditions. Color gradation indicates absolute walking speed. Velocity clearly grows after leaving the room.

Two different configurations were tested using the same geometry and giving the same orders but changing the number of pedestrians occupying the room before the evacuation. In the first configuration 25 participants took part to the experiment and it was repeated 3 times. Considering the 3 repetitions, evacuation time (i.e. the time passing from the first and the last person going through the exit) was 18.53 ± 0.47 s. In the first configuration all the participants equipped with inertial sensors took part (i.e. 20 people in total).

Table 3.18: Details concerning the configurations used in the bottleneck experiment [157, 158]. Density was not uniform and figures are given for reference. Evacuation time is the time passing between the first participant going through the exit door and last one leaving the room, deviation is taken among the several runs. Numbers in bracket refer to tablet participants, smartphones and the ones not equipped with sensors.

Configuration	Participants	Initial density	Runs	Evacuation time
Low density	25 (10 + 10 + 5)	≈ 0.9 m^{-2}	3	18.53 ± 0.47 s
Medium density	43 (10 + 10 + 23)	≈ 1.5 m^{-2}	5	29.95 ± 0.82 s

Later, all participants were asked to take part to the experiment, thus bringing the number of pedestrians to 43 [11]. Also in this second configuration, which was repeated 5 times, all the participants equipped with inertial sensors took part. Evacuation time for this configuration has been about 60% higher than the low density scenario, with the number of participants being more than 70% higher (i.e. a somehow more efficient evacuation).

---

[11]One participants arrived late and did not took part to the chaotic flow experiments.

Results

In the previous derivations, the congestion level was computed over a large surface and only a single value was obtained. To allow getting a map of the congestion level changing over the room considered in the bottleneck experiment, the algorithm described in Figure 3.29 have been applied on the trajectories from participants. Each repetition has been divided in time intervals ranging from 2 to 3 s. Average velocities have been taken during each time interval constituting the velocity vector field used to compute the rotational (also here mesh size has been of 0.2 m), which has been computed in all possible locations (borders and locations with not enough velocity vectors are skipped). A central part in the calculation of the congestion level is given by the difference between the smallest and the largest value for rotation, which was usually taken over the whole surface. Here a Region of Interest (ROI) is used to get the local rotation range and the local average velocity (magnitude). Using those two values the local congestion level for the specific ROI is computed. Later, the ROI is moved by one cell and the local calculation is repeated. The congestion level map is obtained by moving the ROI over the whole surface. Here a ROI of 5 × 5 cells is used (i.e. 1 m × 1 m). Selection of ROI size is important but reasonable values are related with human size and therefore the selection range is limited.

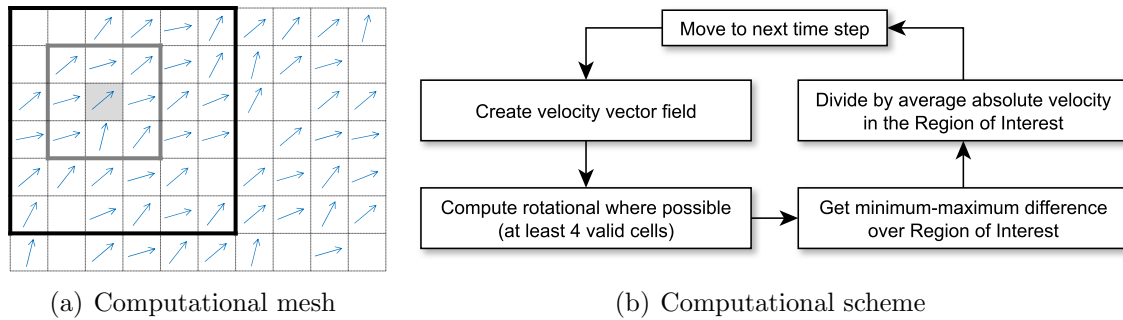(a) Computational mesh   (b) Computational scheme

Figure 3.29: Calculation process to obtain the congestion level map over a given surface [158]. In the example provided here a ROI of 6 × 6 cells is used. In (a) cells in the gray region are used to compute the rotational, black region is the ROI.

By using the algorithm described in Figure 3.29 a congestion level map has been computed for each time interval in each of the repetitions considered in both configurations. Results were first averaged over the different time intervals to get a single result for one execution and later all repetitions were averaged to get a single result for each configuration. The same procedure was also performed for density and velocity to compare the several maps. Flow was obtained by multiplying speed and density in each cell.

Results for the configuration with 25 participants are given in Figure 3.30. Clearly the highest density is found close to the exit, which also constitutes the location with the highest flow. By moving away from the exit, decreasing values for density and flow are observed. The congestion level map generally provides the same results, although the region of highest congestion seems to be translated a small distance from the exit into the room. However, the result for the congestion level seems to be quite noisy and the limited number of participants allowed a calculation only over a small area close to the exit. This is related to the fact that to compute the rotational 4 cells filled with velocity vectors are required and were present only close to the exit where the density is higher. Also, in the first configuration only 3 repetitions were performed, thus creating relatively large differences between each case.

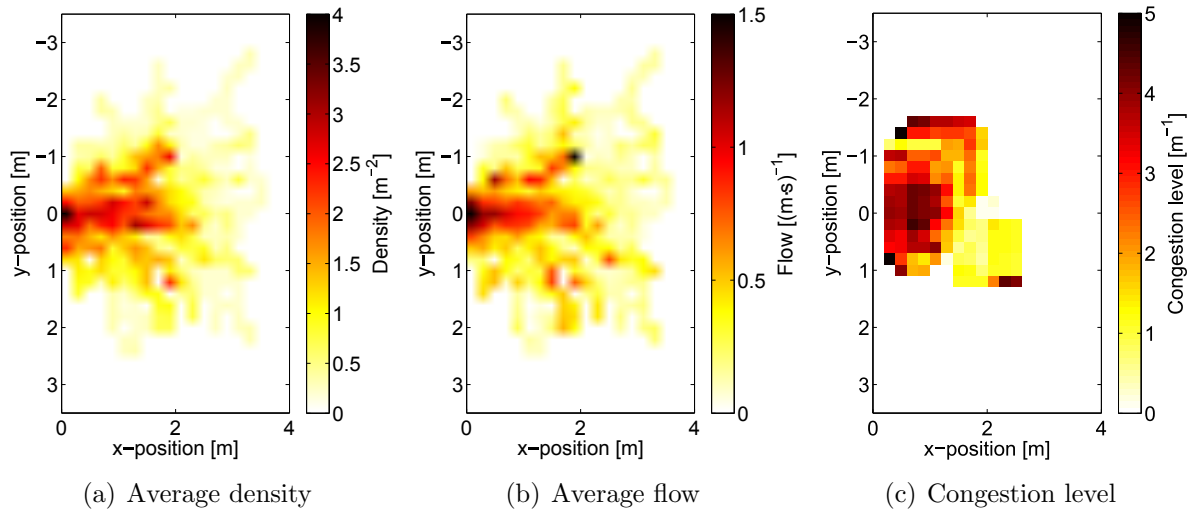(a) Average density   (b) Average flow   (c) Congestion level

Figure 3.30: Floor maps indicating the value of different quantities inside the room for the bottleneck experiment with 25 participants [158]. Maps are averaged over the different time intervals and for the 3 repetitions.

The different maps for the case with 43 participants are given in Figure 3.31. Results are conceptually similar to the previous case, but the map for the congestion level is now more smooth and it appears clear that the highest congestion is found about 80–90 cm in front of the exit. Also the results for density and flow are now more clear and differences between the representation using density and flow appear. A peak of density is found right in the location of the exit, but quite high densities are also found in a region about 1–2 m from the exit. On the other side, change in flow is more steep by approaching the exit location and the high-flow region is more clearly outlined.
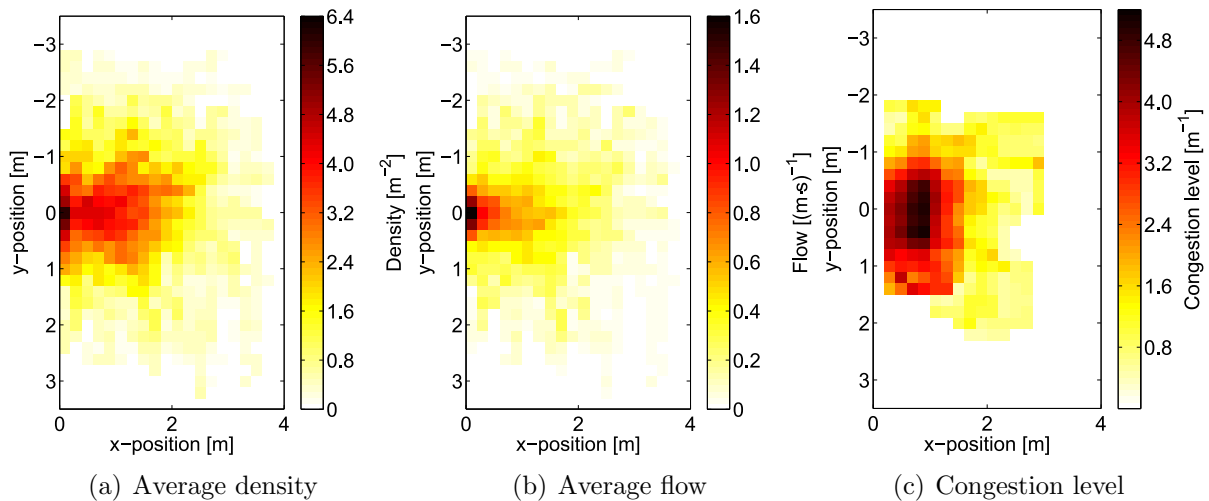

(a) Average density   (b) Average flow   (c) Congestion level

Figure 3.31: Floor maps indicating the value of different quantities inside the room for the bottleneck experiment with 43 participants [158]. Maps are averaged over the different time interval and for the 5 repetitions.

The location for the maximum congestion seem to be in line with conclusions from previous studies which found that by placing an obstacle shortly before the exit, evacuation can be accelerated. In particular, Yanagisawa et al. [159] used a door having 50 cm in

width and found the the obstacle was effective 65 away from the exit (i.e. roughly the size of the door). In our study we found that for a door 80 cm in width the maximum congestion is roughly at the same distance toward the center of the room. This may suggest that by suppressing the peak for congestion a more smooth distribution is found, but further research is required to check this hypothesis.

Nonetheless, the results presented here show that the congestion level can provide relevant information also when used in spatial configuration like the maps provided above. However, it seems to be quite inaccurate for low densities when only few trajectories are available. While the goal is to consider dangerous, high density crowds, more improvements are required to guarantee stability. Considering the results obtained by using the congestion level in the bottleneck experiments, a possible application could be in determining design flaws in existing infrastructures, thus increasing the safety and comfort in regard to pedestrian traffic.

Finally, we want to consider the data gained from the inertial sensors during the evacuations tested here. Results for velocities estimated during two executions belonging to each configuration are given in Figure 3.32.

(a) 25 participants, run 2   (b) 43 participants, run 3
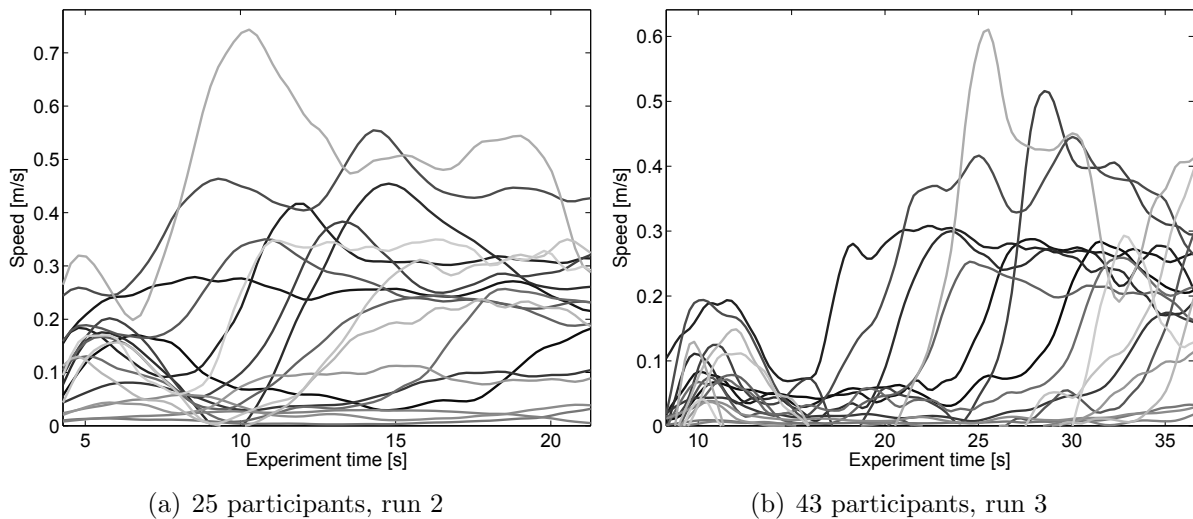
Figure 3.32: Speed during evacuation estimated using information from the inertial sensors [157]. Each line correspond to a different participant. Reference time $t_0 = 0$ is set when the first participant left the room.

To compute the velocity the following steps has been performed. For each device a calibration has been performed using the chaotic experiment described in Chapter 3.5.2. Average values for the linear acceleration (magnitude) were compute for each experiment from C1 to C9 (see Table 3.13) and they were fitted against crowd velocity using a linear function (as discussed earlier). Since individual combination of trajectory and inertial data was not possible here, we assumed that each pedestrian walked at the same velocity during each configuration of the chaotic experiment. Although we know that this assumption is not totally correct, we wanted to test a hypothetical scenario in which only aggregated data are available for calibration.

After obtaining individual parameters for the (participant) linear acceleration – (crowd) walking speed relationship, we used those parameters to determine the velocity of the same individuals equipped with sensors during the bottleneck experiment [12]. From the

---

[12]Participants wearing tablets and smartphones were not changed after the chaotic flow experiment.

results in Figure 3.32 it is seen that, generally, the behavior expected in case of evacuation is reproduced. In Figure 3.32(b) a minimum velocity is found at around 15–20 s, which is possibly in line with the time during which most of the participants equipped with sensors passed through the exit (the case represented in Figure 3.32(b) had a similar initial configuration to Figure 3.27). In this sense, we confirmed that strong differences in crowd conditions can be detected using sensors, but we also found that estimated values for velocities are not reliable without a proper calibration. In fact, negative velocities were often obtained (theoretically impossible since estimated velocity is the absolute value) and the maximum velocity is too low compared with values gained from the camera (around 1.5 m/s when participants left the room). These results possibly confirm that to obtain reliable results, a moderate number of people equipped with inertial sensors is required.

3.6.2   Periodic bidirectional flow (circular flow)

Experimental design

In the bottleneck experiment we have been able to assess the possibility to use the congestion level to analyze a heterogeneous space. Here, we want to focus on changes of the congestion level over time. To do so, an experiment has been designed to allow the creation of organized structures over time and assess the differences between different configurations using the congestion level. After the end of the bottleneck experiment, a circular course has been created by having the camera focusing at the center (examples of frames from the experiment are given in Figure 3.34 and Figure 3.35). Internal radius was of 2 m and external radius of 3.5 m. Total surface was 25.9 m^2 and average one-turn distance about 17 m (taking the midline). The 1.5 m width of the course allowed the formation of 2–3 lanes at maximum. In this set of experiments, participants were divided in two groups: the ones turning clockwise and the ones turning counterclockwise (sense of rotation assigned to each group is given in Table 3.20). In the first configuration, 24 participants (group A) were asked to stay in the room and the remaining ones (group B) were asked to leave it and doors were closed. After closing the doors instructions were given only to group A (group B staying outside could not listen). Half of the participants from group A were asked to walk clockwise and the remaining half in the opposite direction. Participants wearing inertial sensors were equally split [13]. After the "start" signal was given, participants started walking in their respective directions. The configuration with group A was tested 2 times

After the second repetition, group B was allowed into the room and instructions were given to them. Since the number of students showing up for the experiment was much less than the ones who applied, we had to include also some of the participants from group A into group B. For this reason some of the participants of group B had already performed the experiment twice. The second configuration with group B was also tested 2 times with half of the people turning clockwise and the other half turning counterclockwise. Also for group B the number of participants having sensors was equally spitted for each turning direction. In addition, we should mention that group A was composed by smartphone participants only and group B by tablet ones (whose members had changed from the previous chaotic experiment). Turning direction was changed after every repetition as shown in Table 3.20.

---

[13]Participants wearing tablets were changed for this experimental campaign, smartphone participants were the same as for the previous experiments.

Table 3.19: Details on the different configurations tested during the circle experiment [158]. For the first configuration about half of the participants left the room and the experiment was conducted at closed doors (so that participants outside could not see the execution of the experiment). Later, roles were changed by having participants outside coming in to perform the same experiment (because of the low total number 5 of them took part to both groups' executions). Experimental surface was 25.9 m².

Configuration	People	Runs	Comment
Normal walking	24	2	Group A (people in excess left the room)
		2	Group B (with few participants of group A)
Normal walking		2	All participants (group A and B)
Distracted walking	43	3	Walking while solving a written problem
Changing conditions		1	Direction of rotation changed several times

Next, all participants were asked to enter the course and the procedure having all participants was also repeated 2 times. In this case, the number of people turning in each side was not equally split with the values being at 22 for one direction and 21 for the opposite one (participants equipped with sensors were also split in half here). For all the configurations described so far participants were simply asked to walk after the start signal, without any specific order. In all the configurations, yellow and red caps were assigned to each group to allow a quick analysis of the situation by looking at the video recordings.

Table 3.20: Sense of rotation for the various experimental setups and executions [158]. Values in brackets are the number of participants. During run 1 and partially run 2 of the distracted walking procedure a single yellow participant mistakenly walked with the red group (this did not have an influence on the results). Group taking the inner part of the path is given in bold (in run 2 of group A stable lanes did not form)

Configuration	Repetition	Sense of rotation	
		Clockwise	Counterclockwise
Normal walking – Group A	1	**Yellow (12)**	Red (12)
	2	Red (12)	Yellow (12)
Normal walking – Group B	1	**Yellow (12)**	Red (12)
	2	**Red (12)**	Yellow (12)
Normal walking – All	1	Yellow (22)	**Red (21)**
	2	Red (21)	**Yellow (22)**
Distracted walking	1	**Yellow (21)**	Red (22)
	2	Red (21)	**Yellow (22)**
	3	Yellow (22)	**Red (21)**

To make formation of lanes more difficult, we later gave to participants a written problem on a paper and we asked them to solve it while walking. More specifically they had to find some particulars in an image including many elements. Most of the participants were seen being focused on the problem, paying little attention to the surrounding people. This configuration labeled as "distracted walking" was repeated 3 times. Finally, we repeated the normal walking configuration (i.e. without solving the written problem) with all

participants; but gave different orders during the experiment asking for inverting turning direction, moving to the center or moving to the exterior to purposely create congestion during the experiment. This configuration with changing conditions was only executed once. All configurations are summarized in Table 3.19 and Table 3.20.

Between each configuration participants were shuffled randomly to avoid a straightforward formation of lanes soon after the start signal. Staff helped assigning unfavorable positions at the beginning of each experiment, with the aim of creating a chaotic distribution. But obviously participants rapidly learned from the experience of the previous repetitions and lanes formed very quickly in the last executions.

Results

Some of the trajectories gained during the different configurations are given in Figure 3.33. To generate the trajectories the full length of the experiment was considered, i.e. shortly before the "start" signal until the "stop" signal, which was given when stable conditions had formed.

(a) Group B, run 1   (b) Group B, run 2   (c) Group A, run 2

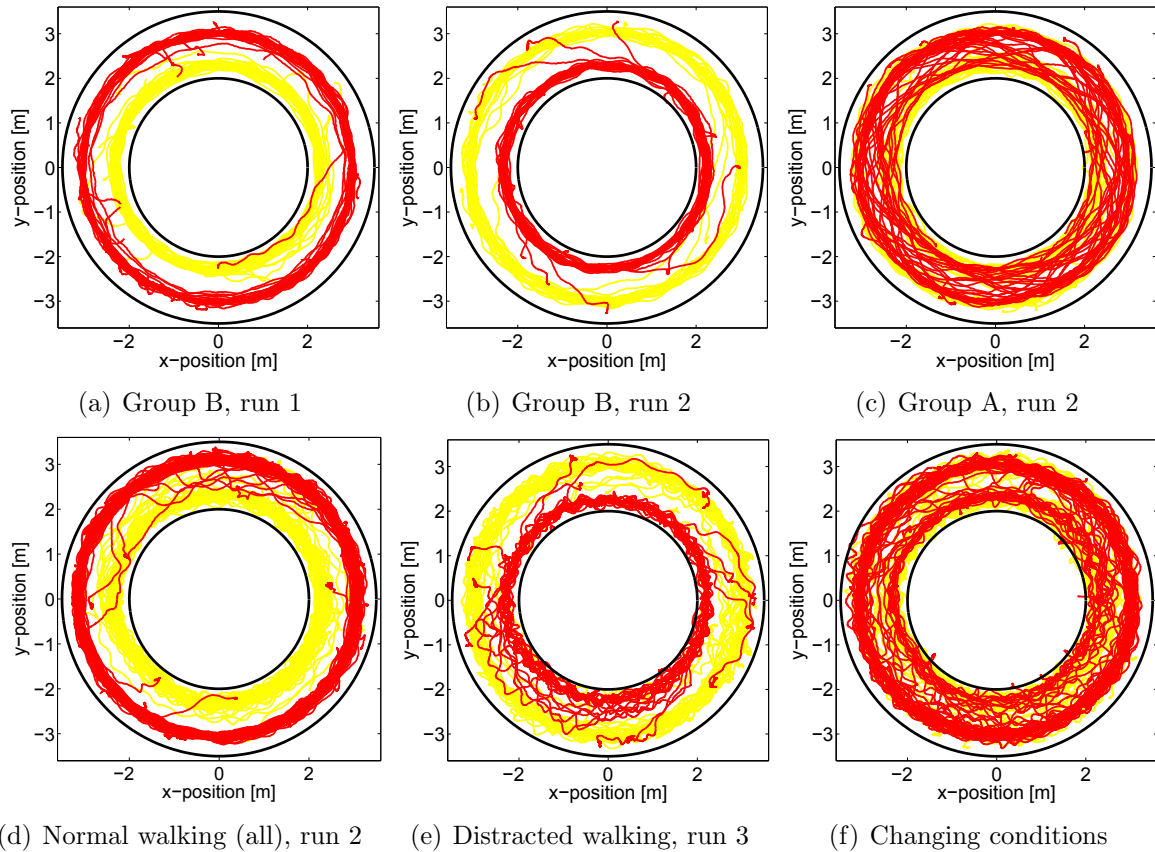(d) Normal walking (all), run 2   (e) Distracted walking, run 3   (f) Changing conditions

Figure 3.33: Trajectories gained during some configurations of the period bidirectional flow experiment [158]. Experiment time changes from configuration to configuration, with most cases lasting about 30–60 s. Each color is relative to a turning direction, details are given in Table 3.20.

Figure 3.33 already allows some initial considerations on the behavior of pedestrians in the different situations. Figure 3.33(a) and Figure 3.33(b) show two cases when separate lanes rapidly formed, by seeing that yellow and red lines take each half of the course. As presented in Table 3.20, lanes for the clockwise and the counterclockwise direction were

not always located in the same region and participants took some time to "determine" which group should take the inner part and which one the outer one (remember that initial position where shuffled).

The cases represented in Figure 3.33(a) and Figure 3.33(b) have been the most common and in the normal cases it usually took less than 10 s to divide both groups. An example for the process of lane formation is given in Figure 3.34 (third run of the distracted walking experiment), whose trajectories are plotted in Figure 3.33(e). Figure 3.34(a) shows a frame taken shortly after the start and it is seen that participants are heterogeneously distributed. The paper in their hand is the problem which was given and most of them are seen looking at it trying to solve it. Shortly after (Figure 3.34(b)), clusters of pedestrians moving in the same direction are formed; but it is seen that yellow pedestrians are divided into a group taking the inner part and another one staying externally. This unstable pattern lasts for a while (Figure 3.34(c)) and as soon as an empty space is spotted in the lane of red pedestrians, yellow ones in the inner loop take the opportunity to join the one in the outer loop (Figure 3.34(d)). Both groups get finally divided after around 20 s (Figure 3.34(e)) and in few seconds position inside each loop becomes homogeneously distributed (Figure 3.34(f)).

Although time to reach stability had been different in each configuration (with the distracted walking generally taking longer), in all experiments with only single exception clockwise and counterclockwise pedestrians divided in groups taking the inner and outer sections. We will consider the single exception more in detail now by examining the frames provided in Figure 3.35 (corresponding to the plot of Figure 3.33(c)). From the first frame (Figure 3.35(a)) relative to few seconds after people started walking it seen that some sort of clusters already existed with red pedestrians being organized in a sort of irregular line and yellow pedestrians forming a small group in the lower part of Figure 3.35(a). Shortly after (Figure 3.35(b)) a configuration formed in which most of the yellow participants took the inner part and 3 of them moved externally. In Figure 3.35(c) it is seen that the same configuration is kept with red pedestrians having to routinely shift inward/outward to avoid collisions with yellow participants. Some seconds later (Figure 3.35(d)) one yellow pedestrian from the inner loop succeed in joining the ones moving externally, but both groups remain splitted as it can be seen in Figure 3.35(e) and Figure 3.35(f). In this unstable configuration, which last for the whole length of the experiment, we observed that walking had not been smooth and at each turn someone had to stop to avoid participants coming from the opposite direction. While the width of the path (1.5 m) theoretically allows the formation of 3 lanes, under these conditions the space for each person become minimal and only a 2-lanes structure allowed smooth motion.

Trajectories gained from video recordings have been analyzed using the same procedure applied on the previous experiments, but with some changes to adapt methods to the peculiarities of this experiment. In the previous experiments we have computed the congestion level by taking time intervals of few seconds. Since changes were really fast in the circle experiment presented here we took a partially different approach. As usual the experimental area has been divided in cells to compute the velocity vector field. However, for this experiment we decided to use a constant time interval of 90 frames (3 s at 30 fps) and move this time interval in steps of 3 frames (i.e. 0.1 s). By doing so we were able to generate a signal for the congestion level having a resolution of 0.1 s. Since we are interested in global changes among the whole experimental section we took the whole surface to determine the rotation range. This means that in this approach we cannot determine precisely where congestion occurred, but we can be accurate concerning the

(a) $t = 1.2$s

(b) $t = 7.3$s

(c) $t = 9.4$s

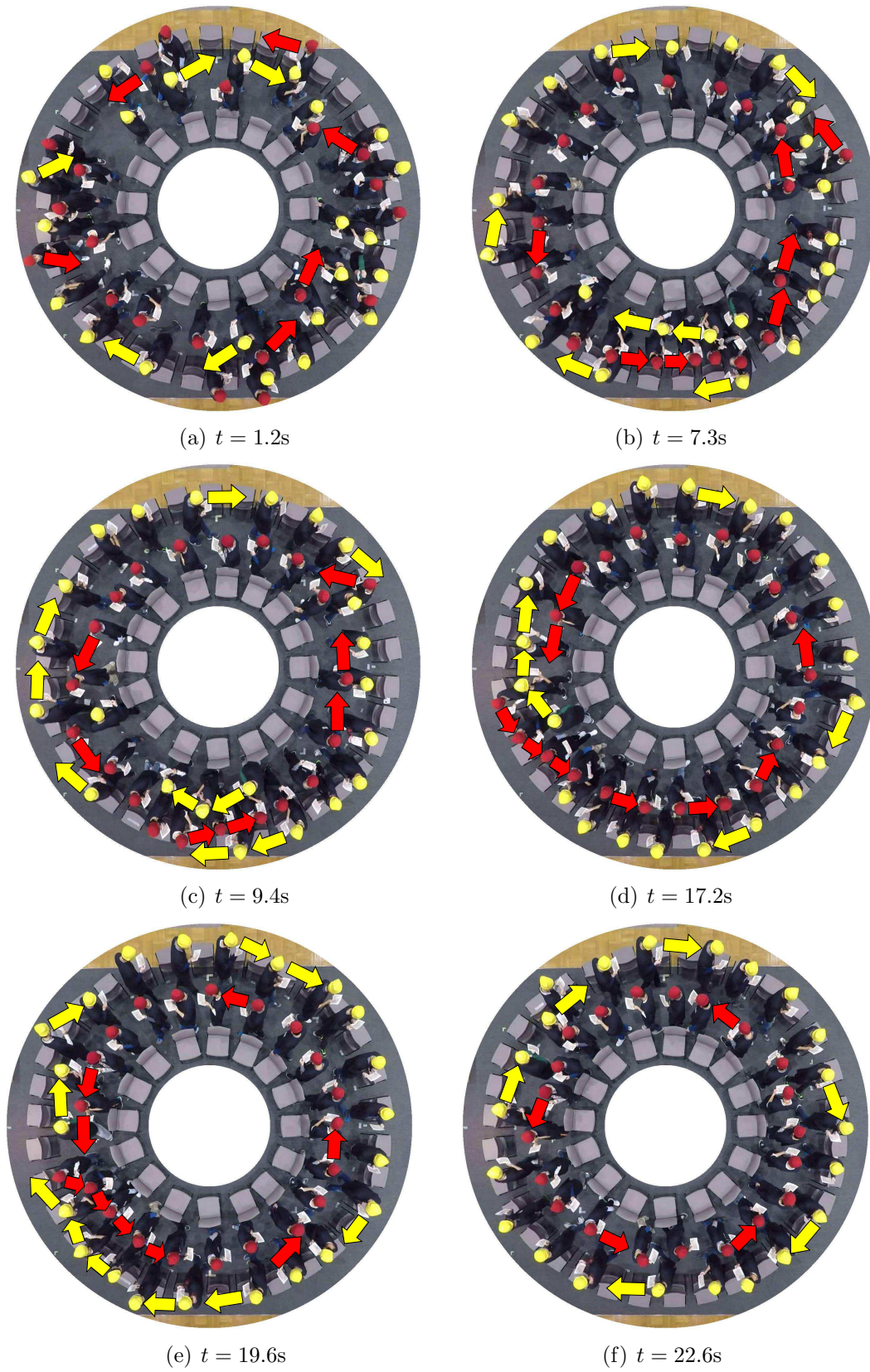(d) $t = 17.2$s

(e) $t = 19.6$s

(f) $t = 22.6$s

Figure 3.34: Frames taken from the third run of the distracted walking experiment. Separate lanes formed after about 20 s. Reference time $t_0 = 0$ is set when average velocity of the group exceeded 0.2 m/s.
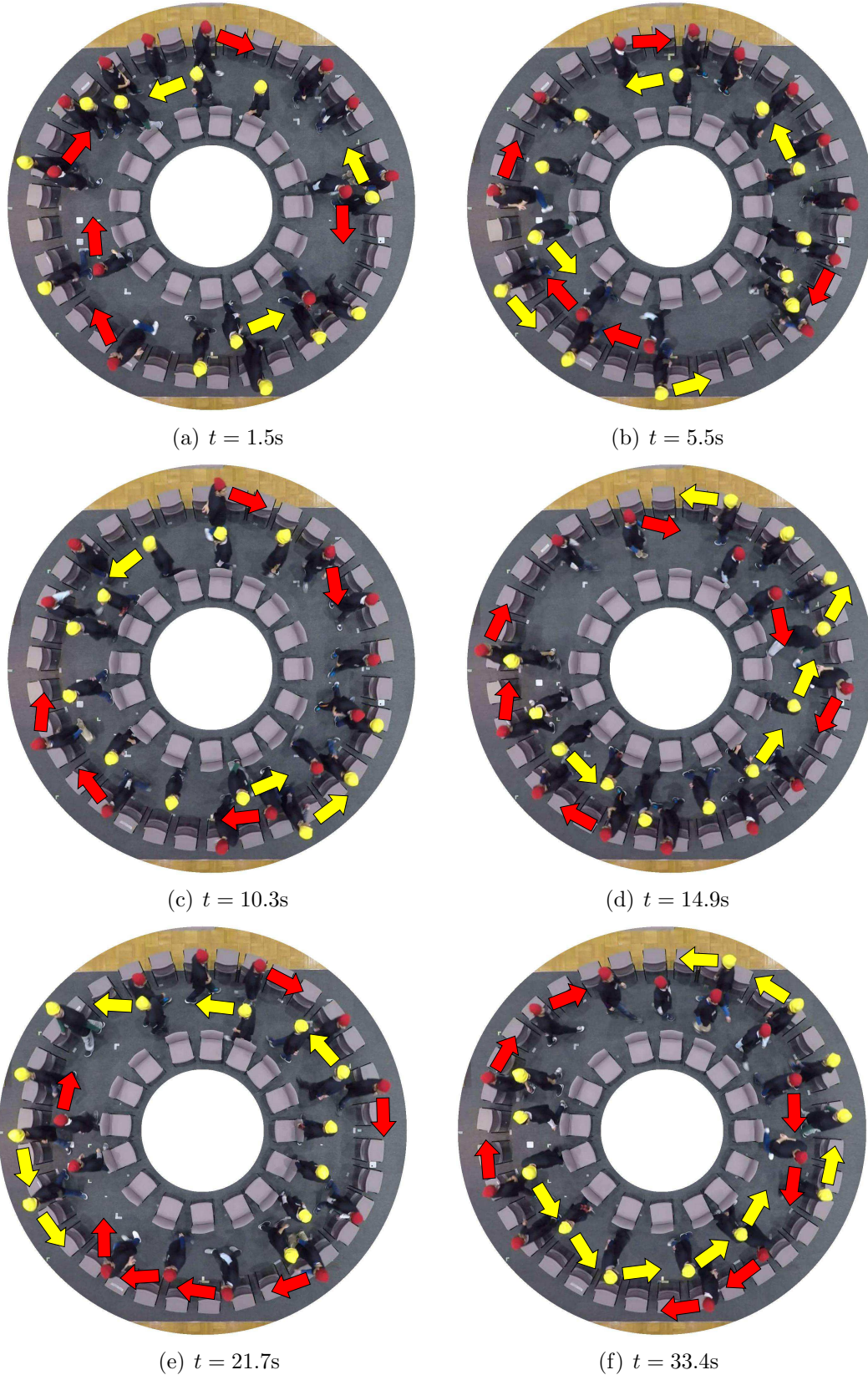
(a) $t = 1.5$s

(b) $t = 5.5$s

(c) $t = 10.3$s

(d) $t = 14.9$s

(e) $t = 21.7$s

(f) $t = 33.4$s

Figure 3.35: Frames taken from the second run of the experiment with group A. An unstable configuration formed with participants having to repeatedly stop or suddenly change direction. Reference time $t_0 = 0$ is set when average velocity of the group exceeded 0.2 m/s.

time when congestion ended.

Results for this type of analysis are presented in Figure 3.36. To allow a comparison of all cases under similar standards we defined the time t_0 when experiments "started" as the time when the average velocity exceed 0.2 m/s. This velocity threshold easily allowed to distinguish a stopping crowd from a moving one also in the congested scenarios of our experiments. When the configurations with 24 people are analyzed using the congestion level (as given in Figure 3.36(a)), it is clearly seen that a low value is quickly reached in most of the cases. Here, we used a threshold of 15 m^{-1} to determine congestion, taking into account the results from the chaotic experiments. The only configuration which did not turn to a stable flow is the second run with group A, which is the one presented earlier having an unstable 3-lanes structure. This shows that the congestion level allows to recognize unstable structures in pedestrian motion. In addition, it is interesting to notice that some sort of learning process is observed when the 4 cases are considered in order of execution. First run of group A is the one taking most time to become stable. If the unstable case of run 2 with group A is excluded, then both executions of group B seem to follow a logical sequence. It should be also reminded that 5 participants from group A were mixed in group B and their experience may have helped the rapid formation of organized lanes observed in both executions of group B.

(a) Low density normal conditions   (b) Medium density normal conditions

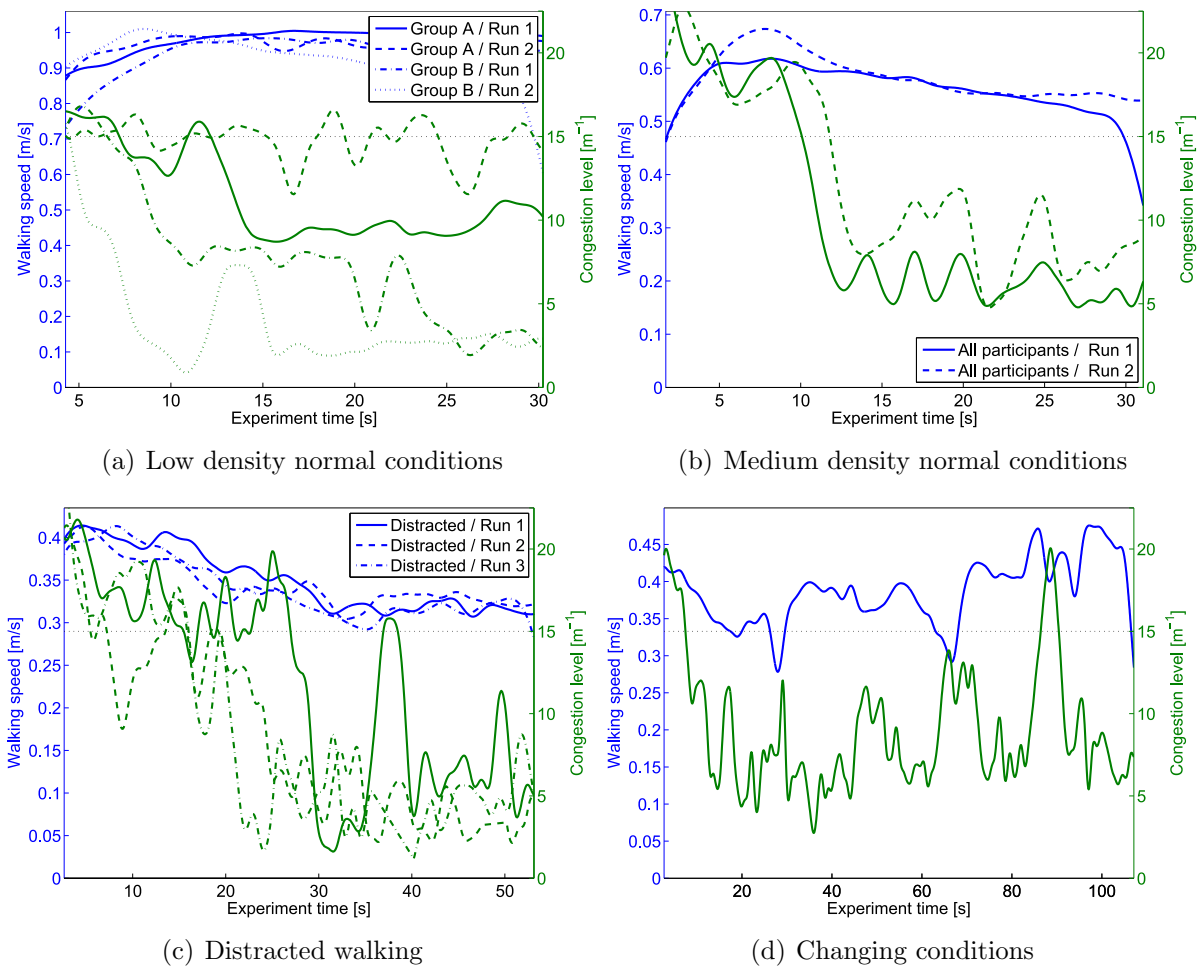(c) Distracted walking   (d) Changing conditions

Figure 3.36: Congestion level and velocity for different configurations [158]. Reference time $t_0 = 0$ is set when average velocity of the group exceeded 0.2 m/s. Signals were filtered to reduce noise.

What it is also interesting to notice is that the congestion level is not related with the walking speed, i.e. it is shown that the congestion level is related with the concept of organization and it is unrelated with flow. In fact, since density is constant in this experiment, flow follows the same behavior of speed here, which is seen taking more or less constant values for the whole length of the experiment. In addition, it seems that the value of 15 m^{-1} obtained for the threshold of the congestion level is appropriate for this situation also, possibly suggesting that it could have some sort of universality.

Next, we can examine the case when all participants took part to the experiment as given in Figure 3.36(b). Qualitatively, the same results as for the previous case are observed, although participants took some more time to reach stable lanes and the transition is sharper compared to the executions with 24 participants. Also here, we can see that changes in velocity (and flow) are not large and changes in the congestion level are not reflected in strong variations of velocity. While this could seem unrealistic, it should be mentioned that the congestion level is computed by taking the whole experimental area and only when stability is reached everywhere low values are obtained. To allow a more accurate analysis a map like the one presented for the bottleneck experiment could be taken for the different time intervals.

(a) Low density normal conditions

(b) Medium density normal conditions
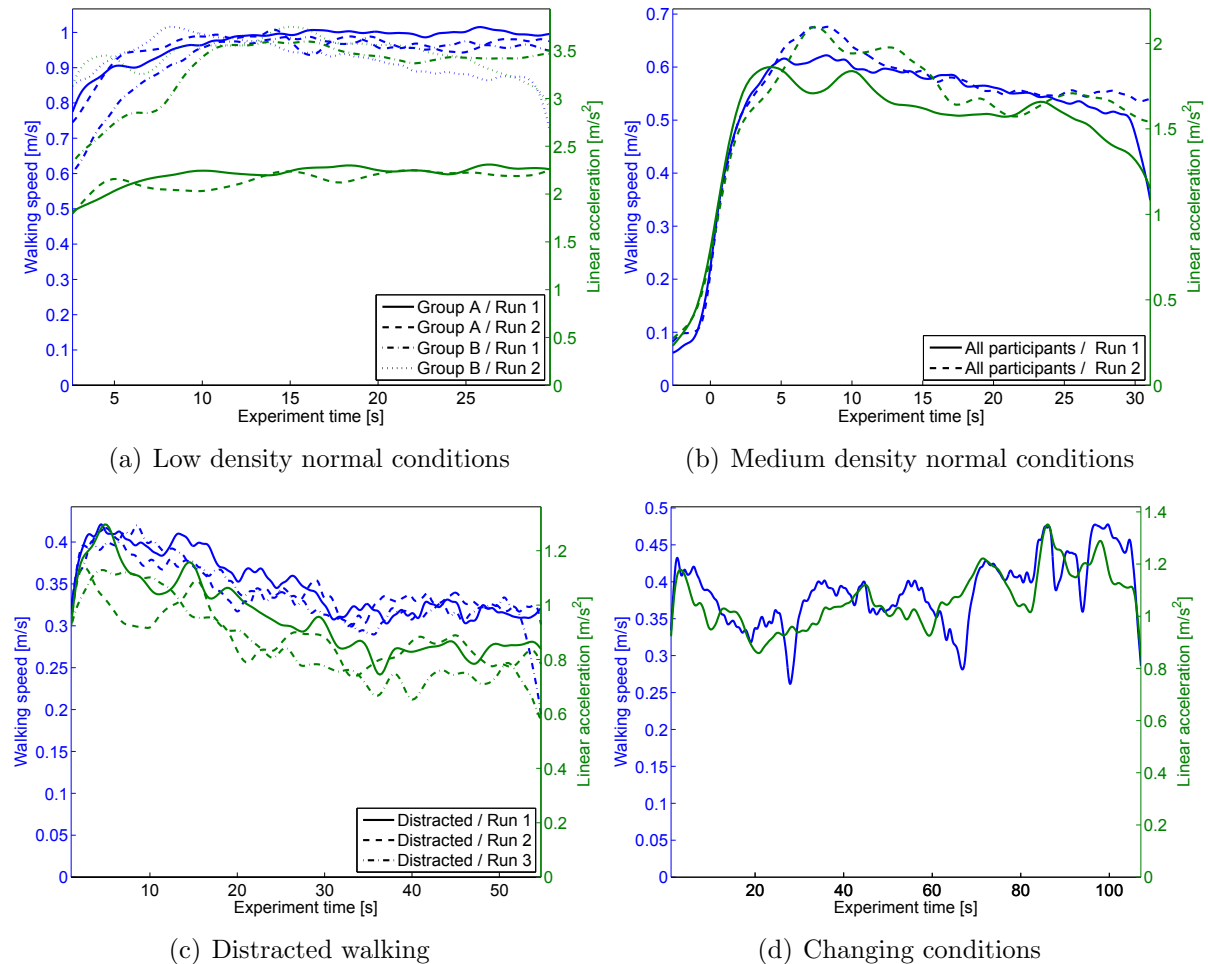
(c) Distracted walking

(d) Changing conditions

Figure 3.37: Walking velocity from computer vision analysis and linear acceleration measured from inertial sensors for different configurations. Reference time $t_0 = 0$ is set when average velocity of the group exceeded 0.2 m/s. Signals were filtered to reduce noise.

Also in the distracted walking scenario of Figure 3.36(c) the same situation is observed

with stable lanes forming about 20 s after the beginning of the experiment. When the 3 cases of Figure 3.36(c) are compared with the observations performed so far, it can be noticed that the congestion level has a similar behavior (with some exceptions) although the velocities are largely different: almost 1 m/s for the low density case, around 0.6 m/s in the second case considered and less that 0.4 m/s in the distracted walking scenario. What is also possible to notice in the graphs of Figure 3.36(c) is that a relatively higher level of noise is observed. While this could be related with the longer experimental time considered, it is also possible that the low velocity creates larger fluctuations in the congestion level (remember that rotation range is divided by the average velocity).

Finally, we can consider the case during which orders were given during the experiment (Figure 3.36(d)). In Figure 3.33(f) it is clearly seen that trajectories of the two colors used for caps overlap, the reason being that after lanes formed we asked participants to switch inner and outer positions and sense of rotation was also changed without previous notification. As a consequence, in some moments all the people turned in the same direction. This is seen in the low values for the congestion level observed in some moments. However, when changes were ordered peaks appear in the graph. In this case, we found that possibly the 3 s interval used to collect velocity vectors is slightly too long to accurately detect rapid changes. In this last case, some changes in walking speed are reflected in peaks of the rotation range (at around 30 s and 70 s), but in general it seems that both signals are not closely related.

To conclude the discussion on the periodic bidirectional flow experiment, we can examine the data collected from the pedestrians equipped with inertial sensors, whose results are given in Figure 3.37. Since tablet pedestrians were changed before this experiment the parameters gained from calibration with the chaotic experiment cannot be used here. As a consequence, in Figure 3.37, velocity obtained from tracking data is compared with the magnitude of the linear acceleration gained from the inertial sensor (which is proportional to the walking speed as discussed earlier). Sampling time to generate an average value of linear acceleration has been of 2 s and time steps of 0.25 s have been used to create a signal which was later filtered to remove noise.

In most of the cases a close relationship between walking speed and linear acceleration measured on the body of participants is seen. In Figure 3.37(a) it is noticed that linear acceleration for group A is very different from the one of group B. The reason for this large difference is that group A is composed only by participants equipped with tablets, while group B only by participants equipped with smartphones. When both classes of pedestrians are mixed in the experiments with all participants, then differences vanish. This clearly shows that while even small changes of velocities are well reflected in the way pedestrians move and accurately measured using inertial sensors (for example in Figure 3.37(c) a slow and light change in velocity is well reported in the trend of the linear acceleration), population composition and different ways of keeping smartphones have large influence on the results. For this reason, further research is required to judge what is the minimum amount of population which should be sensed to have results accurate enough to make judgment related with crowd control. While this research provide some initial evidence for the potential of this approach, verification is required in a real scenarios.

3.6.3   Summary

In this section, we have investigated the application of the the congestion level in scenarios where it changes considerably over space and time. In general, we found that results obtained with the congestion level are in line with previous qualitative results from the literature and mostly follow intuitive observations gained while inspecting the video of the experiments. In addition, we also tested the inertial sensors under changing conditions and found that, while there is a potential in this technology, there are also many limitations which could obstacle the application on real scenarios.

In particular, we have showed that the congestion level applied on a specific surface allows getting a different image from the one obtained by using the density and the flow (including velocity). While all quantities are important to understand different aspects, we believe that also the congestion level should be considered in judging the condition of a crowd of people. However, we found that only at moderate densities and combining several results, accurate maps providing the distribution of the congestion level over space are obtained.

Also in the transient time application, where space was uniformly considered and time had the largest variation, the congestion level allowed to identify the moment when organized structures formed and give some clue on possible cognitive processes occurring among participants. However, there are several aspects which require further investigation, in particular concerning the parameters used in the algorithm for the calculation of the congestion level. Additionally, also here a quite noisy behavior was observed sometimes making it difficult to make considerations on the degree of organization seen in the pedestrian crowd.

3.7   Conclusions and discussion

In this chapter, the central topic of pedestrian crowds' measurement has been considered from two perspectives: on one side the congestion level which was introduced in the frame of the bidirectional flow (where it was originally named as relative rotation range) has been tested in more complex multidirectional structures and on the other side we tested the possibility to judge pedestrian quantities by collecting data on the movements of pedestrians' body.

Concerning the congestion level we showed that, in the case of chaotic motion, it follows the same behavior of flow in regard to changes in density. The "standard" fundamental diagram composed by density and flow had practically the same shape of the congestion level–density relationship, but the approach presented here with the congestion level allowed to measure more universal transitions and returning a value of about 15 m^{-1} as a threshold for congestion. This value has been able to distinguish organized motion and congestion in our experiments, but we later saw analyzing data by other researchers that defining a universal threshold for the congestion level can be a difficult task and only specifically designed experiments may succeed in obtaining an accurate figure determining phase transition (to congestion). Nonetheless, the whole analysis presented so far seems to agree that values for the congestion level below 5 m^{-1} are relative to an uncongested fairly organized motion, with congestion clearly seen over 12.5–15 m^{-1}. Further research should be addressed to test the universality of this threshold with a vaster experimental campaign. If the validity of the congestion level (which based on velocity vectors) would be confirmed, this could help measuring pedestrian crowds with simplified image vision

algorithm (like the optical flow), since, as discussed earlier, velocities are more easily obtained compared to density by using images extracted from surveillance cameras.

The estimation of pedestrian properties based on data gained from inertial sensors contained in commercial electronic devices showed that technical equipment used and position where it is kept have a strong influence on the accuracy of the results. An initial problem was identified in the inability of the accelerometer to provide correct results. While the gyroscope was confirmed being an accurate scientific instrument (at least for the hardware tested), we also showed that its use in pedestrian crowds should be ruled out, since values obtained change depending on the geometry where pedestrians are moving (and the route chosen). On the other side, while inaccurate from a physical point of view, we noticed that the accelerometer can still be used and becomes particularly useful in heterogeneous crowds composed by people using different devices. Our results led to the conclusion that only large crowds can be accurately sensed using inertial sensors, since, in that context, individual differences created by hardware and storing location are reduced. In this regard, it should be noted that, while the 20 participants considered here could be a relatively small number compared to large crowds usually observed in urban spaces, the original idea behind the use of commercial devices was to avoid the constraint of detecting all pedestrians, which is the case in computer vision. As a consequence, if the minimum number of people required to get accurate results from inertial sensors gets too high, then the complexity of the approach may be comparable to those related to computer vision (thus limiting the benefits in the use of inertial sensors).

To summarize, concerning our initial goal of developing a method to judge level of congestion based on an approach different from computer vision, we can conclude that, while we showed that the techniques presented here have some potential, more research is required on the subject. In particular, by combining the linear acceleration obtained from inertial sensors with the congestion level, we showed that a clear transition is seen. This could help signaling changes in crowd motion by using only information from electronic devices, but we also mentioned that results obtained need to be considered with care. Nonetheless, we hope that the techniques presented here may be of inspiration for other researchers, thus finally and definitively moving toward the goals stated in the introduction of this chapter. As a last remark, we should mention that the techniques tested here may have limitations at low densities, but can be useful to study high density crowds which are also the most dangerous and the least investigated empirically, thus representing an additional stimulus for research.

Chapter 4

Pedestrian–vehicle interaction at unsignalized crosswalks

4.1 Introduction

Having vastly considered fundamental aspects of the the bidirectional flow in Chapter 2, we can continue the discussion by considering a particular situation represented by the crosswalk. In our previous analysis, we considered mostly medium to high density crowds and the conclusions can be used to model crosswalks with heavy pedestrian traffic. For the particular case of signalized crosswalks (with a traffic light), pedestrian and vehicular traffic can be considered separately and the methods described in Chapter 2 perfectly suits the modeling on the pedestrian side. But in the case of unsignalized crosswalks, pedestrian flow is usually low and intermittent and very simple considerations are sufficient to study pedestrian motion alone. However, when unsignalized crosswalks are considered, then interaction between pedestrians and vehicles becomes more important than the separate considerations on pedestrian and vehicle traffic. For this reason, this chapter will be devoted in developing a model able to reproduce the interactions between pedestrians and vehicles. Of course, pedestrian and vehicle motion also needs to be considered, but we will keep the discussion on those aspects to basic levels and mostly use well-known models from the literature as foundation. Our goal is to develop a model which can be used both for traffic management (for example in determining if a traffic light would be more appropriate to improve the level of service in a particular location) and for accident prevention (understanding which policy is the most efficient in reducing accident occurrence).

This chapter is organized as follows: at first we will present the motivation of this research, discussing the problematic related to traffic accidents and how pedestrians are involved with this issue. Later, we will provide a literature overview on studies considering the specific aspect of unsignalized crosswalks and discuss more in detail an empirical work which constitute the methodological basis for this study. We will continue presenting the simulation model and perform its validation using the Level of Service (without accidents). Finally, we will implement a method to account for gravity of collisions and discuss ways to reduce fatality among pedestrians. Conclusions and final discussion will conclude this chapter.

4.2   Motivation and statistics on traffic accidents

Traffic accidents have occurred since the introduction of the first engine powered vehicles with initial reported cases dating back at the end of the 20th century [160]. Before the problem became widespread, legislators had already started improving the safety of road users by clearly separating pedestrian and vehicular flows. Traffic lights were first installed in the United Kingdom in 1868 and in 1890 it was suggested to create under/overpasses to physically separate the road surface used by pedestrians and vehicles [160].

More than one century later road safety has greatly improved, with the number of road fatalities reported in the United Kingdom passing from a maximum of 7'952 in 1965 to 3'172 in 2006, this although the number of licensed vehicles has almost tripled [161]. In Japan, a similar trend has been observed with a peak of 16'765 road casualties registered in 1970 when the country fleet size was about 16.5 million vehicles. The number of fatalities has rapidly decreased reaching 3'904 in 2016 (the lowest on record if ratio with the country population is considered), with the number of registered vehicles close to 81 millions or almost 5 times the number of 1970 [162, 163]. Also in Italy (the country which will be the focus of an empirical study discussed later), a situation analogous to the one of Japan was observed in the 20th century: 11'078 road casualties were registered in 1972 when the country fleet size was about 15 million vehicles, but the figure rapidly decreased reaching 4'090 in 2010 (with the number of registered vehicles more than tripled) [164]. However, although in Italy the number of casualties has kept decreasing for a number of years, after 2013 this figure has slightly increased making it questionable whether the objective of 2'057 road traffic victims set for 2020 could be effectively reached [165].

When road safety is considered on a global scale the situation appears different, with emerging economies seeing an increase in road traffic causalities, both in absolute and relative terms. For example, in India traffic fatalities per 100'000 population were about 3 in the 70's but passed to 8 at the end of the 21st century [166]. The situation appears particularly dramatic in south Asia where the number of death in traffic accidents is predicted to more than double during the 2010–2020 period. Globally, traffic injuries were the 11th leading cause of death with the number of fatalities only slightly below the ones caused by malaria [166].

Among all road users, pedestrians are some of the most vulnerable, with the percentage of pedestrians fatalities lying at 25% of the overall traffic victims in the United Kingdom in 2014 [167], at 34.9% in Japan in 2016 (the percentage was 32.3% in 2006) [162] and at 17% in Italy in 2015 [165]. In developing countries pedestrians appear to be also vulnerable road users, in particular in India where they represent the majority of road users killed in accidents with a proportion over 40%. The percentage grows when large cities are considered and in Mumbai 78% of the traffic victims are pedestrians (53% for New Dehli). Worldwide, crashes between vehicles and pedestrians account for more than a third of all road-traffic deaths and injuries [166].

Although in modern countries the number of pedestrians casualties has rapidly decreased in line with a general improvement of road safety and compliance, this figure has been almost unchanged in the recent years. In the United Kingdom the number of pedestrians killed in road accidents has been fairly constant since 2010 [167] and in the U.S. it has not shown any significant trend since 2004 [168], with pedestrians still representing 14% of all fatal crashes in 2013. In Italy, an increase of 4.2% has been recorded for pedestrian fatalities in the period 2014–2015 [165]. In Japan, the situation is slightly better, although the number of pedestrian fatalities only decreased in absolute terms and the proportion

among road users actually increased [162].

While the increasing number of pedestrian fatalities in developing economies can be related to the overall increase of motorized traffic and non-compliance issues, the recent increase of pedestrian's crashes in developed countries appears to be more difficult to explain. Some studies suggest that one of the possible causes for this increase is related with elderly pedestrians [167, 169], which has often been identified as being one of the most vulnerable group of pedestrians [170, 171, 172]. Although, in general, most of the fatalities recorded for pedestrians are relative to the 15–29 age group, results drastically change when the proportion of each age group inside the population is taken into account [171, 166]. Clearly, the reason for the high relevance of fatalities in elderly pedestrians is related to different factors associated with physiological limitations given by their age. In particular, factors limiting their capability to interact with road users are given by: (i) their limited locomotion capabilities (e.g., reduced muscle strength and coordination abilities, posture differences and low walking speed) and (ii) the reduced reliability of perceptive sensors and cognitive functions (e.g., ability to distinguish colors and evaluate lighting conditions, inefficient suppression of background noise, poor attention and reaction time, disorientation and slower decision-making) [173]. Concluding, the importance in improving safety for elderly pedestrians is clearly reported in the "World Report on Road Traffic Injury Prevention", which highlights pedestrian safety as the main safety concern for the elderly road users.

Some of the most critical traffic components in which pedestrians and drivers interact are represented by crosswalks, with unsignalized ones creating an higher risk for pedestrians compared with the one signalized using traffic lights. For example, in the case of Israel, elderly pedestrians crossing the road in locations within a metropolitan/urban area were found as the most common type of road accident leading to death [170].

However, research on pedestrian behavior on crosswalks has been limited by a variety of factors: difficulty in obtaining empirical data through on-field observations, safety and ethical concerns related with experiments involving individuals and the limited scope of the simulation models developed in the past. More recently, virtual reality is offering the possibility to evaluate driver and pedestrian reaction in an environment very close to reality without the risks which would exist in a real scenario [174, 175, 176]. But still, although a variety of simulation software can deal with traffic from both a macroscopic and microscopic point of view, only little attention has been put in developing simulation models to reproduce crossing behavior on the basis of empirical data collected in real situations. Such a simulation tool is required if pedestrian safety and comfort has to be improved and a development in this direction would also lead to an increased accuracy on the macroscopic scale. In addition, a reliable simulation model would allow policy-makers to take decisions based on a more rigorous base thus contributing to the creation of more safe and comfortable areas for pedestrians and road users.

4.3   Literature survey

As the numbers above testify, it is rather easy to find statistical data concerning the relevance of a certain type of accident occurring to pedestrians and most of the countries make those data openly available. However, it is more difficult to find reliable studies describing the behavior of pedestrians in crosswalks and this may be one of the reasons why simulation models developed so far could not be validated using empirical data. Hereafter, we will attempt to summarize some of the most relevant studies considering the

interaction between pedestrians and vehicles at unsignalized crosswalks (when relevant, research on signalized crosswalks will be also considered). We will summarize empirical studies at first and later focus on modeling attempts. Finally, we will summarize the empirical aspects on which our model is based.

4.3.1   Empirical studies

Most of the experimental studies on pedestrian crosswalks focused on measuring walking speed of pedestrians and investigating possible differences with behavior observed in pedestrians in common situations. Pedestrian speed at crosswalks was found roughly following a normal distribution [177, 178, 179, 180, 181], which should not come as a surprise since pedestrian walking speed in general has been long known for being normally distributed [131, 21, 127]. Reported crossing speed change depending on the type of crosswalk considered (signalized or unsignalized) and the physical characteristic of the pedestrians walking on it, with gender and age being statistically relevant (young and males are significantly faster than elderly and women). On the other side, ethnicity of the pedestrian, grouping pattern and lighting condition of the crosswalk were not found to significantly impact the crossing speed [179, 181]. In addition, in the case of signalized crosswalks, pedestrians were shown having significantly higher crossing speeds when attempting to cross in the "don't walk" time [180]. Speed-density relation for the situation of signalized crosswalk showed a linear relationship similar to the one observed in general pedestrian facilities [21, 180].

Other researchers have set their attention on drivers' behavior and speed profiles observed while approaching a (unsignalized) zebra crossing. It was found that drivers do not follow the law concerning speed behavior and that instead, maintaining high speeds or even accelerating was used to signalize to pedestrians that they do not intend to give the way. The region lying between 50 to 40 m before the zebra crossing was found critical for influencing drivers' behavior [182]. Pedestrians' capability to estimate approaching car's speed vary by weather conditions and vehicle speed. If the speed of the oncoming vehicle exceed an upper bound, pedestrians are more likely to underestimate vehicle speed, thus increasing the risk of trying dangerous crossing attempts [183].

Waiting times for pedestrians attempting to cross zebra crossings are typical of the location considered, but in general short waiting times are much more frequent than long intervals, with the distribution rapidly decreasing the as the waiting time grows bigger [178]. In a particular study [184], waiting time has been analyzed based on a number of factors which can potentially have an influence in reducing it, consequently trying risky crossing attempts. Results show that female pedestrians, those having children, those who own and drive a car, elderly pedestrians and people having assisted to traffic accidents are more likely to accept longer waiting time at the curbside. Among factors influencing pedestrians toward more risky behavior were found commuting to work, frequent use of the given crosswalk and crossing in group behavior [184].

Concerning crossing attempts, it has been shown that slightly less than half of pedestrians (41.67%) try to cross at the first attempt and that expected waiting time seems to influence the number of attempts required to cross the street [184]. It has been shown that the perception of ease in regard with the crossing task influences the degree of hazard taken by pedestrians when attempting to cross a road. Those thinking it would be easy to cross are more likely to take risks [185].

Several researchers identified the acceptance gap as one of the main parameters uncon-

sciously used by pedestrians in judging if a crossing attempt can be considered safe or not. The accepted time gap can be defined as the relation between the distance (along the driving direction) and the average speed of oncoming vehicles when pedestrians decided to cross [173]. Although data on this aspect are limited, researchers seem to agree that accepted gaps are in the order of 4–6 seconds [186, 177, 173]. Distributions for accepted and refused gaps are different, but both tend to flatten when accepted gaps get longer and refused gaps shorter. Interestingly, the distributions for accepted gaps by pedestrians waiting and not waiting only differ to a small extent [177]. Finally, time gap (or vehicle headway to use another expression) was found having a positive coefficient toward waiting time, meaning that waiting time seems to decrease for short time gaps.

Other studies considered aspects generally related with city planning and infrastructure selection. A comparative study considered different types of pedestrian crossings (signalized, unsignalized, marked, non-striped, midblock crosswalks...) and analyzed pedestrians preference and compliance observed for each type. Unsignalized midblock crosswalks were among the preferred by pedestrians and high crossing compliance was also observed. However, location of the crosswalk relative to origin and destination was found being the most influential decision factor. Less incisive but still remarkable were the presence of traffic control and vegetation or concrete barriers [187]. The relationship between pedestrian accidents and infrastructure selection has been investigated by considering different types of intersections: three-legged, four-legged, roundabouts and road segments. A function predicting accident's frequency in relationship with pedestrian and traffic flow was derived for each intersection [188].

To conclude this part, a study [189] considered the effect on mobile phone use on the pedestrian crossing behavior at signalized and unsignalized crosswalks. Both males and females surveyed in the study were found crossing at lower speed and taking less attention to surrounding traffic when using mobile phones compared to pedestrians not making use of it.

4.3.2   Previous modeling attempts

Vehicular traffic has been studied for several decades and both mathematical formulations and more sophisticated models are available to perform simulation on traffic flow (an extensive summary including several modeling approaches is given in [190]). Modern software are commercially available to study road networks extending from small neighborhood to large cities. In addition, multiple lanes models have also been developed to simulate lane change and overtaking maneuvers [191]. Pedestrian models have also reached a considerable degree of maturity and have been already discussed in this thesis (for details see Chapter 1.2.4, Chapter 2.3.4 and Chapter 2.7). Specific models designed to deal with elderly pedestrians have been developed by considering different walking velocities for each agent used in simulation [192].

Although both car's and pedestrian's model have been constantly developed separately for decades, attempts to combine both road users are more rare. One of the first modeling attempt to describe unsignalized pedestrian crossing is the mathematical model developed by Griffiths [193]. This model, however, allows only qualitative considerations of purely mathematical nature and it is difficult to adapt to real-life scenarios. Helbing et al. [194] also developed a mathematical model which has been able to grasp delay caused by the intersecting flows of car and pedestrians. However, although this model allows a rigorous analytical treatment of the problem, its foundation is based on many-particle streams,

which does not present some of the heterogeneous aspect found in traffic flow, especially if elderly are considered.

Lawniczak et al. [195, 196] proposed a simple Cellular Automata model to simulate the hypothetical case of creatures crossing a highway. In their model, priority is not set on accurately capturing behaviors found in nature, but rather to create a cognitive process in which each creature tries to cross the highway and following creatures learn from mistakes observed by their predecessors. Knowledge is transferred from one creature to the following one by judging the behavior which resulted in successful and failed crossing attempts. Daganzo and Knoop [197] have considered a similar case in which pedestrians are allowed to cross at any point of a given road, the so-called "pedestrianized streets" (to use their own words). Analytical formulas have been derived to assess the impact of pedestrian's flow on vehicular traffic. The researchers qualitatively concluded that the street's capacity is inversely proportional to the square root of the pedestrian flux for low pedestrian densities.

Yang et al. [186] developed a Cellular Automata model to simulate pedestrian behavior at signalized crosswalks. Although their model is designed for pedestrians crossing in the presence of traffic light, the main goal of their study is to implement two types of behavior observed during red light period: law-obeying pedestrians (waiting until the traffic light turns green) and opportunistic ones (crossing while facing red light). To account for interaction between pedestrians and vehicles in the crossing attempts with red light a distribution for the accepted time gap is used. From this point of view, the model by Yang et al. intrinsically contains behavioral mechanisms proper of unsignalized crosswalks.

More recently, Zeng et al. [76] developed a social force model to simulate pedestrians' behavior at signalized crosswalks. Similarly to the model by Yang et al., also in the approach by Zeng et al. interactions with drivers are considered to account for the effect of turning vehicles which (compliantly) invade the zebra crossing during green light periods. The simulation by Zeng et al. considers a number of phenomena (individual interactions, group behavior, vehicle interaction, speed changes and deviations from zebra stripes) by modeling them using repulsive or attractive forces of different magnitude. Their model predicts very well pedestrians' trajectories observed in reality by even reproducing pedestrians walking outside the boundary, which are usually not considered in typical social force models. However, interaction with incoming vehicles was only considered in terms of deviation from the normal crossing trajectory and compliance has not been an issue in their study. Also, the model by Zeng et al. and all the models presented so far do not consider collisions with vehicles.

Finally, Crociani and Vizzari [198, 199] developed a model with the specific intention to consider both signalized and unsignalized crosswalks. In their model cars move in a continuous space environment, while pedestrians' motion is simulated using a standard Floor Field Cellular Automata model. Interactions at the crosswalks are modeled in an idealistic way: drivers will stop every time a waiting person is spotted on the curbside and pedestrians are capable of precisely estimate car breaking distance based on its speed. One of the limitations of their model is the constant time step (which has to be chosen equal to the drivers' reaction time) which does not allow a smooth variation of pedestrians' walking speed. Also, empirical data have not been used to validate their model, constraining the suitability in evaluating real-life situations.

4.3.3   Short summary of field survey in Milan and main results

Creating a universal model able to reproduce pedestrian behavior observed in different countries and accounting for different type of vehicles would be an extremely difficult and not necessarily indispensable task. On the other side, any new knowledge gained while analyzing a specific traffic scenario will contribute to a better understanding of human behavior in streets, eventually allowing to create increasingly complex and generalized models. It is therefore important to define strength and limitations of the model to be developed and clearly illustrate the context on which it can be applied (scope of application). In the case of this study, rules and parameters implemented into the model have been obtained based on an observation performed in Milan on a unsignalized crosswalk. Main results of the field survey and empirical knowledge used to develop the simulation are presented in this section (a complete analysis of the results is given in [173]).

Figure 4.1: Snapshot from the video relative to the observation in Via Padova.
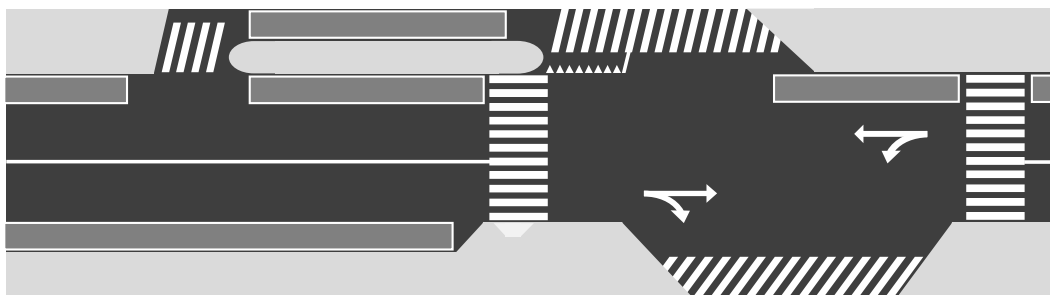
Figure 4.2: Schematic diagram of the investigated crosswalk [173].

An unsignalized crosswalk in a residential area of Milan (Italy) has been chosen for a roughly hour-long observation. The specific location has been selected based on a number of criteria: the high number of accidents with pedestrians reported, a proportionally large elderly population and strategical factors (proximity with public facilities, possibility to obtain video recordings from a tall building...). A schematic representation of the crosswalk studied is given in Figure 4.2. A camera has been used to record a video (for which a snapshot is given in Figure 4.1) which has been later analyzed by means of tracking software and manual analysis. During the 1:15-long observation 1379 vehicles and 585 pedestrians have passed through the target crosswalk. However, after excluding biased vehicle-pedestrian interactions (parked car obstructing the view, turning vehicles, bicycles interfering pedestrians' movements, bikes overtaking cars...), only a dataset with crossing actions involving 50 pedestrians and 79 vehicles (mostly cars) has been used to study in detail the understand decision-making process for both road users.

Vehicular traffic throughout the whole observation was evenly distributed in both directions with a large proportion of cars (67%), followed by bikes (13%), vans (8%), cycles (6%) and heavy vehicles (6%). Measured traffic volume accounted to 1139 vehicles per hour for both directions. Speed limit in the considered section is of 50 km/h, although vehicles have been rarely observed exceeding a speed of 35-40 km/h (with a partial exception for bikes) mostly because of the consecutive presence of several crosswalks before and after the one analyzed. Among pedestrians, many of them have been observed crossing from South to North (relative to the orientation of Figure 4.2), with the largest part being composed by adults (71%) followed by elderly (24%). Most of the pedestrians were walking alone (65%), with groups dominated by dyads (26%) and triples (8%). Pedestrian flow on the crosswalk stood at 8.01 pedestrians per minute. However, if groups are considered as a "single entity" because of their cohesion and synchronized motion, the flow for crossing sets (or blocks) reduces to 5.52 per minute.

Table 4.1: The Level of Service criteria for two-way stop-controlled unsignalized intersections (adapted from [19, 200]).

LOS	Description	Delay per entity [s]	
		Vehicle	Pedestrian
A	· Nearly all drivers find freedom of operation · Very seldom more than one vehicle in queue · Very small delay to cross · Low likelihood of risk-taking behavior by pedestrians	<5	<10
B	· Some drivers consider the delay an inconvenience · Occasionally more than one vehicle in queue · Small delay to cross · Low likelihood of risk-taking behavior by pedestrians	5 – 10	10 – 15
C	· Many times more than one vehicle in queue · Most drivers feel restricted, but not objectionably so · Small delay to cross · Low likelihood of risk-taking behavior by pedestrians	10 – 20	15 – 25
D	· Often there is more than one vehicle in queue · Drivers feel quite restricted · Big delay to cross · Moderate risk-taking behavior by pedestrians	20 – 30	25 – 35
E	· Demand is near or equal to capacity · Almost always more than one vehicle in queue · Drivers find the delay approaching intolerable levels · Very big delay to cross · High likelihood of risk-taking behavior by pedestrians	30 – 45	35 – 50
F	· Forced flow · Intersection failure caused by external factors · Very big delay to cross · High likelihood of risk-taking behavior by pedestrians	>45	>50

The so-called "Level Of Service" (LOS) has been used to grade the quality of the crosswalk facility. The idea behind the LOS (whose details are given in [19] and has been already discussed for the pedestrians-only case in Chapter 1.2.3) is to compute the time

lost due to congestion/delay formed in a given infrastructure (highway, intersection...) and rate its quality/safety on a graded scale. In the case of crosswalks, both the time lost by pedestrians and drivers need to be considered. For drivers, braking, queuing, waiting and accelerating are actions considered to contribute to the time loss. For pedestrians, the time spent while waiting and during start-up at the curbside is used.

In the case of the crosswalk analyzed, delay (or time loss) for both road users was found as 3.20 ± 2.73 s per vehicle and 1.29 ± 0.21 s per pedestrian. In the grading used in the LOS, this corresponds to a A-level (see Table 4.1), meaning that nearly all drivers found freedom of operation and that no pedestrians crossed irregularly (therefore taking very few risks).

Analysis of the velocities from selected pedestrians revealed that three phases are characteristic in a crossing attempt. During the approaching phase pedestrians move toward the crosswalk; here velocities are equivalent to the ones observed during common situations with only density and social structure influencing it. Around 3 m before reaching the curbside (this figure slightly varies among individuals), pedestrians slow down and start assessing the viability of their crossing attempt. If it is considered safe to cross, pedestrians will accelerate (eventually reaching a walking speed slightly higher than their approaching speed) and walk on the opposite side of the crosswalk. Walking speeds during the three phases are different between adults and elderlies (values are reported in Table 4.2), although in general elderly pedestrians tend to consistently walk about 0.25 m/s slower.

Table 4.2: Velocity during different crossing phases (relative for the selected pedestrian-vehicle interaction dataset) [173].

Crossing phases	Adult pedestrians	Elderly pedestrians
Approaching speed	1.28 ± 0.18 m/s	1.03 ± 0.18 m/s
Appraising speed	0.94 ± 0.21 m/s	0.69 ± 0.23 m/s
Crossing speed	1.35 ± 0.18 m/s	1.09 ± 0.17 m/s

Finally, the decision-making process for pedestrians attempting to cross the road has been analyzed by using the time gap previously discussed. Time gaps are obtained by measuring the distance and speed of each vehicle at the time pedestrians decide to cross the road (this moment is represented by the transition between appraising and crossing phase). Results for the 50 pedestrians considered in the dataset are given in Table 4.3.

Table 4.3: Measured car's quantities at the beginning of the crossing phase [173].

Quantity	Final decision to cross	
	Adult pedestrians	Elderly pedestrians
Car distance	16.21 ± 8.09 m	17.61 ± 9.50 m
Car speed	16.54 ± 6.48 km/h	15.15 ± 7.68 km/h

Although deviations are very large, distance from cars accepted by elderly when moving out from the sidewalk are larger compared to adult pedestrians. On the other hand speed of cars appear to be smaller. Based on those two data, it is possible to compute the accepted time gap by simply dividing distance and speed. Results are presented in Table 4.4 with distinction being made for near and far lane.

Table 4.4: Accepted time gaps for different types of pedestrians and each lane [173].

Time gap	Adult pedestrians	Elderly pedestrians
Near lane	3.84 ± 2.87 s	4.43 ± 1.72 s
Far lane	4.22 ± 1.96 s	4.59 ± 1.92 s

Again, elderly appear to be more caution when deciding to cross the road, although deviations are very large making differences statistically insignificant. Differences are smaller when the far lane is considered.

The model that we will introduce in the next section is based on the qualitative aspects apprehended while visioning the video recording and empirical evidence gained. In addition, numerical values obtained in the above analysis has been used to calibrate the model.

4.4   Simulation model

As shortly discussed in Chapter 4.3.2, Crociani and Vizzari already developed a model to simulate interactions between vehicles and pedestrians at unsignalized crosswalks. However, their model had several shortcomings and it was not suitable to use the empirical results previously introduced for calibration. The model presented here represents a substantial improvement from the initial modeling attempt and it allows to perform calibrations based on empirical data gained from field survey reported above.

In this section, the simulation model will be discussed in detail, including geometrical setup for the road (and crosswalk), algorithms to sequentially move pedestrians and cars and the rules governing interactions between both road users.

4.4.1   General structure

The simulation code has been written using Repast Simphony (version 2.4), which has several libraries dedicated to multi-agent simulations and particularly suits to the case of traffic dynamics. The simulated geometry corresponds to the scenario of the observation, whose dimensions are given in Figure 4.3. The portion of road considered has a single crosswalk in the center where pedestrians and cars interact. The crosswalk section contains a "virtual" midblock which allows pedestrians to stop in the middle of the street without colliding with incoming cars (details for this approach will be presented below).
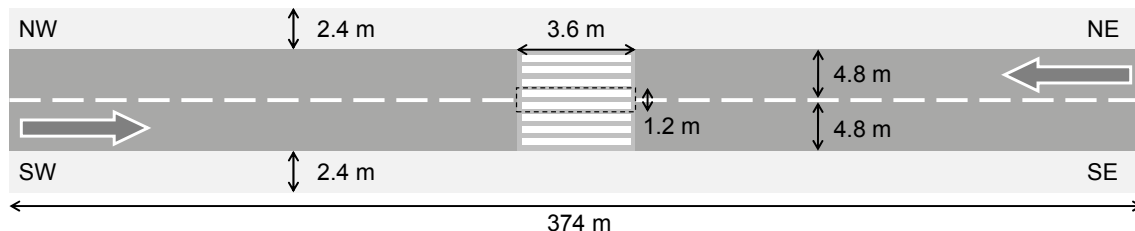

Figure 4.3: Schematic representation with dimensions of the simulated model (dotted area is the "virtual" midblock) [201].

Cars move on each of the two lanes in opposite directions. Periodic boundary conditions are used to allow a continuous flow of cars: once a car leaves from one side of the road

it is (re)created in the next computational step on the opposite side. Pedestrians are randomly generated from one of the cardinal points indicated in Figure 4.3. Origin and destination are randomly chosen by ensuring that the chosen combination will force the given pedestrian to pass through the crosswalk. After reaching the destination each pedestrian is removed from the scenario.
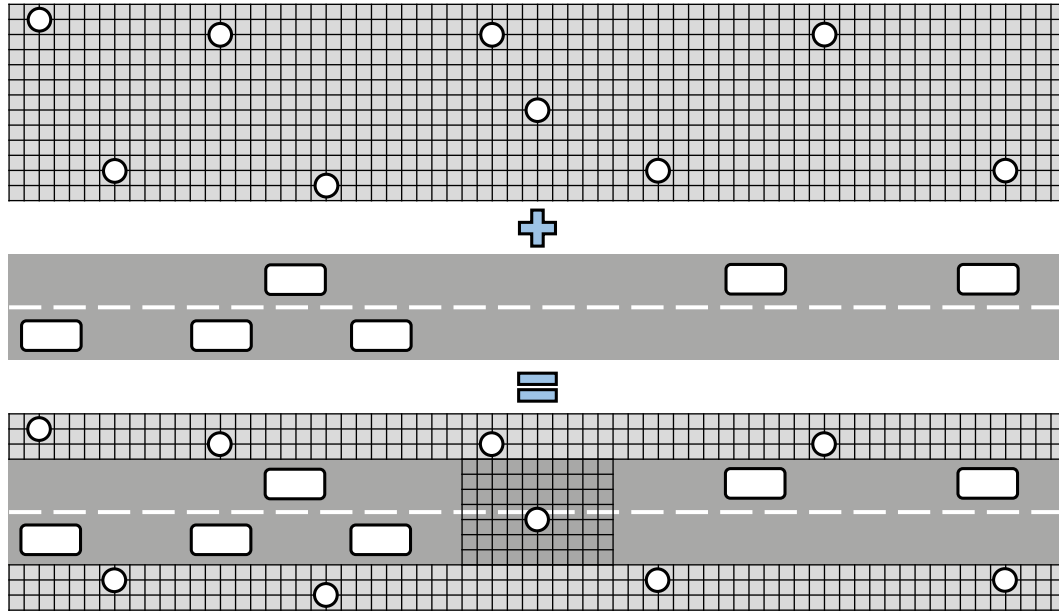

Figure 4.4: Representation of the global environment created by superposition of the vehicular and pedestrian sub-environments [201].

Car and pedestrian environment is modeled using two different approaches, allowing to use the best approach for each type of agent (a schematic representation is given in Figure 4.4). Cars are modeled in a continuous space, in which the position along the lane can be computed in an accurate way limited only by the machine precision (car position will consequently be given as a decimal number). This approach is necessary since cars move with a large range of velocities and a discrete approach would not allow to accurately compute positions at low and high velocities. Pedestrians are modeled using the Floor Field CA approach and can only move in the portion of the grid which is not occupied by the road, with the exception of the crosswalk where both pedestrians and cars are allowed to pass. The advantage of this type of environment is to allow a subdivision between the space occupied by each agent, thus making it possible to simulate each road users in an independent way and considering only interactions as a connective point between both agents.

4.4.2   Pedestrian model

Pedestrian motion inside the computational grid is based on the Floor Field model with parallel update. In this case a Moore neighborhood is used (i.e. diagonal motion is possible) [1]. The static FF has been set like the example shown in Figure 4.5 for a pedestrian moving to the South-West exit. Clearly, the smallest values of the static floor field are found at the left-lower corner (i.e. South-West according to Figure 4.3). As

---

[1]In the model used in the previous chapters Neumann neighborhood was used, i.e. only neighboring 4 cells were considered as candidates for pedestrian motion.

a consequence, the pedestrian will be directed there, with no regard on which corner
is generated. By looking again at Figure 4.3 it can be noticed that the field strength
is symmetrical in both sides of the upper section of the street. This means that if a
pedestrian is generated at the upper sidewalk (no matter if left of right), he will have to
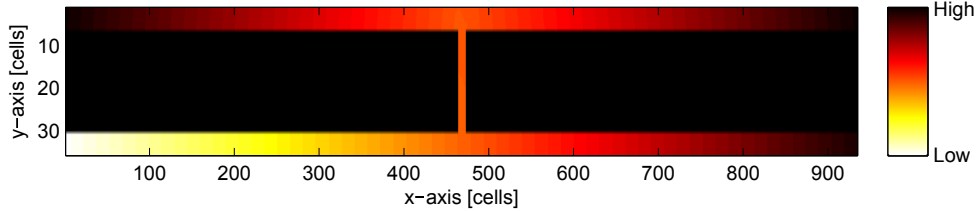cross the road to reach his destination.

Figure 4.5: Static floor field for the scenario considered in simulations (pedestrian desti-
nation is South-West, origin is either North-East or North-West).

In the most simple implementation of the Floor Field model used here each pedestrian
determines his next cell during each time step only based on the static floor field. In
the standard Floor Field model implementation, walking speed is simply considered by
adjusting the size of time step and cell size. Typically 0.4 m cells and time steps in the
order of 0.3 s are used, with a resulting free walking speed of about 1.3 m/s. However,
in our model we wish to consider different walking speeds and a small time step is also
required to accurately represent car behavior. It is therefore important to consider a
system allowing to set pedestrian individual walking speeds. An idea would be to have
pedestrians moving to the next cell with some probability computed to match with the
actual walking speed. This "update probability" μ can be computed as:

$$\mu = v_{ped} \frac{t_{step}}{w_{cell}} \tag{4.1}$$

where v_{ped} is the (desired) pedestrian speed, t_{step} is the time step and w_{cell} is the side
length of the grid's cell. For each iteration a random number $X = [0, 1]$ is generated and
the pedestrian is moved to a neighbor cell if $X < \mu$. The method is simple and efficient,
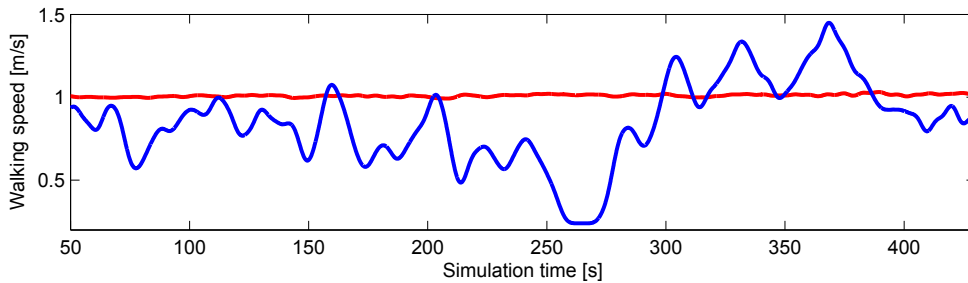but real moving speed tends to have large oscillations as shown in Figure 4.6.

Figure 4.6: Pedestrian velocity computed with (red) and without (blue) moving average
correction (moving average has a period of 10 s).

This happens because of the probabilistic nature of the method employed. The pedestrian
may move sequentially for several time steps and stop a similar long time, thus generating
the oscillations depicted in Figure 4.6. In addition, at the time when update probability is
computed it cannot be known if the pedestrian will move to a side or a corner cell. Since

the center-to-center distance is different by $\sqrt{2} - 1$, the desired velocity is not correctly reproduced in simulation. To improve accuracy and precision of the walking speed we decided to introduce an additional algorithm, which is briefly presented in Figure 4.7(a).
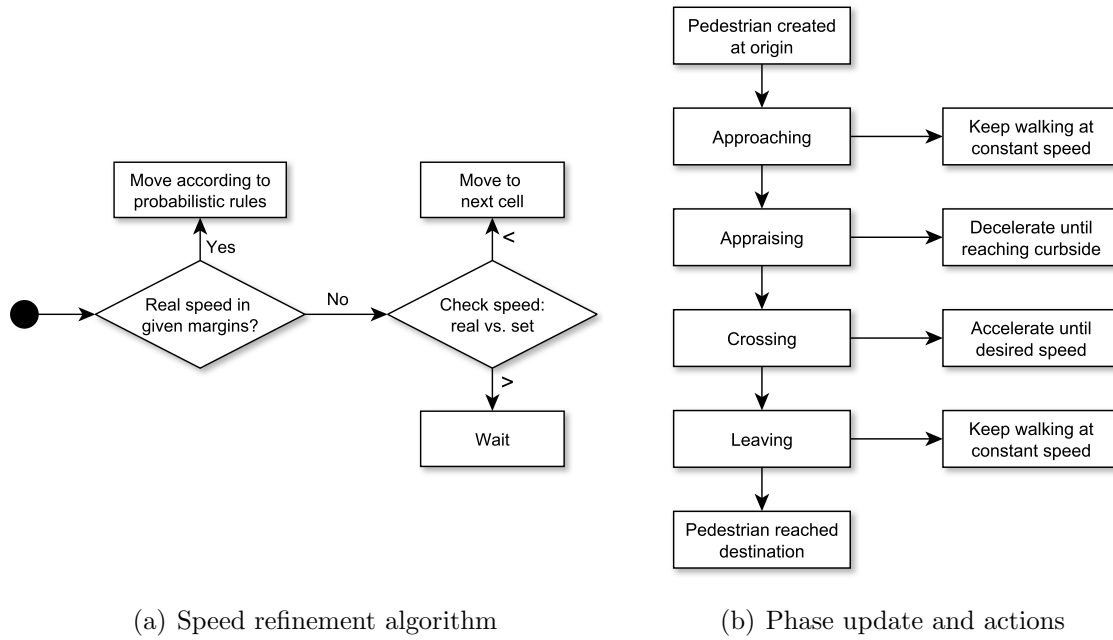

(a) Speed refinement algorithm   (b) Phase update and actions

Figure 4.7: Relevant components of the pedestrian model and update algorithm [201].

At each time step the moving average of the real walking speed v_{avg} (i.e. the velocity actually achieved in simulation) is computed according to:

$$v_{avg} = \frac{d_{tot} \cdot s_{cell}}{N_{avg} \cdot t_{step}} \tag{4.2}$$

where d_{tot} is total distance traveled in cell units (diagonal motion count as $\sqrt{2}$), s_{cell} is the cell's side length, N_{avg} the number of time steps considered and t_{step} the time step length. To avoid cyclic oscillations, the size of N_{avg} is slightly changed every time step. Once v_{avg} has been computed, it is checked if the velocity lies within given margins of the desired walking speed. If this test is passed update is performed according to probabilistic rules (as shown above). If v_{avg} is too large or too low, update is halted or forced accordingly to each case. As the red line in Figure 4.6 shows, the use of this algorithm allows to greatly stabilize the real walking speed.

To conclude the discussion about walking speed, it is important to remember that pedestrians do not only have different individual walking speeds, but also change their speed in accordance with each phase of the crossing attempt. In Figure 4.7(b) the process used to update phase and change the desired speed is illustrated in detail. When a pedestrian is created it is decided if the given individual is an adult or an elderly according to the proportion of each group inside the population. Later, the desired walking speed is assigned to each pedestrian by using the distribution relative to the corresponding age group. By using the walking speed assigned, the pedestrian will move toward the crosswalk. At a given distance from the crosswalk (appraising distance), the pedestrian will start decelerating. The desired walking speed will be consequently changed every time step according to the given deceleration. When the pedestrian reaches the curbside, deceleration will stop and a decision will be taken on whether to cross or not. If safe conditions are met

(details on the decision-making process are presented later) the pedestrian will accelerate until reaching its original walking speed. The destination is reached by keeping walk on that speed for the remaining time.

4.4.3   Vehicular model

The car following computational method is based on a modified version of the Gipps model [202, 203] on which further changes have been made to allow the use of time steps different from the driver's reaction time. In the original formulation of the Gipps model it is assumed that drivers need a time step before reacting to changes occurring in the traffic. This constraint requires the use of a computational time step as close as possible to the typical driver's reaction time (usually in the order of 1 s). When only cars are considered, this limitation does not cause any problem, since space is continuous (thus allowing accurate speed calculations) and on large vehicle fleets the use of constant reaction time is an acceptable approximation. However, since our model include pedestrians which move in a discrete space and need to change their velocity before and during the crossing attempts, choosing time steps equal to the reaction time would not be a satisfactory solution. For this reason, the Gipps model has been further modified allowing the use of time steps much smaller then the driver's reaction time.

According to the time-discrete Gipps model the maximum speed at which a car can travel without colliding with the front vehicle (or obstacle in general) is given by:

$$v_{safe} = b\left(\alpha_{safe} + \beta_{safe}\right) \tag{4.3}$$

where b is the maximum breaking deceleration (given by the car's performance). α_{safe} and β_{safe} are two functions defined as follows:

$$\alpha_{safe} = \left[\sqrt{2\frac{d_p + g}{b} + \frac{1}{4}} - \frac{1}{2}\right] \tag{4.4}$$

$$\beta_{safe} = \frac{d_p + g}{(\alpha_{safe} + 1)b} - \frac{\alpha_{safe}}{2} \tag{4.5}$$

with g being the distance with the front car and d_p the minimum breaking distance which can be computed using:

$$d_p = b\left(\alpha_p\beta_p + \frac{\alpha_p(\alpha_p - 1)}{2}\right) \tag{4.6}$$

where α_p and β_p are defined as the integer and decimal part respectively of the ratio v_{car}/b, being the number of steps required to completely stop the car moving at speed v_{car} (remember that b is the maximum deceleration). As explained above, the reaction time is implicitly included in the fact that each driver can react to changes in traffic conditions only at the next time step, thus requiring the time step being equal (or close) to the reaction time. To allow the use of time steps much smaller than the reaction time it is sufficient considering a gap g_{new} equal to:

$$g_{new} = g - t_{reaction} \cdot v_{car} \tag{4.7}$$

in which the distance traveled by the car during the reaction time $t_{reaction} \cdot v_{car}$ is subtracted from the "real" gap from the front vehicle. By simply using the modified g_{new} in equations

(4.4) and (4.5) it is possible to introduce different reaction times for each driver without having to heavily modify the Gipps model. The only condition for accurate results is to ensure that the time step used is sufficiently smaller than the smallest reaction time (this aspect will be also discussed in the results).

Figure 4.8: Basic algorithm for updating car position and speed [201].

The update of speed and position for each car is performed as indicated in the simple diagram of Figure 4.8 and by using the update rules of the Gipps model (with some small modifications allowing to use different values for acceleration and breaking deceleration). For a given car with current speed $v_{car}(t)$, the velocity at the next time step can be obtained by initially compute v_1 and v_0 as follows:

$$v_1 = min\left[v_{car}(t) + a, v_{max}, v_{safe}\right] \tag{4.8}$$

$$v_0 = v_1 - \epsilon\left(v_1 - (v_{car}(t) - a)\right) \tag{4.9}$$

where a is the maximum acceleration and ϵ is a model parameter typically chosen equal to 0.4. The new velocity is finally computed by taking a random value between v_0 and v_1, or, in mathematical terms:

$$v_{car}(t+1) = \begin{cases} v_0 + (v_1 - v_0) \cdot X, & \text{if } v_0 < v_1 \\ v_1 + (v_0 - v_1) \cdot X, & \text{otherwise} \end{cases} \tag{4.10}$$

where X is a randomly generated number between 0 and 1. As a last step, it is necessary to check the speed change $v_{car}(t+1) - v_{car}(t)$ and, if required, set it to the maximum allowed according to the car's performances (and speed limit). New position for each car is simply computed by multiplying the updated speed with the time step and adding the traveled distance to the old position.

4.4.4 Vehicle–pedestrian interaction

Having discussed how pedestrians and cars move inside their own sub-environment, the next step is to consider the interaction between both agents at the crosswalk, which is the main topic of this study. Here, it is important to remark that the actual definition of a model for the coordination of individual actions between pedestrians and vehicles requires adding specific rules in the behavioral specification of the two distinct types of agents, that are certainly self-interested in general (i.e. they try to pass through the intersection in the smallest possible time) but, at the same time, they are generally benevolent towards the others due to the desire to avoid impacts [204]. Neither a pedestrian nor a vehicle driver wish to have an accident so, despite the possibility of having non-compliant behaviors, both of them are willing to yield either to a crossing pedestrian (whenever a vehicle can safely stop in time) or to a passing car (whenever the vehicle would be too close and/or too fast to yield). To start with, we will begin the discussion by considering the decision making process for cars, which is summarized in Figure 4.9(a).

At first, it is important to define if the considered vehicle is approaching the crosswalk

or not. Obviously, vehicles which just passed the crosswalk do not need to pay attention on pedestrians attempting to cross it (except the case in which only one car is present). If a queue of vehicles is approaching the crosswalk, it is assumed (partially supported by empirical evidence) that only the leading vehicle will consider the presence of pedestrians. The remaining vehicles will only consider the front vehicle as an "obstacle" and adjust their speed accordingly. Next, we need to check if the approaching car is compliant or not. When vehicles are generated, compliance is assigned according to a given probability (obtained empirically). Non-compliant cars will ignore the presence of pedestrians at the curbside (or at the midblock) and will keep driving only caring of the distance from the front vehicle. Here we need to remark (and will be discussed later on) that vehicles are updated before pedestrians in the simulation. As a consequence, when a non-compliant car is approaching, pedestrians are able to judge on its non-decreasing speed that it is not safe to cross. Non-compliant cars ignore pedestrians on the curbside but will always stop if a pedestrian is on their lane (and since pedestrians are very careful before attempting to cross, cars will always have enough distance to stop).

(a) Cars' driver   (b) Pedestrians near and on crosswalk
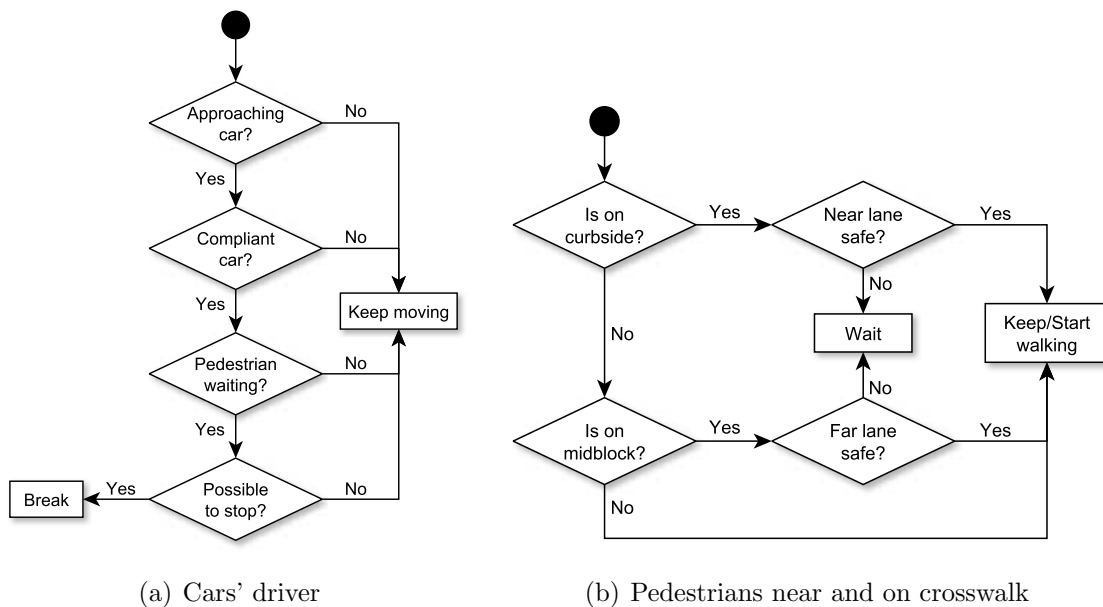
Figure 4.9: Decision-making algorithms for drivers and pedestrians [201].

In the next step of the decision-making algorithm for vehicles, it has to be checked if a pedestrian is waiting on the relative side of the road. If not, there is no need to break before the crosswalk. Waiting pedestrians are only finally considered if all the previous conditions are met: approaching compliant car spotting pedestrian(s) waiting on the side of its lane. In this case, it is important to determine if the car is able to stop in the distance available before the crosswalk. This is performed by using the equations of the Gipps model. If the speed is too high to allow a complete stop, then the driver will abort his stopping attempt and instead adjust his speed by using the distance with the front vehicle. If the speed is low enough to allow a complete stop before the crosswalk, the driver will start breaking eventually arriving at a complete stop just before the crosswalk. As we will see later (and briefly discussed above), pedestrians make similar considerations, which means that they will not attempt to cross if a vehicle cannot or do not want to stop.

Concerning pedestrians, the decision-making process for crossing is summarized in Fig-

ure 4.9(b). After carefully examining the video recording it was concluded that a two-steps crossing mechanism would better summarize the behavior observed in reality (a fact which was also supported by empirical evidence). Pedestrians studied would usually start crossing the road provided the near lane is safe. While crossing the road pedestrians would judge if stepping into the far lane is safe or not and will stop (or slow down) around the middle of the street if the incoming car is deemed as not breaking.

Therefore, the algorithm to assess if a pedestrian can start crossing or not has been designed as follows. At the beginning, we need to check if a pedestrian is on the curbside, since crossing actions start from there. If so, the pedestrian will check the safety of the near lane at first. For this check two different methods have been adopted as listed below.

- Method 1: calculation based on car speed and distance using the same equations of vehicles. If the speed is judged too high to stop in the space provided, the crossing attempt is considered unsafe and the pedestrian will wait.

- Method 2: accepted time gap. When pedestrians are generated, together with the individual walking speed, a specific accepted time gap is assigned to each one according to the distributions for adults and elderly. Because of the statistical nature of distributions, a minimum value for accepted time gap is used to avoid insignificant values (negative numbers in particular which would lead to collisions with cars and are not consistent with observations). Before starting to cross, pedestrian compute the time gap by using speed and distance of the incoming vehicle. If the time gap is larger then the accepted one, then the pedestrian will step into the crosswalk.

Pedestrians judging the near lane as safe will start crossing and after entering the "virtual midblock" the decision-making process is repeated for the far lane. When lanes are not judged as safe pedestrians will simply wait at the same position until safe conditions are met.

4.4.5   Computational loop

After discussing pedestrian, car and interaction modeling, we can now consider how these aspects are combined in the computational loop which is presented in Figure 4.10.
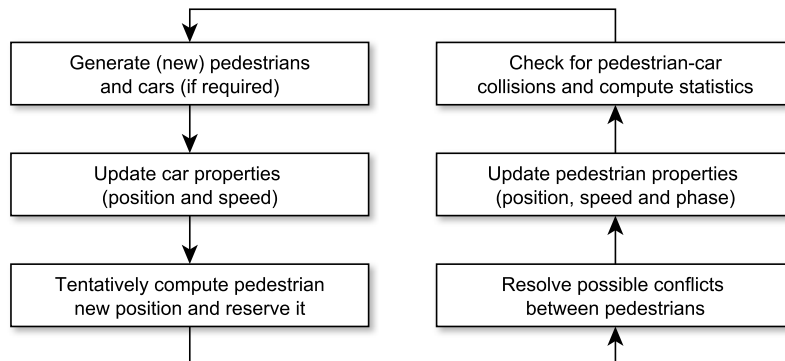

Figure 4.10: Computational loop with update for pedestrians' and cars' properties [201].

Since vehicle and pedestrian sub-environments are independent it is possible to update each class of agent in a predetermined order. At first, if the number of pedestrians

and/or cars is below the input given, pedestrians and/or cars are generated into each sub-environment. Next, each car's speed and position are updated in a sequential way by using the car-following model previously introduced. Here, interactions with pedestrians will be considered while computing the speed of approaching vehicles. Later, pedestrians' new speed and position are also computed, but, since conflicts (with other pedestrians) need to be solved first, pedestrians' do not move yet. Interaction with cars is considered to judge the next move of pedestrians on the curbside or on the midblock. The cell to move in is first reserved and conflicts resulting from pedestrians aiming at the same cells are resolved. When cells reserved by each pedestrian do not overlap, pedestrians are moved in sequential way. Finally, it is checked if collisions did not occur between pedestrians and vehicles on the crosswalk and output values are computed and stored.

In the model presented so far a perfect feedback between vehicles and pedestrians is present and therefore collisions do not occur. In particular, pedestrians, which are more vulnerable than cars, make decisions after drivers and are in a position of advantage in terms of safety. Collisions [2] could be introduced by allowing the accepted time gap to become negative, but this, although mathematically correct, does not correspond to the reality. The first goal is to measure the Level of Service of a crosswalk given the context in which is (or should be) integrated, as consequence, accidents should be excluded from the outcome of simulations (will be considered later on).

4.4.6   Model parameters and constants

To conclude the discussion about the simulation model, it is relevant to define the numerical values which has been used in simulations. This sections is divided into two parts: constants and parameters.

Table 4.5: Constants used in the model [201].

General constants		Pedestrian dynamics	
Time step	0.1 s	Adult walking speed (mean)	1.30 m/s
Pedestrian cell size	0.4 m	Adult walking speed (variance)	0.20 m/s
Scenario dimensions		Elderly walking speed (mean)	1.05 m/s
Road length	374 m	Elderly walking speed (variance)	0.20 m/s
Sidewalk width	2.4 m	Acceleration	0.30 m/s^2
Lane width	4.8 m	Deceleration	0.50 m/s^2
Crosswalk width	3.6 m	Crossing behavior	
Midblock width	1.2 m	Appraising distance	3.0 m
Car (driver) dynamics		Accepted gap adult (mean)	4.0 s
Car length	4.5 m	Accepted gap adult (variance)	2.5 s
Minimum gap	1.0 m	Accepted gap elderly (mean)	4.5 s
Reaction time (mean)	1.1 s	Accepted gap elderly (variance)	1.8 s
Reaction time (variance)	0.2 s	Minimum accepted gap	1.0 s

Although, strictly speaking, both class of numbers can be changed for each simulation, constants are intended for those values which are typical for the scenario considered and are not intended for modification. For instance, walking speeds and driver reaction time

---

[2]Collisions will be included in Chapter 4.6; for the moment we wish to consider the situation observed in the field survey without accidents (and validate the model).

are relative to human nature and will not change much (if not at all) if a different road with similar properties is chosen in a different area (these values will however change from country to country). On the other side, parameters refer here to conditions typical of the time of the day and the weather during which the observation was performed. For example, rainy weather will alter the breaking performance of cars and the flow of pedestrians will also change.

Model constants given in Table 4.5 were mostly obtained from the field study described earlier. Among the values taken from the literature is the drivers' reaction time [205, 206, 207] and the pedestrians' acceleration and deceleration [208]. Although values found in the literature are not specific for the scenario considered here, they refer to phenomena which only slightly change depending on the case considered. Model parameters are given in Table 4.6.

Table 4.6: Parameters used in the model [201].

Car related	
Car density	16.30 cars/km/lane
Maximum (breaking) deceleration	9.0 m/s^2
Maximum acceleration	2.0 m/s^2
Maximum (possible) speed	35 km/h
Non-compliant drivers ratio	0.5 (50%)
Pedestrian related	
Pedestrian flow (both directions)	5.52 min^{-1}
Ratio of elderly pedestrians	0.25 (25%)
Other parameters	
Simulated time (one run)	4500 s (1h:15m)

Some considerations need to be made here concerning the parameters used. During the observation, only car flow has been measured. However, by assuming that traffic conditions allowed to drive at a maximum speed of 35 km/h (data taken from video recording), the relative density can be computed. Car performances are typical of mid-range vehicles. Pedestrian flow refers to the frequency of crossing attempts per minute. Since our simulation model do not consider group cohesion, multiple pedestrians crossing in group in the field study are considered as a single entity (see also previous discussion in Chapter 4.3.3). Non-compliant drivers ratio is obtained from observed behavior and has an important role in balancing pedestrian and vehicular flow on the crosswalk. If this behavioral aspect is excluded, cars will have to continuously stop, thus reducing vehicular flow and allowing pedestrians to cross almost without waiting. Finally, the simulated time for one simulation run has been chosen equal to the total length of the field survey.

4.5   Model validation and results

To check out the capabilities of the model developed and in particular assess its accuracy in estimating motion of cars and pedestrians, different cases have been considered. First of all, it is important to check if the modifications made on the Gipps model allow to correctly estimate the dynamics found in vehicular traffic.

As in the case with pedestrians, to qualitatively assess the degree of congestion in a

given road, the fundamental diagram is typically employed. Average speed and flow are measured during a defined time period (usually 5 or 10 minutes) in the section of the road which is to be analyzed. Density can also be obtained experimentally but it is usually computed by dividing the flow with the average speed. The result for a single measurement of flow and density is plotted in a diagram, resulting in a dispersion of points like the blue crosses shown in Figure 4.11(a). Figure 4.11(a) represents the case of an highway and the speed can be obtained from the slope in the linear part (free flow): 100 km/h for the highway considered.

(a) Density vs. flow   (b) Density vs. speed
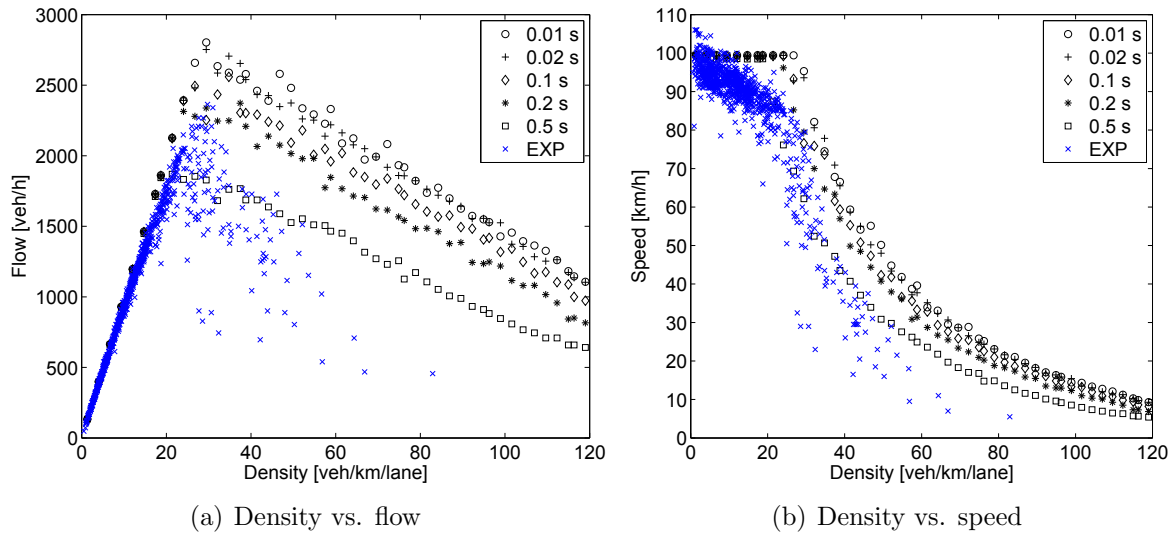
Figure 4.11: Simulated car fundamental diagram for an highway with 100 km/h speed limit. Blue crosses are experimental data. The legend indicates the time steps used in simulation (black symbols). EXP stands for experiment.

To validate the vehicular model used in this study, simulations without pedestrians were performed by changing car density and time step. Results for the highway case with a speed limit of 100 km/h are plotted in Figure 4.11(a) and Figure 4.11(b), showing the density–flow and density–speed diagram respectively. Results were compared with experimental data taken in a section of highway where traffic jams routinely occur. It can be noticed that the fundamental diagram does not significantly change when small time steps are used, meaning that the modifications applied on the Gipps model allow to use variable time steps. However, when the time step grows close to the reaction time, a significant reduction in the maximum flow is observed, which is to be expected since the remainder of the division between reaction time and time step becomes large.

It is remarkable to notice the accuracy in predicting the transition between free flow and congestion, which is observed in Figure 4.11(a) when the initially linearly growing flow reaches a maximum and capacity drops. Both experimental and simulated data agree with a transition around 30 vehicles/km. The maximum flow reached is predicted with less accuracy, but a time step of 0.1 or 0.2 seconds accurately reproduce the experimental case. The simulation model partially fails in computing the behavior of congested flow, but if results are analyzed in terms of speed and density (as shown in Figure 4.11(b)), it can be concluded that the accuracy is sufficient (especially considering that mostly uncongested flow is observed near the crosswalk).

In Figure 4.12(a) and Figure 4.12(b) the results for simulated fundamental diagrams are presented for the case of an urban road (with 50 km/h speed limit), which is more sim-

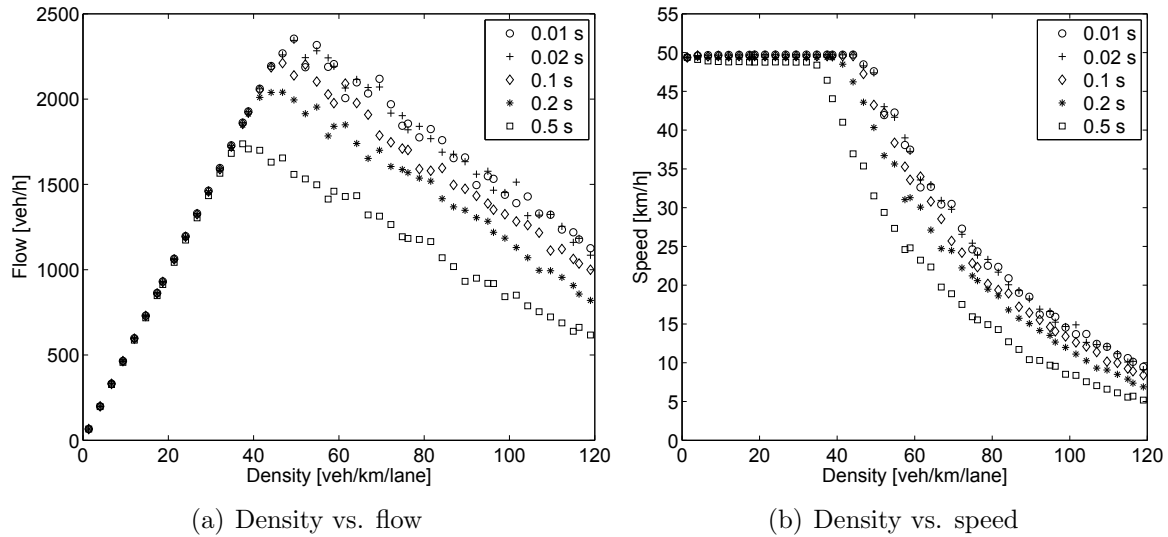(a) Density vs. flow

(b) Density vs. speed

Figure 4.12: Simulated car fundamental diagram for an urban road with 50 km/h. The legend indicates the time steps used in simulation.

ilar to the case considered in this study, but for which large experimental data are not available. Nonetheless, results of the 50 km/h case seem to agree with some simple values from the literature [191], with transition density lying around 40 vehicles/km and a maximum flow of slightly more than 2000 vehicles/hour/lane. Again, in the 50 km/h case also, results are similar when the time step is chosen in the 0.01–0.2 s interval and become significantly different for relatively large time steps (as the case of 0.5 s).

Having verified that the vehicular model allows to correctly simulate car traffic behavior, it is now important to check if the pedestrian model allows to include the features for which it has been developed. In particular, since modeling elderly pedestrians is part of the motivation of this study, we want to check if pedestrians with different velocities are correctly reproduced in the discrete computational space. As discussed before, some specific algorithms were required to assure that pedestrians effectively move at the desired speed and, since distributions are employed, we want to verify if a population of pedestrians actually move with different walking speeds.

In Figure 4.13(a) walking speeds for different pedestrians are plotted against simulation time. Each line corresponds to a single pedestrian which entered the simulation scenario when the line started and was able to reach the "exit" at the end of the line. Two considerations can be done by observing Figure 4.13(a). First of all, it can be concluded that the algorithm previously presented allows to stabilize pedestrians' speed, creating a stable trend similar to situations observed in reality. Next, it can be observed that it is possible to differentiate between individual pedestrian velocities, meaning that it is possible to consider differences between adults and elderly when passing through the crosswalk. However, because of the relatively long moving average interval used, velocity fluctuations during the different crossing phases could not be observed. This can be also clearly understood by looking at Figure 4.13(b), which depicts the difference between the moving average (MA) and the cumulative average (CA) based on results from Figure 4.13(a). In the experimental case, clear variations are seen when pedestrians change (crossing) phase, but in simulation changes are minimal and irrelevant. To observe this type of variations in simulation, small time intervals would have to be used when computing the moving average, but this would result in fluctuations which cannot be removed because of the

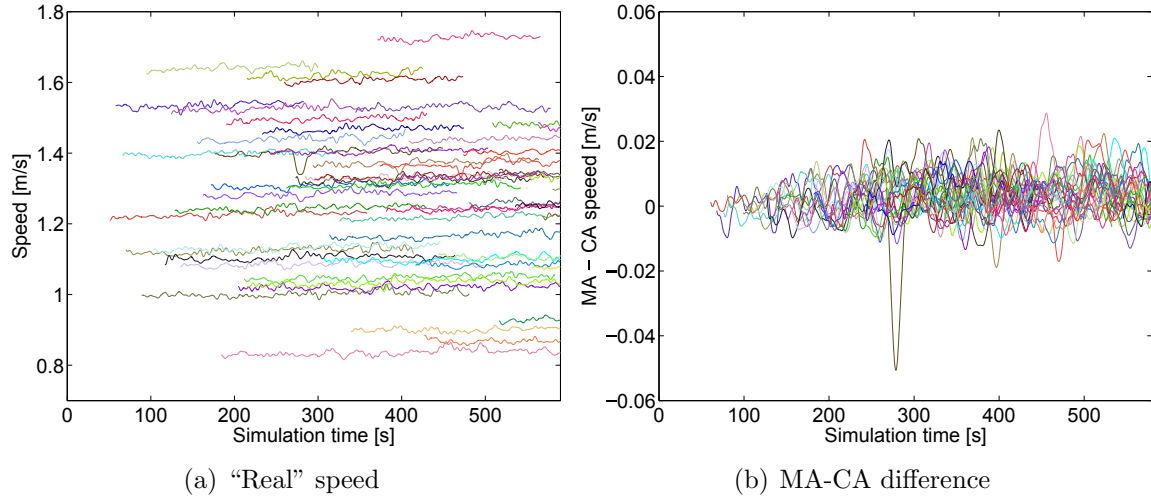(a) "Real" speed

(b) MA-CA difference

Figure 4.13: Pedestrians' speed and speed change during a simulation with different age groups (velocities are averaged over a 10 s interval, pedestrians characteristics are given in Table 4.5). CA stands for cumulative average and MA for moving average.

discrete modeling approach. A solution to see short-term velocity fluctuations would be to use a very small mesh size, but computational time dramatically increases and unrealistic pedestrian densities may form during the simulation.

Finally, we would like to check the validity of the modeling approach used to simulate vehicle-pedestrians interactions. As a comparative quantity to analyze differences between the simulation model and the behavior observed in reality, the delay (or time loss) used to evaluate the Level of Service can be used. Pedestrian delay is simply the time lost while waiting on the curbside. For vehicles the time delay is obtained by computing the difference between the travel time (i.e. the time actually required to go from one side of the simulation model to the other side) and the time it would be required at maximum (allowed) speed (i.e. if no other road user is present at all). Results for vehicular and pedestrian delay and flow of both observation and simulation are presented in Table 4.7.

Table 4.7: Simulation results for vehicle-pedestrian interaction at crosswalk (values used in the simulation are given in Table 4.5 and Table 4.6), letters in brackets refer to the Level of Service.

Quantity observed	Observation	Simulation	
		Method 1	Method 2
Vehicle delay	3.20 ± 2.73 s (A)	3.33 ± 0.34 s (A)	6.20 ± 1.02 s (B)
Pedestrian delay	1.29 ± 0.21 s (A)	1.16 ± 0.18 s (A)	5.81 ± 0.83 s (A)
Vehicle flow	1139 vehicles/h	1028 ± 8 cars/h	963 ± 23 cars/h
Pedestrian flow	5.52 min^{-1}	5.51 ± 0.14 min^{-1}	5.52 ± 0.12 min^{-1}

A set of 100 simulation runs were performed for both methods previously discussed on the pedestrian decision-making process. Method 1 (comparison between vehicle speed and maximum speed allowed for a complete stop) clearly performs better than method 2 (accepted time gap), with delays computed with method 1 lying within the margin of observed quantities. Pedestrian flow appears to be consistent with both methods, but, being an input parameter not related with vehicle interaction is not representative of the

quality of the model and it is only reported for reference. Simulated vehicular flow (which strongly depends on the interaction with crossing pedestrians) is lower than the empirical figure, but it is necessary to remark that observed flow include a variety of vehicles (cars, bikes, bicycles...), while the model has been developed on the assumption that only cars are moving on the road. For example, a bicycle can safely pass on the crosswalk when a pedestrian is walking, a behavior not included in the simulation model. If only cars (or four-wheel vehicles) are accounted for, then the resulting figure for the observed flow will be lowered, getting closer to the simulated value.

The reason for the high delays computed with method 2 may be related to the fact that the distribution of time gaps resulting from the observation is not correctly reproduced in the simulation, where a normal distribution is used [3]. Although the concept of time gap is particularly useful in measuring for example differences between adult and elderly, a direct use in simulation may not be appropriate. Possibly, an extension of the concept of time gap by using different distributions for the accepted and refused time gap as proposed by some researchers [177] may help improving the accuracy of the results. The good agreement between observed delay and the one computed with method 1 possibly suggests that, as some researcher found [183], under clear weather conditions and for low vehicle speeds (like the case of the observation) pedestrians can correctly estimate breaking distance of cars.

Nonetheless, although numerical values for method 2 are much higher than observed delays, results are closest to reality when the Level of Service is adopted. Delays measured in the field study are very low, corresponding to a level A for both vehicular and pedestrian traffic. Both method 1 and 2 are able to obtain the same result numerically (level A). For the vehicular traffic method 2 is only one level above the one observed, meaning that from a qualitative point of view this result can still be considered as satisfactory. In other words, we can conclude that the model developed allowed to correctly assess the LOS found in unsignalized crosswalks (especially when method 1 is employed), thus making it feasible to employ it to assess, for example, if in a given location an unsignalized crosswalk would perform better than a traffic light in terms of quality of service perceived by road users. The particularity of considering elderly pedestrian in the simulation would allow to assess with a better accuracy different areas of a city characterized with different age groups.

4.6   Assessment of pedestrian fatality risk

In the previous discussion we have seen that it is possible to predict delays created by traffic conditions using the simulation model presented. This model can therefore be used to optimize both pedestrian and vehicular traffic in urban environments. However, with the rules and algorithms employed so far, accidents never occur and the model cannot be used to improve pedestrian safety. As we have seen in the introduction, pedestrian safety is an important issue and cannot be studied by experimental methods due to the risks involved and the related ethical concerns. We need therefore to implement some modifications to the model allowing to consider collisions between vehicles and pedestrians.

When distracted, pedestrians or car drivers may not pay attention to the traffic conditions and simply move on the road following their instinct. In the case of vehicles, drivers

---

[3]In the observation a normal distribution was assumed, but data points were not enough to confirm this hypothesis or check for different distributions.

may simply leave the vehicles running without checking road conditions creating a dangerous situations for pedestrians. A similar situation may happen for pedestrians and Hatfield and Murphy found that about 3% of the people crossing the road at unsignalized crosswalks were looking at their phones and did not pay attention to traffic conditions [189] (after the introduction of smartphones this percentage may have increased). Since distraction is one of the leading cause for collisions between vehicles and pedestrians, we can assume in simulations that a given portion of each road user neglects safety in the decision-making process and simply acts as the road would be empty. More specifically, distracted pedestrians do not check if a lane is safe or not and simply cross the road. Distracted drivers do not break even if a pedestrian is on the road. This is different from non-compliant drivers who did not stop when a pedestrian was on the curbside, but did stop if a pedestrian was already crossing. However, in our model, distracted drivers have the ability to perceive other vehicles and so collisions between vehicles do not occur.
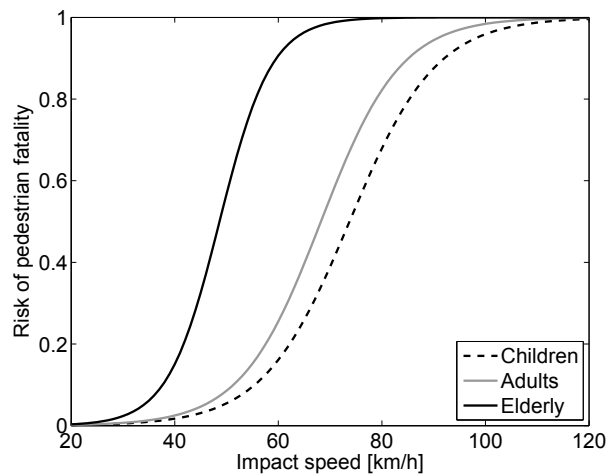
Figure 4.14: Relationship between impact speed and risk of pedestrian fatality [209]. Values for a and b are given in Table 4.8. Children are not considered in this work.

Next, there is an additional important aspect which needs to be considered about collisions between vehicles and pedestrians and it is related with the fatality risk. It is known that collision speed has a strong relationship with the probability of resulting in death of the pedestrian involved. Age of the pedestrians is also relevant, with elderly being more vulnerable then adults as discussed in the introduction. To quantify the relationship between collision speed, pedestrian age and fatality risk, several authors collected data relative to traffic accidents and obtained a function describing the probability of death. D. C. Richards [209] summarized the literature on the subject and presented different functions which can be used to compute the risk of fatality; in this study we will use the following equation [210]:

$$p_{fatality} = 1 - \frac{e^{a-b \cdot v}}{1 + e^{a-b \cdot v}} \qquad (4.11)$$

where v is the collision speed (in km/h and only relative to the vehicle, since pedestrian speed can be neglected) and a and b are empirical parameters obtained by analyzing statistical data for traffic accidents. As stated before, age is a relevant condition in this context and therefore different a and b have to be used depending on the age group of the pedestrian involved. Davis [210] estimated the parameters for children, adults and elderly with the values given in Table 4.8. Figure 4.14 also provides a plot for the three different

curves representing each age group. Database used by Davis refers to data collected in the 1970s and it is possible that technological improvements have contributed in reducing pedestrian fatality risk in the meanwhile. However, we believe that qualitative aspects have remained unchanged since biological processes leading to death are also unchanged.

Table 4.8: Empirical parameters to compute the risk of pedestrian fatality in case of impact with cars for different age groups of pedestrians [209].

Parameter	Children	Adults	Elderly
a	8.85	8.87	9.73
b [h/km]	0.12	0.13	0.20

In Figure 4.14 it is shown that at low velocities (below 50 km/h in the case of adults) the fatality risk is limited, but it quickly grows when speed is increased and after a given value (about 90 km/h for adults) death is almost certain. The same applies to elderly, although the sudden increase in fatality risk occurs at lower speed and the change is more abrupt (compared to adults).

A consequence of the above discussion is that, to measure pedestrian risk in a particular crosswalk using our simulation model, it is not sufficient to simply count the number of collisions occurring, but gravity of the accidents also needs to be accounted for. We therefore decided to include the above equation for pedestrian fatality in our model and evaluate each collision between vehicle and pedestrian using it. Our results are therefore based on the combination between the frequency of collisions and the gravity of them. This means that a crosswalk where collisions occur relatively often at low speed may be considered safer than a crosswalk where collisions are rare but usually result in pedestrian death (due to high speed for example).

To reduce the number and relevance of accidents between vehicles and pedestrians, policies are an effective measure. The "World report on road traffic injury prevention" [166] estimated that serious and fatal road casualty reduction effects related to new policies account for 42% in the case of pedestrians, the highest percentage among road users (the same percentage was 33% for car occupants and 24% for cyclists). We want therefore to investigate which policy is the most effective in reducing road casualties related to the specific case of pedestrians crossing unsignalized crosswalks by using our model, which allows to change different parameters related to traffic conditions and road users' attitude. The standard values used for the simulations presented hereafter are given in Table 4.9.

Table 4.9: Values used in the simulations presented in this work [211]. In each case a single parameter was varied by keeping the remaining ones constant.

Type	Variable	Value
Driver's attitude	Car speed	50.0 km/h
	Non-compliance	0.5
Traffic conditions	Car density	15.0 cars/km/lane
	Pedestrian flow	5.0 min^{-1}
Distraction	Distracted pedestrians	0.02
	Distracted drivers [4]	0.00

---

[4] When amount of distracted drivers was varied, distracted pedestrians was set at 0.

For each simulation we varied the parameter which had to be investigated and kept the
remaining ones constant. Since the case of elderly pedestrians is an important part of
this work three different scenarios were considered: adults-only, a population consisting
of adults and elderly in equal amount and elderly-only. For every parameter-set 72 sim-
ulations each corresponding to 5 hours in reality were performed, totaling 360 hours or
15 days of continuous traffic. If not provided in Table 4.9, values used in simulations
are given in Table 4.5 and Table 4.6 (method 1 was used for the decision-making process
of pedestrians). Pedestrian safety was estimated computing the cumulative fatality risk
over the total simulated time and it is presented in terms of fatalities per hour. Finally,
it should be noted that collisions are only considered once in our model, i.e. even if a
pedestrian suffers a collision on the near lane he/she can continue in the crossing action
and, if a collision also happens in the far lane, this last one is not taken into account.

Drivers' attitude

We can start the discussion on the results by considering drivers' attitude, with speed
and non-compliance analyzed in Figure 4.15. A logarithmic scale is used since the fatality
risk contains exponential terms and changes are extremely quick in a limited speed range.
A first look on Figure 4.15 should suggest that fatalities are intuitively high. Although
it is not possible to provide a direct comparison with empirical data, Figure 4.15(a) in-
dicates that for a speed of 50 km/h one fatality occurs roughly about every 100 hours
or 4 days (in other words almost 90 fatalities per year). To understand these results it
is important to remember that parameters used refer to a moderate level of traffic from
both a vehicular and pedestrian perspective and simulations were performed with the
level of traffic unchanged for 360 hours. In reality, traffic volumes drastically decrease at
nighttime and weekends also have different traffic levels. The results presented here are
therefore intended for comparison between different policies and for qualitative consid-
erations. Quantitative values need to be considered with care. To obtain more realistic
values, simulation should be performed considering the changes in traffic volumes over a
typical week, but on that purpose accurate values for vehicular and pedestrian flow are
required (and not available for the scenario considered here).

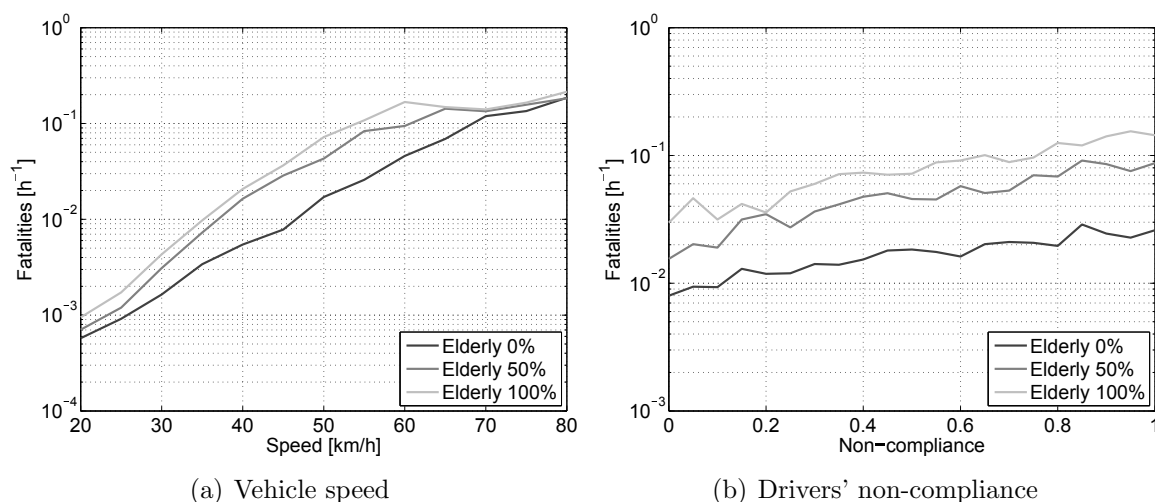(a) Vehicle speed   (b) Drivers' non-compliance

Figure 4.15: Relationship between drivers' attitude (in terms of speed and compliance)
and fatality rate for crossing pedestrians [211].

Figure 4.15(a) shows that speed clearly has an influence on pedestrian fatality for all the cases considered and the ratio of elderly roughly has a linear relationship with frequency of fatality (although, because of the logarithmic scale, mixed population line seems to be shifted toward the one for elderly). On the other side, non-compliance is seen as having only a marginal effect of pedestrian safety since the increase in fatalities in not as marked as in the case of speed. Qualitatively, it can be observed that pedestrians are able to recognize non-compliant drivers, thus preventing them from colliding with them. In this regard, it can be concluded that compliance becomes important for LOS considerations, but its relation with safety is limited.

Traffic conditions

Next, we wish to consider volumes of traffic for both vehicles and pedestrians, whose simulation results are given in Figure 4.15(a).

(a) Pedestrian flow (or frequency)   (b) Car density (related with flow)
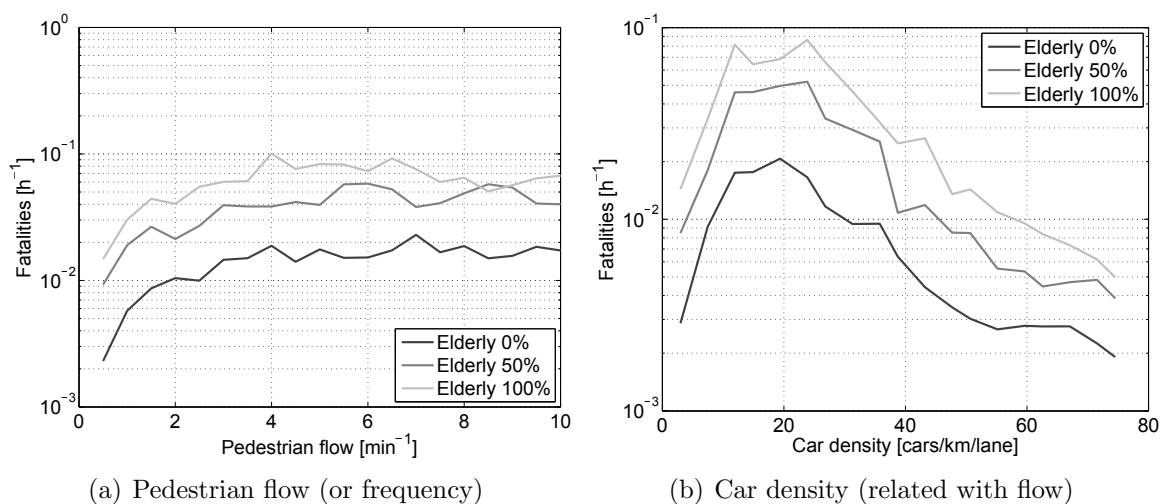
Figure 4.16: Relationship between traffic volumes for vehicles and pedestrians and fatality rate for crossing pedestrians [211].

In the case of pedestrians, it is shown that fatalities grow with the volume of traffic, but a plateau is reached for around 4 $(min)^{-1}$. This could be related with the fact that when the traffic of pedestrians grows, it is more often observed that people have to wait at the curbside. As a consequence, even if a distracted pedestrian crosses without checking, it is more likely that cars already stopped to give way to other pedestrians, thus preventing him/her from suffering a collision. In the case of vehicular traffic (more precisely density is changed in the simulations) the situation is slightly different. At first, the number of pedestrian fatalities grows with an increase in car density, but after reaching a maximum at about 20 cars/km/lane it constantly decreases until the maximum density considered in simulations. This change was created by the formation of traffic jams, which reduced the driving speed for cars consequently reducing the cumulative risk for pedestrians. Considering both pedestrians and vehicles altogether it can be concluded that a dense traffic is beneficial for pedestrian safety. In this regard, it is worth mentioning an experiment which was performed in the town of Drachten in the Netherlands in 2002 by removing almost all traffic signs. It was observed that despite an increase in traffic volumes, number of accidents fell from 8.3 per year between 1992 and 2002 to an average of one in 2005 [212]. The principle of shared space spread to other cities, which later followed the same

example. A similar experiment performed in Auckland (New Zealand) revealed that 80% of pedestrians felt safer and 72% of drivers felt their journey did take either shorter or same as before the removal of traffic signs. Although it seems that psychological aspects also contribute to the improvements of pedestrian safety created by shared spaces [213], results from our simulation seem to agree that an increase in traffic density can reduce fatality risk at unsignalized crosswalks.

Distraction

As a last case we wish to consider distraction and in particular we are interested in investigating which road user is the most dangerous when not paying attention (although, in all the cases, pedestrians will be the ones paying the consequences in case of accident). Results are shown in Figure 4.17; in each case distraction was set at 0 for the road user which was not varied to allow a comparison under equivalent conditions.

(a) Ratio of distracted drivers   (b) Ratio of distracted pedestrians
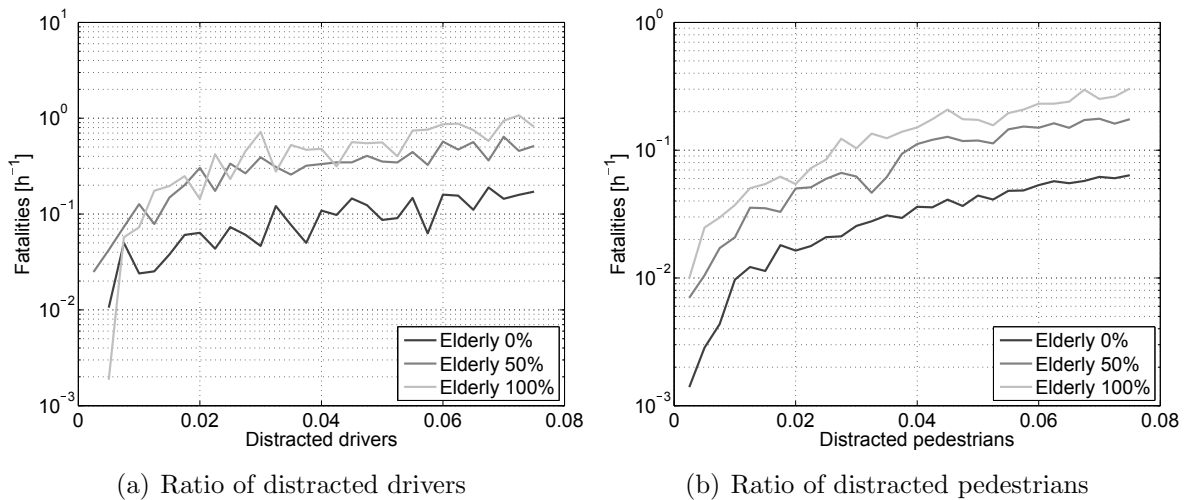
Figure 4.17: Relationship between distraction in drivers and pedestrians and fatality rate for crossing pedestrians [211].

General behavior is similar for both drivers and pedestrians, although distraction in drivers results in a number of fatalities 3–4 times higher compared to distracted pedestrians. Also, from Figure 4.17(a) it can be noticed that the line for the mixed population overlaps with the one for elderly, but this can be caused by issues in statistics related with the high number of collisions (fluctuations are large for all age groups). Nonetheless, these results show that reducing the number of distracted drivers is more efficient than increasing awareness among pedestrians. Being the most vulnerable users, pedestrians are somehow responsible for their own safety regardless on the behavior of drivers, but these results show that policies increasing awareness on traffic accidents are more effective when directed on drivers. In this regard, the use of shared space previously discussed may help increasing the sense of responsibility among drivers possibly reducing their distraction.

4.7 Conclusions and discussion

Based on empirical results from a field survey, a simulation model for pedestrian crossing at unsignalized crosswalks was developed. Although both vehicular and pedestrian motion

are based on classical models found in the literature, specific modifications were required to allow considering important aspects related to vehicle–pedestrian interaction. Concerning pedestrians, small time steps were required to allow considering different walking speeds and therefore making it possible to differentiate between different age group (adult and elderly in particular). In addition, a refinement of the update algorithm was required to remove large fluctuations found in the motion of pedestrians inside the discrete computational grid. Concerning cars, the variable time steps used for pedestrians resulted in the requirement to modify the Gipps car-following model. Driver's reaction time has been explicitly included in the computational loop, also making it possible to consider a distribution for the reaction time which closely reproduce drivers' behavior.

Crossing mechanism of pedestrians has been modeled in a two-step fashion to reproduce behavior observed in the field study. A pedestrian attempting to cross will consider only the near lane first and later check the safety of the far lane while walking on the crosswalk. Results from simulations show that a good agreement with delay of both road users is found when pedestrians are supposed to estimate velocity of incoming vehicles and judge if they can stop in the given distance. The use of the accepted gap also led to somehow acceptable results, but the concept need to be investigated further to allow a successful implementation in simulation.

Inclusion of distracted road users not paying attention to traffic conditions allowed to simulate accidents occurring when crossing pedestrians collide with incoming vehicles. Several scenarios were studied to investigate which factor is the most relevant in reducing accidents and improving pedestrian safety. Speed limit was found as an effective measure to reduce fatality among pedestrians, since probability of surviving an accident is directly related with it. However, we also found that alternative solutions may have the same impact without specifically addressing only one road user. In particular, the shared space concept (in which traffic signs are removed) can automatically reduce traffic speed and at the same time decrease the number of distracted drivers, both leading to a more safe pedestrian environment.

To conclude the discussion, it is important to remark that the model developed in the frame of this research is representative of the phenomena observed during the field study in Milan. This means that, although generally speaking behavior of pedestrians will not largely change in different countries, the accuracy of the model may be limited if, for example, high non-compliance rates are found in drivers or the traffic is composed by a large number of motorbikes. Nonetheless, the approach presented here will surely help developing a partially different model representing the specific behavior found in another country/city.

A possible application of the proposed crosswalk model may be for city planning. In particular, this model can be useful to determine where to place a crosswalk and which LOS can be expected in the given location. Most of the constants used in the simulation will not change to a large extent, especially inside the same city, and expected pedestrian and vehicular flow can be estimated by means of measurements or surveys. With both flows provided, the simulation can easily allow to predict the LOS and thus help decision-makers determining if an unsignalized crosswalk is appropriate or alternative solutions have to be considered (underground passage, traffic light...). The model could also be used to assess pedestrian safety and efficacy of policies, especially where large populations of elderly are found.

Chapter 5

Conclusions and outlook

5.1   Conclusions

In this thesis, properties of pedestrian flows (or more generally pedestrian crowds) and methods to analyze them have been presented and discussed. We started by considering unidimensional pedestrian motion and the literature devoted on the subject, to gradually move toward a full bidimensional treatment where directions become irrelevant. The bidirectional flow has been initially regarded as a system composed by two unidirectional streams which could be analyzed using the typical methods found in the literature. However, during the analysis of the important mechanism of lane formation, we noticed that lateral motion plays an important role and that considering one direction preferentially does not allow to grasp relevant properties. Our on-field observation in the Omote-sando subway station also suggested that body rotation and more generally rotational movements inside the crowd are important, in particular at high densities, partially confirming similar findings reported in the literature. This observation later inspired the formulation of the so-called rotation range used to measure the amount of rotation in pedestrian crowds. The formulation was further improved leading to what we defined as the congestion level: a measure for the amount of congestion (or smoothness in its inverse definition) found in fully bidimensional pedestrian crowds. The different learnings on the behavior of people in pedestrian crowds led to the formulation of a simulation model which considers more precisely motion of pedestrians in high density situations and allowed to reproduce the fundamental diagram for the bidirectional flow for a large range of densities and flow ratios. The simulation model was also validated using empirical data showing a good agreement in different scenarios.

The methods developed by analyzing the bidirectional flow were applied to more complex multidirectional pedestrian crowds obtaining interesting results. In particular, by using the congestion level, we have been able to identity the location possibly responsible for the chaotic situations found in evacuations. When applied on completely chaotic pedestrian motion, the congestion level had a similar behavior to the one of flow in relation to changes in density. However, flow and congestion level got completely unrelated when we applied both on a periodic bidirectional flow with constant density, where a clear transition into organized motion was observed during the experiment and only the congestion level could detect such a change. This shows that the congestion level proposed here has a different nature from the flow usually employed to describe pedestrian streams and can therefore provide an additional type of information and increase the capabilities in examining pedestrian crowds.

During our analysis, we often made use of the fundamental diagram, which has been the most used method to measure capacity and transition to congestion in pedestrian dynamics. While we found that the fundamental diagram allows to recognize differences among pedestrian crowds, our analysis also suggests that it is not universal and therefore it may not be appropriate to measure them. In particular, we noticed that there is a sort of transition in the shape of the fundamental diagram when the dimensionality of motion is increased from the simple unidirectional motion to the most complex chaotic multidirectional dynamics. The congestion level introduced here represents a more universal and versatile approach which could potentially substitute the standard fundamental diagram in the analysis of crowds.

For the particular case of the bidirectional flow we identified three flow regimes (free flow, organized motion and congestion) and defined a method to detect them and describe the transition in terms of the flow ratio. While we have not been able to analyze several types of multidirectional flows, our analysis suggests that with the degree of complexity being increased, more flow regimes (or states) are possible and transition from the different flow regimes may not be universal, but might depend on people's cognition and environment. Throughout our analysis, we noticed that cognitive nature of humans has a remarkable influence on the dynamics of crowds. While this aspect has been known for a long time (and in fact research on crowds started from a humanistic approach), physical and numerical modeling have been preferred with a particular focus on computer simulation. Considering that prediction accuracy for simulation models is rapidly increasing, cognitive aspects should start being considered more systematically. It is possible that only by accounting for cognitive aspects the differences observed in several fundamental diagrams observed at high densities and the multiple phase transitions can be explained.

With this said on cognitive aspects of this research, we showed that some of the methods presented here, such as the congestion or the obstruction index, allow to measure pedestrian crowds, thus creating the fundamentals to compare different cases and examine the relationship with crowd composition, cognitive and environmental factors. In this regard, the system presented here to measure velocity, density and congestion level based on data from inertial sensors (contained in electronic devices) could also help in gaining relevant empirical data, which represent the starting point for a critical analysis. While we showed that such an application may be only feasible for crowds composed of a large number of pedestrians, this is also the condition that needs to be studied the most and possibly the technological limitations are minimized if very crowded spaces are considered. On the other side, the transition observed in the congestion level – body acceleration relationship shows that it could be possible to define a clear threshold outlining congestion occurrence and combining some of the goals identified for this research (i.e. crowd measurement and congestion detection).

Finally, we showed that cognitive aspects had also a central part in modeling the interaction between pedestrians and cars at unsignalized crosswalks. In this regard, the implementation of the decision making process observed in reality had been crucial in determining the accuracy of the results and correctly modeling the waiting times recorded during observation. The calibrated simulation model was later used to investigate dangerous situations not reproducible in experiments, showing that shared spaces could actually lead to a reduction of fatalities caused by collisions between cars and pedestrians. This aspect shows that design of urban facilities accommodating pedestrian traffic needs to be performed considering multiple aspects, with design capacity being also related to the way those facilities are perceived and the interactions among the different users.

5.2   Outlook

While the techniques and methods presented here have shown having some potential, further research is required to validate them and a large amount of empirical data is desired to calibrate the several parameters on which they depend. In particular, spatial and time scale, used to determine the velocity vector field on which most of our analysis is based, could affect the outcome of crowd measurement. While we discussed that selection range is fairly limited and related to typical quantities of human body, the selection within this range is important and need to be investigated further. In addition, we found that most of the measurements introduced here tented to be noisy and although the reason could be related to a non-optimal selection of parameters, the nature of this noise needs to be clarified since it determines the accuracy in predicting future changes in pedestrian crowds.

Also, our research has been mostly based on precisely designed supervised experiments and real situations could be largely different. Although experiments were designed without specific orders, therefore allowing a fairly natural behavior, we excluded many factors which do exist in any urban environment (time pressure, stress, crowd heterogeneous age/gender composition, weather...). As a consequence, the methods presented here represent a starting point on which future technologies may be built, but require an extensive validation before coming to final conclusions/judgments on their accuracy.

In addition, in particular for the case of the bidirectional flow, we understood that indications and more generally the environment has a large influence on the way crowds move and behave. While our analysis mostly considered only changes in density with similar neutral environments, the relationship of the surrounding environment in determining people's movements should be a topic of future research. Similarly to the composition of the crowd, the environment in which people move and more importantly the perception of it (indications, colors, lights, smells...) is also determinant in the analysis of pedestrian dynamics and need to be considered for future research.

Concerning simulation models, we showed that satisfactory results were obtained, but scenarios considered in our simulations were rather simple, both in the bidirectional pedestrian flow and the crosswalk model. For both cases, it is technically feasible to extend each scenario to more complex situations: for example by considering a multidirectional flow with the sub-mesh model or simulating a traffic grid reproducing a neighborhood (or also an entire city) with the crosswalk model. An implementation connecting both models would be also feasible, but it is possibly not relevant for practical applications.

Finally, although probably very difficult, more accurate data on crowd accidents (such as stampedes) would be required to assess the validity of the methods presented here in describing them numerically and potentially preventing them. In this regard, data on velocities (and densities) observed during crowd accidents could help improving the accuracy of the congestion level by including elements related to density as already performed by Helbing et al. for their "crowd pressure". On the other side, a more vast database on traffic accidents could help assessing the reliability of the fatality rates obtained in simulations of the unsignalized crosswalk.

Bibliography

[1] Vicsek, T. & Zafeiris, A. Collective motion. *Physics Reports* **517**, 71–140 (2012).

[2] Schadschneider, A., Chowdhury, D. & Nishinari, K. *Stochastic transport in complex systems: from molecules to vehicles* (Elsevier, 2010).

[3] Cont, R. & Bouchaud, J.-P. Herd behavior and aggregate fluctuations in financial markets. *Macroeconomic dynamics* **4**, 170–196 (2000).

[4] Postmes, T. & Brunsting, S. Collective action in the age of the Internet mass communication and online mobilization. *Social Science Computer Review* **20**, 290–301 (2002).

[5] Kozinets, R. V., Hemetsberger, A. & Schau, H. J. The wisdom of consumer crowds: Collective innovation in the age of networked marketing. *Journal of Macromarketing* **28**, 339–354 (2008).

[6] Dyer, J. R. *et al.* Consensus decision making in human crowds. *Animal Behaviour* **75**, 461–470 (2008).

[7] Moere, A. V. Time-varying data visualization using information flocking boids. In *Information Visualization, 2004. INFOVIS 2004. IEEE Symposium on*, 97–104 (IEEE, 2004).

[8] Helbing, D. & Mukerji, P. Crowd disasters as systemic failures: analysis of the Love Parade disaster. *EPJ Data Science* **1**, 7 (2012).

[9] Desa, UN. World urbanization prospects, the 2014 revision. *United Nations* **366** (2014).

[10] The World Bank. Air transport, passengers carried. http://data.worldbank.org/indicator/IS.AIR.PSGR (2015). Online; accessed 17 March 2017.

[11] Murosaki, Y. Crowd avalanche at the Akashi fireworks show. *Accident Prevention Newsletter (Yobō Jihō)* 8–13 (2002). In Japanese.

[12] BBC. Hajj stampede: At least 717 killed in Saudi Arabia. http://www.bbc.com/news/world-middle-east-34346449 (2015). Online; accessed 17 March 2017.

[13] Zhang, J., Klingsch, W., Schadschneider, A. & Seyfried, A. Transitions in pedestrian fundamental diagrams of straight corridors and T-junctions. *Journal of Statistical Mechanics: Theory and Experiment* **2011**, P06004 (2011).

[14] Steffen, B. & Seyfried, A. Methods for measuring pedestrian density, flow, speed and direction with minimal scatter. *Physica A: Statistical mechanics and its applications* **389**, 1902–1910 (2010).

[15] Oberhagemann, D. Static and Dynamic Crowd Densities at Major Public Events. Tech. Rep. TB 13-01, Vereinigung zur Förderung des Deutschen Brandschutzes (2012).

[16] Helbing, D., Johansson, A. & Al-Abideen, H. Z. Dynamics of crowd disasters: An empirical study. *Physical review E* **75**, 046109 (2007).

[17] Canetti, E. & Stewart, C. *Crowds and power* (Macmillan, 1962).

[18] Fruin, J. J. *Pedestrian planning and design* (Elevator Books, 1971).

[19] Transportation Research Board. *Highway capacity manual* (Transportation Research Board, 2000).

[20] Mōri, M. & Tsukaguchi, H. A new method for evaluation of level of service in pedestrian facilities. *Transportation Research Part A: General* **21**, 223–234 (1987).

[21] Weidmann, U. *Transporttechnik der fussgänger* (ETH, IVT, 1992). In German.

[22] Kuhne, R. D. Greenshields' legacy: Highway traffic. *Transportation Research E-Circular* (2011).

[23] Hankin, B. & Wright, R. Passenger flow in subways. *OR* **9**, 81–88 (1958).

[24] Navin, F. P. & Wheeler, R. J. Pedestrian flow characteristics. *Traffic Engineering, Inst Traffic Engr* **39** (1969).

[25] Oeding, D. *Verkehrsbelastung und Dimensionierung von Gehwegen und anderen Anlagen des Fußgängerverkehrs* (Bundesminister für Verkehr, Abt. Strassenbau, 1963). In German.

[26] Older, S. *Movement of pedestrians on footways in shopping streets* (Traffic engineering & control, 1968).

[27] Predtechenskii, V. M. & Milinskiǐ, A. I. *Planning for foot traffic flow in buildings* (National Bureau of Standards, US Department of Commerce, and the National Science Foundation, Washington, DC, 1978).

[28] Daamen, W. *Modelling passenger flows in public transport facilities*. Ph.D. thesis, TU Delft (2004).

[29] Fruin, J. J. *Design for Pedestrians, A Level-of-Service Concept*. Ph.D. thesis, The Polytechnique Institute of Brooklyn (1970).

[30] Sarkar, A. & Janardhan, K. A study on pedestrian flow characteristics. In *The 76th TRB annual meeting, National Research Council, Washington, DC*, 169–192 (1997).

[31] Lam, W. H., Morrall, J. F. & Ho, H. Pedestrian flow characteristics in Hong Kong. *Transportation Research Record* 56–62 (1995).

[32] Tanaboriboon, Y., Hwa, S. S. & Chor, C. H. Pedestrian characteristics study in Singapore. *Journal of transportation engineering* **112**, 229–235 (1986).

[33] Virkler, M. R. & Elayadath, S. *Pedestrian speed-flow-density relationships* (Transportation Research Board, 1994).

[34] Gupta, A. & Pundir, N. Pedestrian flow characteristics studies: A review. *Transport Reviews* **35**, 445–465 (2015).

[35] Chattaraj, U., Seyfried, A. & Chakroborty, P. Comparison of pedestrian fundamental diagram across cultures. *Advances in complex systems* **12**, 393–405 (2009).

[36] Dambalmath, P., Muhamad, B., Eberhard, H. & Löhner, R. Fundamental diagrams for specific very high density crowds. In *Proceedings of Pedestrian and Evacuation Dynamics 2016*, 6–11 (University of Science and Technology of China Press, 2016).

[37] Feliciani, C. & Nishinari, K. An improved Cellular Automata model to simulate the behavior of high density crowd and validation by experimental data. *Physica A: Statistical Mechanics and its Applications* **451**, 135–148 (2016).

[38] Zhang, J. *et al.* Universal flow-density relation of single-file bicycle, pedestrian and car motion. *Physics Letters A* **378**, 3274–3277 (2014).

[39] Zhang, J. *Pedestrian fundamental diagrams: Comparative analysis of experiments in different geometries.* Ph.D. thesis, Forschungszentrum Jülich (2012).

[40] Zhang, J. & Seyfried, A. Comparison of intersecting pedestrian flows based on experiments. *Physica A: Statistical Mechanics and its Applications* **405**, 316–325 (2014).

[41] Cao, S., Seyfried, A., Zhang, J., Holl, S. & Song, W. Fundamental diagrams for multidirectional pedestrian flows. *Journal of Statistical Mechanics: Theory and Experiment* **2017**, 033404 (2017).

[42] Zhang, J. & Seyfried, A. Comparison of bidirectional pedestrian flows by experiments. *arXiv preprint arXiv:1312.2475* (2013).

[43] Matyus, T., Schrom-Feiertag, H., Seer, S. & Stubenschrott, M. Modelling Pedestrian Overlap from Dense Crowd Observations. In *Proceedings of Pedestrian and Evacuation Dynamics 2016*, 359–363 (University of Science and Technology of China Press, 2016).

[44] Kachroo, P. *Pedestrian dynamics: Mathematical theory and evacuation control* (CRC Press, 2009).

[45] Cristiani, E., Piccoli, B. & Tosin, A. *Multiscale modeling of pedestrian dynamics*, vol. 12 (Springer, 2014).

[46] Lighthill, M. J. & Whitham, G. B. On kinematic waves. II. A theory of traffic flow on long crowded roads. *Proceedings of the Royal Society of London A: Mathematical, Physical and Engineering Sciences* **229**, 317–345 (1955).

[47] Richards, P. I. Shock waves on the highway. *Operations research* **4**, 42–51 (1956).

[48] Whitham, G. B. *Linear and nonlinear waves*, vol. 42 (John Wiley & Sons, 1974).

[49] Zhang, X., Weng, W. & Yuan, H. Empirical study of crowd behavior during a real mass event. *Journal of Statistical Mechanics: Theory and Experiment* **2012**, P08012 (2012).

[50] Papadimitriou, E., Yannis, G. & Golias, J. A critical assessment of pedestrian behaviour models. *Transportation research part F: traffic psychology and behaviour* **12**, 242–255 (2009).

[51] Wąs, J., Porzycki, J., Lubaś, R., Miller, J. & Bazior, G. Agent based approach and Cellular Automata - A promising perspective in crowd dynamics modeling? In *2015 Summer Solstice: 7th International Conference on Discrete Models of Complex Systems* (2015).

[52] Burstedde, C., Klauck, K., Schadschneider, A. & Zittartz, J. Simulation of pedestrian dynamics using a two-dimensional cellular automaton. *Physica A: Statistical Mechanics and its Applications* **295**, 507–525 (2001).

[53] Blue, V. & Adler, J. Emergent fundamental pedestrian flows from cellular automata microsimulation. *Transportation Research Record: Journal of the Transportation Research Board* **1644**, 29–36 (1998).

[54] Kirchner, A. & Schadschneider, A. Simulation of evacuation processes using a bionics-inspired cellular automaton model for pedestrian dynamics. *Physica A: statistical mechanics and its applications* **312**, 260–276 (2002).

[55] Suma, Y., Yanagisawa, D. & Nishinari, K. Anticipation effect in pedestrian dynamics: Modeling and experiments. *Physica A: Statistical Mechanics and its Applications* **391**, 248–263 (2012).

[56] Nishinari, K., Kirchner, A., Namazi, A. & Schadschneider, A. Extended floor field CA model for evacuation dynamics. *IEICE Transactions on information and systems* **87**, 726–732 (2004).

[57] Henein, C. M. & White, T. Macroscopic effects of microscopic forces between agents in crowd models. *Physica A: statistical mechanics and its applications* **373**, 694–712 (2007).

[58] Shimura, K., Ohtsuka, K., Vizzari, G., Nishinari, K. & Bandini, S. Mobility analysis of the aged pedestrians by experiment and simulation. *Pattern Recognition Letters* **44**, 58–63 (2014).

[59] Vizzari, G., Manenti, L. & Crociani, L. Adaptive pedestrian behaviour for the preservation of group cohesion. *Complex Adaptive Systems Modeling* **1**, 7 (2013).

[60] Lämmel, G., Rieser, M. & Nagel, K. Large scale microscopic evacuation simulation. In *Pedestrian and evacuation dynamics 2008*, 547–553 (Springer, 2010).

[61] Mitsubishi Electric. Mitsubishi Electric Develops World's First Real-time Crowd-congestion Estimation System. http://www.mitsubishielectric.com/news/2016/pdf/0818-b.pdf (2016). Online; accessed 17 March 2017.

[62] Muramatsu, M., Irie, T. & Nagatani, T. Jamming transition in pedestrian counter flow. *Physica A: Statistical Mechanics and its Applications* **267**, 487–498 (1999).

[63] Nowak, S. & Schadschneider, A. Quantitative analysis of pedestrian counterflow in a cellular automaton model. *Physical review E* **85**, 066128 (2012).

[64] Kwak, J., Jo, H.-H., Luttinen, T. & Kosonen, I. Jamming transitions induced by an attraction in pedestrian flow. *arXiv preprint arXiv:1701.06909* (2017).

[65] Chandra, S. & Bharti, A. K. Speed distribution curves for pedestrians during walking and crossing. *Procedia-Social and Behavioral Sciences* **104**, 660–667 (2013).

[66] Saberi, M., Aghabayk, K. & Sobhani, A. Spatial fluctuations of pedestrian velocities in bidirectional streams: Exploring the effects of self-organization. *Physica A: Statistical Mechanics and its Applications* **434**, 120–128 (2015).

[67] Kirchner, A., Klüpfel, H., Nishinari, K., Schadschneider, A. & Schreckenberg, M. Discretization effects and the influence of walking speed in cellular automata models for pedestrian dynamics. *Journal of Statistical Mechanics: Theory and Experiment* **2004**, P10011 (2004).

[68] Weng, W., Chen, T., Yuan, H. & Fan, W. Cellular automaton simulation of pedestrian counter flow with different walk velocities. *Physical Review E* **74**, 036102 (2006).

[69] Helbing, D. A mathematical model for the behavior of pedestrians. *Behavioral Science* **36**, 298–310 (1991).

[70] Turchetti, G., Zanlungo, F. & Giorgini, B. Dynamics and thermodynamics of a gas of automata. *EPL (Europhysics Letters)* **78**, 58003 (2007).

[71] Helbing, D. & Molnar, P. Social force model for pedestrian dynamics. *Physical review E* **51**, 4282 (1995).

[72] Helbing, D., Farkas, I. & Vicsek, T. Simulating dynamical features of escape panic. *Nature* **407**, 487–490 (2000).

[73] Lakoba, T. I., Kaup, D. J. & Finkelstein, N. M. Modifications of the Helbing-Molnar-Farkas-Vicsek social force model for pedestrian evolution. *Simulation* **81**, 339–352 (2005).

[74] Zanlungo, F., Ikeda, T. & Kanda, T. Social force model with explicit collision prediction. *EPL (Europhysics Letters)* **93**, 68005 (2011).

[75] Maury, B. & Venel, J. A discrete contact model for crowd motion. *ESAIM: Mathematical Modelling and Numerical Analysis* **45**, 145–168 (2011).

[76] Zeng, W., Chen, P., Nakamura, H. & Iryo-Asano, M. Application of social force model to pedestrian behavior analysis at signalized crosswalk. *Transportation research part C: emerging technologies* **40**, 143–159 (2014).

[77] Duives, D. C., Daamen, W. & Hoogendoorn, S. P. State-of-the-art crowd motion simulation models. *Transportation research part C: emerging technologies* **37**, 193–209 (2013).

[78] Hoogendoorn, S. P. & Bovy, P. H. Pedestrian route-choice and activity scheduling theory and models. *Transportation Research Part B: Methodological* **38**, 169–190 (2004).

[79] Crociani, L., Invernizzi, A. & Vizzari, G. A hybrid agent architecture for enabling tactical level decisions in floor field approaches. *Transportation Research Procedia* **2**, 618–623 (2014).

[80] Matyus, T., Seer, S. & Schrom-Feiertag, H. Simulation-based forecasts of crowd flows at major events using real-time measurements. In *Traffic and Granular Flow'15*, 329–336 (Springer, 2016).

[81] McComas, J., MacKay, M. & Pivik, J. Effectiveness of virtual reality for teaching pedestrian safety. *CyberPsychology & Behavior* **5**, 185–190 (2002).

[82] Kinateder, M. *et al.* Virtual reality for fire evacuation research. In *Computer Science and Information Systems (FedCSIS), 2014 Federated Conference on*, 313–321 (IEEE, 2014).

[83] Ronchi, E. *et al.* A virtual reality experiment on flashing lights at emergency exit portals for road tunnel evacuation. *Fire Technology* **52**, 623–647 (2016).

[84] von Sivers, I., Templeton, A., Köster, G., Drury, J. & Philippides, A. Humans do not always act selfishly: Social identity and helping in emergency evacuation simulation. *Transportation Research Procedia* **2**, 585–593 (2014).

[85] Pelechano, N., O'Brien, K., Silverman, B. & Badler, N. Crowd simulation incorporating agent psychological models, roles and communication. Tech. rep., DTIC Document (2005).

[86] Boltes, M., Seyfried, A., Steffen, B. & Schadschneider, A. Automatic extraction of pedestrian trajectories from video recordings. In *Pedestrian and Evacuation Dynamics 2008*, 43–54 (Springer, 2010).

[87] Boltes, M. & Seyfried, A. Collecting pedestrian trajectories. *Neurocomputing* **100**, 127–133 (2013).

[88] Boltes, M. *Automatische Erfassung präziser Trajektorien in Personenströmen hoher Dichte*. Ph.D. thesis, Forschungszentrum Jülich (2015). In German.

[89] Sun, S., Zhang, C. & Yu, G. A Bayesian network approach to traffic flow forecasting. *IEEE Transactions on intelligent transportation systems* **7**, 124–132 (2006).

[90] Cheung, C.-y. *Pedestrian flow characteristics in the Hong Kong Mass Transit Railway stations*. Master's thesis, The Hong Kong Polytechnic University (1998).

[91] Lam, W. H., Lee, J. Y. & Cheung, C. A study of the bi-directional pedestrian flow characteristics at Hong Kong signalized crosswalk facilities. *Transportation* **29**, 169–192 (2002).

[92] Kretz, T., Grünebohm, A., Kaufman, M., Mazur, F. & Schreckenberg, M. Experimental study of pedestrian counterflow in a corridor. *Journal of Statistical Mechanics: Theory and Experiment* **2006**, P10001 (2006).

[93] Wong, S. *et al.* Bidirectional pedestrian stream model with oblique intersecting angle. *Journal of transportation Engineering* **136**, 234–242 (2010).

[94] Alhajyaseen, W. K. & Nakamura, H. Quality of pedestrian flow and crosswalk width at signalized intersections. *IATSS research* **34**, 35–41 (2010).

[95] Feliciani, C., Murakami, H. & Nishinari, K. A universal function for capacity of bidirectional pedestrian streams: filling the gaps in the literature. *PLoS one* **13**, 1–31 (2018).

[96] Zhang, J., Cao, S. & Seyfried, A. Properties of Pedestrian Movement at Signalized Crosswalk. In *Proceedings of Pedestrian and Evacuation Dynamics 2016*, 126–130 (University of Science and Technology of China Press, 2016).

[97] Zhang, J., Klingsch, W., Schadschneider, A. & Seyfried, A. Ordering in bidirectional pedestrian flows and its influence on the fundamental diagram. *Journal of Statistical Mechanics: Theory and Experiment* **2012**, P02002 (2012).

[98] Jülich Research Center. Database of pedestrian trajectories in controlled experiments. http://www.fz-juelich.de/ias/jsc/EN/Research/ModellingSimulation/ CivilSecurityTraffic/PedestrianDynamics/Activities/database/databaseNode.html (2017). Online; accessed 24 March 2017 (data openly provided).

[99] Saberi, M. & Mahmassani, H. Exploring areawide dynamics of pedestrian crowds: three-dimensional approach. *Transportation Research Record: Journal of the Transportation Research Board* 31–40 (2014).

[100] Helbing, D. A fluid dynamic model for the movement of pedestrians. *arXiv preprint cond-mat/9805213* (1998).

[101] Yamori, K. Going with the flow: Micro–macro dynamics in the macrobehavioral patterns of pedestrian crowds. *Psychological review* **105**, 530 (1998).

[102] Hoogendoorn, S. & Daamen, W. Self-organization in pedestrian flow. In *Traffic and Granular Flow '03*, 373–382 (Springer, 2005).

[103] Rex, M. & Löwen, H. Lane formation in oppositely charged colloids driven by an electric field: Chaining and two-dimensional crystallization. *Physical Review E* **75**, 051402 (2007).

[104] Kaufman, M. *Lane Formation in Counterflow Situations of Pedestrian Traffic.* Master's thesis, Duisburg-Essen University (2007).

[105] AlGadhi, S. A., Mahmassani, H. S. & Herman, R. A Speed-Concentration Relation for Bi-Directional Crowd Moments with Strong Interaction (2002).

[106] Liu, X.-d., Song, W.-g. & Lv, W. Empirical data for pedestrian counterflow through bottlenecks in the channel. *Transportation Research Procedia* **2**, 34–42 (2014).

[107] Flötteröd, G. & Lämmel, G. Bidirectional pedestrian fundamental diagram. *Transportation research part B: methodological* **71**, 194–212 (2015).

[108] Blue, V. & Adler, J. Cellular automata microsimulation of bidirectional pedestrian flows. *Transportation Research Record: Journal of the Transportation Research Board* 135–141 (1999).

[109] Jian, L., Lizhong, Y. & Daoliang, Z. Simulation of bi-direction pedestrian movement in corridor. *Physica A: Statistical Mechanics and its Applications* **354**, 619–628 (2005).

[110] Blue, V. J. & Adler, J. L. Cellular automata microsimulation for modeling bi-directional pedestrian walkways. *Transportation Research Part B: Methodological* **35**, 293–312 (2001).

[111] Xue, S., Jia, B. & Jiang, R. A behaviour based cellular automaton model for pedestrian counter flow. *Journal of Statistical Mechanics: Theory and Experiment* **2016**, 113204 (2016).

[112] Bandini, S., Crociani, L., Gorrini, A. & Vizzari, G. An agent-based model of pedestrian dynamics considering groups: A real world case study. In *Intelligent Transportation Systems (ITSC), 2014 IEEE 17th International Conference on*, 572–577 (IEEE, 2014).

[113] Sarmady, S., Haron, F. & Talib, A. Z. Simulating crowd movements using fine grid cellular automata. In *Computer Modelling and Simulation (UKSim), 2010 12th International Conference On*, 428–433 (IEEE, 2010).

[114] Wąs, J. & Lubaś, R. Towards realistic and effective agent-based models of crowd dynamics. *Neurocomputing* **146**, 199–209 (2014).

[115] Muramatsu, M. & Nagatani, T. Jamming transition in two-dimensional pedestrian traffic. *Physica A: Statistical Mechanics and its Applications* **275**, 281–291 (2000).

[116] Tajima, Y., Takimoto, K. & Nagatani, T. Pattern formation and jamming transition in pedestrian counter flow. *Physica A: Statistical Mechanics and its Applications* **313**, 709–723 (2002).

[117] Alonso-Marroquin, F., Busch, J., Chiew, C., Lozano, C. & Ramírez-Gómez, Á. Simulation of counterflow pedestrian dynamics using spheropolygons. *Physical Review E* **90**, 063305 (2014).

[118] Yanagisawa, D. *et al.* Study on efficiency of evacuation with an obstacle on hexagonal cell space. *SICE Journal of Control, Measurement, and System Integration* **3**, 395–401 (2010).

[119] Yamamoto, K., Kokubo, S. & Nishinari, K. Simulation for pedestrian dynamics by real-coded cellular automata (RCA). *Physica A: Statistical Mechanics and its Applications* **379**, 654–660 (2007).

[120] Yanagisawa, D. Coordination Game in Bidirectional Flow. *Collective Dynamics* **1**, 1–14 (2016).

[121] Oliveira, C. L. N., Vieira, A. P., Helbing, D., Andrade, J. S. & Herrmann, H. J. Keep-Left Behavior Induced by Asymmetrically Profiled Walls. *Physical review X* **6**, 011003 (2016).

[122] Ikeda, K. & Kim, K. Lane formation dynamics of oppositely self-driven binary particles: Effects of density and finite system size. *Journal of the Physical Society of Japan* **86**, 044004 (2017).

[123] Tokyo Metro Co.,Ltd. Ranking of subway stations by ridership. http://www.tokyometro.jp/corporate/enterprise/passenger_rail/transportation/passengers/ (2015). Online; accessed 29 March 2017 (in Japanese).

[124] Feliciani, C. & Nishinari, K. Phenomenological description of deadlock formation in pedestrian bidirectional flow based on empirical observation. *Journal of Statistical Mechanics: Theory and Experiment* **2015**, P10003 (2015).

[125] Seyfried, A., Steffen, B., Klingsch, W. & Boltes, M. The fundamental diagram of pedestrian movement revisited. *Journal of Statistical Mechanics: Theory and Experiment* **2005**, P10002 (2005).

[126] Finnis, K. K. & Walton, D. Field observations to determine the influence of population size, location and individual factors on pedestrian walking speeds. *Ergonomics* **51**, 827–842 (2008).

[127] Feliciani, C. & Nishinari, K. Empirical analysis of the lane formation process in bidirectional pedestrian flow. *Physical Review E* **94**, 032304 (2016).

[128] Gorrini, A., Vizzari, G. & Bandini, S. Granulometric Distribution and Crowds of Groups: Focusing on Dyads. In *Traffic and Granular Flow'15*, 273–280 (Springer, 2016).

[129] Gorrini, A. *et al.* Social Groups and Pedestrian Crowds: Experiment on Dyads in a Counter Flow Scenario. In *Proceedings of Pedestrian and Evacuation Dynamics 2016*, 179–184 (University of Science and Technology of China Press, 2016).

[130] Feliciani, C. & Nishinari, K. Pedestrians rotation measurement in bidirectional streams. In *Proceedings of Pedestrian and Evacuation Dynamics 2016*, 76–83 (University of Science and Technology of China Press, 2016).

[131] Henderson, L. & Lyons, D. Sexual differences in human crowd motion. *Nature* (1972).

[132] Garcimartín, A. *et al.* Flow and clogging of a sheep herd passing through a bottleneck. *Physical Review E* **91**, 022808 (2015).

[133] Karamouzas, I., Skinner, B. & Guy, S. J. Universal power law governing pedestrian interactions. *Physical review letters* **113**, 238701 (2014).

[134] Ivancevic, V. G. & Reid, D. J. Turbulence and shock-waves in crowd dynamics. *Nonlinear Dynamics* **68**, 285–304 (2012).

[135] Crociani, L. *et al.* Micro and Macro Pedestrian Dynamics in Counterflow: The Impact of Social Group. In *International Conference on Traffic and Granular Flow*, 423–431 (Springer, 2017).

[136] Zanlungo, F., Brščić, D. & Kanda, T. Spatial-size scaling of pedestrian groups under growing density conditions. *Physical Review E* **91**, 062810 (2015).

[137] Intelligent Robotics and Communication Laboratories. Dataset: Pedestrian tracking with group annotations. http://www.irc.atr.jp/sets/groups/ (2010). Online; accessed 26 April 2017.

[138] Gertman, D. *et al.* The SPAR-H human reliability analysis method. *US Nuclear Regulatory Commission* (2005).

[139] Blackman, H. S., Gertman, D. I. & Boring, R. L. Human error quantification using performance shaping factors in the SPAR-H method. In *Proceedings of the human factors and ergonomics society annual meeting*, vol. 52, 1733–1737 (SAGE Publications Sage CA: Los Angeles, CA, 2008).

[140] Nagy, M., Ákos, Z., Biro, D. & Vicsek, T. Hierarchical group dynamics in pigeon flocks. *Nature* **464**, 890–893 (2010).

[141] Feliciani, C. & Nishinari, K. An Enhanced Cellular Automata Sub-mesh Model to Study High-Density Pedestrian Crowds. In *International Conference on Cellular Automata*, 227–237 (Springer, 2016).

[142] Yu, Y. & Song, W. Cellular automaton simulation of pedestrian counter flow considering the surrounding environment. *Physical Review E* **75**, 046112 (2007).

[143] Weifeng, F., Lizhong, Y. & Weicheng, F. Simulation of bi-direction pedestrian movement using a cellular automata model. *Physica A: Statistical Mechanics and its Applications* **321**, 633–640 (2003).

[144] Wilensky, U. NetLogo (1999).

[145] Johansson, A., Helbing, D., Al-Abideen, H. Z. & Al-Bosta, S. From crowd dynamics to crowd safety: a video-based analysis. *Advances in Complex Systems* **11**, 497–527 (2008).

[146] Daamen, W., Yuan, Y. & Duives, D. Comparing three types of real-time data collection techniques: counting cameras, Wi-Fi sensors and GPS trackers. In *Proceedings of Pedestrian and Evacuation Dynamics 2016*, 568–574 (University of Science and Technology of China Press, 2016).

[147] Kok, V. J., Lim, M. K. & Chan, C. S. Crowd behavior analysis: A review where physics meets biology. *Neurocomputing* **177**, 342–362 (2016).

[148] Junior, J. C. S. J., Musse, S. R. & Jung, C. R. Crowd analysis using computer vision techniques. *IEEE Signal Processing Magazine* **27**, 66–77 (2010).

[149] Hoogendoorn, S. P., Daamen, W. & Bovy, P. H. Extracting microscopic pedestrian characteristics from video data. In *Transportation Research Board Annual Meeting*, 1–15 (2003).

[150] Corbetta, A., Meeusen, J., Lee, C.-m. & Toschi, F. Continuous measurements of real-life bidirectional pedestrian flows on a wide walkway. In *Proceedings of Pedestrian and Evacuation Dynamics 2016*, 18–24 (University of Science and Technology of China Press, 2016).

[151] Seer, S., Brändle, N. & Ratti, C. Kinects and human kinetics: A new approach for studying pedestrian behavior. *Transportation research part C: emerging technologies* **48**, 212–228 (2014).

[152] Abedi, N., Bhaskar, A., Chung, E. & Miska, M. Assessment of antenna characteristic effects on pedestrian and cyclists travel-time estimation based on Bluetooth and WiFi MAC addresses. *Transportation Research Part C: Emerging Technologies* **60**, 124–141 (2015).

[153] Feliz Alonso, R., Zalama Casanova, E. & Gómez García-Bermejo, J. Pedestrian tracking using inertial sensors (2009).

[154] Kazuya, M. *et al.* Development of emergency rescue evacuation support system (ERESS) in panic-type disasters: disaster recognition algorithm by support vector machine. *IEICE Transactions on Fundamentals of Electronics, Communications and Computer Sciences* **96**, 649–657 (2013).

[155] Sekimoto, Y. *et al.* Real-time people movement estimation in large disasters from several kinds of mobile phone data. In *Proceedings of the 2016 ACM International Joint Conference on Pervasive and Ubiquitous Computing: Adjunct*, 1426–1434 (ACM, 2016).

[156] Yamamoto, H., Yanagisawa, D., Feliciani, C. & Nishinari, K. Body-rotation behavior of pedestrians for collision avoidance in passing and cross flow. *Transportation Research Part B: Methodological* **122**, 486–510 (2019).

[157] Feliciani, C. & Nishinari, K. Estimation of pedestrian crowds' properties using commercial tablets and smartphones. *Transportmetrica B: Transport Dynamics* **7**, 865–896 (2019).

[158] Feliciani, C. & Nishinari, K. Measurement of congestion and intrinsic risk in pedestrian crowds. *Transportation research part C: emerging technologies* **91**, 124–155 (2018).

[159] Yanagisawa, D. *et al.* Introduction of frictional and turning function for pedestrian outflow with an obstacle. *Physical Review E* **80**, 036110 (2009).

[160] Short, J. R. & Pinet-Peralta, L. M. No accident: Traffic and pedestrians in the modern city. *Mobilities* **5**, 41–59 (2010).

[161] Department for Transport. Road Casualties Great Britain: 2006 - Annual Report. http://webarchive.nationalarchives.gov.uk/+/http://www.dft.gov.uk/adobepdf/162469/221412/221549/227755/rcgb2006v1.pdf (2007). Online; accessed 14 April 2017.

[162] National Police Agency. Occurrence of traffic accidents – 2016 report. https://www.npa.go.jp/publications/statistics/koutsuu/H28_zennjiko.pdf (2017). Online; accessed 14 April 2017 (in Japanese).

[163] Automobile Inspection & Registration Information Association. Private car ownership – 2016 report. http://www.airia.or.jp/publish/statistics/ub83el00000000wo-att/hoyuudaisuusuiihyou.pdf (2017). Online; accessed 14 April 2017 (in Japanese).

[164] Istituto nazionale di statistica & Automobile Club d'Italia. Le statistiche degli incidenti stradali in Italia dagli anni trenta ad oggi. http://www.aci.it/fileadmin/documenti/studi_e_ricerche/dati_statistiche/incidenti/Incidenti_Stradali_dal_1930.pdf (2011). Online; accessed 17 July 2017 (in Italian).

[165] Istituto nazionale di statistica. *Road traffic accidents in Italy in 2015* (2016). Online; accessed 14 April 2017 (in Italian).

[166] Peden, M. *et al.* World report on road traffic injury prevention (2004).

[167] Department for Transport. Reported Road Casualties Great Britain: 2014 – Annual Report. https://www.gov.uk/government/uploads/system/uploads/attachment_data/file/467465/rrcgb-2014.pdf (2015). Online; accessed 14 April 2017.

[168] U.S. Department of Transportation. *Traffic Safety Facts – 2013 Data* (2015). Online; accessed 14 April 2017.

[169] Asher, L., Aresu, M., Falaschetti, E. & Mindell, J. Most older pedestrians are unable to cross the road in time: a cross-sectional study. *Age and ageing* **41**, 690–694 (2012).

[170] Prato, C. G., Gitelman, V. & Bekhor, S. Mapping patterns of pedestrian fatal accidents in Israel. *Accident Analysis & Prevention* **44**, 56–62 (2012).

[171] Al-Ghamdi, A. S. Pedestrian–vehicle crashes and analytical techniques for stratified contingency tables. *Accident Analysis & Prevention* **34**, 205–214 (2002).

[172] National Police Agency. Particularities in the occurrence of fatal traffic accidents in Japan in 2015. https://www.npa.go.jp/toukei/koutuu48/H27_setsumeishiryo.pdf (2016). Online; accessed 14 April 2017 (in Japanese).

[173] Gorrini, A., Vizzari, G. & Bandini, S. Towards Modelling Pedestrian-Vehicle Interactions: Empirical Study on Urban Unsignalized Intersection. In *Proceedings of Pedestrian and Evacuation Dynamics 2016*, 25–33 (University of Science and Technology of China Press, 2016).

[174] Roenker, D. L., Cissell, G. M., Ball, K. K., Wadley, V. G. & Edwards, J. D. Speed-of-processing and driving simulator training result in improved driving performance. *Human factors* **45**, 218–233 (2003).

[175] Lobjois, R. & Cavallo, V. Age-related differences in street-crossing decisions: The effects of vehicle speed and time constraints on gap selection in an estimation task. *Accident analysis & prevention* **39**, 934–943 (2007).

[176] Lobjois, R., Benguigui, N. & Cavallo, V. The effects of age and traffic density on street-crossing behavior. *Accident Analysis & Prevention* **53**, 166–175 (2013).

[177] Jiangang, S., Zhenhua, W. & Yanyan, C. Analysis on behaviors and safety of VRUs at unsignalized roadway crosswalk. In *ICTCT Extra Workshop, Beijing* (2008).

[178] Ibrahim, N. I., Kidwai, F. A. & Karim, R. Motorists and pedestrian interaction at unsignalised pedestrian crossing. In *Proceedings of the Eastern Asia society for transportation studies*, vol. 5, 120–125 (2005).

[179] Goh, B. H., Subramaniam, K., Wai, Y. T., Mohamed, A. A. & Ali, A. Pedestrian crossing speed: the case of Malaysia. *International Journal for Traffic and Transport Engineering* **2**, 323–332 (2012).

[180] Park, H. J. *et al.* Pedestrian crossing behavior and compliance at signalized intersections. In *17th International Conference Road Safety On Five Continents (RS5C 2016), Rio de Janeiro, Brazil, 17-19 May 2016.* (Statens väg-och transportforskningsinstitut, 2016).

[181] Perumal, V. *et al.* Study on pedestrian crossing behavior at signalized intersections. *Journal of traffic and transportation engineering (English edition)* **1**, 103–110 (2014).

[182] Varhelyi, A. Drivers' speed behaviour at a zebra crossing: a case study. *Accident Analysis & Prevention* **30**, 731–743 (1998).

[183] Sun, R., Zhuang, X., Wu, C., Zhao, G. & Zhang, K. The estimation of vehicle speed and stopping distance by pedestrians crossing streets in a naturalistic traffic environment. *Transportation research part F: traffic psychology and behaviour* **30**, 97–106 (2015).

[184] Hamed, M. M. Analysis of pedestrians' behavior at pedestrian crossings. *Safety Science* **38**, 63–82 (2001).

[185] Evans, D. & Norman, P. Understanding pedestrians' road crossing decisions: an application of the theory of planned behaviour. *Health Education Research* **13**, 481–489 (1998).

[186] Yang, J., Deng, W., Wang, J., Li, Q. & Wang, Z. Modeling pedestrians' road crossing behavior in traffic system micro-simulation in China. *Transportation Research Part A: Policy and Practice* **40**, 280–290 (2006).

[187] Sisiopiku, V. P. & Akin, D. Pedestrian behaviors at and perceptions towards various pedestrian facilities: an examination based on observation and survey data. *Transportation Research Part F: Traffic Psychology and Behaviour* **6**, 249–274 (2003).

[188] Gomes, S. V. The influence of the infrastructure characteristics in urban road accidents occurrence. *Accident Analysis & Prevention* **60**, 289–297 (2013).

[189] Hatfield, J. & Murphy, S. The effects of mobile phone use on pedestrian crossing behaviour at signalised and unsignalised intersections. *Accident analysis & prevention* **39**, 197–205 (2007).

[190] Nagel, K., Wagner, P. & Woesler, R. Still flowing: Approaches to traffic flow and traffic jam modeling. *Operations research* **51**, 681–710 (2003).

[191] Nagel, K., Wolf, D. E., Wagner, P. & Simon, P. Two-lane traffic rules for cellular automata: A systematic approach. *Physical Review E* **58**, 1425 (1998).

[192] Bandini, S., Crociani, L. & Vizzari, G. Pedestrian simulation: considering elderlies in the models and in the simulation results. In *Ambient Assisted Living*, 11–21 (Springer, 2015).

[193] Griffiths, J. A mathematical model of a nonsignalized pedestrian crossing. *Transportation science* **15**, 222–232 (1981).

[194] Helbing, D., Jiang, R. & Treiber, M. Analytical investigation of oscillations in intersecting flows of pedestrian and vehicle traffic. *Physical Review E* **72**, 046130 (2005).

[195] Lawniczak, A., Ernst, J. & Di Stefano, B. Creature learning to cross a ca simulated road. *Cellular Automata* 425–433 (2012).

[196] Lawniczak, A. T., Di Stefano, B. N. & Ernst, J. B. Stochastic Model of Cognitive Agents Learning to Cross a Highway. In *Stochastic Models, Statistics and Their Applications*, 319–326 (Springer, 2015).

[197] Daganzo, C. F. & Knoop, V. L. Traffic flow on pedestrianized streets. *Transportation Research Part B: Methodological* **86**, 211–222 (2016).

[198] Crociani, L. & Vizzari, G. An integrated model for the simulation of pedestrian crossings. In *International Conference on Cellular Automata*, 670–679 (Springer, 2014).

[199] Sporchia, M. *Simulazione integrata dell'interazione tra pedoni e veicoli in intersezioni regolate e non.* Master's thesis, Università degli Studi di Milano Bicocca (2013). In Italian.

[200] Milazzo II, J., Rouphail, N., Hummer, J. & Allen, D. Quality of service for interrupted-flow pedestrian facilities in highway capacity manual 2000. *Transportation Research Record: Journal of the Transportation Research Board* 25–31 (1999).

[201] Feliciani, C. *et al.* A simulation model for non-signalized pedestrian crosswalks based on evidence from on field observation. *Intelligenza Artificiale* **11**, 117–138 (2017).

[202] Gipps, P. G. A behavioural car-following model for computer simulation. *Transportation Research Part B: Methodological* **15**, 105–111 (1981).

[203] Krauß, S., Wagner, P. & Gawron, C. Metastable states in a microscopic model of traffic flow. *Physical Review E* **55**, 5597 (1997).

[204] Ciancarini, P., Omicini, A. & Zambonelli, F. Multiagent system engineering: The coordination viewpoint. In *International Workshop on Agent Theories, Architectures, and Languages*, 250–259 (Springer, 1999).

[205] Jurecki, R. S., Jaśkiewicz, M., Guzek, M., Lozia, Z. & Zdanowicz, P. Driver's reaction time under emergency braking a car-research in a driving simulator. *Eksploatacja i Niezawodność* **14**, 295–301 (2012).

[206] Mehmood, A. & Easa, S. M. Modeling reaction time in car-following behaviour based on human factors. *International Journal of Applied Science, Engineering and Technology* **5**, 93–101 (2009).

[207] Taoka, G. T. Brake reaction times of unalerted drivers. *ITE journal* **59**, 19–21 (1989).

[208] Zębala, J., Ciępka, P. & Reza, A. Pedestrian acceleration and speeds. *Probl. Forensic Sci* **91**, 227–234 (2012).

[209] Richards, D. Relationship between speed and risk of fatal injury: pedestrians and car occupants (2010).

[210] Davis, G. Relating severity of pedestrian injury to impact speed in vehicle-pedestrian crashes: Simple threshold model. *Transportation Research Record: Journal of the Transportation Research Board* 108–113 (2001).

[211] Feliciani, C. *et al.* Assessment of pedestrian fatality risk at unsignalized crosswalks by means of simulation. In *International Conference on Traffic and Granular Flow*, 423–431 (Springer, 2017).

[212] Senthilingam, M. Shared space, where the streets have no rules. http://edition.cnn.com/2014/09/22/living/shared-spaces/ (2014). Online; accessed 19 April 2017.

[213] Schulz, M. European Cities Do Away with Traffic Signs. http://www.spiegel.de/international/spiegel/0,1518,448747,00.html (2006). Online; accessed 14 April 2017.

Relevant publications

Most of the contents of the current thesis were published and presented in international journals and conferences, as presented below (the list has been updated after the official thesis submission):

[1] Claudio Feliciani and Katsuhiro Nishinari, *Phenomenological description of deadlock formation in pedestrian bidirectional flow based on empirical observation*, Journal of Statistical Mechanics: Theory and Experiment, IOP Publishing, 2015, https://doi.org/10.1088/1742-5468/2015/10/P10003

[2] Claudio Feliciani and Katsuhiro Nishinari, *An improved Cellular Automata model to simulate the behavior of high density crowd and validation by experimental data*, Physica A: Statistical Mechanics and its Applications, Elsevier, 2016, https://doi.org/10.1016/j.physa.2016.01.057

[3] Claudio Feliciani and Katsuhiro Nishinari, *Empirical analysis of the lane formation process in bidirectional pedestrian flow*, Physical Review E, APS, 2016, https://doi.org/10.1103/PhysRevE.94.032304

[4] Claudio Feliciani and Katsuhiro Nishinari, *An Enhanced Cellular Automata Sub-mesh Model to Study High-Density Pedestrian Crowds*, International Conference on Cellular Automata, Springer, 2016, https://doi.org/10.1007/978-3-319-44365-2_23

[5] Claudio Feliciani and Katsuhiro Nishinari, *Pedestrians rotation measurement in bidirectional streams*, Proceedings of Pedestrian and Evacuation Dynamics, University of Science and Technology of China Press, 2016, https://doi.org/10.17815/CD.2016.11

[6] Andrea Gorrini, Luca Crociani, Claudio Feliciani, Pengfei Zhao, Katsuhiro Nishinari and Stefania Bandini, *Social Groups and Pedestrian Crowds: Experiment on Dyads in a Counter Flow Scenario*, Proceedings of Pedestrian and Evacuation Dynamics, University of Science and Technology of China Press, 2016, https://doi.org/10.17815/CD.2016.11

[7] Claudio Feliciani, Luca Crociani, Andrea Gorrini, Giuseppe Vizzari, Stefania Bandini and Katsuhiro Nishinari, *A simulation model for non-signalized pedestrian crosswalks based on evidence from on field observation*, Intelligenza Artificiale, IOS Press, 2017, https://doi.org/10.3233/IA-170110

[8] Claudio Feliciani, Luca Crociani, Andrea Gorrini, Giuseppe Vizzari, Katsuhiro Nishinari and Stefania Bandini, *Assessment of pedestrian fatality risk at unsignalized crosswalks by means of simulation*, Proceedings of Traffic and Granular Flow '17, Springer, 2019, https://doi.org/10.1007/978-3-030-11440-4_46

[9] Luca Crociani, Andrea Gorrini, Claudio Feliciani, Giuseppe Vizzari, Katsuhiro Nishinari and Stefania Bandini, *Micro and macro pedestrian dynamics in counter flow: the impact of social groups*, Proceedings of Traffic and Granular Flow '17, Springer, 2019, https://doi.org/10.1007/978-3-030-11440-4_18

[10] Claudio Feliciani and Katsuhiro Nishinari, *Measurement of congestion and intrinsic risk in pedestrian crowds*, Transportation research part C: emerging technologies, Elsevier, 2018, https://doi.org/10.1016/j.trc.2018.03.027

[11] Claudio Feliciani, Hisashi Murakami and Katsuhiro Nishinari, *A universal function for capacity of bidirectional pedestrian streams: filling the gaps in the literature*, PLoS one, Public Library of Science, 2018, https://doi.org/10.1371/journal.pone.0208496

[12] Claudio Feliciani and Katsuhiro Nishinari, *Estimation of pedestrian crowds' properties using commercial tablets and smartphones*, Transportmetrica B: Transport Dynamics, Taylor & Francis, 2019, https://doi.org/10.1080/21680566.2018.1517061

[13] Hiroki Yamamoto, Daichi Yanagisawa, Claudio Feliciani and Katsuhiro Nishinari, *Body-rotation behavior of pedestrians for collision avoidance in passing and cross flow*, Transportation Research Part B: Methodological, Elsevier, 2019, https://doi.org/10.1016/j.trb.2019.03.008

Acknowledgment

Revisions

This chapter contains a list of revisions made on this document after the submission to the university. Changes made have not been reviewed by referees and only refers to minor errors found after submission. References and literature related documentation have also been updated to reflect changes occurred after official submission. Readers requiring the original copy are referred to the library system of the University of Tokyo.

List of revisions

- September 2017: "open space" corrected with "shared space".

- October 2017: reference [159] added, reference [154] corrected (first name was used instead of family name).

- November 2017: Figure 2.62 modified (related discussion remains unchanged).

- November 2017: caption of Figure 3.15 corrected.

- April 2018: "congestion level" used instead of "congestion index" and units for rotation and related quantities corrected.

- May 2018: text in Figure 3.29(b) corrected ("4" instead of "9").

- May 2018: scale of Figure 3.31(a), Figure 3.31(b) and Figure 3.31(c) corrected (results were divided by the total number of experiment, 8, instead of the number of experiments with 43 participants, being 5).

- May 2018: scale of several graphs related to rotation (curl) corrected. Results were not divided by the mesh size (0.2 m) resulting in reduced values (content of the text remains unchanged). Figures affected are: 2.42, 2.45, 2.49, 2.50(a), 2.50(b), 2.51(a), 2.51(b), 2.52(a), 2.52(b), 2.57(a), 2.57(b), 2.57(c), 3.16(b), 3.19(a), 3.19(b), 3.22(b), 3.24(a), 3.24(b), 3.26(b), 3.30(c), 3.31(c), 3.36(a), 3.36(b), 3.36(c) and 3.36(d).

- August 2018: Figure 3.9 corrected, x and y-axis were inverted.

- October 2019: references [201, 158, 157, 95, 156, 211, 135] updated (papers published)

Latest update: October 30, 2019